Nature-inspired humectants and plasticisers for use in aqueous confectionery fillings

Andrew James Maneffa

Submitted for the degree of Doctor of Philosophy

University of York

Chemistry

September 2020

Abstract

With an ever-increasing global population and incidence of health-related non-communicable diseases (diabetes, cancer, cardiovascular disease), there is growing pressure on confectionery manufacturers to improve the nutritional profile of their products by reducing the content of undesirable free/added sugars. This is particularly challenging within aqueous confectionery fillings as sugars provide not only sweetness but also humectancy and plasticisation by lowering the water activity (a_w) and glass transition temperature (T_g), which is necessary for maintaining product safety and quality. This thesis investigates both theoretical and practical aspects of replacing common confectionery sugars within model aqueous confectionery fillings using novel, nature-inspired approaches.

Initial attention focussed on rationalising the a_w of aqueous solutions containing archetypal or unheralded humectants via application of statistical thermodynamics. This revealed that a_w manifests as a result of the interplay between the hydration (reduces a_w) and clustering of solutes (increases a_w). A second aspect of the thesis examined the humectant and plasticisation properties of two unheralded natural osmolytes; 2-*O*-α-D-glucopyranosyl glycerol (glycoin) and 2-*O*-α-D-galactopyranosyl glycerol (floridoside) and involved direct extraction of the latter from a natural biomass (*Palmaria palmata*). Both glycoin and the floridoside extract were found to exhibit low T_g values and effective a_w reducing capacities that were equivalent or superior to common confectionery sugars (sucrose, fructose). Two previously unforeseen crystal forms of floridoside were also identified and subsequently characterised in detail. The development and characterisation of several novel 'deep' eutectic mixtures formed using naturally-occurring, food-grade components as 'proof-of-concept' humectant/plasticisers were also described. The performances of one such eutectic mixture, in addition to glycoin and the floridoside extract were evaluated within a model aqueous confection and found to be very comparable to D-fructose, suggesting that they all have potential as drop-in humectants and plasticisers for use within sugar-reduced confectionery and broader food sector applications.

Dedication

I would like to dedicate this thesis to my family who have supported me throughout all stages of my education both financially and emotionally and in particular, for providing me with a comfortable place to live in and write up from during the COVID-19 pandemic. Thank you.

List of Contents

List of Figures

List of Tables

Acknowledgements

I would like to thank my academic supervisors Dr Avtar Matharu and Prof James Clark for giving me the opportunity to undertake PhD research at the Green Chemistry Centre of Excellence (GGCE, York). I also gratefully acknowledge the Biotechnology and Biological Sciences Research Council (BBSRC) for provision of a CASE studentship (award number BB/P504919/1) and the industrial partner for this project Nestlé along with my supervisors at the Nestlé Product Technology Centre Confectionery (NPTC Confectionery, York); Dr Steve Whitehouse, Dr Hugh Powell and Dr Stewart Radford. Special mention must go to Steve and Stewart who not only facilitated but actively partook in various aspects of the experimental work from which I learnt a lot.

My sincerest thanks must go to Dr Seishi Shimizu (University of York) for taking a keen interest in my work, sharing his expert knowledge and acting as an excellent independent panel member and collaborator. Thanks must also go to the various technical staff who either provided training and analysis, both within the GCCE, wider Department of Chemistry within the University of York and research labs at NPTC Confectionery. I would especially like to acknowledge Mr Paul Elliott of the GCCE for sharing his knowledge and many hours of his time to help prepare and facilitate experiments - I hope retired life is treating you well. I am also grateful for the inputs of Dr Rob McElroy (GCCE) and Dr James Sherwood (GCCE) particularly in the earlier stages of the project in addition to those of Dr Aris Lazidis (NPTC Confectionery).

Finally, thank you to all of the students and staff that I have met over the years since arriving at York both past and present, it has been most enjoyable spending time with and learning from you (I hope you enjoyed the coffee).

Declaration

I declare that this thesis is a presentation of original work and I am the sole author unless otherwise clearly indicated. This work has not previously been presented for an award at this, or any other, University. All sources are acknowledged as References. Aspects of the work have been published as the following peer-reviewed journal articles:

1. **A. J. Maneffa**, R. Stenner, A. S. Matharu, J. H. Clark, N. Matubayasi, and S. Shimizu, Water activity in liquid food systems: a molecular scale interpretation, *Food Chemistry*, 2017, **237**, 1133–1138.

2. **A. J. Maneffa**, A. B. Harrison, S. J. Radford, A. S. Whitehouse, J. H. Clark, and A. S. Matharu, Deep eutectic solvents based on natural ascorbic acid analogues and choline chloride, *ChemistryOpen*, 2020, **9**, 559–567.

3. **A. J. Maneffa**, A. C. Whitwood, A. S. Whitehouse, H. Powell, J. H. Clark, and A. S. Matharu, Unforeseen crystal forms of the natural osmolyte floridoside, *Communications Chemistry*, 2020, **3,** 128.

The author would like to declare the contributions made to the above-mentioned works by the respective co-authors:

1. SS conceived of the research question and developed the theoretical framework in collaboration with NM. AJM collected and analysed the data along with RS and developed the research question, draughted the manuscript and responded to reviewers in collaboration with SS. ASM and JHC contributed to proofreading and editing.

2. AJM conceived of the research question, planned and performed the majority of experiments and subsequent data analyses, draughted the manuscript and responded to reviewers. ABH conducted the bacterial toxicity testing analysed the resulting data. ASM, JHC, SJR and ASW contributed to proofreading and editing.

3. AJM conceived of the study, planned and performed the majority of experiments and subsequent data analyses, draughted the manuscript and responded to reviewers. ACW performed single crystal X-ray diffraction experiments and generated/refined the resulting single crystal structural data. ASW conducted isothermal optical microscopy along with AJM and contributed to proofreading and editing. ASM, JHC and HP contributed to proofreading and editing.

All other collaborators (namely those involved in experimental analyses) are duly declared where appropriate.

How to use this thesis

It is intended that this thesis be used by both experienced researchers and/or those who may be less familiar to the areas of green and sustainable and/or confectionery chemistry (undergraduates, postgraduates etc). The thesis comprises eight main chapters which have been prepared and presented according to the rules and regulations set out by the University of York (as of September 2020), with various aspects of Chapters 3, 5 and 6 having been published in peer-reviewed journals as outlined within the Declaration. A collated appendices, references and list of abbreviations/symbols can all be located at the end of the thesis. The appendix has been arranged into individual sections (A - E) which each provide supplementary information for Chapters 3 – 7 based on numerical order (i.e. A corresponds to Chapter 3 and E to Chapter 7).

Chapter 1: This chapter provides a general technical and non-technical background for the main aspects of research that are covered within the thesis. It initially introduces the main national and international drivers for sugar reduction followed by a brief technical summary which describes the role of sugars within aqueous confections. Many of the current state-of-the-art sugar reduction strategies are then discussed before the specific aims of the thesis are presented, each accompanied with their own separate focussed mini-literature reviews.

Chapter 2: This section provides details concerning the materials, methods and analytical/instrumental techniques that were used during the work.

Chapter 3: This chapter begins with a short literature review that critically summarises the various conflicting hypotheses that have been posited regarding the molecular origin of water activity (a_w) in aqueous solutions of sugars and sugar alcohols. This origin is subsequently investigated using the Kirkwood-Buff (KB) theory of solutions, which is also employed to rationalise the humectancy of several relatively unheralded natural osmolytes.

Chapter 4: The humectant and plasticising properties of the natural osmolyte 2-*O*-α-D-glucopyranosyl glycerol (glycoin) and its aqueous solutions are characterised in detail and both the corresponding Norrish constant and Gordon-Taylor constant for the glycoin-water binary solution calculated. The experimentally measured a_w and glass transition temperature (T_g) are compared to those of a range of common confectionery humectants/plasticisers, enabling evaluation of glycoin as a potential replacement for sugars within aqueous confections.

Chapter 5: This chapter investigates the clean, food-grade extraction of the osmolyte 2-*O*-α-D-galactopyranosyl glycerol (floridoside) from natural macroalgal biomass (*Palmaria palmata*) and subsequent physicochemical characterisation (a_w and T_g) thereof. It also reports on the identification and detailed characterisation of two previously unforeseen crystal forms of floridoside which may have important ramifications for future anthropocentric applications and natural biochemistry research.

Chapter 6: This chapter describes the development and preparation of novel eutectic mixtures as 'proof-of-concept' humectants and plasticisers using non-sugar, food-grade components based on several naturally-occurring lactones (including vitamin C). The thermal characteristics of these mixtures are investigated in detail and other physicochemical properties including rheology and a_w are also evaluated.

Chapter 7: The performances of the novel humectants and plasticisers that are presented within Chapters 4 to 6 are evaluated within a model aqueous confectionery filling based on a low 'added' sugar glucose syrup. Following initial characterisation of the base syrup, the influence of the neoteric additives on the principal physicochemical properties (a_w, T_g and viscosity) of the resulting sugar-reduced confections are appraised and compared with those prepared using archetypal confectionery ingredients (glycerol and D-fructose).

Chapter 8: This Chapter provides a general summary of the main outcomes presented within each of Chapters 3 to 7 and also offers suggestions for future work that have arisen as a result.

Chapter 1: General Introduction and Thesis Aims

1.1. General background: Drivers for sugar reduction

Confectionery-based goods are amongst the most popular of all foodstuffs and are enjoyed by consumers across almost virtually every part of the anthropocentric world. Most typically consumed on account of the sense of pleasure and indulgence they bestow, confections also often act as a convenient and readily portable source of energy which can be purchased cheaply and subsequently stored for relatively long periods without spoiling. Unsurprisingly, this popularity is reflected economically, with the global market for confectionery being projected to reach well in excess of $200 billion by the end of 2020.[1] Concerns about obesity and non-communicable diseases have led to increasing demand from government and consumers to reduce the sugar content of packaged foods including confectionery. Incredibly, it has been reported that over 2 billion people worldwide are now overweight or obese,[2] which is especially alarming considering that the latter is known to promote the development of various non-communicable diseases (NCDs) including diabetes, cardiovascular disease and cancer.[3]

In an attempt to curb the prevalence and severity of such maladies, higher authorities have begun to implement sweeping new agendas and policies on both national and international levels.[4] On the global stage, the campaign against NCDs has been reflected most notably, in Goal 3.4 of the seventeen 'Sustainable Development Goals' (Goal 3: Good Health and Well-being) introduced by the United Nations (**Figure 1.1**), which aims to "reduce by one third premature mortality from non-communicable diseases through prevention and treatment" as part of the 2030 Agenda for Sustainable Development.[5] Furthermore, in 2015 the World Health Organisation (WHO) published an overarching guideline which recommended that daily so-called 'free' sugar consumption should represent less than 10 % of an individual's total energy intake.[6] Here, 'free' or 'added' sugar refers to any mono- and di-saccharide used within a food not including that which is naturally present in *intact* fruit, vegetables, milk and dairy products. From a chemical perspective, the IUPAC loosely define a sugar as a "monosaccharide or lower oligosaccharides" where a 'monosaccharide' is a polyhydroxy aldehyde or ketone with three

or more carbon atoms that have the chemical formulae H-[CHOH]$_n$-CHO and H-[CHOH]$_n$-CO-[CHOH]$_m$-H respectively.[7] Within this thesis, the term sugar has also been extended to include higher oligosaccharides and polysaccharides which comprise multiple monosaccharide units joined via glycosidic linkages.

Figure 1.1: The seventeen Sustainable Development Goals of the United Nations.[13] Originally in colour.

Following on from the WHO's recommendation, the United Kingdom Scientific Advisory Committee on Nutrition then produced a report entitled "Carbohydrates and Health" which suggested that the daily free sugar consumption for adults and children in the UK should represent less than 5% of total calorie intake.[8] As a consequence of this, in 2016 Public Health England (PHE) initiated a landmark target of 20 % reduction in the total sugar content of those food products which "provide the majority of sugar in the diets of children" by 2020 compared to the levels of 2015.[9] These commitments have led most noticeably to the 'Soft Drinks Industry Levy', which began in April 2018 and taxes UK producers and

importers of highly sugar-sweetened beverages.[10] They have also been complemented more recently by a targeted 20 % sugar reduction in the fermented yoghurt drinks category which commenced in 2019 and will run up to 2021.[11] However, overall progress appears to have been slow according to the latest progress report published by PHE in late 2019 which suggested that only a 2.9 and 4.9 % reduction had been achieved in the period 2015 – 2018 in the home (retailers and manufacturers) and out of home (restaurants, public houses, cafes etc.) sectors respectively.[12]

With all of the aforementioned considerations in mind, there is ever-growing pressure on producers of sugar-containing goods, including confectionery, to improve the nutritional profile of their products by reducing the content of free or added sugar. Naturally, this has therefore become a key objective of responsible food and beverage multinationals such as Nestlé who as part of their support for the Sustainable Development Goals, have previously stated their aim to reduce added sugar content across their collective product portfolio by 5 % by 2020.[14] Until now, the most common approach towards 'sugar reduction' taken by confectionery manufacturers has been to reduce portion size. This can be somewhat effective as a short-term strategy although it is generally unpopular with consumers as it reduces perceived value for money and has become colloquially termed 'shrinkflation'.[15] Therefore, it is not a sustainable approach in the longer term and manufacturers are in need of alternative strategy - namely product reformulation and innovation. In practice however, the implementation of novel, innovative solutions into the public consumer marketplace can be very challenging and there is no guarantee that new products will be accepted even if they are technologically sound. This difficulty is evidenced by the recent withdrawal of various sugar-reduced products from the UK marketplace.[16, 17]

In any case, irrespective of other barriers that may play a role in preventing wider reaching adoption of sugar-reduced goods (e.g. marketing, consumer education, economics etc.), it is imperative that research

and development continues to make progress in bringing new ideas and approaches to the table so that manufacturers can be empowered to employ the best technical solutions at their disposal.

1.2. Technical background

As mentioned previously, under current WHO guidelines the term 'free sugars' refers to any mono- or disaccharide that is added into a foodstuff (or beverage). This definition is also extended to include sugars that may be naturally released following treatment of natural sugar-containing foodstuffs such as fruit during juicing or pureeing, whilst those sugars present within the corresponding intact foods (e.g. milk) are not considered.[18] The most common added free sugar is the disaccharide sucrose i.e. α-D-glucopyranosyl-(1→2)-β-D-fructofuranose (**Figure 1.2a**), whilst its constituent monosaccharides; glucose (**Figure 1.2b**) and especially fructose (**Figure 1.2c**) are also ubiquitous. Other common free sugars include monosaccharides galactose (**Figure 1.2d**), mannose (**Figure 1.2e**) and the disaccharides maltose (**Figure 1.2f**, α-D-glucopyranosyl-(1→4)-α-D-glucopyranose) and lactose (**Figure 1.2g**, β-D-galactopyranosyl-(1→4)-β-D-glucopyranose). All of these molecules except sucrose can also be described as 'reducing' sugars as they can tautomerise in solution through hemiacetal/hemiketal intermediates (the principal atoms involved are depicted in red and blue within **Figure 1.2**) to form acyclic isomers containing aldehydes. These aldehydes can then undergo oxidation reactions and hence act as 'reducing' agents. This is instead not possible for sucrose because it lacks the necessary hemiacetal/hemiketal moiety that is required for tautomerisation to occur.

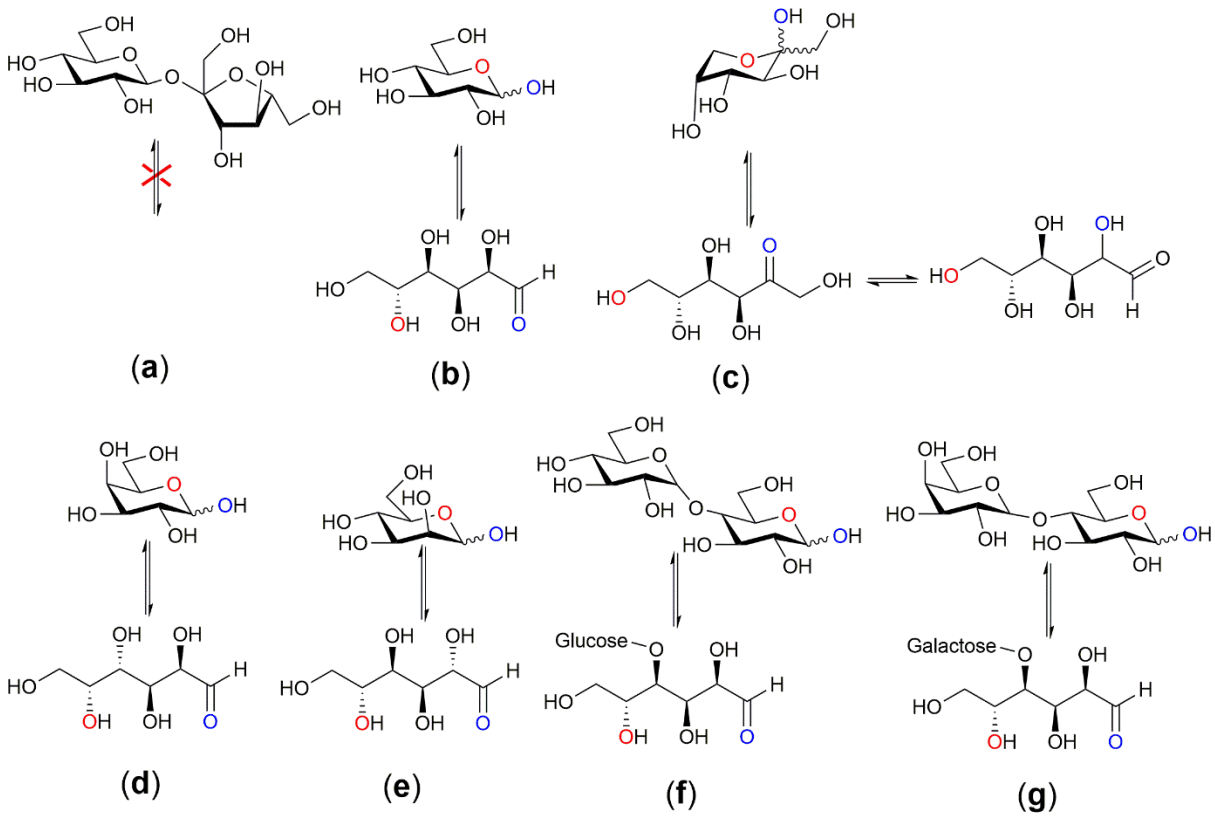

Figure 1.2: Structural formulae of the most common 'free' added sugars; (**a**) sucrose, (**b**) glucose, (**c**) fructose, (**d**) galactose, (**e**) mannose, (**f**) maltose and (**g**) lactose. Originally in colour.

In addition to providing sweetness, a key property of the aforementioned sugars is to contribute literal 'bulk' to a product by increasing density, volume and generally satiety following consumption. Importantly, within aqueous confections they also provide so-called 'humectancy' and/or 'plasticisation' and therefore act as 'humectants' and/or 'plasticisers'.[19] Neither of these terms are particularly well defined but in this context a 'humectant' refers to a substance which lowers the 'water activity' (a_w) or 'effective concentration' of water within a product, which is critical for increasing shelf-life and managing moisture migration. A 'plasticiser' contributes towards maintaining product fluidity or plasticity which essentially describes the ability of a confection to continuously and permanently deform without rupturing during the application of a force sufficient to induce flow.[20] This

coincides with a reduction of the glass transition temperature (T_g) and viscosity which have a dominant influence on sensorial properties such as softness and adhesiveness.[21]

In order to provide sufficient humectancy, large quantities of free sugars are required and it is common for them to constitute > 60 % of the total weight of a confection. Following consumption, the introduction of common sugars into the oral cavity begins a series of metabolic processes which start via initial metabolism by oral bacteria and result in the production of lactic acid and subsequent demineralisation/remineralisation (caries/calculus formation) of the teeth.[22] This development of dental caries can have a profoundly detrimental impact on quality of life, adversely affecting eating, sleeping and in severe cases even leading to the development of chronic infections.[23] After passing through the oral cavity, monosaccharides (either as consumed or formed via the digestion of disaccharides) are absorbed into the small intestine before eventually reaching the liver wherein they are ultimately metabolised into carbon dioxide and water, generating energy in the process (*ca*. 17 kJ g^{-1}).[24] Yet the exact details concerning how and the extent to which these conditions actually manifest following sugar consumption is still under considerable debate.[25]

As discussed in section **1.1**, because of their negative effects on health, there has been and still remains a strong desire to minimise the addition of free sugars into foodstuffs and beverages. In the case of confectionery, this is especially challenging because these ingredients account for the majority of the product and whilst the loss of sweetness can be somewhat mitigated through the use of alternative sweeteners or recipe alterations, neither the humectancy nor plasticisation can be controlled in the absence of sugars. This has led to the development of various alternative 'reduced-sugar' technologies, many of which will now be highlighted.

1.3. Current state-of-the-art sugar replacement strategies

1.3.1. Polyols

The current most commonly used humectants within sugar-reduced confections are polyols or sugar alcohols, which are generic terms that describe typically sweet tasting partially or completely acyclic, polyhydroxylated species that are hydrogenated derivatives of mono- and di-saccharides.[26] As they are often only partially metabolised following consumption, polyols contribute a considerably lower amount of energy than common mono- and di-saccharide sugars. For instance, sorbitol, xylitol and mannitol (**Figure 1.3a-c**) only provide *ca*. 10, 10 and 7 kJ g^{-1} respectively compared to the *ca*. 17 kJ g^{-1} of common free sugars.[27] It has been suggested that this can be largely attributed to the absence of both a reducing aldehyde group and specific glycosidic linkages between saccharide units in polyols which hinders their digestion (by stereospecific enzymes e.g. α-amylase, sucrase-isomaltase etc.) and limits absorption via the stomach and/or small intestine.[28] In addition to contributing reduced energy, they are either non, or minimally cariogenic (as little or no metabolism by bacteria via acidogenesis occurs within the oral cavity) which makes them attractive sugar replacement options and although various hypotheses have been advanced (e.g. selective inhibition of deleterious bacterial enzymes and/or protectful salivary proteins and enhanced complexation of calcium ions which promotes remineralisation), the reasons for this appear to remain poorly understood.[29] The industrial production of various polyols (via chemocatalytic hydrogenation) is now very well established and many are readily available at cheap prices, leading to widespread use within the sugar-reduced marketplace.

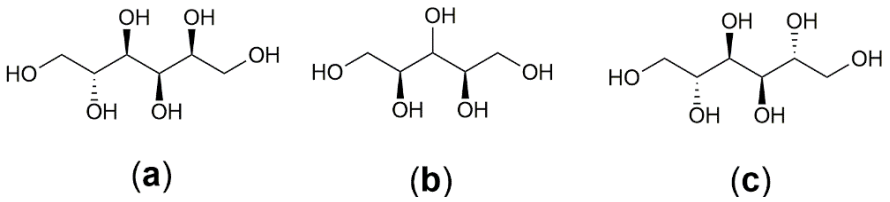

Figure 1.3: Structural formulae of; (**a**) sorbitol, (**b**) xylitol and (**c**) mannitol.

Sugar alcohols function well because they tend to have comparable solubility to most common free sugar humectants and are also similar in molecular mass (only hydrogen has been added). In addition to effective humectancy, a particularly attractive property of most polyols is their higher plasticity or lower T_g relative to their parent sugars. The fundamental mechanism for this remains unclear, although it is typically attributed to a greater degree of 'free volume' which originates from the enhanced flexibility of the aliphatic chains with respect to the more rigid, cyclic mono- and di-saccharides. Others have recently suggested that it may instead be linked to a decreased tendency to participate in *intermolecular* hydrogen bonding (as a result of increased molecular flexibility) within a condensed, hydrogen bond-dominated matrix such as an aqueous confectionery filling, although conclusive evidence for this has not yet been forthcoming.[30, 31]

Partial and slower metabolism of polyols ensures that they are less calorific with respect to normal sugars, but limited absorption in the small intestine can lead to fermentation and lowering of environmental a_w within the lumen, which subsequently draws water into it from the surrounding intestinal epithelium.[26] These phenomena result in undesirable so-called 'laxative' side-effects including bloating/flatulence, abdominal pain and irritable bowel syndrome, although only when the polyols are consumed in large amounts. Another potential issue with commercial sugar alcohols is that they are currently made via a 'synthetic' approach, leading some consumers to regard them as 'artificial' and unsafe for consumption. Although some studies have shown it is possible to extract moderate to high amounts of certain polyols from natural sources - such as mannitol from brown seaweeds (e.g. *Laminaria digitata*), this can require the use of problematic auxiliaries (e.g. HCl) and is currently uneconomical.[32]

Whilst not strictly a polyol in the same sense as those derived via hydrogenation of free sugars, glycerol (i.e. 1,2,3-propanetriol) is another aliphatic polyhydroxyl which is probably the most common

confectionery humectant/plasticiser outside of sucrose and fructose. Its popularity stems from a combination of its mildly sweet taste, extremely low glass transition temperature (- 83 ^{o}C),[30] small molecular mass and complete miscibility with water, which combine to make it a very powerful plasticiser and also potent humectant. It can be derived cheaply from natural triglycerides (for instance as by-product of biodiesel production) yet this requires extensive purification, giving it a 'synthetic' label. Another issue is that its caloric density is very comparable to free sugars although it is not cariogenic.

In any case, although common polyols have attractive humectant/plasticising properties and also potential health benefits, the applications of these materials are already well-described in the academic literature and established within industry. Therefore, they were not considered for further study within the present thesis.

1.3.2. High intensity sweeteners

In addition to polyols, perhaps the next most common approach to reducing sugar content has involved the use of so-called 'high intensity sweeteners' (HIS). Some of the most common examples of HIS, which are highlighted in **Figure 1.4,** include aspartame (**a**), stevioside (**b**), saccharin (**c**) and neotame (**d**) which have been reported to be 180 - 200, 250 - 300, 300 and *ca*. 8000 times sweeter than sucrose (as determined by human sensory panels), respectively.[33, 34] Even though some HIS actually have comparable energy values with respect to common sugars, as so few molecules are required to achieve a comparable level of sweetness, their absolute energy contribution following consumption is negligible, making them popular for use across many sugar-reduced drink and food categories, including confectionery.

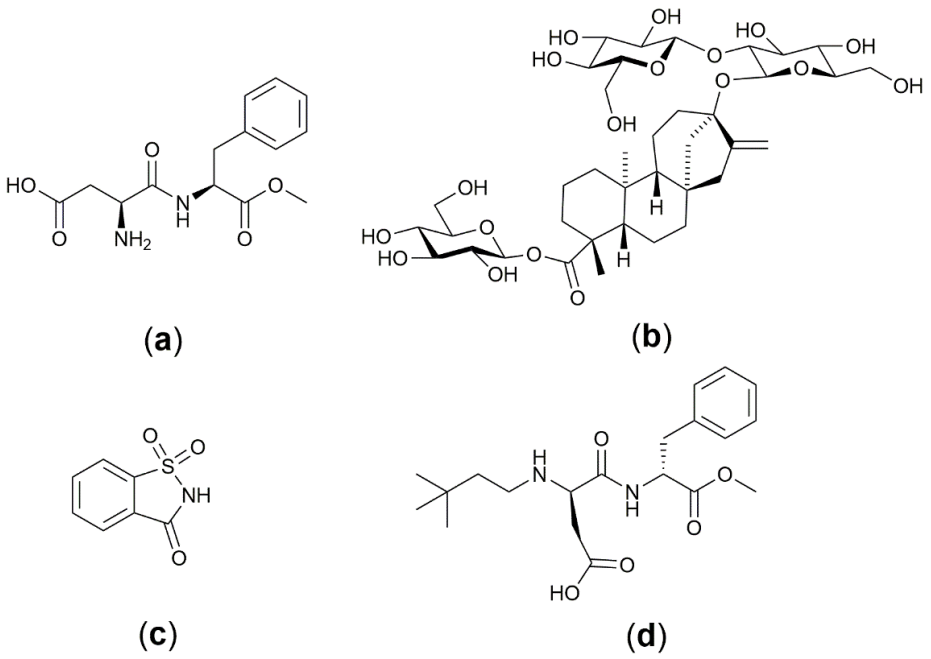

Figure 1.4: Structural formulae of several common high-intensity sweeteners; (**a**) aspartame, (**b**) stevioside, (**c**) saccharin and (**d**) neotame.

Whilst the application of HIS can be effective in products where sugar is primarily added to impart taste only (e.g. sugar-sweetened beverages), it fundamentally cannot be used as a strategy to replace the 'bulk' characteristics that are also provided through the use of sugars/derivatives - namely humectancy and plasticisation. In the case of the former, this is obvious when considering that a_w reduction proceeds predominantly via Raoult's Law, which ultimately necessitates the reduction of the mole fraction of water, x_w. Therefore, it is essential that they are combined with other low-sugar humectant and plasticisers if they are to be used in confections. Outside of these technical issues, many of the most common HIS also do not exist naturally and must be 'synthetically' produced, which is unpopular with consumers who often presume that this makes them detrimental to health. Although such concerns are unsubstantiated for most HIS, there have been persistent doubts surrounding the safety of several compounds - most infamously aspartame, whose metabolism in humans results in the formation of methanol within the gastrointestinal tract.[35]

Linked to HIS is the concept of using sweet taste 'modifying' or 'enhancing' molecules, which boost the sweetness intensity of another semi-/sweet 'bulk' or HIS ingredients thereby reducing the amount required to elicit the same sweet taste. One class of such modifiers is based on a central pyrimidine-type moiety (**Figure 1.5a** - **c**) and function by binding to and modulating the human sweet taste receptor.[36] Others include natural phenols such as phloretin (**Figure 1.5d**) which are capable of masking bitter off-tastes (e.g. from steviol glycosides) and can be extracted from apple tree bark.[37, 38] Yet in all cases there remains the same fundamental issue as with HIS in that they cannot replace the humectancy and/or plasticisation which is lost upon removal of large quantities of sugars/polyols.

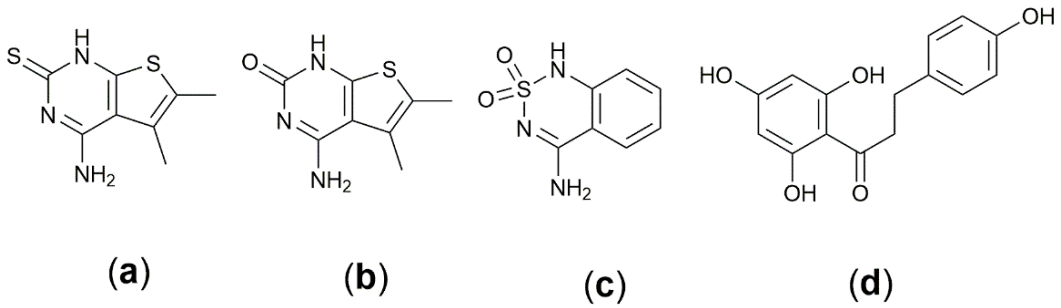

Figure 1.5: Several pyrimidine-based taste-modifying compounds (**a** - **c**) and the natural phenol phloretin (**d**).

1.3.3. Fibres

Within the context of foods and beverages, the term 'fibre' or 'dietary fibre', generally (although ambiguous) refers to non-digestible, saccharide-based oligomers or polymers that are derivatives of plant materials.[39] Fibres are typically classified according to their (relative) solubility in water, with polymers such as cellulose and hemicellulose being considered 'insoluble' and others including pectins, gums and mucilages 'soluble'. From a functional perspective, as a significant reduction in a_w requires solute dissolution, the former 'insoluble' group can be considered as being virtually osmotically inactive and thus completely unsuitable as a humectant. Similarly, even though the latter group are soluble

relative to the first, they are not particularly soluble on an absolute basis and therefore also exhibit poor a_w lowering capabilities compared to common sugars.

Other soluble dietary fibres based on smaller oligomeric and polymeric species do however, find application within confectionery such as inulin and polydextrose. Polydextrose is a generic term that describes synthetic glucose-based polymers (< 5000 g mol^{-1}) that are produced via vacuum condensation of glucose, sorbitol and citric acid.[40] Inulin are mixed oligomers constituted of β-D-fructofuranosyl-(2→1)-β-D-fructose that typically have a degree of polymerisation (*DP*) between 2 to 60 (often terminated by an end glucopyranose unit, **Figure 1.6a**) and which exist naturally within various biomasses including chicory, artichoke and asparagus.[41] This also includes 'fructooligosaccharides' or 'oligofructose' which more specifically refer to lower molecular weight inulin (2 – 10 monomers) that have become popular for use within certain reduced-sugar confectionery products.[42] In addition to fructooligosaccharides, there are various other non-digestible and so-called 'prebiotic' oligosaccharides each based on different monosaccharides e.g. galactooligosaccharides (galactose) and xylooligosaccharides (xylose) although they are generally less abundant and their use far less established than fructooligosaccharides.[43] Whilst not strictly dietary fibres as they are digested upon consumption, maltodextrins represent the current preeminent class of mixed oligosaccharides used within the food industry and already find extensive application in confectionery.[44] Maltodextrins are mixed oligomers based on α-(1→4)-linked glucopyranose (**Figure 1.6b**) that are classified according to their so-called dextrose equivalence (*DE*). This describes the amount of reducing aldehyde groups within the mixed system relative to that of D-glucose (dextrose which has a *DE* = 100 by definition) on a dry weight basis. Any mixed α-(1→4)-glucopyranose oligomers with a *DE* < 20 are classified as maltodextrins whereas those of *DE* > 20 are referred to as 'glucose syrups' which are ubiquitous within most aqueous confectionery fillings (see section **1.4**). It should be noted that non-digestible so-called 'resistant' maltodextrins produced via heat and enzymatic treatment of starch and which contain α-(1→2) and (1→3) glycosidic linkages are commonly employed as soluble dietary fibre.[45]

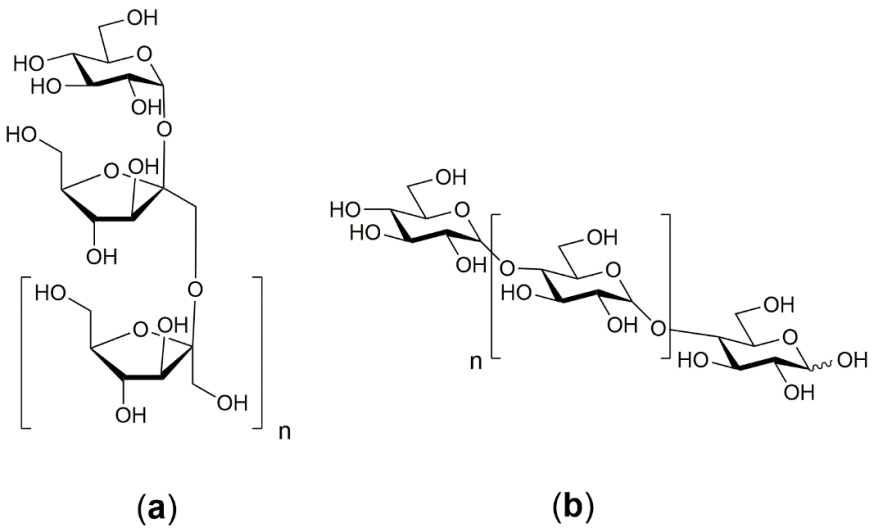

Figure 1.6: Generalised structural formulae of (**a**) inulin and (**b**) maltodextrin.

Whilst the aforementioned oligo- and poly-saccharides are very effective at increasing the T_g/viscosity and 'bulk' of a confectionery product at even low levels of addition, they are relatively ineffective at reducing a_w on a wt. % basis due to their high molecular weight (cf. Raoult's Law – see section **1.4**). This is problematic from a humectancy perspective because most fibres have only limited solubility, making it very challenging to achieve low a_w using solely fibres as 'drop-in' type sugar replacers and necessitating blending with smaller, more osmotically active solutes. Similarly, as T_g tends to be very strongly correlated with molecular weight (see section **1.4**),[46] high levels of direct substitution by even relatively small oligomers ($DP \geq 4$) will result in a confection with an unacceptably viscous or even glass texture.

1.3.4. Natural syrups

Natural sugar-containing syrups are probably the oldest confections known to human kind. Consumption of honey for instance, has been recognised for at least 4000 years and was used by various

ancient civilisations in order to preserve and increase the palatability of other foodstuffs.[47] The consumption of maple syrup, which is produced via concentration of the sap collected from the sugar maple (*Acer saccharum*), has also been documented for centuries in North America.[48] Depending on the location, the saps of many other trees such as the birch (*Betula pendula*) and oil palm (*Elaeis guineensis*) are already used or have been considered as natural humectants across virtually all parts of the world.[49, 50] Within western countries, the popularity of other natural plant-derived syrups such as sorghum (extracted from *Sorghum bicolor*) has also increased greatly in recent years and they are typically marketed as healthy alternatives to common free sugars.[51]

All of the aforementioned substances are natural, can provide sufficient humectancy and plasticity and may also bestow some other health benefits due to the presence of other trace 'bioactive' compounds. However, a fundamental issue in each case is that the vast majority ($\geq$ 95 %) of the constituent solutes are either glucose, fructose and/or sucrose and hence their application would not offer any reduction in the amount of undesirable free sugars. In several syrups including agave (*Agave tequilana/salmiana)*[52] and most notably yacon (derived from the tuber of *Smallanthus sonchifolius*), some non-negligible proportion of the solutes are instead fructooligosaccharides, which can constitute up to 50 wt. % of the total solids in the case of the latter.[53] However, there remains limited information concerning the physicochemical properties of yacon syrup (a_w and T_g) which are likely to resemble those of the large constituent oligomers at higher concentrations and may therefore, limit overall applicability due to the reasons outlined previously in section **1.3.3**.

1.3.5. Rare Sugars

The term 'rare sugars' refers to thirty-five of the total forty-two currently known monosaccharides that exist within the natural world but in amounts that are far lower than the common free sugars introduced in section **1.2.**[18] Of all the various rare sugars that exist, current commercial interest is limited to just

several particular compounds namely; D-allose, D-tagatose, D-allulose and D-sorbose. Like archetypal monosaccharides such as glucose and galactose, they are also pyranoses, differing only in the orientation of the hydroxyl groups. From a sugar-reduction perspective, the application of such species is attractive as they tend to display comparable humectancy/plasticisation to common sugars which is unsurprising given their high structural similarities. Allulose for example, has recently been shown by Wang and Hartel to act as an effective sugar-reduced plasticiser within model aqueous confectionery binders.[54] Yet rare sugars are typically only partially metabolised within the body, contributing for instance only 6 – 12 kJ g^{-1} and 0 kJ g^{-1} in the cases of tagatose and allulose, respectively compared to *ca*. 17 kJ g^{-1} for common free sugars.[18]

Although promising, perhaps the greatest current issue surrounding the use of rare sugars is their inherent lack of availability and high cost of production, which continues to improve through the development of novel technologies (namely genetically engineered enzymes) yet must be greatly further advanced before they can be brought into the mainstream market. To circumvent this issue several workers have attempted to develop of a so-called 'rare sugar' syrup via an alkaline catalysed (0.1 M NaOH) isomerisation of commercial high-fructose corn syrup, followed by subsequent treatment using a base ion exchange resin at moderate temperatures.[55, 56] Whilst this resulted in a syrup that contained approximately 6.0 and 7.5 wt. % solids allulose and sorbose/mannose, respectively which the authors claimed could be used to reduce weight. However, the vast majority (> 75 wt. solids %) of the constituent carbohydrate species were still either glucose or fructose, representing only a modest reduction in calorific free sugar content compared to the initial syrup (wherein glucose/fructose constituted ≈ 95 wt. % of the overall solids).

1.3.6. Structured sugar-reduced composites

Another recent novel solution towards sugar reduction includes Nutrition Innovation's Nucane® which involves the use of a non- or low-calorie support material such as protein or fibre that is coated with relatively unrefined sugars/derivatives to give an apparently sweet-tasting powdered product that is considerably less energy dense than neat crystalline sucrose.[57] A similar technique has been employed by the food-tech company DouxMatok, which patented a reduced-sugar alternative that comprises insoluble silica or cellulosic nanoparticles coated in soluble carbohydrates (namely sucrose).[58] The company claim that such products provide comparable sweetness sensation following dissolution of the coating sugar to that of native sugar, thus allowing the overall sugar content to be reduced on weight-by-weight basis. However, both approaches utilise supports that are either completely or significantly insoluble which makes them unsuitable for use in amorphous aqueous confectionery products as the coating would simply dissolve within the boiling syrup during product formulation. Because the insoluble component would contribute negligibly towards the reduction of a_w or T_g, there would be an insufficient degree of humectancy or plasticisation to justify the use of the aforementioned products.

Recently, Nestlé announced a related approach which involves the use of stable porous amorphous particles produced via spray drying a high-pressure mixture of sugar, bulking agent (e.g. maltodextrin) surfactant and inert gas (N_2, CO_2 etc).[59] These particles can be dispersed into media such as cocoa liquor without collapsing and the retention of the aerated structure/amorphous nature of the particle/sugar component results in a low density material which apparently elicits a sweet taste that is at least equivalent to or greater than the corresponding crystalline sugar. Again however, the porous structure would be lost via dissolution within aqueous-based confections, preventing application of this technology within the systems of interest.

A simplified comparison of relevant characteristics for each of the aforementioned sugar replacement strategies is provided in **Table 1.1** (n.b. the relative ratings have been designed to act as an approximate guide for the reader and not an exact quantification).

Table 1.1: Comparison of relevant characteristics of common free sugars and various current state-of-the-art sugar replacement strategies.

Strategy (Examples)	**Sweetness**	**Humectancy**	**Plasticisation**	**Cario-genicity**	**Calorific value**	**Example application**
'Free' sugars						
Sucrose	++	++++	+++	+++++	+++++	Various
Fructose	+++	+++++	++++	+++++	+++++	Various
Polyols						
Glycerol[A]	+	+++++	+++++	+	+++++	Binder
Sorbitol[B]	+	++++	++++	+	+++	Hard candies
Xylitol[C]	++	++++	++++	-	+++	Chewing gum
HIS						
Aspartame[D]	+++++	-	-	-	-	Tabletop Sweetener
Stevioside[D]	+++++	-	-	-	-	"
Saccharin[D]	+++++	-	-	-	-	"
Fibres						
Maltodextrins[E]	+	+	+	+++	+++++	Bulking agent
Inulins[F]	+	+	++	+	++	Chocolate
Polydextrose[G]	+	+	+	+	+	Bulking agent
Natural Syrups						
Honey[H]	++	++++	++++	+++++	+++++	Condiment
Maple[I]	++	++++	+++	+++++	+++++	Condiment
Agave[J]	+++	++++	+++	+++++	+++++	Binder
Rare sugars						
Allulose[K]	+	++++	++++	+	+	Gel candies
Tagatose[L]	++	++++	++++	+	+++	Chocolate

Trehalose[M]	+	++++	++	+	+++++	Ice cream
Structured Sugars						
DouxMatok[N]	++	+	+	+++	+++	Chocolate
Nestlé[O]	+++	+	+	+++	+++	Chocolate

+++++ = Highest (relative) rating, + = Lowest (relative) rating, - = Not applicable, References: A: Nakagawa and Oyama,[60] B: Lenhart and Chey,[26] C: Ur-Rehman *et al*.,[61] D: Chattopadhyay *et al*.,[33] E: Roos and Karel,[62] F: Mensink *et al*.,[63] G: Ribeiro *et al*.,[64] H: Lazaridou *et al*.,[65] I: Bhatta *et al*.,[66] J: Willems and Low,[52] K: Mu *et al*.,[67] L: Roy *et al*.,[68] M: Roe and Labuza,[69] N: US8911806B2,[58] O: WO2017093309A1.[59]

1.4. Thesis Aims

The global aim of this thesis is to investigate and ultimately evaluate the performance of innovative solutions towards sugar-reduction within model aqueous confectionery fillings, which can be sub-divided into four sections covering both theoretical and practical aspects and are outlined through Aims 1 to 4. **Thesis hypothesis**: The main hypothesis of this thesis is that the humectant and plasticising properties of common 'free' sugars used in aqueous confectionery systems (e.g. syrup binders, caramels) could be effectively replaced by nature-inspired, 'drop-in' alternatives including natural small organic osmolytes and low melting, food-grade eutectic mixtures.

- ***Aim 1****: To investigate the molecular basis of 'water activity' within aqueous binary solutions containing both common (sugars/polyols) and non-traditional natural humectants (such as* N-*methyl glycines) (**Chapter 3**). The impetus for this investigation is a result of confusion within the literature as to what the molecular basis for water activity actually is and thus, what causes some humectants to perform better than others. This will be achieved via application of the statistical Kirkwood-Buff theory of solutions which is able to quantify the various interactions*

*that take place within solution, thus providing a clearer interpretation of what drives water activity at the fundamental level (see **Chapter 3**). In particular the specific aims are:*

(i) Can the water activity of solutions containing sugars and polyols be rationalised through the KB theory?

(ii) If so, can this rationalisation indicate which (if any) of the current theories concerning a_w are correct?

(iii) Is it also possible to understand the humectancy of several natural osmolytes containing unusual and even counterintuitive molecular features?

The term 'activity' was first introduced as a thermodynamic descriptor of a chemical species by Lewis over a century ago,[70] to describe the "escaping tendency" or "fugacity" of a substance with respect to its concentration, although it is more intuitive to consider it as an 'effective concentration'. The activity of water like any other species, is equal to the ratio of its fugacity in solution and its fugacity at an arbitrary standard state (at thermodynamic equilibrium and constant temperature).[71] If the water vapour escaping from solution behaves as an ideal gas (well approximated at ambient temperatures) then the water activity, a_w is equivalent to the partial vapour pressure of water in equilibrium with either its solution p_w or pure liquid water p_w° respectively (**Equation 1.1**):

$$a_w = \frac{p_w}{p_w^\circ} \qquad \textbf{Equation 1.1}$$

Equation 1.1 is often able to give a good representation of the true a_w and it has become the *de facto* definition for "water activity". As such, the most common methods of a_w measurement typically involve quantifying the water vapour pressure above an analyte.[72] a_w is directly related to the equilibrium relative humidity (ERH) of a system through **Equation 1.2**:

$$ERH = 100\, a_w \qquad \textbf{Equation 1.2}$$

In a so-called 'ideal' solution, the vapour pressure of water in solution is equal to the product of vapour pressure of pure water and its mole fraction, x_w (again at equilibrium and constant temperature/external pressure) as defined by Raoult's Law (**Equation 1.3**):[73]

$$p_w = x_w\, p_w^{\circ} \qquad \textbf{Equation 1.3}$$

The existence of the molar term here gives rise to what is commonly described as the 'colligative effect', where the reduction of water vapour pressure (and other related properties) in solution is principally governed by the *number* of solute molecules rather than their identity. Therefore, most of the commonly employed 'humectants' or a_w suppressing additives tend to be relatively small, highly soluble molecules and also electrolytes that can dissociate into multiple ions within solution, namely salts (e.g. NaCl and KCl). A particularly important early treatment of this phenomenon was made by van't Hoff, who introduced a now familiar formula that linked the number of discrete solute entities formed following dissolution (the van't Hoff 'factor', i) to the osmotic pressure of a solution through the following equation (**Equation 1.4**):[74]

$$\pi = \text{iMRT} \qquad \textbf{Equation 1.4}$$

Where M, R and T correspond to the; solution molarity, universal gas constant and absolute temperature, respectively. π represents the osmotic pressure, defined as the pressure that must be applied to a solution separated from pure solvent by a semipermeable membrane in order to prevent the pure solvent from flowing into it. Note that for virtually all confectionery ingredients, i is taken to be 1. This is related to a_w (in aqueous solutions) via **Equation 1.5** (where V_w is the molar volume of water, 18.1 $cm^3\ mol^{-1}$):

$$a_w = e^{\left(-\frac{\pi V_w}{RT}\right)}$$ **Equation 1.5**

In reality, few solutions and particularly those encountered in confectionery behave ideally and there is deviation from **Equation 1.3** which can either be 'negative' or 'positive', i.e. there is a more or less pronounced reduction in vapour pressure (activity) than would otherwise have been predicted. The extent of this non-ideal behaviour depends principally on the size/structure of the dissolved solute/s and is represented through a coefficient term; the water activity coefficient, γ_w which is used to calculate a_w through **Equation 1.6**:

$$a_w = \gamma_w x_w$$ **Equation 1.6**

For an ideal solution γ_w = 1 but in non-ideal cases it can theoretically take any value above 0 and is often found to be 0.6 – 1.1 for most food-related solutes. Because of the large size disparity between water and virtually any added solute, x_w will always remain relatively high (> 0.5) and so significant lowering of a_w can only be realised when both terms on the right-hand side (r.h.s.) of **Equation 1.6** are reduced concomitantly. This is exemplified when using sugars to reduce a_w as there is often a balancing act between the utility of mono- and di-saccharides with the former offering more significant reduction through lowering x_w (smaller mass) whilst the latter can reduce y_w to a greater extent.

In food science, the concept of water activity was popularised by Scott, who first described it as a representation of the "availability" of water in food articles.[75] By this point, ERH had already been recognised as being useful descriptive property of a food and particularly as a predictor of microbiological safety for which, it was far superior than simple water content.[76] It is now generally accepted that most bacteria struggle to proliferate at $a_w \leq 0.85$ and all other microorganisms by *ca*. 0.60

(at ambient temperatures).[77] Given that most confections are expected to typically last for one year once produced, lowering the a_w to levels that prevent microbial growth is of critical importance.

Within composite confectionery products, relatively dry and crisp components (a_w < 0.6, < 10 wt. % water) including wafers, biscuits and cereals are typically combined with water-based fillings such as a syrup binder or caramel that may contain up to 20 wt. % water depending on the application.[78] In the absence of sufficient humectant dissolution into the aqueous component, moisture will naturally tend to migrate from it into the dry component until the a_w of both components are equivalent.[79] The additional moisture in the initially crisp constituent will almost certainly result in a change of texture, and typically towards something that is softer and often described as 'soggy' or 'leathery' which is unacceptable from a quality control perspective.[80] Because water acts a potent plasticiser that can significantly influence product fluidity, a_w can often be directly correlated to other important sensorial properties that rely on mass transfer, such as aroma.[81] Additionally, it has also been shown to have a notable impact on the chemical and biological reactivity of food articles (Maillard reaction kinetics, lipid oxidation, hydrolytic reactions, non-enzymatic browning etc.), as summarised in **Figure 1.7**.[80]

As mentioned previously, the most effective way to reduce a_w is to effectively 'dilute' (decrease x_w) the water via use addition of a solute/s. In the preparation of aqueous confections, this is primarily achieved via the dissolution of sugars and/or their derivatives in order to create a supersaturated 'solution' that is typically *ca*. 80 – 95 wt. % solids. The preparation of such a solution generally proceeds via progressive removal of water by boiling the mixture at elevated temperatures (*ca*. 105 – 155 °C) and often under reduced pressure. Boiling point elevation is inversely related to a_w (by definition, due to reduction in p_w as x_w decreases) and water content and an accurate knowledge of their relationship with the so-called 'cook temperature' (i.e. final boiling point) is crucial for ensuring product quality, safety and reproducibility.[19]

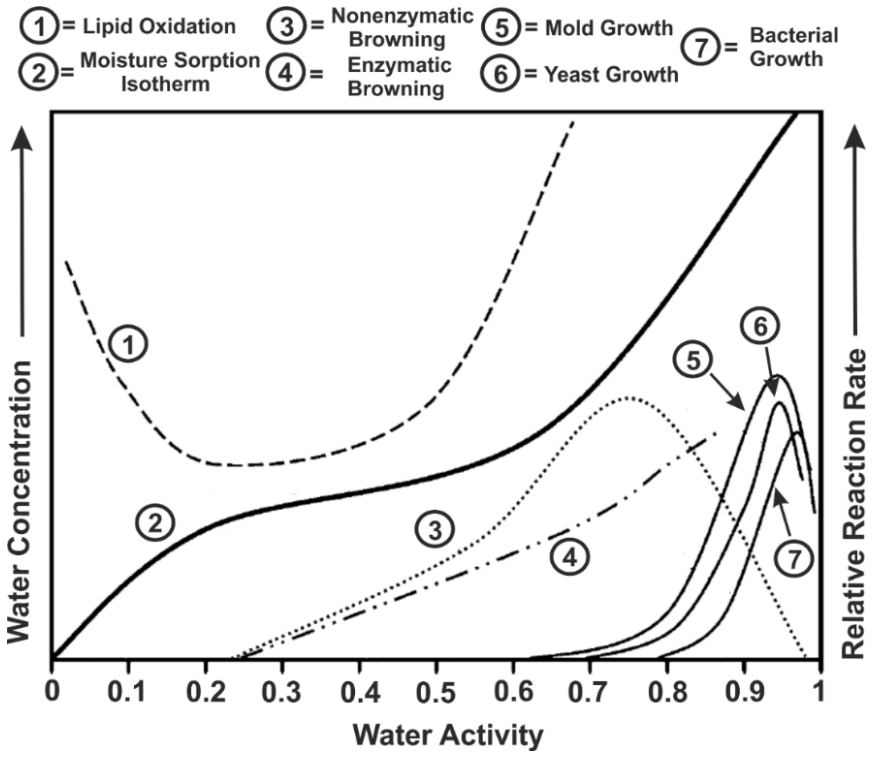

Figure 1.7: Influence of water activity on various food-related phenomena. Adapted from Labuza.[80] Arrows indicate directions of increases properties.

A large amount of research has focussed on the development of predictive models for confectionery ERH/a_w, starting with Grover (1947)[82] and subsequently Money and Born (1951),[83] who each utilised empirically determined constants for common confectionery ingredients. However, these approaches drew criticism for lacking a thermodynamic basis and sometimes giving illogical results,[84] which fuelled the development of various later more rigorous predictive models using empirical or semi-empirical approaches. Due to the sheer number and general similarity of many of the models that exist within the literature, only the most widely applied examples - namely the Norrish and the Ross equations will be discussed in any detail here. For more comprehensive summaries of other models, the reader is directed towards reviews on the subject by Lewicki or Sereno *et al*.[85, 86]

In the mid-1960s, Norrish demonstrated that a semi-empirical equation (**Equation 1.7**), based on thermodynamic principles could be used to predict the water activity of binary solutions containing small non-electrolyte species such as sugars:[87]

$$a_w = x_w e^{K_N x_s^2} \qquad \textbf{Equation 1.7}$$

Where x_s represents the mole fraction of solute and K_N is a constant, the so-called 'Norrish constant' which is obtained from empirical a_w measurements and is closely related to y_w through **Equation 1.8**:

$$y_w = e^{K_N x_s^2} \qquad \textbf{Equation 1.8}$$

K_N can be determined via linearising **Equation 1.8** through a plot of ln y_w vs. x_s^2 as the value of the slope which passes through the origin. This method has been used to calculate K_N for many of the common food humectants, where $K_N \approx -2$ to -7 or *ca*. -1 for sugars or polyols respectively (at least in the form that is given in **Equation 1.8**). Using just a single value of K_N, the Norrish equation has been reported by many to provide an accurate prediction of a_w in solutions comprising a wide range of different solutes up to and in some cases, even well past the solubility limit (at *ca*. 25 °C). Although the number of publications is too many to fully summarise, particularly relevant examples include the works of for instance; Chrife *et al*. (polyols),[88] Baeza *et al*. (sugars and polyols)[89] and Fyusn *et al.* (sorbitol, glycerol).[90]

Whilst the Norrish equation is only used for predicting the a_w of binary solutions containing one solute, aqueous multisolute systems are often treated using the Ross equation (**Equation 1.9**).[91] This simply states that the water activity of the mixed solution ($a_{w,mix}$) is equal to the product of the solution a_w measured for the binary solutions of each component *i*, $a_{w,i}$ (where $i = 1, 2 \ldots \infty$) at the concentration in which they are present within the mixed solution:

$$a_{w,mix} = a_{w,1}a_{w,2} \dots a_{w,i}$$ **Equation 1.9**

Because of its simplicity, the Ross equation has been found to give reasonably accurate predictions of a_w in multicomponent solutions containing sugars. Mauer and co-workers for instance have reported that it can be used to estimate the water activity of saturated solutions of glucose and fructose, sucrose and glucose and sucrose, glucose and fructose within $\pm$ 0.01, 0.02 and 0.05 a_w respectively.[92] Over the years, various authors have attempted to offer modifications in the hope of improving accuracy, yet the addition of extra semi-/empirical constants has rarely produced noticeably better results whilst greatly increasing complexity for the user.

Although it can generally be well predicted, the molecular basis for what gives rise to a_w in aqueous confectionery solutions is still poorly understood, as evidenced by the existence of multiple and sometimes contradictory hypotheses that exist within the literature. A greater comprehension of water activity appears necessary for improving our understanding of how current humectants function and could provide some further insights that may also aid in the rational selection of new sugar-replacers. As such, this aspect has been investigated in greater detail within **Chapter 3**.

- ***Aim 2****: To investigate the humectant and plasticising properties of the natural osmolytes 2-O-α-D-glucopyranosyl glycerol (glycoin,* ***Aim 2a****) and 2-O-α-D-galactopyranosyl glycerol (floridoside,* ***Aim 2b****) in order to assess suitability as sugar replacements within a model aqueous confectionery filling. In the case of glycoin, which is already produced commercially under the tradename Glycoin® natural, this will specifically involve (see* ***Chapter 4****):*

  (2ai) *Characterisation of the received Glycoin® natural in order to confirm the presence/quantity of glycoin.*

*(**2aii**) Investigating the humectancy (*a_w*) and plasticity (*T_g*) of glycoin and its aqueous solutions as a function of solute concentration and subsequent comparison against current archetypal confectionery solutes (sucrose, fructose etc).*

*For floridoside, which is not commercially available but naturally bioaccumulated within abundant and renewable macroalgal biomass, the specific aims are (see **Chapter 5**):*

*(**2bi**) To establish a 'clean' and food-grade route for extracting high purity floridoside from natural macroalgae (*Palmaria palmata*).*

*(**2bii**) To investigate the relevant physicochemical properties (*a_w *and* T_g*) of floridoside extracted according to **Aim 2b(i)** and compare these against current archetypal confectionery solutes (sucrose, fructose).*

Organisms from all three domains of cellular life produce a plethora of compounds in order to combat the stresses of their environments. Elevated external osmotic pressure or reduced a_w (also referred to as hypertonicity or hyperosmolarity) is a prominent example of such a stress and its control (i.e. osmoregulation) plays an important role in homeostasis across many eukarya, bacteria and archaea.[93] Typically resulting from exposure to saline environments that contain high concentrations of dissociating salts, if osmotic stress is not properly alleviated then it can result in potentially deleterious phenomena, namely cell shrinkage and ultimately cell death.[94] One of the most efficient mitigative strategies is the intercellular accumulation of water-soluble, organic species and/or (to a lesser degree) inorganic salts.[95] Of the former group, which are commonly termed 'osmolytes' and number over 100 examples,[96] several major molecular classes appear to be ubiquitous including; carbohydrates, amino acids, methylamines, methylsulfoniums and many of their derivatives (**Figure 1.8**).[97] Such solutes are often then further defined (sometimes misleadingly) as being 'compatible' or 'perturbing' depending on whether they facilitate or disrupt the function of essential intercellular machinery (protein, membranes etc).[98]

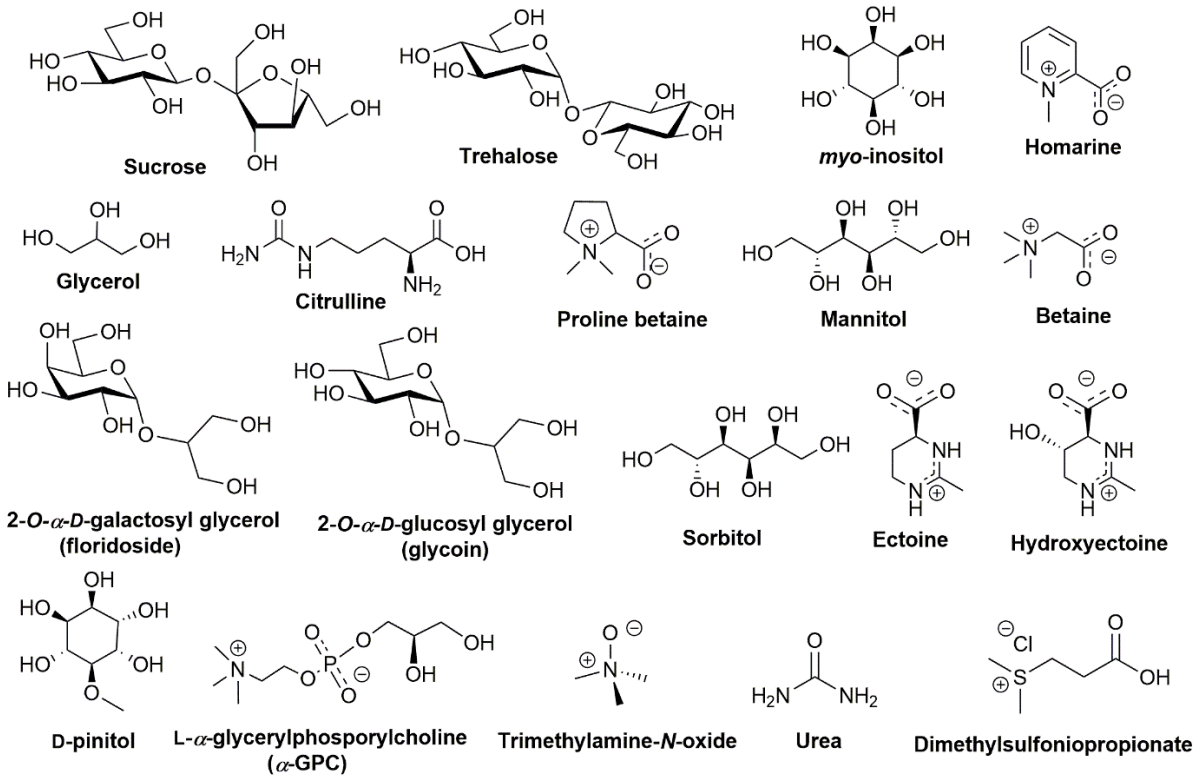

Figure 1.8: A selection of the most common naturally-occurring 'osmolytes'.

From the perspective of this thesis, it is interesting to note how many of these osmolytes or structurally similar analogues already find use within the food industry, particularly mono- (e.g. fructose, glucose) or di-saccharides (trehalose, sucrose) in addition to aliphatic polyols (mannitol, sorbitol and glycerol). Their utilisation as humectants in foodstuffs is perhaps not surprising given that one of their main roles is *in-vivo* reduction of a_w and therefore essentially function as intracellular humectants. Their ability to effectively lower a_w can in large part, be attributed to a combination of high solubility and relatively low molecular mass given that it is most effectively reduced through minimising x_w (cf. Raoult's law). Their small size is also attractive from a plasticisation perspective as T_g tends to exhibit a strong positive correlation with molecular weight, whilst the presence of multiple 'polar' groups within most of the compounds should intuitively afford sufficient compatibility with the matrices that constitute aqueous confections (namely aqueous oligo-/poly-saccharides).

Considering these desirable physicochemical properties and the precedent for using such solutes in foodstuffs, it appears as though the area of natural osmolytes might prove fruitful in the search for novel, replacement humectants and plasticisers for common free sugars. However, outside of the application of the traditional aforementioned solutes, there appears to have been only limited exploration of this concept within the confectionery and wider food industry to the best of this author's knowledge. In the 1980s, Chirife and co-workers evaluated the a_w lowering capacities of various amino acids (lysine, ornithine, proline etc.) and polyol osmolytes (D- and L-arabitol, glycerol) which could be well described via the Norrish equation with appropriate values of K_N.[88, 99] In later reviews by prominent aficionados including Slade *et al*. and Aguilera and Karel, the potential application of compatible solutes within food-relevant technologies was highlighted yet apparently unable to catalyse any interest in the use of neoteric osmolytes within food and particularly confectionery systems.[100, 101]

Aside from the aforementioned preeminent polyhydroxy humectants that already find extensive utilisation (glucose, sucrose, trehalose, sorbitol etc.), there are many nitrogen-containing osmolytes (commonly referred to as *N*-osmolytes) most of which, contain an α-*N*-carboxylate moiety and exist as zwitterions. Proline is the most ubiquitous of such solutes and is a well-known flavour ingredient in the food and beverage industries,[102] however its application in certain products such as confectionery is limited by its propensity to undergo significant (and potentially undesirable) Maillard browning reactions with reducing sugars. L-citrulline can be found naturally in watermelon but would presumably encounter a similar problem and is also limited by its relatively low solubility.[103] Proline betaine (stachydrine) is present within various natural foodstuffs and particularly citrus juice (< 1.1 g L^{-1}),[104] yet its use appears to be currently restricted by a lack of availability. On the other hand, urea is already a commodity chemical and a known ingredient in some chewing gums.[105] However, it is unlikely to be popular with consumers given its obvious link to urine, with recent studies also indicating that it may exhibit in-/direct toxicity both *in vivo* and *in vitro*.[106] Similarly, trimethylamine-*N*-oxide has recently

been linked (albeit not definitively) to several serious maladies including insulin resistance, cardiovascular disease and cancer which suggests that it is likely to be unsuitable for human consumption.[107, 108]

There are however, some structurally unusual *N*-osmolytes which could make for promising humectants/plasticisers, namely ectoine, hydroxyectoine, betaine and L-α-glycrophosphorylcholine (α-GPC). Ectoine and hydroxyectoine are widely accumulated within various species of halophilic bacteria and their ability to act as effective humectants has already generated significant interest in the cosmetic sector.[109]Notably, the former has also been applied within medicinal products designed for direct human consumption (e.g. throat and nasal medications),[110] detected naturally in some cheeses,[111] and has recently been implicated as a functional food ingredient for enhancing the probiotic profile of yoghurt.[112] However, cost of production (which currently proceeds via bacterial milking)[113] is still prohibitively high for large-scale industrial usage and there remains a lack of clarity surrounding its safety for human consumption in significant quantities (gram scale). Betaine (betaine glycine or trimethylglycine) can be obtained as a by-product of the molasses produced from the widely cultivated *Beta vulgaris altissima* (sugar beet) via relatively simple filtration/chromatographic treatment and within which it often constitutes up to 1.5 wt. % dry mass.[114] Notably, it has already been patented for use in the confectionery sector as a crystallisation inhibitor and a general humectant for use within foods and nutritional products.[115, 116] α-GPC is considered safe for human consumption (apparently even up to 1.2 g day^{-1})[117, 118] whilst also being potentially derivable from natural sources including soybean lecithin and via wheat fermentation,[119, 120] making it a promising future target from a 'clean-label' functional food perspective. It is perhaps surprising that α-GPC along with betaine, ectoine and hydroxyectoine are amongst the most ubiquitous natural osmolytes given that the molecular structures are very dissimilar with respect to traditional anthropocentric humectants such as sugars and polyols. This is especially true of α-GPC and betaine which both contain counterintuitive 'hydrophobic'

trimethylammonium groups, yet the reasons for their potent humectancy remains poorly understood and will be subsequently explored in greater detail within **Chapter 3.3**.

An interesting and currently understudied class of osmolytes, particularly with respect to their potential utilisation in food are non-saccharide aglycone glycosides, i.e. those containing a glycosidic linkage to a non-sugar species. Some 'synthetic' examples including lactitol (4-*O*-α-D-galactopyranosyl-D-sorbitol, **Figure 1.9a**), maltitol (4-*O*-α-D-glucopyranosyl-D-sorbitol, **Figure 1.9b**) and isomalt (a mixture of 1-*O*-α-D-glucopyranosyl-D-mannitol (**Figure 1.9c i**) and 6-*O*-α-D-glucopyranosyl-D-sorbitol (**Figure 1.9c ii**) derived from lactose, maltose, sucrose respectively are already popular 'sugar free' humectants/plasticisers on account of their limited digestibility and non-carcinogenicity.[121] However, because they do not exist in nature, they are often considered to be 'unnatural' and excessive consumption can lead to laxative effects. The aforementioned solutes are anticipated to have display broadly comparable a_w lowering capabilities with respect to those of their parent disaccharides as the humectancy of structurally similar solutes is primarily dependent on the size and far less on the spatial distribution of individual functional groups (see **Chapter 3**). As highlighted in **1.3.1.** aliphatic polyhydroxy species tend to exhibit lower T_g values then analogous cyclic mono- or di-saccharides of the same molecular weight which is also true of lactitol (*ca*. 40 ºC for lactitol monohydrate) versus *ca*. 110 ºC for lactose)[122] and maltitol (*ca*. 40 ºC versus *ca*. 90 ºC for maltose)[123] and makes them well suited as confectioner plasticisers.

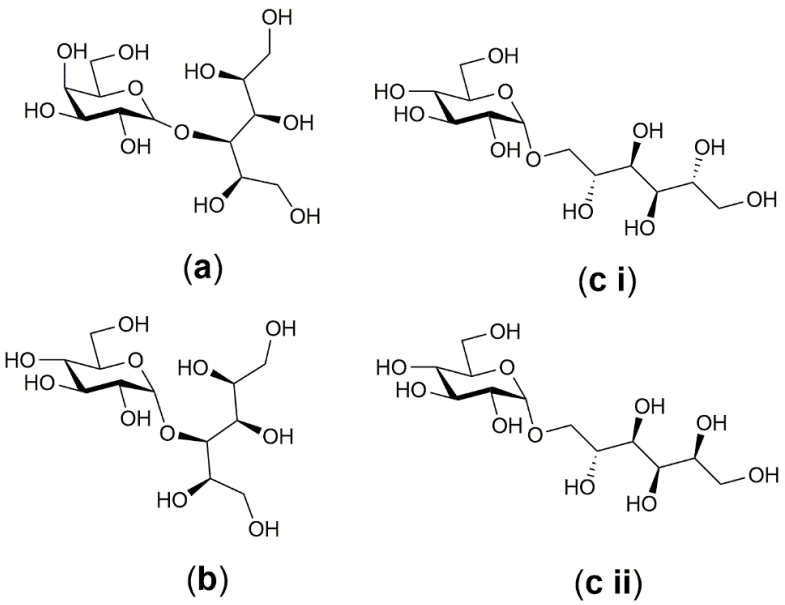

Figure 1.9: Structural formulae of commercial polyol glycosides; (**a**) lactitol, (**b**) maltitol and (**c**) isomalt (**i** = 1-*O*-α-D-glucopyranosyl-D-mannitol, **ii** = 6-*O*-α-D-glucopyranosyl-D-sorbitol).

It is hypothesised that the same should therefore also be true for structurally similar natural glycosides that contain aliphatic polyhydroxy aglycone functionalities. The two preeminent members of this class are 2-*O*-α-D-glucopyranosyl glycerol (glycoin) and 2-*O*-α-D-galactopyranosyl glycerol (floridoside), in which either α-glucopyranose or α-galactopyranose forms a glycosidic bond with the secondary hydroxyl of a glycerol molecule (**Figure 1.8**). Glycoin is a primary osmolyte of various moderately halotolerant cyanobacteria whereas floridoside is accumulated by most of the *Rhodophyta* (red macroalgae).[124,125] Both have already received some attention as natural and functional food ingredients and as food or cosmetic 'humectants', are potentially already available at scale with reportedly low digestibilities, a lack of cariogenicity and sweet or neutral tastes.[126, 127] Indeed, glycoin is produced commercially by the German company bitop AG under the tradename Glycoin® natural whereas floridoside can often constitute a significant proportion (up to 25 dry wt. %) of certain *Rhodophyta*, with some members of this phylum already being harvested at over the one million-ton (wet basis) scale.[128-130]

Yet there appear to be no published details concerning the a_w lowering or plasticisation properties of glycoin or floridoside or their utilisation within confectionery products to the best of this author's knowledge. Due to their small size and high structural similarity with respect to common free sugars, it is anticipated that both glycoin and floridoside could be effective natural humectants/plasticisers within aqueous confections yet this must first be confirmed via rigorous experimental characterisation before any further evaluations can take place. Therefore, one of the main goals of this research was to undertake detailed physicochemical characterisation of both glycoin and floridoside, the results of which have been presented in **Chapters 4** and **5** respectively.

- ***Aim 3****: To develop and characterise a nature-inspired and 'proof-of-concept' food-grade, eutectic mixture for application as a potential sugar-reduced humectant and plasticiser within a model aqueous confectionery filling (see* ***Chapter 6****). More specifically this will involve:*
  (i) Initial screening of a variety of mixtures constituted of food-grade components in order to assess their potential to form stable eutectic melts that can meet a sugar-reduced mandate.
  (ii) Characterisation of any leading candidate eutectic mixtures resulting from Aim 3(i) in order to appraise suitability for application as potential replacement humectants/plasticisers within a low-sugar, model confectionery system.

Eutectic melting in solid mixtures describes the phenomenon of melting point depression of the mixture with respect to the melting points of any of its constituents (in pure form) and has been known for many years. Within the simplest of such systems, which consists of an intimately mixed binary blend of two components (at constant pressure) that are immiscible in the solid phase but miscible in the liquid phase, there is a minimal temperature at which eutectic melting occurs, termed the solidus or eutectic temperature.[131] At a specific, system-dependent composition the solid mixture will completely liquefy once it reaches the solidus, corresponding to the so-called eutectic point. For all other compositions, the formation of a fully liquified melt occurs at a temperature higher than the solidus, referred to as the

liquidus, which increases towards the fusion temperature of an individual constituent as the mixture becomes increasing enriched with it. A graphical summary of these phenomena is presented in **Figure 1.10**. Within the area of green chemistry, the interest in the study of eutectic mixtures has increased exponentially over the past twenty years or so owing to the seminal contribution of Abbott and co-workers, who introduced the concept of 'deep eutectic solvents' (DES).[132] These 'solvents' could be formed via simple blending of quaternary ammonium salts with various amides (most notably urea) and were shown to yield mixtures that were capable of liquifying at around room temperature despite the fact their native components melted at > 100 °C and thus, appeared to represent a 'deep' eutectic melting point depression (dashed lines, **Figure 1.10**).[133]

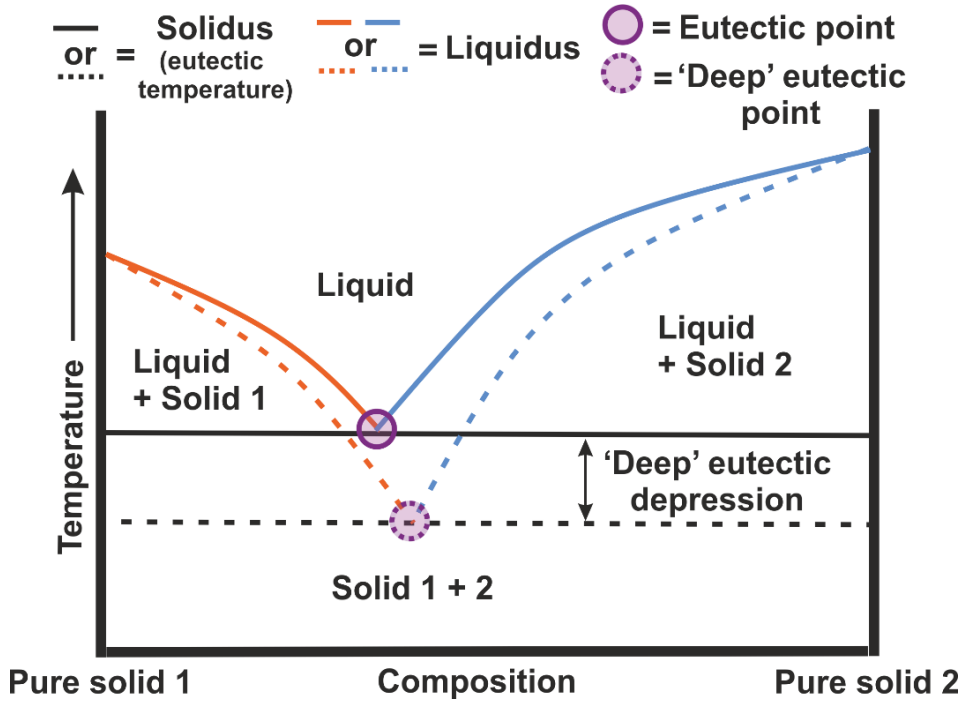

Figure 1.10: Graphical schematic of a simple binary eutectic mixture comprising hypothetical solids 1 and 2. Arrow indicates direction of increasing temperature. Originally in colour.

Following the work of Abbott *et al.*, DES are now considered to be amongst the most promising 'green' technologies and hundreds of different eutectic mixtures now been documented within the literature.[134] Most are based on mixtures of naturally-occurring including sugars, sugar alcohols, natural quaternary ammonium salts, organic acids, amino acids of which many also fall into the classification of 'osmolytes' that were highlighted previously.[135, 136] Whilst the properties of specific DES are naturally highly dependent on the individual components that constitute them, they tend to broadly share some attractive physiochemical characteristics including *inter alia* minimal vapour pressure, lack of toxicity, biodegradability, facile preparation, broad polarity range, good thermal stability and excellent solubilising capabilities.[137, 138] These properties have facilitated successful application of DES within various fields such as organic synthesis, biomass pre-treatment, CO_2 capture and biocatalysis amongst many others.[139-142] DES can be broadly classified into five types depending on their constituents; (i) metal chloride plus quaternary ammonium salt, (ii) metal chloride plus quaternary ammonium salt hydrate, (iii) general hydrogen bond donor plus quaternary ammonium salt, (iv) hydrogen bond donor plus metal chloride hydrate and (v) non-ionic mixtures based on weak and strong hydrogen bond donors/acceptors.[143]

Although the exact mechanisms that underpin the formation of DES are still under debate and vary depending on the constituents that are present, an underlying assumption is that the formation of the interactions which manifest within mixed liquid melt must be more favourable overall than those which exist within the native solids. Currently there appears to be confusion in the literature as to what constitutes a 'deep' eutectic mixture, with some authors suggesting that it the term should simply describe systems that exhibit melting points below those of their constituents and if these are around or below room temperature.[137] However, this definition has been criticised because it encompasses virtually every mixture, including binary aqueous solutions containing water and any solute.[144] This has led to some to invoke the term 'low transition temperature mixtures' to describe such systems,[145] but for sake of consistency the terms 'DES' or 'eutectic mixture' will be used herein.

Notably, many eutectic mixtures can be formed using naturally-occurring food ingredients such as sugars and polyols which are often referred to as 'natural deep eutectic solvents' (NADES). The concept of NADES was introduced by Choi *et al*. who speculated that specific mixtures of natural plant metabolites, namely sugars, amino acids, choline and organic acids and water may form *in-situ* intracellular eutectics on account of their inexplicably high *in-vivo* concentrations.[146] It has been hypothesised that such media could play a role in for instance; the cryoprotection, biosynthesis/solubilisation of poorly water-soluble compounds and the stabilisation of proteins within various organisms.[147, 148] Owing to the fact that many such NADES are formed from edible components, one of their most promising areas for application is the food sector. Various studies have proven the utility of NADES as extractants for natural food additives and nutraceuticals including flavonoids,[149] phenolics and terpenoids.[150, 151]

Most interesting from the perspective of this thesis is that many of the food-grade eutectic mixtures appear to display an attractive combination of potent humectancy and strong plasticisation. Indeed, many DES are found to vitrify upon cooling and exhibit very low T_g values (often < - 40 ^oC) in addition to minimal a_w (< 0.2) due mainly to fact that only a small amount of (if any) water is required to achieve liquefaction.[152] Previous studies have indicated that many of the eutectic 'networks' or 'structures' which give rise to the augmented properties of DES, are reasonably resilient to water addition and can persist following even significant dilution (> 40 wt. %).[153-155] In this way, the sequestration of water within the eutectic phase appears to be an effective strategy for maintaining a low a_w,[147] and could also hypothetically remain operative within most aqueous confectionery matrices (syrup-based binders, caramels etc.) which typically contain moderate amounts of water (< 20 wt. %).

Given their inherently low T_g, is not surprising that DES have becoming increasingly utilised as plasticisers for a variety of different biopolymers; most typically starch[156, 157] but also chitosan,[158]

cellulose acetate[159] and agarose for instance.[160] As discussed briefly in section **1.3.3**, saccharide-based oligomers and especially those based on α-(1→4)-linked glucopyranose (i.e. glucose syrups) are the main ingredients within virtually all aqueous confectionery fillings. Given their high degree of structural similarity with respect to polymeric starch (they are essentially highly concentrated aqueous mixtures of partial starch hydrolysates), it is hypothesised that DES could also act as effective plasticisers of confectionery matrices based on glucose syrups. However, very few studies have actually explored the use of eutectic systems as food additives, with only one patent describing the use of "eutectic flavour systems" comprising mixtures of food-grade carbohydrates, sugar alcohols, acids, non-aqueous solvents and/or salts with minimal levels of water addition for delivery of active ingredients (namely flavour compounds) into food or beverage products.[161] Another somewhat related patent has described their use as solvent/direct precursors to food flavours.[162]

A recent study has developed a NADES based on glycerol and choline chloride which is designed to act as a direct oral delivery system for the bioactive curcumin.[163] Some authors have also advocated that NADES themselves could serve as ingredients for "desserts" or even as being "drinkable".[135, 164-166] It is interesting to note that a very recent article has invoked the concept of using NADES as food plasticisers and a sugar replacement strategy.[167] However, the authors only examined the properties of several aqueous amino acids (glycine, proline) and their influence on some food-related (starch gelatinisation, protein denaturation, biopolymer melting etc.) phenomena although they did not investigate glucose syrup-based models or even the application of any NADES themselves. Thus, there is an outstanding question regarding whether food-grade eutectic mixtures could be successfully applied as neoteric, nature-inspired humectants/plasticisers for use within an aqueous glucose syrup-based confectionery system. In particular, it is hypothesised that the formation of a highly plastic (i.e. very low T_g) molten eutectic phase which is also capable of effectively sequestering water should be able to act as an effective functional replacement for sugar within a hydrophilic, oligosaccharide-based matrix

which, in the opinion of this author merits further investigation, the results of which have been presented in **Chapter 6**.

- ***Aim 4****: To evaluate the performance of the novel humectants/plasticisers developed as part of Aims 2 and 3 alongside archetypal confectionery humectants within a model aqueous confectionery system based on a low 'added' sugar glucose syrup (see* ***Chapter 7****). More specifically, this will involve:*

  (i) Preliminary analysis of the as-received glucose syrup in order to confirm low 'added' sugar composition.

  (ii) Preparation of model confections based on said low-sugar glucose syrup and added neoteric humectants/plasticisers developed earlier within the thesis (glycoin, floridoside and a novel food-grade 'deep' eutectic mixture) or archetypal confectionery solutes (fructose and glycerol).

  (iii) Evaluation of additive influence on key physicochemical properties (a_w*,* T_g *and viscosity) of the model aqueous confections prepared according to Aim 4(i) in order to assess potential as 'drop-in' humectants/plasticisers for reduced-sugar, aqueous confectionery fillings.*

In addition to a_w reduction, the second fundamental role of any small molecular sugar is to increase product fluidity or plasticity. Most aqueous confections can be described as 'amorphous' materials in which the constituent molecules lack the long-range, periodic ordering that characterises a crystalline solid although some structuring does exist on the local level. As mentioned earlier, from a technical perspective the preparation of amorphous confectionery 'solutions' is necessitated by the need to reduce a_w, whilst the lack of crystallinity can also be sensorially desirable as it results in a faster dissolving product with a smoother mouth feel.

Depending on a variety of internal (namely composition) and external factors (temperature, pressure etc.), these amorphous materials can exist in either an ultra-high viscosity ($10^{10} – 10^{14}$ Pa), brittle glassy state or viscous rubbery state whereby the crossover point between the two is referred to as the glass transition temperature, T_g.[168] Unlike other commonly encountered phase transitions such as fusion or vaporisation, the T_g is a second order transition in that is does not involve the release or absorbance of latent heat by the analyte. During the transition, there are significant changes in numerous thermal and physical properties of the analyte including; viscosity, dielectric constant, specific heat capacity and expansion coefficient which tend to more closely resemble either solid-like or liquid-like values below or above T_g.[169] By monitoring their change as a function of T, the T_g can be determined, yet rather than occurring at a singular value it instead manifests over a relatively broad range depending on the experimental conditions and nature of the sample.

Although the concept of the glass transition has been recognised within broader polymer science since the 1940s, its mainstream application in food and confectionery systems did not occur until later (1980s - 1990s) through the seminal work of Slade and Levine.[100] They analogised the carbohydrate (or peptide)-based polymers which constituted foodstuffs to traditional synthetic archetypes and suggested that the small molecular species which are typically also present (e.g. sugars and water) act so as to plasticise them. Knowledge of the T_g is now widely accepted to be crucial for the control and optimisation of both the sensorial characteristics and stability of any food product.[77] Yet despite its ubiquitous application, the fundamental mechanisms underpinning the glass transition phenomenon still remain poorly understood, although there have been many theoretical models and frameworks advanced over the years. Whilst detailed discussion of these theories is outside the scope of the present work, it is briefly worth mentioning that the currently most accepted theory concerning the T_g of amorphous food matrices is based on the concept of ‘free volume’. The free volume model essentially considers that the volume of an amorphous material above its T_g is made up of two main contributions; the inherent volume occupied by the atoms/molecules of its constituents and some amount of ‘free’ excess volume

which arises from their atomic/molecular motion.[169] As the material is progressively cooled, the motion of the constituents diminishes and reduces the available free volume, eventually to the point (T_g) where long-range motions can no longer occur and only the inherent volume is left. A more comprehensive review covering free-volume and other theories of the glass transition in food systems can be found in, for instance, Abaid *et al*.[170]

Within amorphous food matrices including confectionery, the most important influence of T_g is that on viscosity (and thus texture). It has been widely reported that the viscosity of such systems is linked to the difference between T_g and the temperature of its external environment i.e. $T = T_g + X$ (K).[168] Over the most common temperature range of interest for aqueous confections where $X \approx 20$ to 70 K, the T/viscosity relationship exhibits an exponential like-character and can be effectively modelled using the so-called Williams-Landel-Ferry (WLF) equation (**Equation 1.10**):[171]

$$log_{10}\left(\frac{\eta\,(T)}{\eta\,(T_g)}\right) = \frac{-C_1\,(T - T_g)}{C_2 + (T - T_g)} \qquad \textbf{Equation 1.10}$$

$\eta\,(T)$ and $\eta\,(T_g)$ are the viscosity (in Pas) of the amorphous confection at a certain operating temperature and T_g respectively, with the latter often taken to be 10^{10} - 10^{14} Pas. C_1 and C_2 are constants that are related to the fractional free volume at T_g and its ratio with the thermal expansion coefficient of the free volume for which 17.44 and 51.66 K, respectively have historically been described as 'universal' values.[168] Yet, it is often necessary that modifications to C_1 and/or C_2 be made in order to optimally fit experimental data.[172, 173] From a thermodynamic perspective, amorphous materials are inherently unstable due to supersaturation and will eventually spontaneously crystallise, with the crystallisation rate also principally being correlated with $T_g + X$. For this reason, some confections with very high T_g ($T < T_g$) such as hard candies can retain microbial and sensorial integrity for many years following preparation if stored at ambient temperatures.

In most aqueous confections, it is desirable that $T \approx T_g$ + 20 to 70 K in order to generate an appropriate semi-fluid or 'tacky' texture (e.g. for a binder syrup), yet crystallisation could occur quite rapidly within this temperature region.[54] In order to prevent crystallisation within most aqueous-based confections, it is necessary to use a so-called 'doctoring agent' that typically consists of a 'glucose syrup' (also known as corn syrup or confectioner's glucose) which is a general term that describes an aqueous mixture of partially hydrolysed starch constituents based on α-1,4-linked glucose i.e. D-glucose (dextrose), maltose, maltotriose etc. akin to maltodextrins but where $DE > 20$.[40] In addition to preventing crystallisation, glucose syrups also contribute towards the sweetness, plasticisation and a_w reduction within a confection, all of which are highly dependent on the syrup composition with a greater amount of glucose and maltose and thus greater *DE*, resulting in lower a_w and T_g/viscosity.[19] It is also very common to use a 'high fructose corn syrup' (HFCS), wherein half or more of the glucose is isomerised enzymatically to fructose or to use so-called 'invert sugar' syrup which is an approximately equimolar aqueous mixture of glucose/fructose that is obtained via acid or enzyme catalysed hydrolysis of sucrose. Both HFCS and invert sugar syrups are typically sweeter and of lower viscosity than regular glucose syrups due to their high fructose content.[19] As glucose, maltose and fructose all represent undesirable free sugars (and especially the latter), manufacturers are becoming increasingly interested in utilising mixed syrups that contain greater amounts of maltotriose and larger maltooligosaccharides which fall outside the 'added' sugar classification (although may still be calorific).

Despite their attractive reduced-sugar status, the use of solely low *DE*, oligosaccharide-based glucose syrups is not technically feasible within most aqueous confections given that there exists a strong negative relationship between *DE* and T_g (viscosity). As a general heurism, the level of plasticity or reduction in T_g is often inversely correlated to the molecular mass or size of an ingredient, with smaller species providing greater reduction.[46] This is classically attributed to an enhanced penetration into the amorphous oligomeric/polymeric matrix, wherein the small additives are capable of disrupting of inter/intramolecular hydrogen bonding that exists between the larger chains. This leads to an increase

in chain mobility, flexibility and molecular spacing and ultimately results in greater free volume.[174, 175] Although size is generally the main determining factor, the shape, spatial distribution and nature of the functional groups of a plasticiser can also be highly influential,[176] yet the underlying reasons remain poorly understood. Water is an extremely potent plasticiser with a T_g of *ca*. – 135 °C and plays the predominant role in the maintenance of a rubbery or plastic consistency in aqueous confectionery (and general food) matrices. As such, there is a very strong negative correlation between water content and T_g/viscosity (at least outside the low water concentration regime where so-called 'anti-plasticisation' may occur).[177] Because the removal of water is required in order to reduce a_w to a safe level, a dramatic increase in T_g is inevitable and especially so if other small species such as glucose, maltose and sucrose are also absent as part of a sugar-reduced mandate. A graphical representation of the interrelationship between a_w/water content, T_g/viscosity and glucose syrup *DE* is shown in **Figure 1.11**.

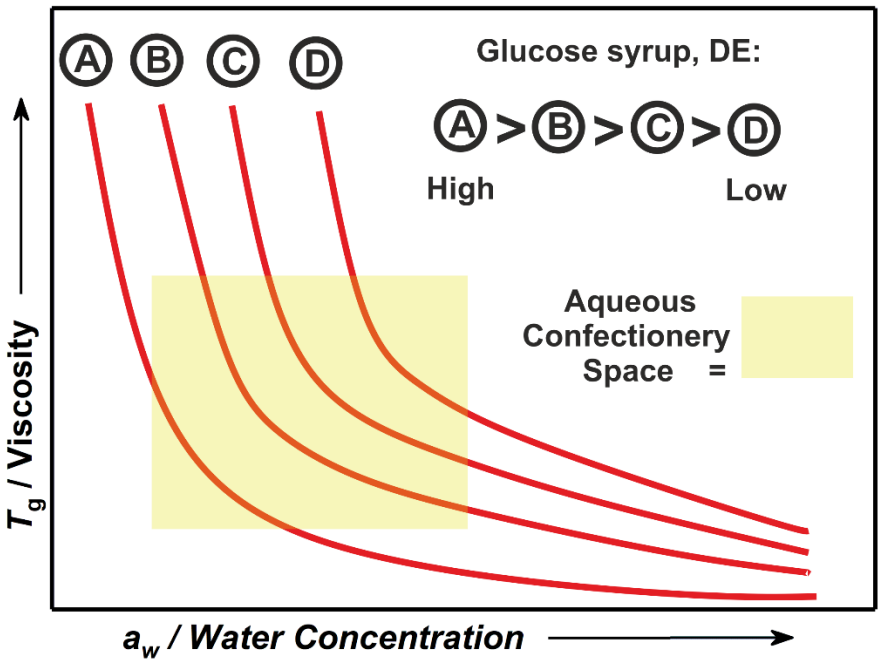

Figure 1.11: Graphical representation of the interrelationships between T_g/viscosity, a_w/ water concentration and glucose syrup *DE* within aqueous confectionery systems. Arrows indicate direction of increased *x* and *y* axis properties. Originally in colour.

It is therefore critical that any potential new sugar-replacement strategy must offer effective plasticisation of the base glucose syrup-rich matrix. Given that T_g is generally highly correlated with molecular mass, it follows that small molecules are most likely to behave as effective plasticisers, which is further justification for the investigation of small natural osmolytes and eutectic mixtures formed using combinations of low molecular weight components. **Chapter 7** investigates the influence of common confectionery solutes (fructose and glycerol) on the T_g and viscosity (and also a_w) of a model aqueous confectionery system in which their performance is evaluated along with several novel, food-grade alternatives introduced within **Chapters 4 - 6**.

Chapter 2: Experimental

This Chapter outlines the various Materials and Methods that were employed throughout the work described within this thesis. In the case of key analytical techniques (infrared spectroscopy, rheology, thermal analyses, a_w measurement and XRD), the basic working principles/theory that are relevant to results discussed herein are also outlined.

2.1. Materials

The chemicals and reagents used within this work are presented in **Table 2.1**, unless specified otherwise. Deionised water was used throughout. All common solvents were used without any further purification.

Table 2.1: Summary of materials used within this thesis.

Material (Abbreviation)	Identifier (CAS)	Purity (%, if given)	Supplier[a]
α-D-glucose	492-62-6	96	SA
Calcium chloride ($CaCl_2$)	10043-52-4	96	Acros
Choline chloride (ChCl)	67-48-1	≥ 98	SA
D_2O	7789-20-0	99.9 atom D	SA
D_6-DMSO	218-617-0	99.9 atom D	SA
D-Fructose (FRU)	57-48-7	-	NPTCC
D-glucono-1,5-lactone (Glu-1,5-Lac)	90-80-2	≥ 99	SA
D-glucurono-6,3-lactone (GluLac)	32449-92-6	≥ 99	SA
D-gulono-1,4-lactone (D-GLac)	6322-07-2	98	AA
Dulse macroalgae	*Palmaria palmata*	-	Ebbtides
Ectoine (Ect)	96702-03-3	> 99	bitop AG
Folic acid (FolAc)	59-30-3	≥ 97	SA
Glycerol (GLY)	56-81-5	-	NPTCC
Glycoin natural ® (glycoin)	22160-26-5	-	bitop AG
Hydranal Composite 5 K	-	-	TFS
Hydranal Composite 5	-	-	TFS
Hydranal Ketosolver	-	-	TFS

Hydroxyectoine (HyEct)	165542-15-4		bitop AG
L-ascorbic acid (Asco)	50-81-7	≥ 99	SA
L-citrulline (Cit)	372-75-8	98	AA
L-gulono-1,4-lactone (L-GLac)	1128-23-0	95	SA
Lithium chloride (LiCl)	7447-41-8	≥ 99	SA
Mylose 351® (MYL)	-	*ca*. 80% solids	Tereos Syral
Myo-inositol (Inos)	87-89-8	≥ 99	SA
Nicotinic acid (NicAc)	59-67-6	≥ 98	SA
Pantothenic acid (PanAc)	599-54-2	100	Bulk powders
Potassium bromide (KBr)	7758-02-03	99	Acros
Potassium carbonate (K_2CO_3)	584-08-7	99	AA
Potassium chloride (KCl)	7447-40-7	≥ 99	SA
Potassium sulfate (K_2SO_4)	7778-80-5	≥ 99	SA
Silicone oil (5 cSt at 298 K)	63148-62-9	-	SA
Sodium chloride (NaCl)	7647-14-5	99.5	TFS
Sodium sulfate (Na_2SO_4)	7757-82-6	> 99	SA
Viscosity standard (0.990 Pas at 25 ºC)	D1000 (supplier code)	-	SA
Viscosity standard (10.030 Pas at 25 ºC)	N4000 (supplier code)	-	SA
Viscosity standard (72.238 Pas at 25 ºC)	S30000 (supplier code)	-	SA

[a]SA = Sigma Aldrich, NPTCC = Nestlé Product Technology Centre Confectionery, TFS = ThermoFisher Scientific, AA = Alfa Aesar.

Dulse seaweed (*Palmaria palmata*) was used as a source of floridoside and was harvested off the coast of Otterton Ledge, East Devon, UK (approximate Latitude: 50.6273 º, Longitude: -3.2955 º) in late September 2018 (average water temperature of 15 ºC and salinity of 34 g kg^{-1} seawater) and purchased from Ebbtides UK, Devon, United Kingdom. Prior to delivery, the biomass underwent

preliminary drying in a commercial dehydrator (5 min at 70 °C then 80 min at 40 °C) and was subsequently stored in sealed plastic containers under ambient conditions upon being received.

2.2. Methods

2.2.1. Preparation of aqueous glycoin solutions

Aqueous glycoin solutions (discussed in **Chapter 4**) were prepared in one of two ways depending on the target concentration. For solutions < 62 wt. %, the as-received glycoin solution was simply diluted with water until the desired concentration was reached. For targets > 62 wt. %, the as-received glycoin solution was dried under elevated temperature *in vacuo* (> 3h, > 80 °C, *ca*. 20 mbar) before being allowed to cool naturally whilst remaining under reduced pressure (*ca*. 20 mbar) until < 40 °C to yield an 'anhydrous' material (Gly-T, 100 wt. % according to STA). This material was subsequently dissolved in the desired amount of water and stirred at sufficient temperature to ensure visible homogeneity (*ca*. 80 °C). All masses were recorded using a Kern ACS-ACJ balance (0.1 mg resolution). The relationship between water concentration and a_w of the binary glycoin-water system was also assessed using Isopiestic moisture sorption studies which consisted of accurately weighing aliquots (*ca*. 0.1 – 1.0 g) of anhydrous Gly-T into plastic vessels and subsequently storing them in separate sealed receptacles containing saturated salt slurries of KCl, NaCl, $Mg(NO_3)_2$, K_2CO_3 or LiCl corresponding to a_w or $(\frac{RH}{100}) =$ 0.851, 0.755, 0.544, 0.432 or 0.113 respectively (at 20 °C).[178] Initial masses and changes thereof were monitored periodically (typically every 7 – 14 days) using a Kern ACS-ACJ balance (4 d.p.) until a plateau had been reached (measured over 69 days). All experiments were conducted in duplicate.

2.2.2. Screening of deep eutectic solvent (DES) formation

The screening of DES mixtures involved initially weighting desired amounts of components according to pre-determined molar ratios and briefly hand mixing (30 s) to ensure homogeneity. The resulting solid blends were quickly transferred into sealed glass vials which were then placed onto a pre-heated hotplate and stirred at temperature ($\geq$ 100 ^{o}C) for at least 1 hour during which time, they were checked periodically for liquid formation. Following heating, samples were allowed to naturally cool to room temperature. Lactone and Asco-based DES used for further testing (rheological, NMR and DSC analysis or within a model aqueous confectionery system) were stored in a vacuum desiccator until required (typically < 48 h following preparation). A summary of the mixtures that were investigated within **Chapter 6** is provided in **Table 2.2**.

Table 2.2: Summary of the mixtures screened for eutectic melting.

Component 1	Component 2	Molar ratio (Component 1:2)
Citrulline	ChCl	2:1, 1:1, 1:2
Ectoine	ChCl	2:1, 1:1, 1:2
Hydroxyectoine	ChCl	2:1, 1:1, 1:2
Folic Acid	ChCl	2:1, 1:1, 1:2
myo-inositol	ChCl	2:1, 1:1, 1:2
Nicotinic acid	ChCl	2:1, 1:1, 1:2
Pantothenic acid	ChCl	2:1, 1:1, 1:2
L-ascorbic acid	ChCl	2:1, 1.5:1, 1:1, 1:1.5, 1:2
L-gulonolactone	ChCl	2:1, 1.5:1, 1:1, 1:1.5, 1:2
D-gulonolactone	ChCl	2:1, 1.5:1, 1:1, 1:1.5, 1:2
Glucuronolactone	ChCl	2:1, 1.5:1, 1:1, 1:1.5, 1:2
Glucono-1,5-lactone	ChCl	1:1[a]

[a]Only a 1:1 mixture could be prepared due to lack of available material.

2.2.3. Preparation of *Palmaria palmata* (dulse) extracts

Several different extracts were produced through either refluxing water, EtOH Soxhlet or simple mechanical treatment of *Palmaria palmata* biomass with the corresponding characterisation thereof being subsequently discussed in detail within **Chapter 5**.

2.2.3.1. Water extract

As-received dulse was dried *in vacuo* (24 h, 80 °C, *ca*. 20 mbar) before being ground using a commercial coffee grinder (Kitchen Perfected, Lloytron) and sieved (< 500 μm). The resulting biomass (*ca*. 80 g) was then heated under reflux in water (*ca*. 900 mL) for 24 h, cooled, filtered and the filtrate (brown-coloured) was subsequently dried *in vacuo* (first using a rotary evaporator and then vacuum oven operating at ≤ 80 °C, *ca.* 20 mbar) to yield a brown, glassy solid (approximately 15 wt. % yield based on the initial biomass) that was analysed using DSC, TGA, CHN microanalysis and NMR spectroscopy. The spent macroalgae (i.e. residue following filtration) was isolated and dried *in vacuo* prior to further characterisation (optical microscopy).

2.2.3.2. Ethanol extractives

As-received dulse was dried, ground and sieved as described above. The resulting biomass (*ca*. 80 g) was placed into a cellulose extraction thimble and subjected to exhaustive extraction (Soxhlet) in ethanol (*ca*. 900 ml) for 24 h resulting in the formation of a green coloured suspension containing an off-white solid. The latter ('inorganic solid') was collected via vacuum filtration, washed with ethanol (*ca*. 25 mL) and subsequently dried *in vacuo* (5 h, 80 °C, *ca*. 20 mbar) and corresponded to a *ca*. 2 – 3 wt. % yield with respect to the initial mass of biomass used before being subjected to TGA, pXRD, FTIR and NMR analyses. The washings were combined with the filtrate before concentration *in vacuo* which yielded a dark brown/green coloured, syrup-like material that was subsequently collected, resuspended into fresh ethanol and stirred at room temperature overnight. Following this period, the resulting sandy/cream coloured precipitate ('organic extract') was collected via vacuum filtration, washed with ethanol and subsequently dried *in vacuo* (5 h, 80 °C, *ca*. 20 mbar) and corresponded to a *ca*. 15 – 20 wt. % yield with respect to the initial mass of

biomass used. A schematic overview of the extraction process in presented in **Figure 2.1**. Ethanol extractives were subjected to NMR, polarimetry, FTIR, pXRD, DSC, TGA, STA, CHN/Cl, and optical microscope analysis along with a_w and KF measurement (of the corresponding aqueous solutions). The (dried) spent biomass that was obtained following Soxhlet extraction was also characterised via CHN analysis.

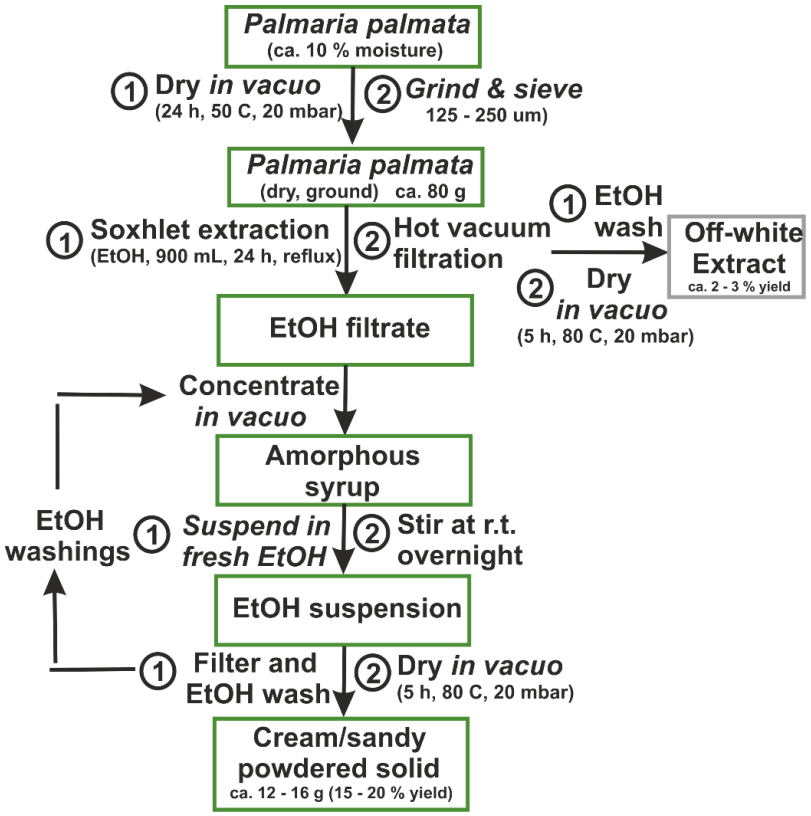

Figure 2.1: Schematic overview of the Soxhlet extraction procedure of *Palmaria palmata* developed in this work. Originally in colour.

2.2.3.3. Preparation of untreated crystalline materials

Untreated (pale-pink coloured) crystalline material (UCM) was produced via physical scraping of the surface of the as-received dulse biomass, with an aliquot thereof being subjected to drying *in vacuo* (5 h, 80 °C, *ca*. 20 mbar) leading to the generation of a second solid (UCM-T). Both materials were stored in sealed glass vials until further use, with UCM-T being used within $\leq$ 7 days of

preparation. Any visible pieces of biomass flesh that remained following collection were discarded prior to analysis (DSC/TGA/STA/TGIR, IR and NMR spectroscopy). The collated UCM was used to prepare crystalline anhydrous (F_I and F_{II}) and monohydrated floridoside (F_h) as described in **2.2.4**.

2.2.4. Preparation of floridoside crystals

All of the floridoside crystals described below and discussed in **Chapter 5** were characterised using IR spectroscopy (ATR and DRIFT), thermal analyses (DSC, hot-stage microscopy and in some cases TGIR), XRD (single crystal and variable temperature) and isothermal optical microscopy.

2.2.4.1. Anhydrous floridoside Form 'II' (F_{II})

UCM was boiled in neat MeOH (*ca*. 25 mg mL^{-1}) before hot-filtering (cotton wool plug) to give a pale-yellow solution which was stored in a sealed glass vial and allowed to naturally cool to room temperature (20 ^{o}C). Transparent, colourless polyhedral crystals could typically be observed following ambient storage over around 1 - 7 days. Crystals used for further analysis were removed from the mother liquor, collected via vacuum filtration and washed with EtOAc before being dried *in vacuo* ($\geq$ 2 h, 80 ^{o}C, *ca*. 20 mbar) prior to use.

2.2.4.2. Monohydrated floridoside Form 'h' (F_h)

The crystal submitted for XRD analysis was prepared as described for F_{II} (**2.2.4.1**) except that the MeOH filtrate was left in an unsealed vial and underwent partial, slow evaporation (under a fume hood at *ca*. 20 ^{o}C). After a period of several days, colourless crystals could be observed within the thickened yellow liquor. Crystals used for other analyses were removed and dried *in vacuo* ($\geq$ 2 h, 25 ^{o}C, *ca*. 20 mbar) prior to use.

2.2.4.3. Anhydrous floridoside Form 'I' (F_I)

UCM was processed in the same way as described for F_{II} (**2.2.4.1**) except that a large excess (~ 3:1 v/v) of EtOAc (room temperature) was immediately added directly into the MeOH filtrate. This was left overnight in a sealed vial at *ca*. 20 °C and resulted in the concomitant formation of small clusters of colourless needle-like crystals (F_I) and polyhedral crystals (F_{II}) which could be separated manually. Crystals used for all other analyses were typically spherulitic-type clusters of very fine needles prepared by immediate addition of EtOAc to the MeOH filtrate (~ 5:1 v/v) until the formation of a turbid, white suspension which was subsequently stored for 2-3 h in a sealed vial at *ca*. 20 °C. Crystals used for thermal, thermogravimetric and spectroscopic analyses were removed from the mother liquor following this time, collected and washed with EtOAc before being dried *in vacuo* ($\geq$ 2 h, 80 °C, *ca*. 20 mbar) prior to use.

2.2.4.4. Floridoside crystal calculations

Calculations of torsion angles, H-bond lengths and simulated pXRD patterns (2Θ = 5 to 90 °, 0.1 ° step) corresponding to the various floridoside polymorphs were generated from the single crystal structural data using Mercury (v 4.1.0).[179] The criteria used for hydrogen bonding included: inter- and intra-molecular donor and acceptor (A) atoms separated by > 1 bond, $\leq$ 3.00 Å (H···A), $\geq$ 90 ° (O-H···A) and OH donor only.

2.2.5. Preparation of model confections

The model confections that are discussed in **Chapter 7** were produced via a direct formulation approach which consisted of accurately weighing (to 0.01 g) 1 kg Mylose 351 glucose syrup (MYL, nominally 80 wt. % solids) into a stainless-steel pan followed by an additive humectant/plasticiser at a level such that the solute concentration of the latter was set consistently at 10 wt. % of the syrup solids (see **Table 2.3**). The pan was transferred onto an electric hotplate and heated to *ca*. 70

- 80 °C with manual stirring in order to facilitate sample homogenisation. Once homogenisation had been achieved (determined visually), an initial aliquot was withdrawn within the aforementioned temperature range and subsequent aliquots (up to six) were taken following the onset of boiling (*ca*. 105 °C) at approximately 5-minute intervals (typically corresponding to an increase of 2 – 3 °C). Once removed from the cooking vessel, samples were immediately wrapped in a waterproof silicone paper in order to prevent further moisture loss/gain and laid on a metal tray to quicken cooling. Once cooled, the wrapped confections were stored in sealed plastic containers prior to analysis (KF titration, HPLC, DSC, rheology and a_w determination) for variable lengths of time depending on technique but all measurements were conducted within 7 days of production. The preparation of model confections was conducted in collaboration with Dr Steve Whitehouse (NPTC Confectionery).

Table 2.3: Model confectionery systems prepared in this work.

System (Abbreviation)	MYL mass (g)	Additive mass (g)
Mylose, neat (MYL)	~ 1000.0	-
Mylose and fructose (MYL+FRU)	1009.4	80.10[a]
Mylose and glycerol (MYL+GLE)	1001.2	80.04[a]
Mylose and floridoside extract (MYL+FLO)	1000.2	80.01[b]
Mylose and GluLac:ChCl, 1:1 (MYL+DES)	1000.5	79.95 (99.75 $\pm$ 0.03 wt. % solids)
Mylose and glycoin (MYL+GLO)	1000.1	88.84 (90.84 $\pm$ 0.18 wt. % solids)

[a]Used as-received (presumed pure).[b]Dried *in vacuo* (5 h, 80 °C, *ca*. 20 mbar) prior to use.

2.3. Analysis and Instrumentation

2.3.1. Infrared spectroscopy (IR)

Infrared (IR) spectroscopy concerns the study of the interaction of matter with light that falls within the so-called 'infrared' range of the electromagnetic spectrum, corresponding to radiation of wavelengths

(λ ≈ 0.78 – 1000 μm) and frequencies (ν ≈ 384 to 0.3 THz) that are intermediate with respect to the visible and microwave regions. The IR region can be further subdivided into the near- (NIR, λ ≈ 0.78 – 2.5 μm), mid- (λ ≈ 2.5 – 25 μm) and far-IR (λ ≈ 25 – 1000 μm). The energy (*E*) associated with such radiation (where $E = h\nu$ and *h* is the Planck constant = 6.626 x 10^{-34} J s^{-1}) is sufficient so as to induce vibrational excitation of molecular bonds following photon absorption. Absorption only occurs however, when the frequency of the IR radiation exactly matches that of a particular vibrational mode whose motion results in a change of the overall molecular dipole moment.[180] In general, bonds that are more polarised (resulting from significant differences in the electronegativities of the constituent atoms) tend to give rise to larger changes in the dipole moment upon excitation and thus exhibit stronger absorption.

To a good approximation, the vibrational frequency, ν of a diatomic bond can be well-described using the so-called 'harmonic oscillator' model by considering the bond as a spring with atoms A and B positioned at either end. In this case, ν can be calculated via **Equation 2.1**:

$$\nu = \frac{\sqrt{k(\frac{M_A + M_B}{M_A M_B})}}{2\pi} \qquad \textbf{Equation 2.1}$$

where M_A and M_B are the masses of atoms A and B and *k* is the force constant of the spring which essentially represents the force required to restore its original position following displacement (in this case following a specific mode of vibration e.g. stretch or bend). According to **Equation 2.1**, bonds comprising lighter atoms e.g. H, C, N, O etc. and/or with a higher *k* (e.g. greater number of shared electrons within the bond) will vibrate at greater ν and thus absorb IR radiation of greater *E* (lower λ). This *E* corresponds to the difference in the potential energy between individual vibrational energy levels, *n*, where *n* = 0 (the ground state), 1, 2, 3... etc.[181] Within IR spectroscopy, the frequency has historically been represented in the form of 'wavenumbers', $\tilde{\nu}$ which take the unit cm^{-1} (i.e. the number

of wave cycles that occur within 1 cm) where $\tilde{\nu} = 1/\lambda$ and $\tilde{\nu} = \nu/c$ (where c is the speed of light = 2.988 x 10^{10} cm s^{-1}), thus increasing cm^{-1} corresponds to a reduction in λ and increase in ν and E. The NIR, mid-IR and far-IR regions broadly encompass $\tilde{\nu} \approx$ 4000 - 12800, 400 - 4000 and 10 - 400 cm^{-1} respectively.

Within the harmonic oscillator model, only transitions between *adjacent* vibrational levels are permitted (i.e. $\Delta n \pm 1$) during photon absorption/emission. In real systems, which are actually 'anharmonic' (as a bond will eventually break following sufficiently large displacement from its equilibrium position), Δn can take any integer value, with transitions from $n = 0$ to $n = 2$, $n = 3$ or $n = 4$ etc. being referred to as the second, third, fourth etc. 'overtones'. Such transitions are less intense than the fundamental vibration i.e. $n = 0$ to $n = 1$ (which often occurs in the mid-IR) and as they involve absorption of comparatively higher energy photons, it is common to find them within the NIR region alongside so-called 'combination' bands which manifest as a result of simultaneous excitation of two or more fundamental vibrations. Another consequence of anharmonicity is that the energy difference between adjacent vibrational states is not constant and instead continually diminishes with increasingly higher values of n. Whilst the fundamental vibrational frequency is often close to that calculated via **Equation 2.1**, transitions where $\Delta n \geq 2$ (and especially at higher n) have frequencies which are (considerably) lower than the relevant multiple of the fundamental frequency. (i.e. $\nu_{n=1\rightarrow n=3} < 2\,\nu_{n=1\rightarrow n=2}$).

Given that ν is very sensitive to the constituent atoms and nature of a bond, different functional groups will absorb photons of varying characteristic frequencies which can therefore be used to aid in molecular identification and interaction studies. Within a typical FTIR spectrometer, IR radiation is generated at a source and is passed through a so-called interferometer before reaching the sample and then a detector.[182] The interferometer splits the source IR beam into two via a beamsplitter, sending one to a mirror of fixed location and the other to a mirror whose position can instead be moved, which can result

in an optical pathlength difference between the two. Movement of the mirror leads to varying degrees of constructive/destructive wave interference (depending on the pathlength difference and particular wavelength involved) once the two beams are recombined. Recombination of the beam results in the generation of a complex overall 'interference pattern' which effectively represents the sum of the different electromagnetic waves with varying (IR) frequencies. Once passing through an IR-active sample, a portion of the frequencies are effectively removed (due to absorption) creating a different interference pattern which then undergoes a so-called Fourier Transform (FT, hence FTIR) that allows for the constituent frequencies (and their relative intensities) to be extracted and compared with those sans sample.

There are various different FTIR sampling techniques of which, attenuated total reflectance (ATR, ATR-FTIR) and diffuse reflectance (DRIFT) are amongst the most common. In ATR, the recombined IR radiation exiting the interferometer is focused onto a high refractive index crystal (with respect to the sample) which is in contact with the sample.[183] At a specific angle, the beam is totally reflected from the internal surface of the crystal, resulting in the generation of a so-called evanescent wave which extends beyond the surface and partially penetrates into the sample layer contacting the crystal. The sample then absorbs some portion of the evanescent wave, attenuating its intensity before the beam enters back into the crystal and eventually leaves to the detector. In DRIFT, incoming IR radiation is focussed onto a particulate sample (e.g. finely ground powder) and may in some circumstances (along with specular reflectance off the particle surface sans penetration), penetrate into the particle matrix and subsequently scatter therefrom following partial absorbance before being collected and directed towards the detector.

Within this thesis, ATR-FTIR analysis was principally employed to characterise a variety of *Palmaria palmata* derived extracts (in the mid-IR range) as discussed in **Chapter 5**. Analyses were

performed using a Perkin Elmer FTIR Spectrum 400 spectrometer operating under ambient conditions in transmittance mode from 650 – 4000 cm^{-1} at a resolution of 4 cm^{-1} and with an acquisition of at least 16 scans per sample. A blank background subtraction (of ambient air, also 16 scans) was performed for each experiment and smoothing/baseline corrections (using OPUS software) were applied following data collection. Analysis (of the aforementioned samples) within the NIR range was conducted via DRIFT spectroscopy using a Bruker Equinox 55 IR spectrometer fitted with a ZnSe window and MCT detector (liquid N_2 cooled) using neat, lightly ground analyte and referenced against a ground KBr background. Measurements consisted of collecting 128 scans per spectra (256 for background) between 4000 – 8500 cm^{-1} at a 4 cm^{-1} resolution and at *ca*. 20 ^{o}C.

2.3.2. Rheology

Rheology describes the study of the flow and deformation of matter and represents an important area of interest within food and general materials science. Many aqueous based sugar systems (glucose syrups, honey etc.) can be characterised according to their 'shear viscosity', which is a measure of the resistance of a fluid to deformation following the application of shear stress (i.e. stress acting parallel to the fluid surface) and is linked to relevant sensory and processing properties. The shear viscosity of a fluid is related to the shear stress via the following equation (**Equation 2.2**):

$$\tau = \eta\dot{\gamma} \qquad \textbf{Equation 2.2}$$

where τ, η and $\dot{\gamma}$ represent the shear stress (in Pa), viscosity (in Pas) and shear rate (i.e. the rate at which the fluid is sheared, in s^{-1}). A large proportion of fluids exhibit so-called Newtonian flow behaviour whereby their viscosity is independent of shear rate (i.e. η within **Equation 2.2** is constant), as is the case for many 'simple' molecular liquids such as water and also most aqueous sugar solutions.[65] For other substances, especially those that are 'semi-solid' (e.g. aqueous biopolymer dispersions), η is

greatly dependent on $\dot{y}$ and it is more appropriate to consider an 'apparent' viscosity. In such non-Newtonian fluids, the application of shear has some type of disruptive influence on the local structural level (e.g. polymer chain alignment or entanglement) which ultimately results in an increase (for shear 'thickening' or 'dilatant' substances) or decrease (for shear 'thinning' or 'pseudoplastic' substances) in the macroscale viscosity of the material.

In this thesis, the flow behaviours of both food-grade eutectic melts and model aqueous confections (subsequently discussed in **Chapters 6** and **7** respectively) were characterised using a Brookfield CPS+ rotational rheometer operating under a cone/plate geometry and controlled shear rate mode at atmospheric pressure. The cone had a diameter of 25 mm, angle of 2 ^{o} and a gap between it and the fixed bottom plate set to 0.045 mm in all experiments and calibration was performed prior to sample measurement using viscosity standards ranging from 1 to 72 Pa s at 25 ^{o}C (see **Table 2.1**). The basic operating principle of the rheometer involves measuring the torque required to induce rotation of the cone, which experiences some degree of resistance upon contacting the fluid placed between it and the bottom plate.[184] For a rotational cone/plate rheometer of known geometry, this torque (M) is proportional to τ as described via **Equation 2.3** whilst $\dot{y}$ can related to the RPM of the rotating cone via **Equation 2.4**:

$$\tau = \frac{3}{2}\frac{M}{\pi r^3} \qquad \textbf{Equation 2.3}$$

$$\dot{y} = \frac{\left(\frac{\pi RPM}{30}\right)}{\sin\theta} \qquad \textbf{Equation 2.4}$$

where r and θ are the cone radius and angle. If both τ and $\dot{y}$ are known then η can be readily determined through **Equation 2.2**. It should be noted that the aforementioned instrumental setup had an upper operating limit of M = 0.050 N m which corresponded to $\tau \approx 12223$ Pa.

.

In **Chapter 6** of this thesis, rheological analysis of various lactone-based eutectic mixtures (GluLac:ChCl, L-GLac:ChCl, D-GLac:ChCl and Asco:ChCl at 1:1 and 1:5 lactone:ChCl ratios) was undertaken in order to characterise their general flow properties, which is of particular interest from an application and processing perspective. In each experiment, a fresh aliquot of sample (*ca*. 0.3 mL) was applied to the bottom measuring plate at 20 °C onto which the top measuring cone was very quickly lowered before both silicone oil and a solvent trap were placed around the cone/plate geometry and excess sample was removed from the outer edge. The measuring programme used was based on a modification of a previous description in the literature.[185] Briefly, the sample was heated to and equilibrated at the desired temperature (20 – 60 °C) for 10 minutes before being subjected to a 120 s pre-shear at 20 Pa followed by a second 60 s equilibration at temperature to remove rheological history. Isothermal flow curves of each DES were obtained using a controlled shear rate regime whereby the shear rate was increased linearly from 5 to 500 s^{-1} over a period of 100 s (i.e. a 5 s^{-1} increase per second). Each reported result reflects the average of at least two replicates.

The aforementioned method (i.e. equilibration at temperature, pre-shear and further equilibration) was also used for viscosity determination of model confections (**Chapter 7**) except that an excess of sample (*ca*. 0.4 mL) was purposefully applied to the bottom measuring plate at $\geq$ 80 °C and not removed prior to measurement. Once equilibrated, samples were subjected to a cooling temperature sweep starting from the initial equilibration temperature (80 – 120 °C) which proceeded at 0.1 °C s^{-1} until the torque limit of the rheometer was reached. Each reported result reflects the average of at least two replicates.

2.3.3. Thermal Analyses

Another one of the key classes of analysis that was conducted within this thesis was thermal analysis, which broadly describes analysis of the change in the physicochemical properties of a substance when it is subjected to varying thermal conditions. Four main thermal analytical techniques were performed;

differential scanning calorimetry (DSC), thermogravimetric analysis (TGA), simultaneous thermal analysis (STA) and thermogravimetric analysis – infrared spectroscopy (TGIR). For each of the techniques, the basic principles are introduced and experimental details relevant to the results and discussion described within later chapters are outlined hereafter. The procedure employed for hot stage optical microscopy is also provided.

2.3.3.1. Differential Scanning Calorimetry (DSC)

Calorimetry broadly describes the measurement of the heat change of a substance as a function of temperature and time under a controlled temperature program. It is common to analyse or 'scan' such a measurement over a temperature (or time in the case of an isothermal experiment) range given that the temperature (n.b. system pressure is typically kept constant) at which a calorimetric process occurs and the energy associated with it provide useful information regarding the nature of the event/substance under investigation. The term 'differential' stems from calorimetric comparison of the sample being analysed (isolated within a sample pan) and a separate reference entity (typically an empty sample pan) operating under the same controlled temperature/temporal program. There are two main DSC designs that are utilised within commercial instruments; 'heat flux' and 'power compensation'.[186] In the former, both sample and reference pans are placed within the same furnace and the temperature difference between the two which manifests during experimentation is recorded and converted to a heat flow equivalent using a suitable calibration factor. In the 'power compensation' method, the sample and reference are instead placed into two separate but identical furnaces and the temperature difference between the two minimised by varying the amount of power that is supplied to them (in order to maintain equivalent temperature) and measured directly.

Due to the presence of the analyte, the sample pan exhibits a greater (specific) heat capacity (C_p, n.b. at constant pressure) with respect to the reference given that some extra amount of energy (heat) is

required to increase the temperature of the material under investigation (in addition to that required for heating the measuring receptacles of both sample/reference systems). Upon undergoing a first-order phase transition (e.g. fusion), a characteristic quantity of so-called latent heat is either absorbed or released by the material during an endothermic or exothermic event respectively whilst the temperature of the material remains constant. In a heat flux DSC, this results in a detectable temperature difference between the sample and reference as a significant quantity of (latent) heat can be absorbed/evolved by the former without resulting in a temperature change yet the same is not true for the latter. Similarly, in the power compensation method a comparatively greater/reduced amount of power must to be supplied to the sample with respect to the reference during an endothermic/exothermic event in order to maintain equivalent temperatures.

The results of a DSC experiment are typically presented as a plot of the differential heat flow rate (*y*-axis) versus temperature (or time, *x*-axis) wherein first-order transitions appear as peaks in the thermogram (n.b. exothermic/endothermic events are assigned positive/negative heat flow rates by convention). Given that the heat flow (and specific heat capacity are related via **Equation 2.5**, then the latent heat of the corresponding transition (a.k.a. heat or enthalpy of transformation) can be calculated via integration of C_p over the temperature range of interest (between temperatures T1 and T2, **Equation 2.6**):

$$C_p = \frac{\frac{dH}{dt}}{\frac{dT}{dt}m} \qquad \textbf{Equation 2.5}$$

$$\Delta H = \int_{T1}^{T2} C_p \, dT \qquad \textbf{Equation 2.6}$$

where dH/dt is the heat flow (in W = J s^{-1}), dT/dt is the heating rate (in K s^{-1}) *m* is the sample mass (in g), C_p is the specific heat capacity (in J K^{-1} g^{-1}), *T* is the temperature (in K) and ΔH is the enthalpy of transformation (in J g^{-1}). So-called second order transitions in which no latent heat is transferred but

abrupt discontinuities to material properties namely C_p are also commonly encountered, the most pertinent of which is the glass transition, which manifests as a step-change in the measured heat flow rate signal. A typical DSC trace is presented in **Figure 2.2** in which a hypothetical substance initially undergoes melting during heating as evidenced by a sharp endotherm (1) before partial recrystallisation (cf. exotherm at point 2) and subsequent partial vitrification (cf. glass transition at point 3) on cooling. Upon re-heating, the glass then transitions back into an amorphous rubber (4) and there is sufficient molecular mobility for some extent of 'cold crystallisation' to occur (5) before the crystalline matter formed during (2) and (5) melts once again (6).

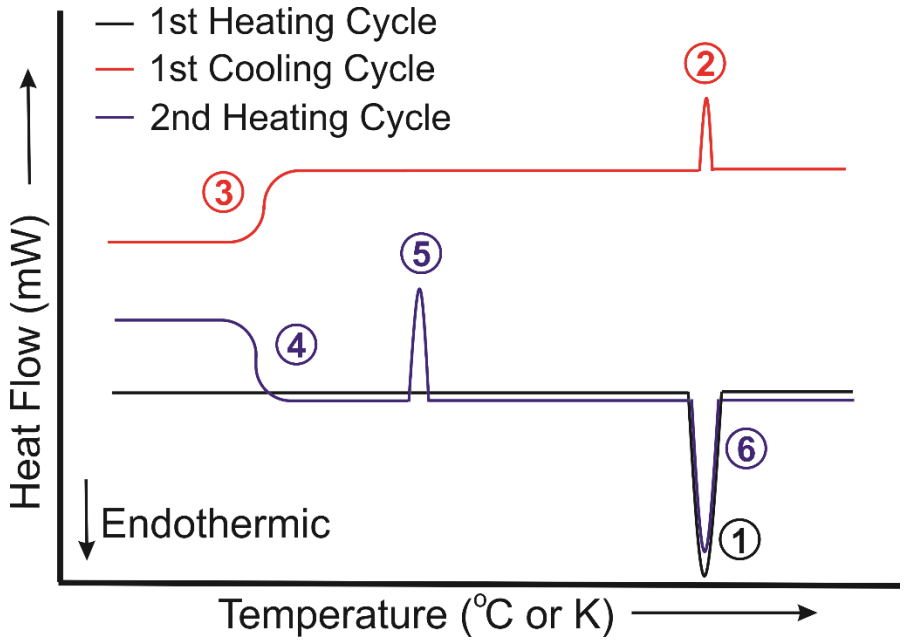

Figure 2.2: Exemplar DSC trace of a hypothetical material wherein axis arrows indicate direction of increased quantity. Originally in colour.

Within this thesis, DSC analyses were undertaken in order to determine either T_g (of aqueous glycoin and model aqueous confections) and/or more general thermal behaviour (identification of phase transitions of *Palmaria palmata* extracts, floridoside polymorphs and eutectic melts). All DSC experiments were performed using a TA Instruments Q2000 Modulated DSC (heat flux

design) under a flowing nitrogen atmosphere (50 mL min^{-1}) and Tzero hermetically sealed aluminium pans (TA instruments) containing *ca*. 5-15 mg of sample. Glass transition temperatures (T_g) were calculated as either the onset or midpoint of the step-change in heat flow that occurred during the second heating cycle. Any quoted maximum fusion temperature, T_{max} corresponds to the temperature recorded at the maximum of the most significant melting endotherm detected during the first heating scan.

Different DSC methodologies were employed depending on the analyte. Characterisation of 'anhydrous' glycoin (Gly-T, discussed in **Chapter 4**) consisted of heating a freshly dried sample (prepared according to section **2.2.1** and analysed within minutes of being removed from the vacuum oven) from 20 to 80 ^oC at rate of 5 $^oC\ min^{-1}$, isothermal storage thereat for 5 min before cooling to - 80 ^oC at 5 $^oC\ min^{-1}$, subsequent isothermal storage at – 80 ^oC for 5 min before reheating back to 80 ^oC and repetition of the same heat/cool cycles a further twice. Binary aqueous solutions containing glycoin (> 62 wt. %, also prepared as described in section **2.2.1**) were subjected to an identical program (using a heating/cooling rate of 5 $^oC\ min^{-1}$). The as-received glycoin solution (*ca*. 62 wt. %) was also subjected to an identical program except that a heating rate 10 $^oC\ min^{-1}$ was used during heating/cooling.

Within **Chapter 5**, *Palmaria palmata* extracts and crystalline floridoside samples (described in sections **2.2.3** and **2.2.4**) were heated from 20 °C to 150 °C at 5 $^oC\ min^{-1}$, held isothermal for 5 min, cooled to −80 °C at 5 $^oC\ min^{-1}$ and held isothermal for 5 min before being reheated to 150 ^oC and repetition of the same heat/cool cycles a further twice. In the case of UCM-90, an identical program was used except that the upper temperature was limited to 90 ^oC.

Thermal characterisation of the lactones used to prepare the DES mixtures discussed in **Chapter 6** consisted of heating the neat, as-received compounds from 20 ^oC to 180 (GluLac) or 195 ^oC (L- and D-GLac) at 3 $^oC\ min^{-1}$. *in-situ* DES formation experiments (also discussed in detail in **Chapter 6**) were designed to replicate the conditions of the screening process (described in section **2.2.2**).

They involved heating solid mixtures of lactone and ChCl of appropriate stoichiometric ratio (1:1 or 1:1.5 lactone:ChCl) from 20 to 100 ^{o}C at 3 ^{o}C min^{-1} and holding at 100 ^{o}C for 20 min. Samples were subsequently cooled to – 80 ^{o}C (at 10 ^{o}C min^{-1}) and held for 5 min before re-heating and two further repetitions of the same full cycle. Preformed DES (both 1:1 and 1:1.5 lactone:ChCl systems) were analysed in the same way except using fully molten eutectic mixtures that had been prepared via stirred heating on a hotplate (section **2.2.2**) prior to analysis. For the preformed Glu-1,5-Lac:ChCl, 1:1 DES, a heating and cooling rate of 10 ^{o}C min^{-1} was instead used and operated up to a limit of 80 ^{o}C followed by the same number of repeat cooling/heating cycles.

For the model aqueous confections that are described in **Chapter 7**, samples were heated from 20 ^{o}C to either 100 or 120 ^{o}C, held isothermally for 5 min, cooled to - 80 ^{o}C, held isothermally for 5 min and subsequently reheated to 100 or 120 ^{o}C. Heating and cooling rates of 5 ^{o}C min^{-1} were used throughout.

2.3.3.2. Thermogravimetric analysis (TGA)

Thermogravimetric analysis involves measurement of the mass (weight) of a substance as a function of temperature and time within a controlled reactive, inert (e.g. N_2/Ar) or an oxygen-rich purge gas (e.g. air/O_2) environmental atmosphere operating under a regulated temperature program.[187] Heating to relatively low temperatures (< 150 ^{o}C) is generally sufficient to drive off volatile components including physisorbed and crystallisation water in addition to residual organic solvents. The thermal decomposition of most organic compounds begins at *ca*. 180 - 250 ^{o}C although the exact nature of the decomposition event/s is highly dependent on various experimental factors (intrinsic properties of the sample, heating rate, purge gas identity/flow rate, sample size/morphology etc).[188] The volatilisation of organic matter is typically well advanced at *ca*. > 550 ^{o}C such that under pyrolytic conditions (i.e. in the absence of oxygen), only a carbon-rich 'char' and (relatively) thermally stable inorganics e.g. salts, silicas and metals (collectively termed 'ash') remain. If thermal decomposition instead proceeds within an oxygen-rich atmosphere then only the

inorganic constituents persist (due to combustion of any organics), allowing for potential ash quantification. Increasing the temperature further may be sufficient to induce the volatilisation of certain salts and can also result in sample mass increases via oxidation reactions.

The results of TGA are typically presented as a plot of the weight (mass) or weight percent (y-axis) vs. temperature or time (x-axis) in the case of non-isothermal or isothermal experiments respectively. Visualisation can be improved through a plot of the first derivative of the mass change (with respect to time/temperature) vs. time/temperature - collectively termed derivative thermogravimetry (dTG). The peak of the dTG curve signifies the point at which the rate of mass change is greatest, whilst integration of the curve over a specific time/temperature range yields the mass change involved. An exemplar TGA trace (**a**) for a hypothetical material along with its corresponding dTG signal (**b**) are shown in **Figure 2.3**.

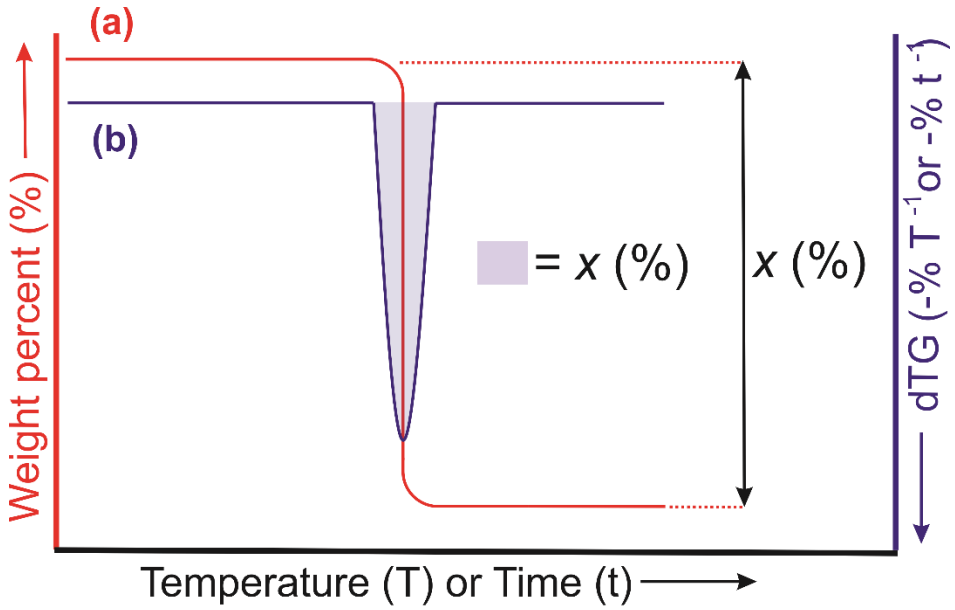

Figure 2.3: Exemplar TGA (**a**) and dTG (**b**) traces of a hypothetical material wherein axis arrows indicate direction of increasing quantity. Originally in colour.

In this thesis, high temperature TGA was carried out using a Netzsch 409 STA wherein samples (*ca*. 50 mg) were placed within an open alumina crucible and heated under either flowing N_2 (100

mL min^{-1}) or in a mixture of air/N_2 (100/20 mL min^{-1}) at 5 or 10 ^oC min^{-1}, typically up to 1300 ^oC. It should be noted that in all high temperature TGA experiments, there appeared to be a systematic increase in measured mass over 100 wt. % related to a buoyancy phenomenon as evidenced by a blank run (i.e. only crucible) which displayed the same trend (**Figure 2.4**). The aforementioned experimental procedure was used to characterise the thermogravimetric behaviour of 'anhydrous' glycoin, *Palamaria palmata* biomass and extracts thereof as discussed in **Chapters 4** and **5** respectively.

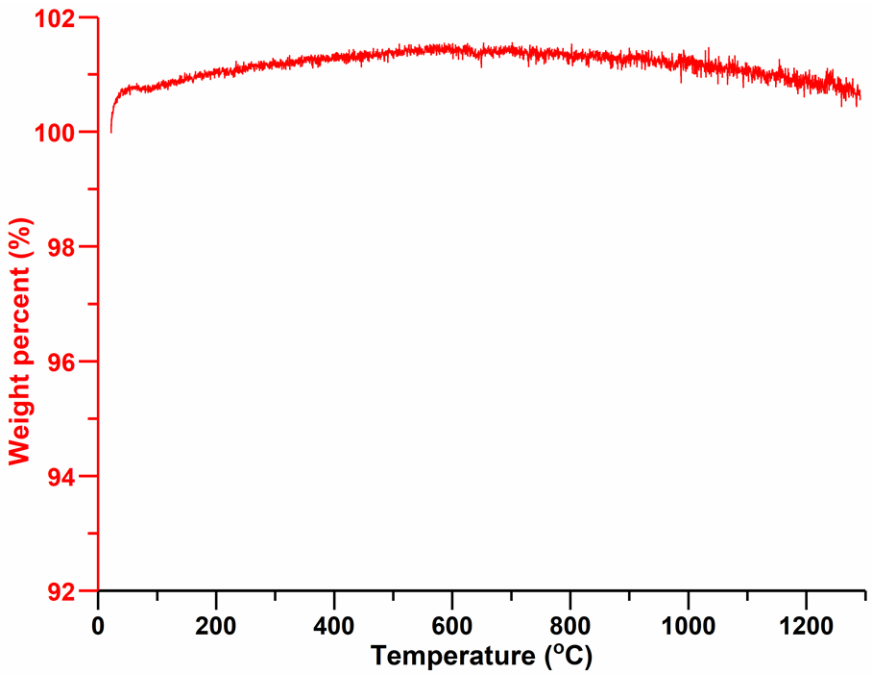

Figure 2.4: Blank TGA experiment (100:20 mL min^{-1}, air:N_2, 5 ^oC min^{-1}) based on a sample mass of 50.0 mg. Originally in colour.

2.3.3.3. Simultaneous Thermal Analysis (STA)

In most instances, it is desirable to conduct both TGA and DSC experiments (i.e. measurement of *both* the heat flow and mass change of a sample under varying thermal conditions) 'simultaneously' to ensure an accurate correlation of events that occur during each set of measurements.[189] This enables differentiation between both mass loss (e.g. endothermic evaporation vs. exothermic

combustion) and non-mass loss events (e.g. melting/freezing, glass transition etc.) that may otherwise be difficult or impossible to interpret solely using TGA, which itself can be more useful than DSC for investigating volatilisation/decomposition behaviour and performing certain compositional analyses (e.g. ash determination).

In this work, STA was conducted using a PL Thermal Sciences STA 625 and consisted of heating samples (approximately 5 - 12 mg) in an open aluminium cup under a flow of either air or nitrogen (*ca*. 50 mL min^{-1}) typically from *ca*. 20 – 625 ^{o}C at 5 ^{o}C min^{-1} unless otherwise stated. DSC signals were obtained simultaneously via reference against an empty sample pan. This procedure was employed for the thermal characterisation of 'anhydrous' glycoin (Gly-T, **Chapter 4**) and various floridoside-rich extracts of *Palmaria palmata* (**Chapter 5**). Additionally, it was also used to investigate the thermal decomposition (pyrolysis) of various 'neat' lactones (up to 250 ^{o}C, using a heating rate of 3 ^{o}C min^{-1}) and to estimate the water content within preformed Asco-based DES (using a heating rate of 10 ^{o}C min^{-1}), both of which are discussed in **Chapter 6**.

2.3.3.4. Thermogravimetric analysis - Fourier Transform Infrared spectroscopy (TG-IR)

In addition to DSC, another useful analytical technique that can be interfaced with TGA is FTIR (i.e. TG-IR), in which gases that are evolved from a sample during heating are subjected to FTIR spectroscopy, thus providing potential information concerning the functional groups present within fugacious components and aiding in species identification (cf. section **2.3.1**). Given that many of the common purge gases (e.g. N_2 and O_2) are IR inactive, band assignment of the evolved matter is significantly simplified, whilst band resolution is maximised due to limited intermolecular interactions within the gas phase during detection. Additionally, the relatively high purge gas flow rates (coupled with a heated transfer pipe to connect the two instruments) ensure the rapid delivery

of the volatiles to the FTIR spectrometer, allowing for effective *on-line* analysis with a high degree of temporal resolution.[190]

In this work, TGIR was carried out using a Netzsch 409 STA that was connected to a gas cell within a Bruker Equinox 55 infra-red spectrometer via heated (160 ^{o}C) transfer pipe. Once loaded in the crucible, samples were placed under reduced pressure following backfilling with N_2 (repeated twice). Samples were then heated from 24 - 300 ^{o}C at 5 ^{o}C min^{-1} under flowing N_2 (100 mL min^{-1}) with spectra collected from 550 – 4000 cm^{-1} approximately every 34.5 s (2.83 ^{o}C) at a resolution of 4 cm^{-1} This was used to augment the thermal characterisation of UCM obtained directly from *Palmaria palmata* biomass as described within **Chapter 5**.

2.3.3.5. Hot-stage optical microscopy

Hot-stage microscopy was conducted in order to compliment the DSC analysis of crystalline floridoside (pseudo) polymorphs as discussed in **Chapter 5**. Covered, sample-containing glass slides were mounted onto a Zeiss Axioskop 40Pol microscope fitted with a temperature-controlled Mettler FP82HT hot stage and Mettler FP90 central processor. Samples were subsequently heated at 5 ^{o}C min^{-1} and photomicrographs taken at frequent intervals using an InfinityX-21 MP digital camera mounted atop of the microscope. All hot-stage optical microscopy experiments were performed by Dr Richard Mandle (Department of Chemistry, University of York).

2.3.4. Water activity (a_w) determination

As discussed in section **1.4**, a_w is one of the key properties that must be considered when preparing confections and especially aqueous-based systems which inherently contain considerable amounts of water (up to *ca*. 20 wt. %). In this work, the a_w of all samples was analysed using a Novasina LabMaster-aw meter in which a sample is housed within a sealed, temperature-controlled chamber

alongside a sensor that comprises an electrolyte film immobilised onto an inert support.[191] Upon sealing the chamber, water vapour is evolved from the sample until a characteristic equilibrium vapour concentration/pressure (which is reflective of sample a_w cf. **Equation 1.1**) is established within the headspace above the surface. Depending on this concentration, the sensor will absorbs/desorbs a characteristic amount of the vapour which results in a detectable change in its conductivity. Greater moisture absorption increases ionic mobility of the supported electrolyte, improving charge carrying ability and thus overall electrical conductivity. All a_w determinations were recorded at the NPTC Confectionery (York) using an instrument operating at 25 $\pm$ 0.1 °C that had been previously calibrated using at least two saturated salt solutions (depending on sample a_w) with a_w = 0.113 to 0.973 $\pm$ 0.003. Samples (*ca*. 1.5 mL and no older than 48 h) were allowed to equilibrate at temperature for at least 20 minutes before measurement which was conducted in duplicate and reported as an average. Where large discrepancies existed between replicates (> 0.010), a further one or two repeats were taken with the reported values representing the mean of all results. a_w analyses were performed on binary aqueous solutions of hydroxy-/ectoine (**Chapter 3**), glycoin (**Chapter 4**) and floridoside-rich extracts (**Chapter 5**) in addition to deep eutectic melts (**Chapter 6**) and also model confectionery systems (**Chapter 7**).

2.3.5. X-ray Diffraction (XRD)

X -ray diffraction (XRD) is a technique that measures the diffraction of X-ray radiation ($\lambda \approx 0.1 – 100$ Å) following interaction with matter. During XRD, X-rays (typically generated via bombardment of a metallic target e.g. Cu, Mo, Co with high-energy electrons) are directed at a crystalline sample in which the constituent molecules/atoms are arranged periodically within a repeating lattice. This lattice can be intersected by a series of equally spaced parallel planes (lattice planes) which are separated from their closet adjacent neighbours by a characteristic distance, *d* (which is on the order of Å). Upon contacting the electrons of atoms that constitute a particular lattice plane, incoming (incident) X-rays can be

redirected and undergo coherent scattering i.e. they retain the same λ and *v* following redirection. Under certain circumstances, X-rays that are coherently scattered from a pair of parallel lattice planes may be completely in-phase with each other and constructively interfere, resulting in wave amplification and so-called diffraction.[192] Such a scenario (illustrated in **Figure 2.5**) can only occur when the Bragg equation (**Equation 2.7**) is satisfied;

$$x\,\lambda = 2\,d\,sin\,\theta \qquad \textbf{Equation 2.7}$$

where λ is the X-ray wavelength, Θ corresponds to the angle formed between the incident (or diffracted) X-ray and diffracting lattice plane and *x* is an integer value. In a typical XRD experiment, the diffracted X-rays are detected by a moving detector unit whose position, along with that of the sample is systematically altered (with respect to the incident X-ray beam of fixed λ) in order to scan for diffraction over a range of (2) Θ angles, and the diffracted X-ray intensity at each position counted.

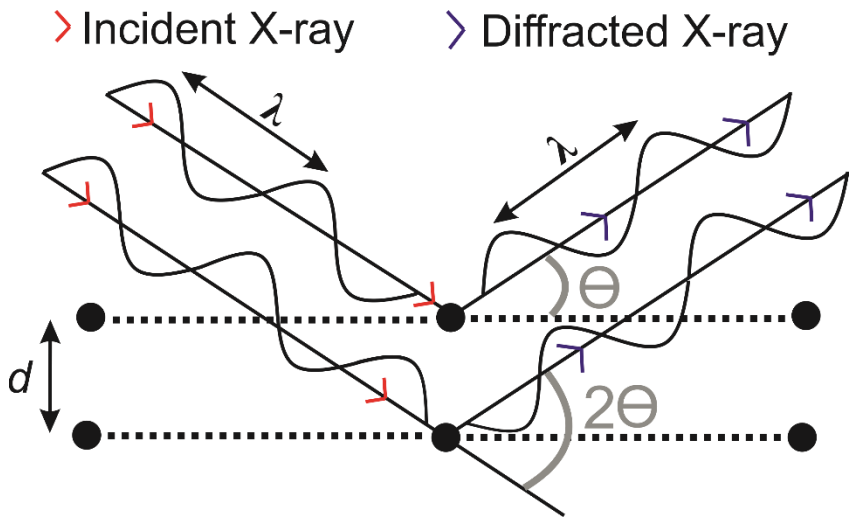

Figure 2.5: Schematic representation of X-ray diffraction satisfying the Bragg equation. Originally in colour.

XRD can be used in the structural characterisation of both bulk polycrystalline samples - referred to as 'powder' XRD (pXRD) and also large, unfractured and optically clear single crystals i.e single crystal XRD. The former is primarily used for species identification and the results thereof are typically presented as a plot of diffraction intensity (*y*-axis) vs. 2 Θ (*x*-axis) which is unique for each individual crystalline phase. The latter yields precise information regarding the position of atoms (and hence bond lengths/angles etc.) and dimensions of the unit cell within a crystal lattice, yet it can be challenging to obtain a crystal of sufficient quality and data collection is a considerably more involved and time-consuming process.

In thesis, both isothermal (at room temperature *ca*. 21 ^{o}C) pXRD and variable temperature XRD (VTXRD) were used to characterise various floridoside-containing crystalline solids as discussed within **Chapter 5**. Room temperature diffractograms of pre-ground materials were recorded using a Bruker D8 powder diffractometer equipped with a Cu source operating under ambient conditions with a scanning range of between 5 and 90 *2* Θ, a scanning speed of 2 ^{o} min^{-1} at an increment of 0.1^{o} with the power and current set to 40 kV and 40 mA respectively. VTXRD studies were performed using a Bruker X8 diffractometer equipped with a custom-built temperature-controlled, bored graphite rod furnace (University of York) using CuKα radiation (λ = 1.54056 Å) from a 1 μS microfocus source. Diffraction patterns were recorded using samples that were filled into 0.9 mm borosilicate glass capillary tubes (Capillary Tube Supplies Ltd) and a Bruker VANTEC 500 area detector set at a distance of 128 mm from the sample. Diffractograms were collected at 2 Θ $\leq$ 24 ^{o} as a function of temperature which involved heating the samples at progressively increasing increments of *ca*. 2 ^{o}C at a heating rate of 10 ^{o}C min^{-1}. At each interval, samples were equilibrated (45s) at temperature prior to irradiation which lasted for 60 s. The collected data were subsequently processed using Bruker DIFFRAC.SUITE EVA software. All VTXRD analyses were conducted by Dr Stephen Cowling (University of York).

In addition to measurements involving bulk powdered floridoside-containing crystallite samples, single crystal XRD of F_I, F_{II} and F_h was undertaken in order to obtain a more detailed picture of the internal lattices (namely covalent and hydrogen bond length/angles – see **2.2.4.4**) of each (pseudo) polymorph (as discussed later within **Chapter 5**). Single crystals (obtained directly from the crystallisation liquor as prepared according to the methodology outlined in section **2.2.4**) were cooled with an Oxford Instruments Cryojet with data being collected using an Oxford Diffraction SuperNova diffractometer with Cu-K_α radiation (λ = 1.54184 Å) operating at 110K fitted with an EOS CCD camera. "Crysalis" was employed to carry out diffractometer control, data collection, initial unit cell determination, frame integration and unit-cell refinement.[193] Face-indexed absorption corrections were applied using spherical harmonics, implemented in SCALE3 ABSPACK scaling algorithm.[194] OLEX2 was used for overall structure solution,[195] refinement and partial preparation of computer graphics (ORTEPs/solvate structure) within which structure solution was completed using the "ShelXT dual-space" algorithm.[196] Refinement by full-matrix least-squares used the SHELXL-97 algorithm within OLEX2.[197] All non-hydrogen atoms were refined anisotropically. C-H hydrogen atoms were placed using a "riding model" and included in the refinement at calculated positions. O-H hydrogens were located by difference map and allowed to refine after all other atoms were located and refined. Crystal and collection data for F_h and F_{II} have been deposited in the CCDC under the codes of 2004260 and 2004259 respectively. All single crystal structures were solved and refined by Dr Adrian Whitwood (Department of Chemistry, University of York).

2.3.6. Elemental microanalysis

2.3.6.1. CHN

The CHN contents of *Palmaria palmata* and extractives thereof **(Chapter 5**) were determined using a CE-440 Analyser (Exeter Analytical Inc.) coupled with a Sartorius S2 analytical balance and

involved combusting samples at 975 °C followed by subsequent analysis of the resulting products via thermal conductivity detection.

2.3.6.2. S/Cl/Br/F

S/Cl/Br/F microanalysis consisted of combusting samples (*Palmaria palmata* and extractives thereof) in O_2 followed by ion chromatography (Dionex Aquion IC system fitted with an IonPac AS22 column). All elemental microanalyses were conducted in duplicate by Dr Graeme McAllister (Department of Chemistry, University of York).

2.3.7. High Performance Liquid Chromatography (HPLC) and Liquid Chromatography - Mass Spectrometry (LC-MS)

HPLC was used to characterise as-received Mylose glucose syrup and to investigate the extent of thermal degradation within model, Mylose-based aqueous confections (**Chapter 7**). Aqueous solutions of *ca*. 0.5 - 2 mg mL^{-1} of sample dissolved in HPLC grade water were initially syringe filtered ($\leq$ 0.45 μm) before being injected into an Agilent Hi-Plex H column (internal diameter and length of 7.7 and 300 mm respectively, particle size = 8 μm) running at 60 ^{o}C in isocratic mode with pure water (0.400 mL min^{-1}) as the eluent. Detection was achieved using an Agilent 1260 Infinity II Series Refractive Index Detector operating at 55 ^{o}C. All HPLC analyses were conducted by Dr Richard Gammons (Green Chemistry Centre of Excellence, University of York). LC-MS was employed to aid characterisation of the constituents within as-received glycoin (**Chapter 4**). Chromatography was conducted under conditions that were identical to those used for HPLC whilst MS was achieved via electrospray ionisation using a Bruker Compact® Time of Flight mass spectrometer operating in positive mode. All LC-MS analyses were carried out by Mr Karl Heaton (Department of Chemistry, University of York).

2.3.8. Inductively Coupled Plasma Optical Emission Spectroscopy (ICP-OES)

ICP-OES was used to determine the most abundant metal-/loids in *Palmaria palmata* biomass (**Chapter 5**). A weighted aliquot of analyte and mixture of HNO_3/HCl (3:1, v/v) were sequentially added into a microwavable digestion tube and subjected to microwave digestion (Mars Xpress). Following digestion, samples were made up to 25 mL using deionised water, filtered and subsequently analysed on an axial Varian VISTA ICP whereby results were automatically corrected for dilution factor. All ICP-OES analyses were conducted by YARA Analytical Services (Pocklington, York).

2.3.9. Isothermal Optical Microscopy

Isothermal optical microscopy was employed in order to characterise the morphology of *Palmaria palmata* biomass, various extractives thereof in addition to crystalline floridoside pseudo-/polymorphs (**Chapter 5**). This was conducted using an Olympus BH2 microscope operating in reflected light mode equipped with digital camera image capture (Visicam) and under ambient conditions (21 ^{o}C) at the NPTC Confectionery in collaboration with Dr Steve Whitehouse.

2.3.10. Karl Fischer (KF) titration

Volumetric Karl Fischer titration was used to assess the water content of a commercial as-received glycoin solution (**Chapter 4**), the saturation limit of a floridoside-rich extract derived from *Palmaria palmata* (**Chapter 5**) in addition to the water content of the eutectic melts and model aqueous confections discussed within **Chapters 6** and **7** respectively. KF analyses of model aqueous confections and their constituent ingredients were conducted at the NPTC Confectionery (York) using a jacketed KF Turbo operating at 40 $\pm$ 0.1 ^{o}C employing a mixed solvent system of MeOH:Formamide (2:1 v/v) and Hydranal Composite 5 as the titrant. Briefly, the method consisted

of addition of the confection (*ca*. 0.5 – 1.0 g) into the titration vessel followed by a five-minute period of shearing and then two minutes equilibration time prior to addition of the titrant. Reported water contents typically reflect the average of at least two replicates. Calibrations using pure water were conducted prior to use for each experimental set. All other samples were analysed using a 907 Titrando unit (Metrohm) whereby Hydranal Composite 5K and Hydranal KetoSolver were used as the titrant and working medium respectively. A polarizing current of 50 μA, stop voltage of 250 mV and a drift end-point criterion (20 μL min^{-1}) was applied in all cases. All titrations were carried out at *ca*. 21 °C with a minimal duration of 120 s and sample sizes of 0.01 – 2.00 g (depending on H_2O concentration). Each titration was repeated at least twice and calibrations using pure water were conducted prior to sample analysis.

2.3.11. Matrix-assisted Laser Desorption Ionisation – Time of Flight Mass Spectrometry (MALDI-TOF-MS)

MALDI-TOF-MS was used to assess the range of glucooligomers present within as-received Mylose 351 glucose syrup (**Chapter 7**). A small aliquot of anhydrous Mylose 351 syrup solids (< 0.1 mg) was taken up in water (100 μL) before spotting 1:1 with 2,5-dihydroxybenzoic acid matrix solution (1:1 v/v). The dried spot was analysed by MALDI-TOF using a Bruker Ultraflex III. Spectra were acquired in reflection mode over a m/z range of 100 - 6000. MALDI-TOF-MS analysis was conducted by Dr Adam Dowle (Centre of Excellence in Mass Spectrometry, University of York).

2.3.12. Nuclear Magnetic Resonance Spectroscopy (NMR)

NMR spectroscopy was used to characterise glycoin (**Chapter 4**), *Palmaria palmata* extracts (**Chapter 5**) and molten eutectic mixtures (**Chapter 6**). All NMR experiments were performed using a JEOL JNM-ECS400A spectrometer operating at a temperature of 25 °C and a frequency of 400 MHz (^1H) or 101 MHz (^{13}C). All samples were dissolved in either D_2O or DMSO-d_6 to give

solutions or suspensions of *ca.* 20 – 40 mg mL^{-1} (unless overwise stated) which were filtered through a cotton wool plug prior to analysis. ^{1}H chemical shift values were obtained via internal referencing against the residual protic solvent resonances (D_2O = 4.75 ppm, DMSO-d_6 = 2.50 ppm).

2.3.13. Polarimetry

Polarimetry was used to corroborate the purity of floridoside-rich *Palmaria palmata* extracts (**Chapter 5**) and was carried out using a Bellingham & Stanley ADP450 Peltier Polarimeter (using Sodium D-line, 598 nm) operating at approximately 20 ^{o}C. All samples were dissolved in distilled water (HPLC grade) at concentrations of *ca*. 10 mg mL^{-1} with measurements taking place following $\geq$ 16 hours equilibration. The specific rotation values reported represent the average of at least four replicates (± 0.010 °).

Chapter 3: A molecular scale interpretation of water activity in simple, confectionery-relevant solutions

Aspects of the work reported in this chapter have been published in: **A. J. Maneffa**, R. Stenner, A. S. Matharu, J. H. Clark, N. Matubayasi, and S. Shimizu, Water activity in liquid food systems: a molecular scale interpretation, *Food Chemistry*, 2017, **237**, 1133–1138.

The purpose of this Chapter is to investigate **Aim 1** as described previously within section **1.4**. Specifically, it deals with a molecular scale interpretation of the concept of 'water activity' within binary aqueous solutions and particularly those comprising confectionery-relevant solutes such as sugars and sugar alcohols. The Chapter is made up of three sections:

(i) **Section 3.1**: A brief critical review of the currently prevailing hypotheses regarding the molecular basis of a_w is provided before a potential solution via an unheralded statistical thermodynamics approach to the problem, the Kirkwood-Buff (KB) theory of solutions is then introduced.

(ii) **Section 3.2**: Using KB theory, a molecular level analysis of solution a_w is presented through interpretation of the preeminent Norrish constant. This enables identification of the main contributors towards solution a_w and allows for scrutiny of the current hypotheses that describe its origin.

(iii) **Section 3.3**: Applying the same analysis developed in section **3.2**, some rationalisation for the efficacy of several unheralded and structurally counterintuitive natural osmolytes is given.

3.1. Reviewing 'water activity' in liquid food systems

Starting from its initial inception as a concept in food science, Scott described the term "water activity" as a representation of the "availability" of water in food articles during his foundational work on the topic.[75] This appears to have been a sentiment that has since been adopted by various researchers over

the years who have subsequently refined it to consider a_w as simply a reflection of the degree of either 'bound' ('unavailable') or 'free' ('available') water within a solution.[198-200] What is actually meant by the two aforementioned terms appears ambiguous,[201, 202] although it is generally understood that a greater degree of bound water, which encompasses interactions between solutes/water leads to the diminution of a_w whereas a higher concentration of free water, which is presumably reflective of interactions between water molecules (akin to those which occur within pure water), drives it up. It is possible that this view has developed as a carry-over from the study of a_w relations in solid foodstuffs that contain relatively static surfaces onto which associated water could conceivably be considered 'bound' (in the traditional sense of the word) and unable to easily exchange from (as indicated by NMR relaxation rates for instance).[203] However, the direct application of this concept towards the interpretation of solution water activity, in which the interactions are highly dynamic and transient in nature has been criticised by various authors as being oversimplistic.[80, 204]

A connected and perhaps more refined concept which has also been posited is that of stoichiometric 'hydration' models. These appear to have been popularised by the early seminal work of Scatchard, who suggested that the a_w of aqueous solutions of sucrose was a consequence of that fact that they appeared to be "semi-ideal" in that the activities of each component were proportional to their molar fractions after accounting for dissociation, association and compound formation.[205] Of these phenomena, the original author asserted that only the self-association of water or association of sucrose and water i.e. hydration should take place in solution, simply based on the relatively small number of sucrose molecules relative to water ($x_s \approx 0.1$ in a saturated sucrose solution of *ca*. 67 wt. %) and hence, a low likelihood of sucrose self-association. Whilst water-self association was indicated to have relatively little influence on a_w, Scatchard suggested that water-sucrose interactions could give a reasonable description if the existence of either a stable hexa- and/or hepta-hydrated sucrose molecule (i.e. $C_{12}H_{22}O_{11}.6H_2O$ or $C_{12}H_{22}O_{11}.7H_2O$) was considered.[206]

A well-known extension was later presented by Stokes and Robinson within the framework of the semi-ideal solution, whereby the hydration of each solute was not limited to a specific stoichiometric ratio and was instead described via a series of varying empirical equilibrium constants between hydrates with differing integers (an 'average hydration number') of associated water molecules.[207] Yet the authors themselves suggested at the time that their theoretical approach was somewhat "incomplete" on a fundamental level. More recently, the modulation of solution a_w by solely stoichiometric hydration of saccharide non-electrolytes has continued to be invoked by various authors including Zavitsas, Gharsallaoui *et al*. and Subbiah *et al.* based on the inference of non-integer hydration numbers from the measured water activity.[208-210] However, these descriptions have drawn criticism from others,[211, 212] who claim that they are nothing more than parameter fitting exercises for which the purported hydration numbers have little or no basis in reality and cannot be applied from one system to another. Perhaps an even more fundamental issue (as highlighted by Zavitsas himself) is that the definition of what constitutes 'hydration' is highly ambiguous and it is possible to find that the same system can give different experimental 'hydration numbers' depending on the method used to obtain them.[213]

Some aficionados have advocated that solute clustering or self-association must be also factored in order to properly consider the basis of a_w in nonelectrolyte solutions.[214, 215] Indeed, according to a detailed analysis of the sucrose-water system Starzak and co-workers concluded that of the available models,[216, 217] the unusual behaviour of y_w could be best described by that of van Hook which incorporated hexameric non-hydrated sucrose clustering.[218] However, despite some promising insights, little advancement in the overall concept of solute hydration/clustering has been forthcoming in recent years to the best of this author's knowledge.

The final popular hypothesis regarding the origin of water activity is that it directly results from the "structure" of the water molecules within a solution. This idea most likely stems from the classical

classification of solutes as “makers” or “breakers” of the structure of water as advocated early-on by for instance Frank and Evans and Frank and Franks.[219, 220] Although the term ‘structure’ here is often ill-defined, it classically refers to the arrangement of water molecules in normal ice (i.e. hexagonal crystalline H_2O, ice I_h), whereby the waters adopt an almost perfect tetrahedral structure. There does not appear to be any clear consensus on what determines whether a solute classifies as a structure maker or breaker, although it is most commonly linked to the magnitude of the water activity coefficient whereby $y_w > 1$ or < 1 signifies water ‘breaking’ and ‘making’ respectively.[221-223] As y_w is found to be below 1 for virtually all sugars and sugar alcohols, they should therefore classify as structure ‘makers’, yet there appear to be conflicting accounts which suggest they are water structure makers, breakers or even both depending on concentration.[224-226]

An interesting and potentially pertinent conceptual off-shoot of the water structure hypothesis that is worth mentioning is the so-called “specific hydration” model of saccharides, which attributes various solution properties including the a_w of sugars to their ‘fit’ into the structure of ice-like water. This theory seems to have originated from Kabayama and Patterson and then popularised by later authors such as Warner and then Tait *et al*., who postulated that the enhanced hydration of D-glucose could be the result of a better fit “with the tetrahedral arrangement of water molecules”.[227-229] This assertion was based on fact that the distance between oxygen atoms in nearest-neighbour equatorial OHs appeared to be very close to the spacing between oxygens in water molecules that adopted an ice-like tridymite structure (**Figure 3.1**). A decade or so after this, the model was further embellished by Franks and co-workers, who claimed that it gave a better thermodynamic description of aqueous carbohydrate solutions compared to for instance, the semi-ideal solution extension proposed by Stokes and Robinson.[230, 231] Yet, various others and even Franks himself later highlighted weaknesses in the model such as its inability to explain the behaviour of furanoses for example, whose spatial OH-OH measurements do not fit into the ice-like structure and the unrealistic nature of such an idealised water structure existing in close proximity to a solute molecule which exhibits local perturbations (e.g. mutarotation).[232]

Nevertheless, several recent authors have still insisted on the link between the number of equatorial OH groups belonging to a sugar molecule and the extent to which it is hydrated/ fits into the water structure.[224, 233, 234]

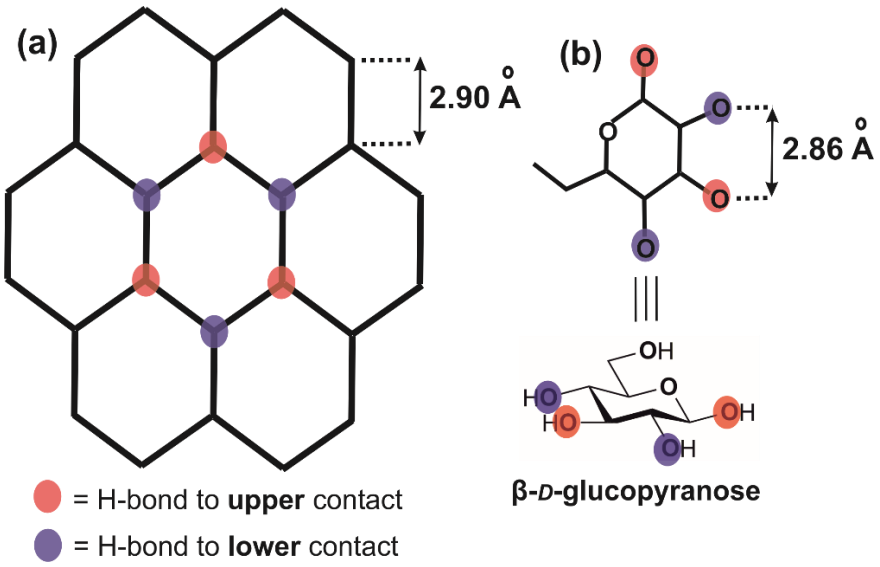

Figure 3.1: Graphical representation of the hypothetical 'specific hydration' model of saccharides; (**a**) an idealised tridymitic water structure in which hexagon points represent an oxygen atom and (**b**) β-D-glucopyranose. Adapted from Kabayama and Patterson and Tait *et al*.[227, 229] Originally in colour.

In the opinion of this author, invoking the concept of a rigid 'structure' to describe liquid water in the traditional sense is somewhat misleading as pure water itself and its resulting solutions appear for all intents and purposes, to be highly dynamical and transient in nature. This should be especially true of sugars which can often exhibit very significant conformation changes e.g. mutarotation in solution. It follows therefore, that the study of 'structure' in such systems should be a statistical exercise and hence, lends itself to investigation by statistical approaches. To this end the Kirkwood-Buff (KB) theory of solutions, first introduced by Kirkwood and Buff,[235] is a rigorous branch of statistical thermodynamics which provides a relation between macroscopic properties and local solution structure via the so-called

Kirkwood-Buff integrals (KBIs). The KBIs, denoted G_{ij} are related to corresponding radial distribution functions (RDFs), g_{ij} which describe the probability of finding the centre of a particle *j* at a certain distance (r, extending out to ∞) from the fixed centre of a second reference particle *i* with respect to that in the bulk. Essentially this provides a means of quantifying the affinity of *i* for *j* (and vice-versa). This relation is as follows (**Equation 3.1**):

$$G_{ij} = 4\pi r^2 \int [g_{ij}\,(r) - 1]\, dr \qquad \textbf{Equation 3.1}$$

The - 1 term simply removes the background level of the RDF and $4\pi r^2$ is used as we are dealing with a 3-D solution sphere around the central molecule. For a binary aqueous solution which contains a solute (e.g. sugar) and the solvent (water), there are three KBIs that correspond to the RDFs of water-water, solute-solute and solute-water affinities; G_{ww}, G_{ss} and G_{sw} respectively, where G_{sw} is equivalent to G_{ws}. Because the integral operates starting from r = 0, there is some distance extending from the centre of fixed molecule out to the centre of the second which simply cannot be occupied due to the fact that the molecules cannot overlap which represents an 'excluded volume'. This part of the normalised RDF is therefore always < 0 and because it contributes towards a significant portion of the overall integral, G_{ij} is typically found to be negative, especially as the molecules in question become larger. If molecule *j* has high affinity towards molecule *i* greater than in the bulk (or vice versa), then this will result in peaks in the RDF that lie above the bulk baseline i.e. > 0, which makes g_{ij} and thus G_{ij} more positive. Conversely, if *j* is preferentially excluded from *i* with respect to the bulk then peaks will be < 0 and g_{ij} and G_{ij} will become more negative.

Although the original authors suggested that the microscopic scale KBIs could be used to calculate macroscopic solution properties, the seminal work of Ben-Naim demonstrated that the reverse process is also possible i.e. deriving the KBIs from experimental bulk properties (namely density and the osmotic pressure).[236] Within the area of food science, this approach has recently found application

within for instance, in the study of carageenan,[237] and caffeine.[238] More related to the objectives of the current thesis, it has also been used in order to rationalise changes in the a_w of the archetypal sucrose-water solution by Shimizu.[239] Yet this has not been extended more generally towards a broader understanding of what gives rise to the measured 'water activity' in aqueous solutions comprising common sugars and sugar alcohols to the best of this author's knowledge.

3.2. KB-based analysis of 'water activity' in liquid food systems

As discussed in **Chapter 1**, the Norrish equation ($a_w = x_w\, e^{(K_N\, x_s^2)}$) is currently the preeminent relation that is used in food science to predict a_w of a binary solution containing water and a non-volatile solute. The Norrish constant, K_N is simply related to the water activity coefficient, y_w through (**Equation 3.2**):

$$K_N = \frac{\ln\, y_w}{x_s^2} \qquad \textbf{Equation 3.2}$$

K_N can be found through linearisation of **Equation 3.2** via a plot of ln y_w against x_s^2 as the slope through the origin. The most accepted K_N values of various common confectionery solutes that have previously been determined by other workers are collated in **Table 3.1** alongside graphically estimated values for relevant trisaccharides; maltotriose and raffinose (the plots are shown in **Appendix Figure A.1**) for which no literature K_N could be found but vapour pressure data did exist.[240, 241] Given a recent interest in the use of amino acids as sugar replacers,[167] the K_N values of several such solutes are also included in **Table 3.1**.

Table 3.1: Summary of K_N values for various common sugars, sugar alcohols and amino acids provided in the literature.

Type	Solute	K_N	Ref.	Type	Solute	K_N	Ref.
Polyol (C3)	Glycerol	-1.16	A	Monosaccharide	Fructose	-2.25	B
Polyol (C4)	Erythritol	-1.34	A	Monosaccharide	Glucose	-2.25	B
Polyol (C5)	Arabitol	-1.41	A	Monosaccharide	Galactose	-2.24	C
Polyol (C5)	Ribitol	-1.49	A	Monosaccharide	Xylose	-1.54	C
Polyol (C6)	Xylitol	-1.66	A	Monosaccharide	Mannose	-2.25	D
Polyol (C6)	Sorbitol	-1.65	A	Disaccharide	Sucrose	-6.47	B
Polyol (C6)	Mannitol	-0.91	A	Disaccharide	Maltose	-4.54	B
Amino acid (C5)	Proline	-3.9	C	Disaccharide	Trehalose	-6.66	E
Amino acid (C3)	Alanine	-2.52	C	Disaccharide	Lactose	-10.2	B
Amino acid (C2)	Glycine	0.87	C	Trisaccharide	Maltotriose	-6.66	TW[a]
				Trisaccharide	Raffinose	-5.38	TW[a]

[a]This work, using a_w data from Miyajima *et al*. (Maltotriose)[240] or Ellerton *et al*. (Raffinose).[241] A: Chirife *et al*.,[88] B: Taoukis and Richardson,[21] C: Lewicki,[85] D: Labuza and Altunakar,[80] E: Galmarini *et al.*[242]

Inspection of **Table 3.1** indicates that the K_N of virtually all of the most common confectionery solutes take a negative sign (at least in the form that is presented in **Equation 3.2**) and that the corresponding solutions display negative deviations from Raoult's law and $y_w < 1$. This is useful from a practical perspective because one of the main functions of an added humectant is to reduce a_w. Another notable trend is that within a specific molecular class, K_N is primarily dependent on the mass/size of the solute and generally increases in larger molecules. Norrish himself noted an almost linear relationship between the magnitude of K_N and the number of OHs for several polyhydroxyls which was later suggested by Miyawaki *et al.* to be better correlated with the number of equatorial OHs only.[87, 223] However, much like in the case of a_w itself, there remains uncertainty surrounding what really influences the magnitude and sign of K_N. Yet knowledge of this would surely be useful for rationalising and predicting the solution properties of new humectants.

A previous result in KB theory has shown that in a binary solution of water and solute, the KBIs describing the self-interaction between water (G_{ww}), solute (G_{ss}) and also the interaction between the two (G_{sw}) can be linked to the change of y_w as a function of x_s (at constant temperature and pressure) through the following (**Equation 3.3**):[239]

$$\left(\frac{\partial ln\, y_w}{\partial x_s}\right)_{T,P} = \frac{1}{x_w}\left[1 - \frac{1}{1+nx_w x_s(G_{ww}+G_{ss}-2G_{sw})}\right] \qquad \textbf{Equation 3.3}$$

where R is the universal gas constant (8.314 J K mol^{-1}), T is the temperature (298 K), x_s and x_w are the mole fractions of solute and water respectively and c_w is the molar concentration of pure water (0.0555 mol cm^{-3}).

The term 'interaction' in this context does not correspond to a specific stoichiometric binding of molecules, but to the overall net accumulation or deficit of a species relative to the solution bulk value, as described via the RDF.[243] If the system is considered at infinite dilution of the solute (denoted by the superscript ∞), then **Equation 3.3** can eventually be re-evaluated (see **Appendix Equations A1 - A3** for a more complete derivation) in terms of K_N via **Equation 3.4**, where V_w^∞ corresponds to the partial molar volume of pure water (18.1 cm^3 mol^{-1}):

$$K_N = \frac{1}{2V_w^\infty}\left(G_{ww}^\infty + G_{ss}^\infty - 2G_{sw}^\infty\right) \qquad \textbf{Equation 3.4}$$

According to **Equation 3.4** K_N will become more negative (i.e. non-ideal, a_w depression will be increased) if the value of the $G_{ww}^\infty + G_{ss}^\infty$ term is more negative and/or G_{sw}^∞ is less negative. Intuitively, this seems reasonable because it should ultimately be the affinity of water and the added solute that lowers a_w (i.e. a more positive G_{sw}^∞ or overall net accumulation of water around the solute with respect to the bulk). This affinity is diminished if the solute and/or water strongly associates with itself and thus not the other species (i.e. which would be indicated by increasingly positive values of G_{ss}^∞ and G_{ww}^∞).

Importantly, **Equation 3.4** can be used to quantify the contribution of each KBI towards the magnitude of K_N and therefore the change in solution a_w. It is known that G_{ww}^{∞} and G_{sw}^{∞} can be determined via **Equation 3.5** and **Equation 3.6** respectively:[244]

$$G_{ww}^{\infty} = RT\kappa_T^{\infty} - V_w^{\infty} \qquad \textbf{Equation 3.5}$$

$$G_{sw}^{\infty} = RT\kappa_T^{\infty} - V_s^{\infty} \qquad \textbf{Equation 3.6}$$

V_s^{∞}corresponds to the partial molar volume of solute at infinite dilution. κ_T^{∞} is the isothermal compressibility of pure liquid water at 298 K (4.53×10^{-10} Pa^{-1}). Thus, if these quantities are known (along with K_N), then G_{ss}^{∞} can then also be readily computed via rearranging **Equation 3.4** to give (**Equation 3.7**):

$$G_{ss}^{\infty} = (K_N\, 2V_w^{\infty} + 2G_{sw}^{\infty}) - G_{ww}^{\infty} \qquad \textbf{Equation 3.7}$$

It should be noted that for the systems considered here, all G_{ij}^{∞} values are negative simply due to the aforementioned excluded volume effect, yet some are significantly less/more negative than others. Graphical summaries of these G_{ij}^{∞} values as determined via **Equation 3.5**, **Equation 3.6** and **Equation 3.7** for each of the sugars and polyols using the relevant K_N and V_s^{∞} data (summarised in **Appendix Table A.1**) are shown in **Figure 3.2** and **Figure 3.3**, respectively.

In general, G_{sw}^{∞} and G_{ss}^{∞} consistently make by far the most significant contributions to K_N, whilst that from G_{ww}^{∞} is negligible by comparison. This is in-keeping with the previous findings of Shimizu, who indicated that the change in a_w of the sucrose-water system was mainly driven by the competition between solute-water and solute-solute interactions at low to moderate solute concentrations.[239] Notably, the relative insignificance of G_{ww}^{∞} in modulating the change in water activity appears to be at

odds with the hypothesis that 'water structure' is a dominant influence,[223, 224, 245] as the water-water self-interaction i.e. G_{ww}^{∞} should play a prominent role in determining a_w in that case.

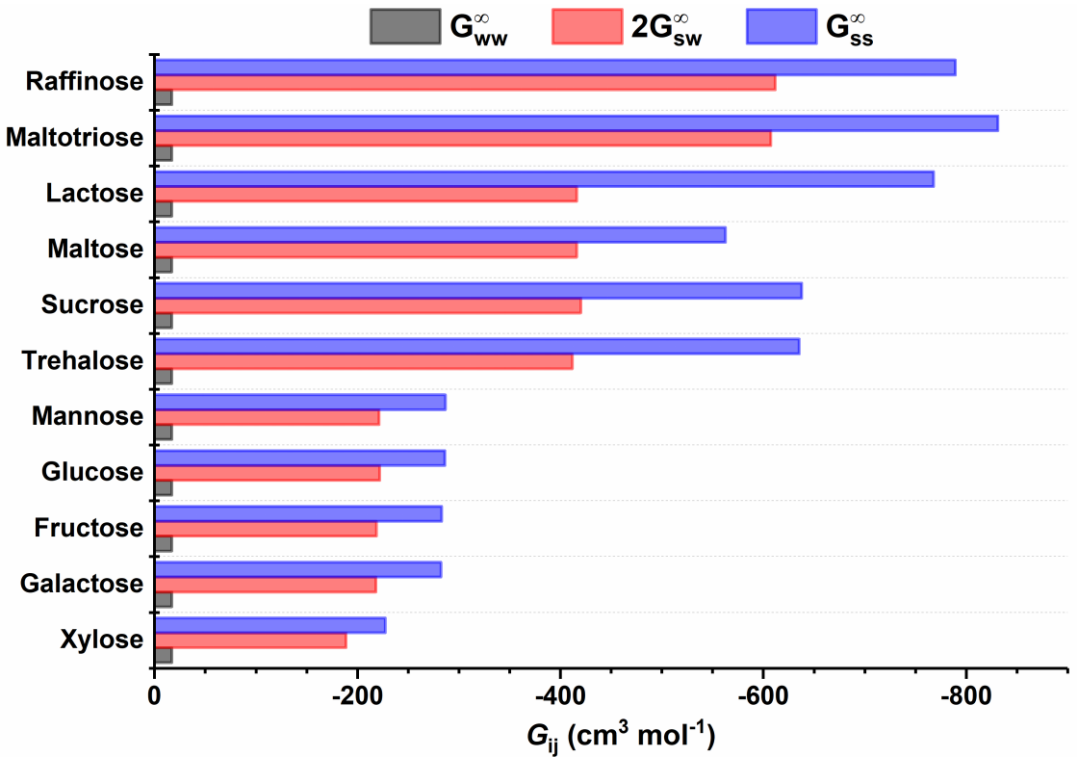

Figure 3.2: KBIs (G_{ww}^{∞}, G_{sw}^{∞} and G_{ss}^{∞}) of various common mono-, di- and trisaccharides as calculated via **Equation 3.5**, **Equation 3.6** and **Equation 3.7**. Originally in colour.

Similarly, the idea of water activity as a compensation between 'free' or 'available' and 'bound' or 'unavailable' water assumes that the former and latter increase and reduce a_w respectively, suggesting that the interplay between G_{ww}^{∞} and G_{sw}^{∞} should be dominant.[201] Although G_{sw}^{∞} is found to be important, it is actually the compensation between it and G_{ss}^{∞} that really determines K_N. A more nuanced interpretation of the broader bound vs. free water concept might suggest that there is an underlying assumption that the 'binding' of water molecules by the solute cannot occur if the latter is already 'bound' to another solute. However, the balance between solute-solute clustering and exclusion (captured through the magnitude of G_{ss}^{∞}) is now explicitly implicated.

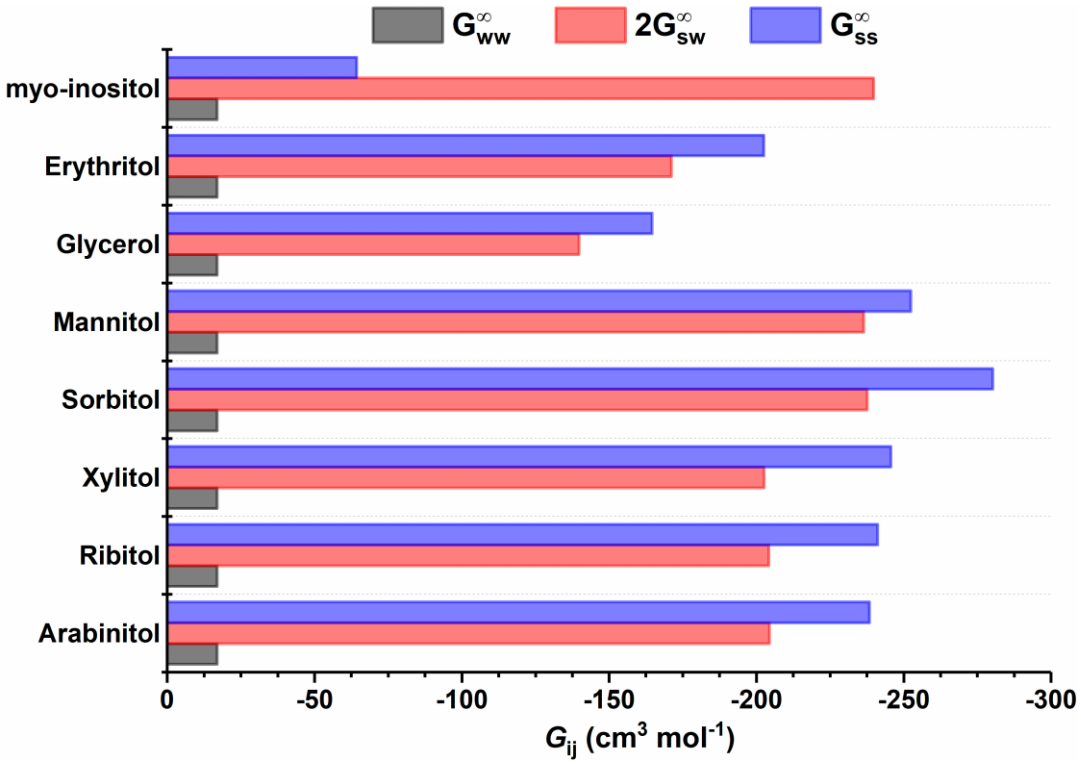

Figure 3.3: KBIs (G^{∞}_{ww}, G^{∞}_{sw} and G^{∞}_{ss}) of various common polyols via **Equation 3.5**, **Equation 3.6** and **Equation 3.7**. Originally in colour.

The findings are instead in qualitive agreement with previous descriptions based on the competition between solute clustering and hydration as is illustrated in **Figure 3.4**, which may explain why models accounting for both phenomena could best describe the experimental a_w data of sugar solutions.[216] Notably, this conclusion has now been reached without invoking the use of heuristic stoichiometric models based on solute/solvent binding, dimerisation or other specific interactions.

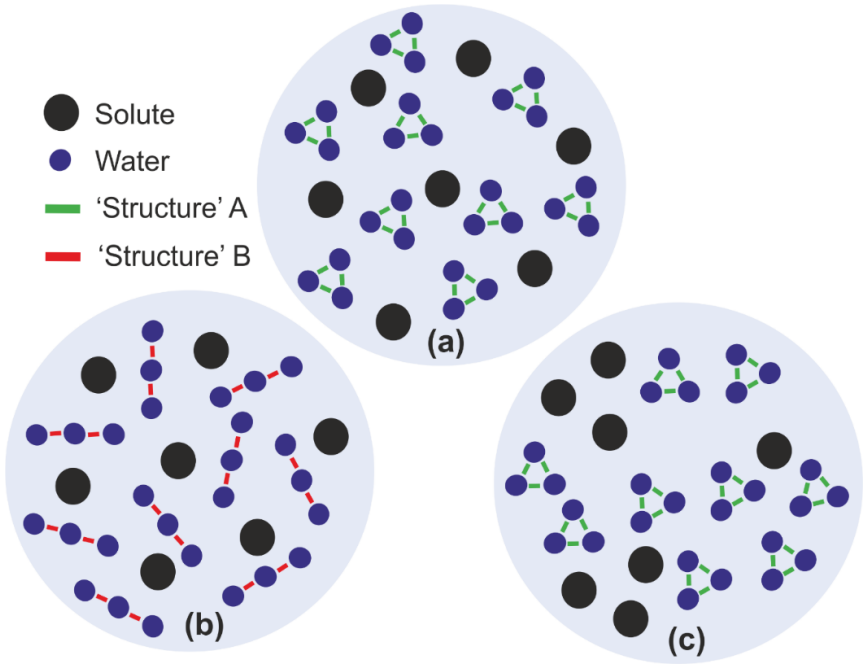

Figure 3.4: Simple illustrative representation of molecular basis for water activity within a binary solute-water solution; a_w in (**a**) and (**b**) is very similar despite any differences in local 'water structure' around the solute whereas a_w increases with greater solute-solute clustering/interactions (**c**). Originally in colour.

According to **Equation 3.4**, G_{sw}^{∞} comes directly from the (infinite) partial molar volume of the solute in water which is obviously greater for larger molecules that otherwise contain highly similar functionalities i.e. pyranose/furanose rings and hydroxyls for sugars or carbon atoms and hydroxyls for sugar alcohols. Also, G_{sw}^{∞} and K_N are both virtually identical for the same size sugars, irrespective of the orientation of their hydroxyl groups suggesting that this molecular feature has little influence on the extent of solute-water interaction. This conclusion is in disagreement with the popular 'specific hydration' model of sugars which advocates that more equatorial OHs provide greater hydration. In the cases where some differences between K_N do exist amongst similarly sized sugars e.g. trehalose (- 6.66) vs. maltose (- 4.54) vs. lactose (-10.2), the only discrepancy is the G_{ss}^{∞} term suggesting that the extent to which they cluster/self-exclude is the main discriminator. Yet how subtle structural modifications

such as OH orientation influence a_w actually manifest remains unclear and could be a goal for future investigations.

As mentioned previously, the individual KBIs are in principal concentration dependent outside of the infinite dilution range (cf. **Equation 3.3**). However, it is very interesting to note that Rösgen *et al*. have demonstrated that both G_{sw}^{∞} and G_{ss}^{∞} change only very slowly as the concentration changes.[246] According to their analysis, both become increasingly positive but continue remain large negative values even at > 3 mol kg^{-1} (the upper limit of their data), whilst G_{ww}^{∞} remains fairly constant and very small by comparison. The continued lack of influence from G_{ww}^{∞} again lends support to the idea that 'water structure' has very little, if any influence on determining a_w. Also, the comparable contributions of $G_{sw}^{\infty}/G_{ss}^{\infty}$ and the similar rates at which they change indicates that the solution behaviour of virtually all sugars and sugar alcohols must be underpinned by broadly general phenomena.[246] Importantly, as the positive increases in G_{ss}^{∞} and G_{sw}^{∞} occur concomitantly, they somewhat cancel each other out and (along with the continually small influence of G_{ww}^{∞}) result in the near constancy of K_N. This would explain why previous experiments have found that the a_w of highly supersaturated solutions of both sugars/polyols even down to a_w = 0.5 – 0.7 could be well predicted using just one value of K_N.[89] This finding is likely to be important for sugar-reduction strategies involving new 'drop-in' saccharide-based molecules as it indicates that their humectancy should be very predictable and primarily depend on size and much less on the orientation of functional groups.

3.3. New insights into solute 'humectancy' from naturally-occurring osmolytes?

As discussed in **Chapter 1.4**, there are various small molecule osmolytes which exist in nature and are often accumulated *in-vivo* to increase internal osmotic pressure and reduce a_w. Several examples are shown in **Figure 3.5**.

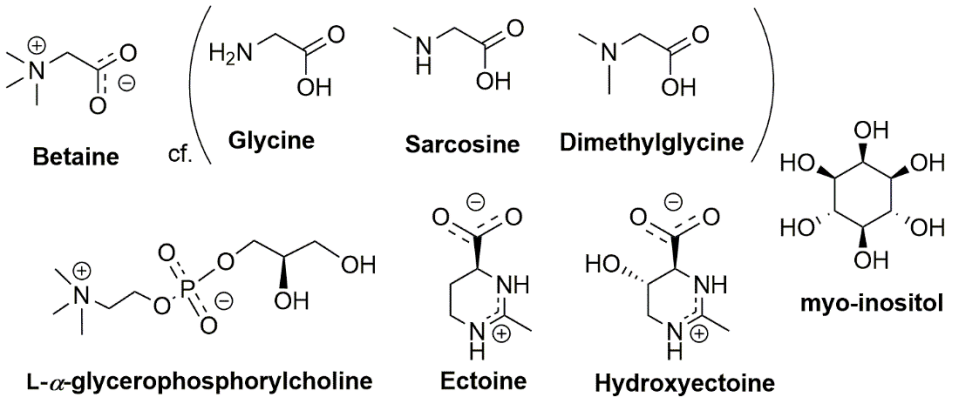

Figure 3.5: Structural formulae of several naturally-occurring osmolyte 'humectants'; L-α-glycerophosphorylcholine, hydroxyectoine, ectoine, myo-inositol and betaine (which is shown alongside analogous (methyl-) glycines for reference).

The K_N values of these solutes as with the archetypal sugars/polyols have been calculated graphically (see **Appendix Figure A.1**) using the relevant a_w data from literature or generated via experiment (in the case of hydroxy-/ectoine, which are shown separately **Appendix Figure A.2**), and summarised in **Table 3.2**. It should be noted that the K_N have only been determined using VLE data up to 2 mol kg^{-1} (*ca*. 34 wt. %) corresponding to an a_w of around 0.937 although its solubility limit is likely considerably higher. Similarly, the VLE data used for sarcosine (*N*-methylglycine), *N*,*N*-dimethylglycine (DMG) and betaine (*N*,*N*,*N*-trimethylglycine) are also considerably lower than the solubility limit of each respective solute as complete data sets could not be found within literature.

It can be seen that like many common sugars and sugar alcohols, many of these solutes induce negative, non-ideal solution behaviour ($K_N << 0$) that is generally quite comparable or even superior to common free sugar humectants in some cases. As with the sugars/polyols discussed in section **3.2**, these K_N have been employed to calculate the individual KBIs via **Equation 3.5**, **Equation 3.6** and **Equation 3.7** using V_S^{∞} values taken from the literature (summarised in **Appendix Table A.1**) (shown in **Figure 3.6**), although no such data was forthcoming for hydroxy-/ectoine.

Table 3.2: Summary of calculated K_N values (via a linear plot of ln y_w vs. x_s^2) of various natural osmolytes and their structural analogues.

Solute	K_N	Range (mol kg^{-1})[a]	R^2	Ref.
α-GPC	-23.70	≤ 2.000	0.999	Jackson-Atogi *et al*.[247]
Betaine	-10.23	≤ 4.941	1.000	Smith and Smith[248]
Dimethylglycine (DMG)	-13.79	≤ 1.600	0.999	Miyawaki *et al*.[249]
Sarcosine	-3.10	≤ 7.544	0.994	Smith and Smith[248]
myo-inositol	3.28	≤ 1.000	0.998	Jackson-Atogi *et al*.[247]
Ectoine	-7.44	≤ 5.812	0.982	TW[b]
Hydroxyectoine	-4.01	≤ 7.130	0.972	TW[b]

[a]Concentration range over which K_N has been determined.[b]This work.

It is interesting to note that myo-inositol displays unusual behaviour as K_N is positive i.e. $y_w > 1$. In this case, G_{ss}^{∞} is calculated to be far less negative (- 64.3 cm^3 mol^{-1}) than the other solutes and also significantly lower than G_{sw}^{∞} (- 99.9 cm^3 mol^{-1}) which is instead very comparable to that of other six carbon molecules (both sugars and polyols). This indicates that solute-solute affinity must be sufficiently large so as override the contribution made by the excluded volume G_{ss}^{∞}. This is surprising because the structure of myo-inositol appears similar to common monosaccharides for which $K_N < 0$ with the major difference being the replacement of the pyranose with a cyclohexane ring. It is not immediately clear why this is the case and thus more, detailed empirical and computational studies appear necessary. Similar behaviour also appears to be true of the amino acid glycine which has a G_{ss}^{∞} (- 35.8 cm^3 mol^{-1}) that is slightly less negative than G_{sw}^{∞} (- 42.1 cm^3 mol^{-1}) and a positive experimental K_N of 0.87. The self-association of glycine in aqueous solution has been heavily implicated by various experimental techniques including dynamic light scattering, diffusion-ordered NMR and neutron scattering.[250, 251] This is consistent with the relatively positive value calculated for G_{ss}^{∞} and the general notion that the clustering of a solute limits its ability to lower a_w.

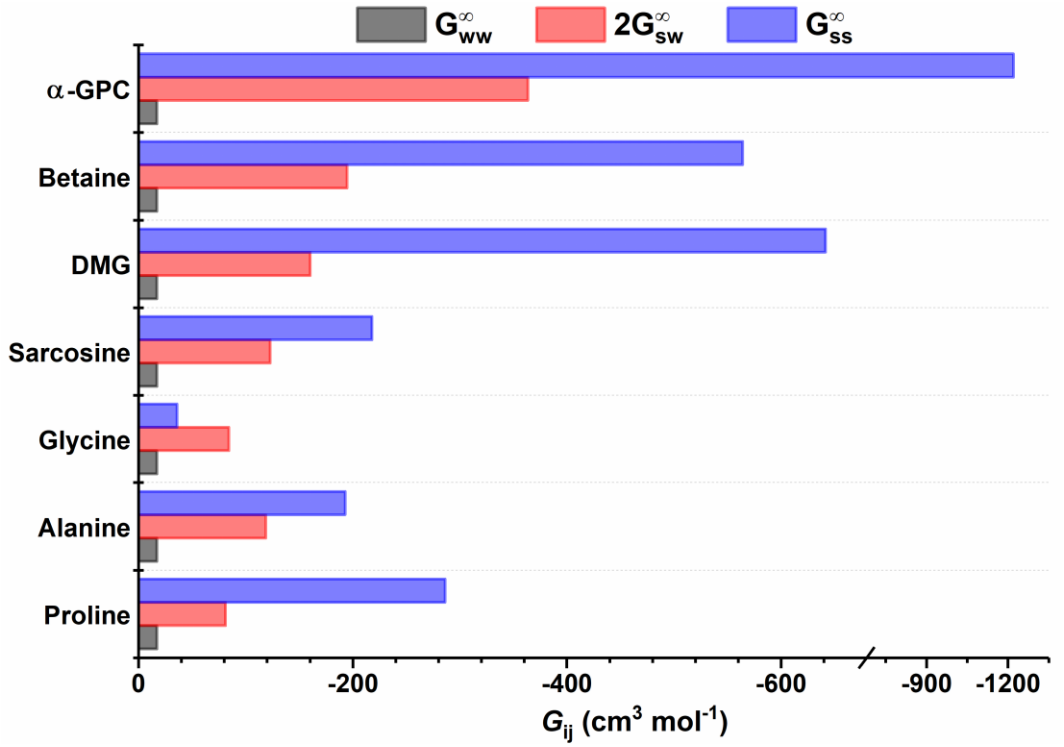

Figure 3.6: KBIs (G^{∞}_{ww}, G^{∞}_{sw} and G^{∞}_{ss}) of various natural osmolytes and comparison with selected *N*-containing species as calculated via **Equation 3.5**, **Equation 3.6** and **Equation 3.7**. Originally in colour.

It is very interesting to consider the differences within the homologous glycine family, wherein the addition of an extra methyl group to give methyl-, di- and finally tri-methyl glycine leads to a substantial decrease in K_N which is actually highly negative in the case of the latter two and to an even greater extent than that found for the di- and tri-saccharides. In these molecules the carbocation becomes increasingly shielded by the additional methyls, presumably discouraging interactions between it and the delocalised carboxylate anions of the other solute molecules. Indeed, Jackson-Atogi et. *al.* have suggested that trimethylglycines can be regarded as 'hard-sphere' self-excluders within solution.[247] A study in the literature has suggested that having a trimethyl moiety alone may not facilitate strong solute self-exclusion, as indicated by the apparent tendency of *tert*-butyl alcohol (TBA) to aggregate in dilute aqueous solution.[252] Instead, it was suggested that the presence of a hydrophilic group which could be very strongly hydrated (to a greater extent than the TBA hydroxyl) was also necessary. Such a balance

may also explain why other amino acids such as alanine and proline and related derivatives e.g. hydroxy-/ectoine which all exist as zwitterions in aqueous solution (and hence should form strong ion-dipole interactions with water) but also contain some 'hydrophobic' alkane functionalities, all exhibit considerably more negative K_N values with respect to glycine which contains no hydrophobic moiety. A similar combination also appears manifest in the strongly non-ideal solution behaviour of α-GPC (K_N = - 23.70) which contains the trimethyl ammonium group but this time in combination with a phosphate monoanion. Surprisingly, the K_N value calculated for DMG is found to be higher than that of betaine but it should be noted that the DMG activity data were measured over a considerably smaller and more dilute concentration range ($\leq$ 4.94 vs. $\leq$ 1.60 mol kg^{-1}).[224, 225] Given that K_N tends to slowly fall (at least for sugars/polyols) with increasing solute addition,[77, 215, 222] this may account for part of the discrepancy and should be confirmed via further measurements that ideally span the entire limit of solubility for each of the glycine derivatives. This also applies to α-GPC whose K_N can currently only be evaluated up to < 2.00 mol kg^{-1} owing to limited experimental data. Interestingly, although it may have been expected that molecular features that appear to give rise to decreased solute-solute interactions such as methylation are not necessarily detrimental to solubility as evidenced by the trend in the respective aqueous saturation limits of the *N*-methyl glycines; glycine = 3.0, sarcosine = 18.5, dimethylglycine = 8.3 and glycine betaine = 11.3 mol kg^{-1} (all at 25 ºC) and even the complete water miscibility of TBA.[103, 249] This family of solutes also exemplify the fact that a greater number of OH or heteroatoms more generally which are capable of interacting with water through H-bonding should not be assumed *a priori* to offer superior humectancy.

3.4. Summary

Water activity has historically been and continues to be recognised as a key concept in confectionery and broader food science. Despite this, the literature which discusses the origin of a_w within aqueous sugar and polyol solutions has been conflicting over the proceeding decades and can be broadly classified according to three main hypotheses; free vs. bound/hydration water, solute hydration vs.

clustering or non-equivalent water 'structuring' by solutes. Via application of the Kirkwood-Buff theory of solutions, the preeminent Norrish constant (K_N) which is commonly used to describe the non-ideality of aqueous food solutions, can be described in terms of water-water, solute-water and solute-solute interaction parameters. The magnitude of K_N was influenced predominantly by the solute-water and solute-solute interactions parameters, whilst the water-water parameter was found to have a negligible influence on determining the extent of solution non-ideality. This finding is at odds with idea of water structuring dictating a_w as this should presumably be captured mainly through water self-interaction. Similarly, it questions the simplified picture of 'free' water and instead highlights that the extent of solute-solute interactions are highly operative in determining a_w. Greater solute self-exclusion is found to decrease a_w whilst increased solute-solute interactions pushes it up, which is in qualitative agreement with previous models based on a competition between solute clustering and hydration.

The a_w lowering behaviour of solutes belonging to the same class e.g. mono- or di-saccharides was found to depend primarily on the molecular mass/size and far less on specific stereochemical effects e.g. hydroxyl orientation, questioning the 'specific hydration' model of sugars. It was also possible to rationalise the efficaciousness of several, structurally unusual and somewhat counterintuitive 'osmolytes' which are based on the tri-/methyl ammonium moiety, namely betaine, other *N*-methyl glycines and α-GPC using the KB-based interpretation. Their potent a_w lowering ability can be predominantly attributed to significant solute self-exclusion (i.e. large, negative solute-solute interaction) which presumably occurs through mainly steric effects, whilst some degree of strong solute hydration also seems prerequisite.

Chapter 4: Glycoin (2-*O*-α-D-glucopyranosyl glycerol) as an unusual but promising natural humectant and plasticiser

The purpose of this Chapter is to investigate **Aim 2a** as described previously within section **1.4**. Specifically, it deals with the evaluation of the natural osmolyte 2-*O*-α-D-glucopyranosyl glycerol (glycoin) as a potential replacement humectant and plasticiser for common confectionery sugars. The Chapter is divided into two main sections:

(i) **Section 4.1**: Presents a brief preamble that provides further contextualisation for the choice of the glycoin as a potential neoteric food and specifically confectionery humectant and plasticiser.

(ii) **Section 4.2**: Provides characterisation of a commercial glycoin-containing product before investigating the humectant and plasticisation properties of the binary water-glycoin system in terms of a_w and T_g with comparison against traditional confectionery solutes (sucrose, fructose glucose and glycerol).

4.1. Preamble

As previously discussed in **Chapter 1**, the application of natural so-called 'compatible solutes' or 'osmolytes' as replacements for archetypal sugars, on account of precedent within not only the food, but other consumer-facing industries (pharmaceutical, personal care etc.) in addition to high structural similarity with the existing solutes. 2-*O*-α-D-glucopyranosyl glycerol a.k.a. glycoin (**Figure 4.1**) is considered to be the preeminent osmolyte of many marine-dwelling cyanobacteria wherein it is primarily produced in response to external osmotic stress (although the influence of other factors e.g. limited nitrogen/CO_2 content have also been implicated).[124, 253, 254]

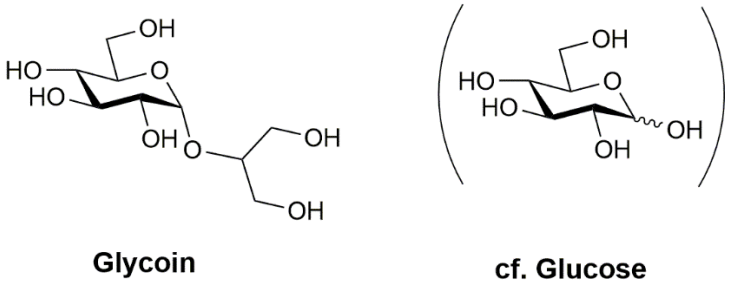

Figure 4.1: Structural skeletal formulae of glycoin (2-*O*-α-D-glucopyranosyl glycerol).

In addition to marine organisms, glycoin has been reported to exist naturally (along with 1-*O*-isomers) within several Japanese staple foodstuffs produced using the koji fungus (*Aspergillus oryzae* i.e. rice malt),[255] namely sake, mirin and miso and has also been detected within several Spanish red wines.[256] Intuitively, the presence of glycoin in these products suggests that it should be safe for human consumption, although its reported content within them is low. A single published study by Takenaka and Uchiyama suggests that glycoin may have; low digestibility, low Maillard reactivity, a "clear-cut" sweetness (*ca*. 0.55 that of sucrose) and lack of cariogenicity,[257] all of which are attractive from a confectionery ingredient perspective. These properties along with its purported potential as a prebiotic,[258] have led to commercial interest in glycoin as a functional food and beverage ingredient (nutritional supplement, sweetening agent, blood glucose suppressant, humectant), as described in several Japanese and worldwide patents.[259-262] However, its specific usage in confectionery and related systems has not yet been disclosed to the best of the author's knowledge.

Interestingly, apart from the aforementioned study by Takenaka and Uchiyama, there appear to be no published studies on the physicochemical properties of glycoin or its aqueous solutions in terms of water activity and glass transition temperature. This is surprising given that many important characteristics including a_w are likely to have direct impact on the shelf life and quality of glycoin-containing products, some of which are already commercialised (e.g. cosmetics). Such knowledge

should also allow for a more complete understanding of the biophysical properties of organisms wherein glycoin is employed *in-vivo* as an osmolyte to lower intracellular a_w and ultimately facilitate homeostasis.

Notably, glycoin is already produced commercially by the German company bitop AG who market it (in the form of an aqueous solution) under the tradename of Glycoin® natural as an active cosmetic ingredient.[263] The current process involves enzymatic synthesis from sucrose and glycerol via application of the enzyme sucrose phosphorylase wherein the glucose constituent of sucrose undergoes glycosylation through covalent attachment to the 2-*O*-position of glycerol, resulting in (a relatively) enantiomerically pure product.[128] It should be noted that overall production is currently somewhat limited in scale at ~ 10 tonnes per annum according to the relevant European Chemicals Agency (ECHA) registration page.[264] However, there may be scope for significantly increased capacity as both of the main chemical substrates are highly abundant and cheap. In this vein, a considerable amount of research continues to be dedicated to augmenting the industrial viability of glycoin including via novel biochemical routes and process intensification.[265-267]

According to the brief preamble presented above it appears as though glycoin is ideally suited for use as a novel and healthful sugar-reduced humectant/plasticiser and is already established as an industrial product. However, a lack of relevant physicochemical data concerning its a_w lowering ability and glass transition temperature prevent any meaningful conclusions from being drawn in this regard and will now be addressed.

4.2. Results and Discussion

4.2.1. Preliminary characterisation of Glycoin® natural

Initial experiments concerning glycoin involved characterisation of the material (Glycoin® natural) received from bitop AG (Dortmund, Germany) in order to confirm identity and estimate purity which would be necessary for appraising the efficacy of the molecule as a potential humectant and plasticiser. The presence of other carbohydrate impurities resulting from the production process had been indicated in the Certificate of Analysis provided by the supplier (**Appendix Table B1**).

LC-MS analysis on the as-received sample revealed the presence of four distinguishable species with retention times (t_R) of 13.4, 15.0, 15.7 and 16.4 minutes, respectively (**Figure 4.2**). Inspection of the relevant ESI (positive) fragmentations patterns indicated that the first peak was consistent with sucrose, with strong signals at m/z = 325.1153 and 360.1137 which are assigned to $[M\text{-}H_2O+H]^+$ and $[M+NH_4]^+$ respectively ($M = C_{12}H_{22}O_{11}$) based on the best-fitting molecular formulae. The subsequent peaks at t_R = 15.0 and 15.7 min gave virtually identical patterns with intense signals at m/z = 255.1047 and 272.1376, consistent with fragments $[M+H]^+$ and $[M+NH_4]^+$ for M = $C_9H_{18}O_8$ and hence, the presence of glycoin in addition to a structural isomer. The final pattern was in-keeping with a monosaccharide with strong signals visible at 180.09 and 198.10 being attributed to $[M\text{-}H_2O+NH_4]^+$ and $[M+NH_4]^+$ respectively ($M = C_6H_{12}O_6$). It is currently unclear why many of detectable fragments within the analysis were ammonium adducts, although they are very commonly encountered in positive mode mass spectrometry. It was not possible to detect any signals corresponding to glycerol which was found to have a much greater t_R (~ 20 min) under experimental conditions. The parity in relative intensity of the two peaks corresponding to glycoin and its 1-*O*-isomer was unexpected given that the concentration of the former was expected to be almost an order of magnitude higher and necessitated verification via use of a second technique - NMR (^1H and ^{13}C).

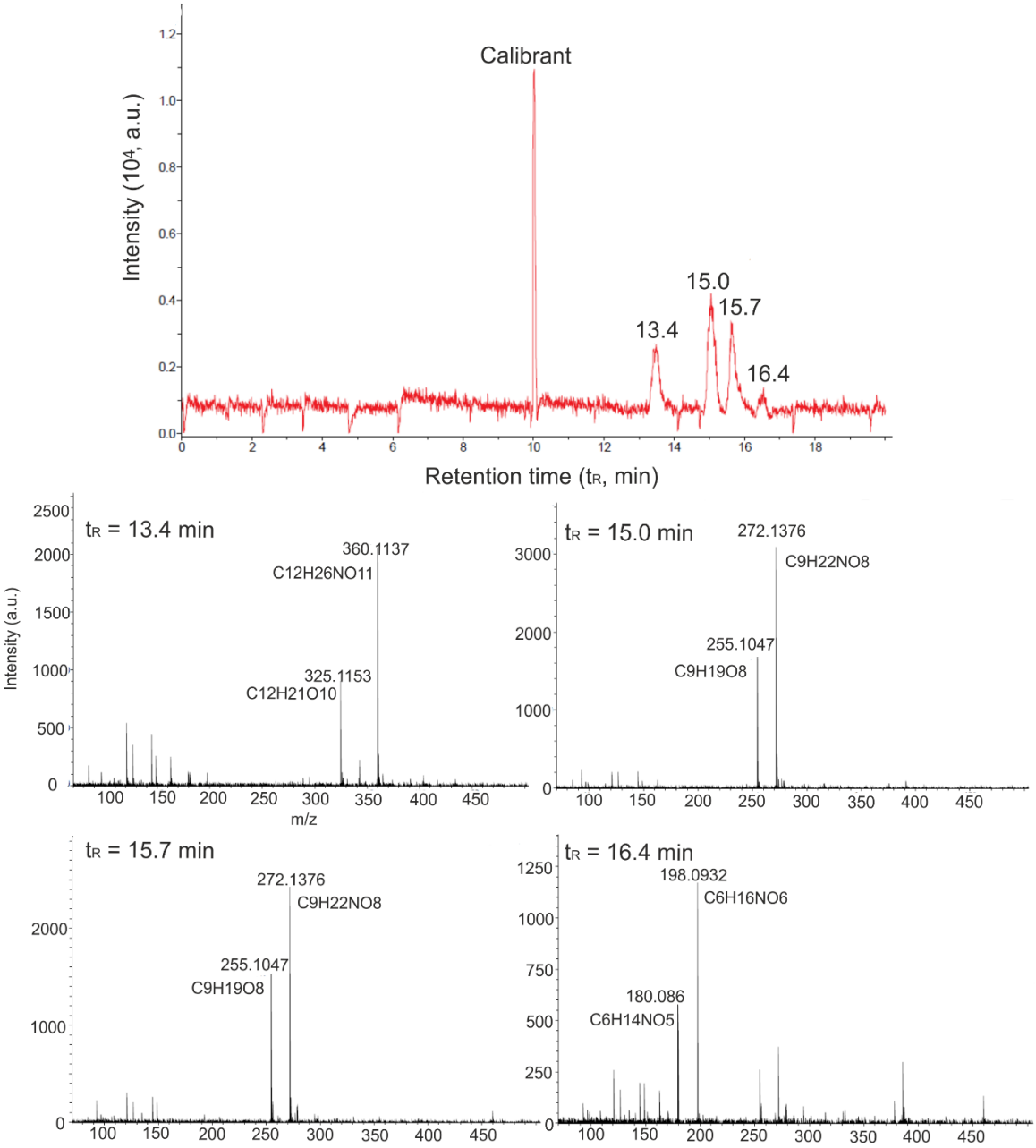

Figure 4.2: LC spectrum (top) of as-received Glycoin® natural and positive ESI fragmentation patterns of the signals at t_R = 13.4, 15.0, 15.7 and 16.4 minutes. Originally in colour.

The ^{1}H NMR (400 MHz) spectrum of glycoin in D_2O (**Figure 4.3a/b**) indicated the presence of a prominent doublet at δ = 5.05 ppm (referenced with respect to HOD at 4.75 ppm) which displayed a coupling constant of 4.1 Hz (full signal assignments are given in **Appendix Table B.2**). The

relatively low J-value of this latter signal can be attributed to a gauche relationship between the vicinal protons situated on C1 (equatorial) and C2 (axial) ($^{3}J_{H1,H2}$) (see **Figure 4.3a**) as described by the well-known relation introduced by Karplus and which is indicative of an α-substituted pyranose system.[268] This is exemplified via comparison with the ^{1}H spectrum of α-D-glucose (**Figure 4.3c/d**), wherein the presence of both α- and β- pyranoses can be readily observed at 5.16 and 4.57 ppm with $^{3}J_{H1,H2}$ = 3.7 and 8.1 Hz respectively at approximately 90 minutes following dissolution (in D_2O at *ca*. 298 K).

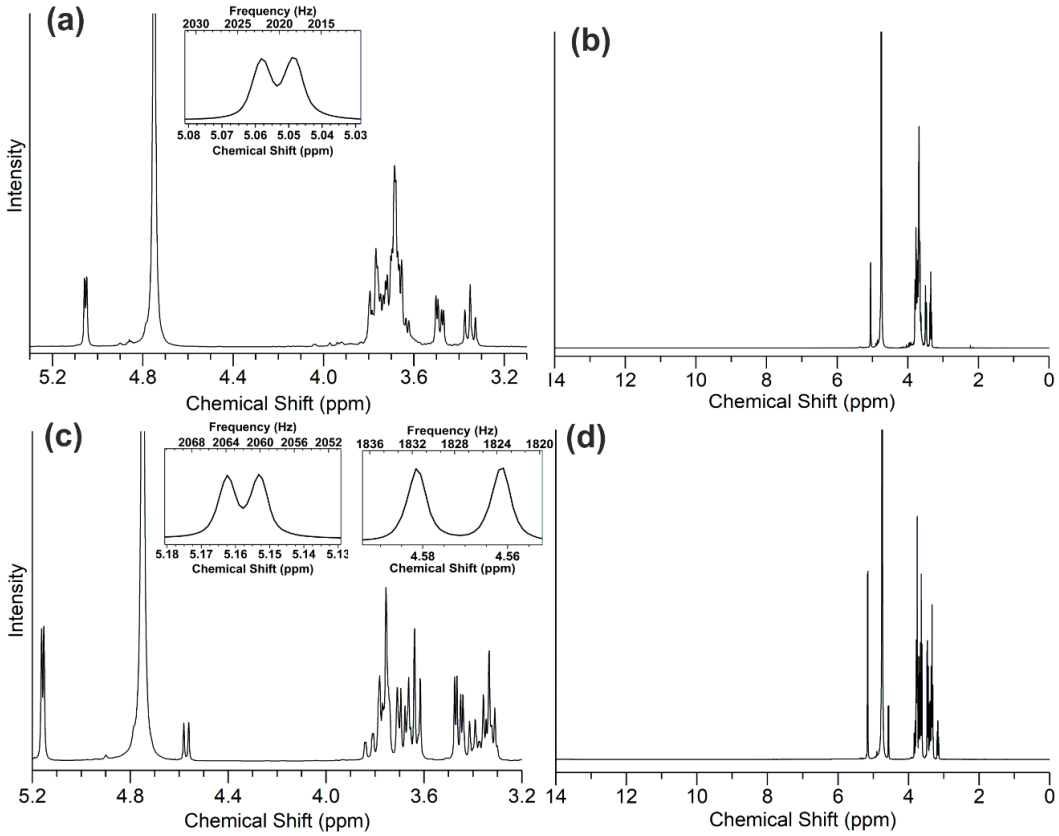

Figure 4.3: ^{1}H NMR spectra (400 MHz) of freshly prepared glycoin (**a**/**b**) and D-glucose (**c**/**d**) solutions in D_2O (referenced with respect to HOD at 4.75 ppm).

Following further storage (under ambient conditions) over *ca*. 72 hours, the concentration of the α-glucopyranose anomer was found to decrease due to progressive mutarotation. This resulted in an

equilibrium composition that was approximately 32:68, α:β glucopyranose (**Figure 4.4**) - in close agreement with common literature values (n.b. the significantly less populated α/β-furanoses and open chain form were virtually undetectable).[269] Conversely, no such signals corresponding to β-glycoin, namely the anomeric proton which should be shifted considerably further downfield (δ = 4.51 ppm) and display a significantly larger *J*-value (~ 8 Hz),[270] could be detected - even following storage > 100 days (**Figure 4.4a/b**).

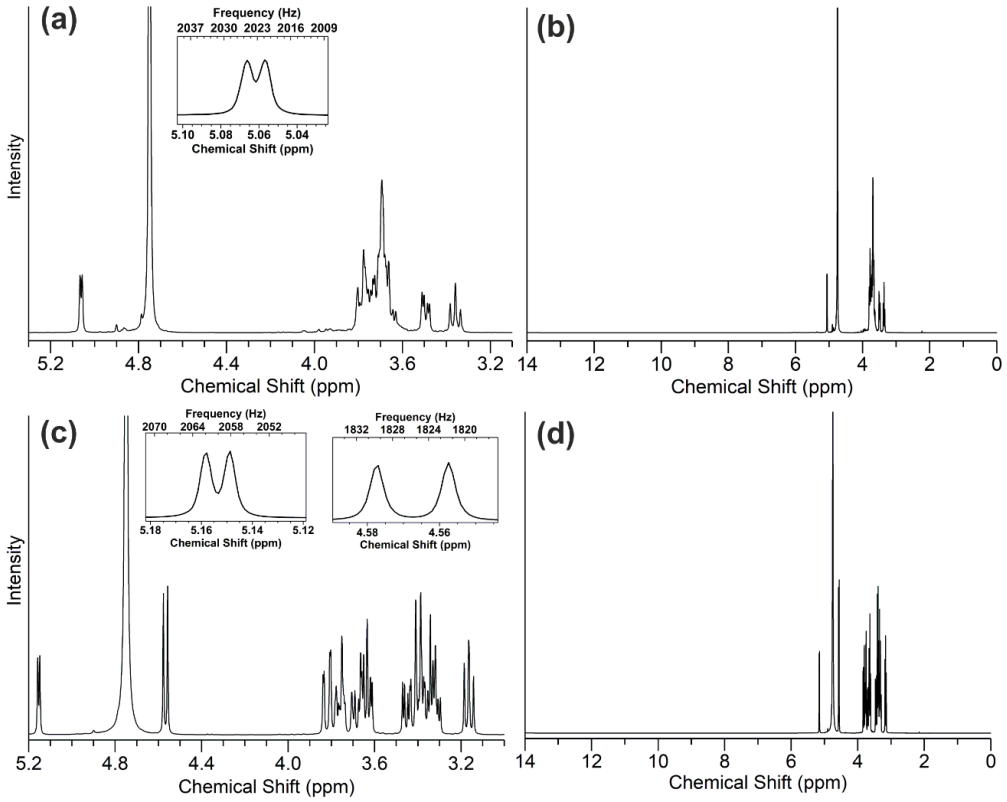

Figure 4.4: ^{1}H NMR spectra (400 MHz) of equilibrated glycoin (> 100 days, **a**/**b**) and D-glucose (> 72 hours, **c**/**d**) solutions in D_2O (referenced with respect to HOD at 4.75 ppm).

This was again consistent with the assignment of C1 as an acetal as this would inhibit anomeric interconversion. It should be noted that it was possible to observe other comparatively very weak signals within the ^{1}H NMR spectra of glycoin, which presumably correspond to the aforementioned impurities given that they manifested in the spectral regions that are typical of sugars-/derivatives

(*ca*. 3.10 – 4.20 and 4.80 – 5.40 ppm). Their presence would also explain why the measured integration values were somewhat greater than that expected for pure glycoin (referenced with respect to the isolated doublet at 5.05 ppm – see **Appendix Figure B.1)** although direct quantification was not possible to the complex and overlapping nature of such signals.

The ^{1}H analyses were also corroborated via ^{13}C/- DEPT-135 NMR (101 MHz) which highlighted the presence of nine unique carbon environments in glycoin (**Figure 4.5a/b**); six methine and three methylene carbons, again consistent with the expected structure. It should be noted that the upfield methylenes in the DEPT spectrum are very weak but can be assigned based on δ values which are virtually identical to those in the regular ^{13}C experiment. The fact that all three of the methylenes are considerably upfield shifted (< 62 ppm) is indicative of a 2-*O* linked structure given that if bonding occurred through either of the primary glycerol hydroxyls, then the secondary methylene carbon of the glycerol moiety would be expected to display a significantly higher chemical shift (e.g. ~ 73 ppm for glycerol in D_2O).[271] This, along with the aforementioned spectral features described for the ^{1}H results is in-keeping with previous structural characterisation of glycoin via NMR.[272, 273]

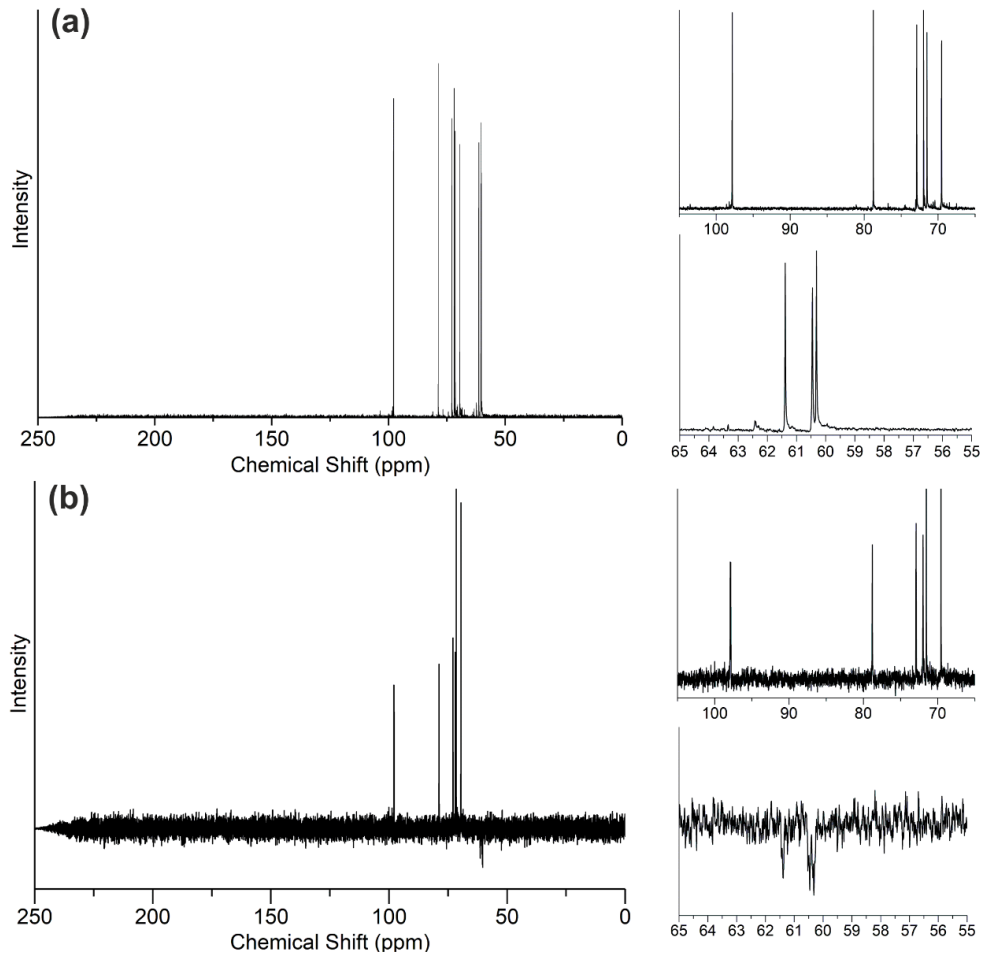

Figure 4.5: Regular (**a**) and DEPT-135 (**b**) ^{13}C NMR spectra (101 MHz) of glycoin (in D_2O) with zoomed regions shown alongside whole traces; 65 – 105 (top) and 55 – 65 ppm (bottom).

4.2.2. Physicochemical characterisation of the glycoin-water system

Following confirmation of the high purity of the as-received Glycoin® natural, efforts were subsequently focussed on assessing its physicochemical properties and particularly those of its aqueous solutions. As the supplied product was already relatively concentrated (*ca*. 62 wt. % based on Karl Fischer titration), a series of comparatively diluted solutions could be produced via simple dilution. For more concentrated mixtures, water removal was achieved via thermal treatment *in vacuo*, with the most efficient method being a combination of initial concentration via rotary evaporation (*ca*. 65 ^{o}C, 40 mbar) and subsequent heating in a vacuum oven (100 ^{o}C, 2h, ~ 20 mbar)

followed by natural cooling (whilst remaining under vacuum) to ambient temperature. It should also be noted that although the analyses involving Gly-T were conducted in an expedient manner (within approximately 5 minutes) following generation of the 'anhydrous' material, a small amount of moisture may have been adsorbed during the course of sample preparation due to the significant hygroscopicity of the material under laboratory conditions. If such moisture adsorption can take place during experimentation, then this necessitates the use of an inert atmosphere e.g. glove box when handling anhydrous Gly-T. However, such facilities were unavailable during the undertaking of this work and hence the results presented herein must be evaluated with this caveat in mind.

The aforementioned drying regime resulted in the formation of a solid, brittle material (Gly-T) which was apparently devoid of water i.e. 'anhydrous' (~ 100 wt. %) according to the absence of any loss of voltailes upon heating during STA (N_2, 10 K min^{-1}, **Figure 4.6**). Inspection of the corresponding trace shows that the majority of mass loss occurred in a generally concerted fashion, beginning at approximately 200 ^oC and reaching a maximum at *ca*. 326 ^oC, suggesting that the thermal stability of glycoin should be sufficient from a confectionery production perspective (cook temperatures are typically ~ 105 – 155 ^oC). Notably, there was no significant endotherm detectable via DSC prior to the main mass loss event, suggesting that Gly-T was entirely amorphous, even following complete water removal. The small endothermic peak that occurs at around 40 ^oC is attributed to an enthalpic relaxation (recovery) event which originates from relatively small, spontaneous structural adjustments within the analyte towards a more thermodynamically stable state during storage below T_g.[274]

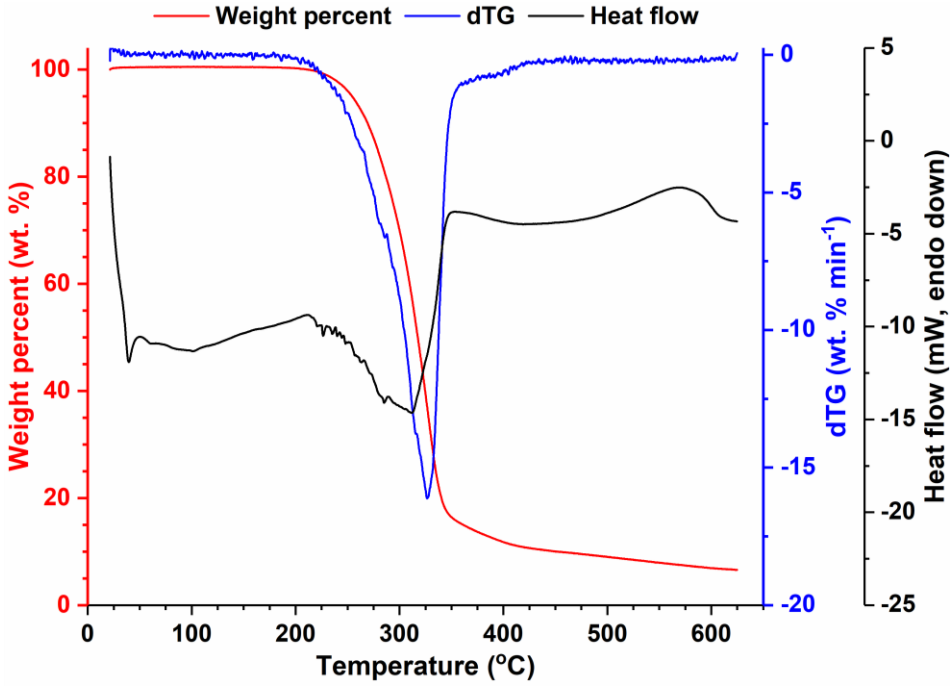

Figure 4.6: STA trace of Gly-T (T = 21 - 625 °C, 10 K min^{-1}, N_2). Originally in colour.

A similar result was also obtained during high temperature TGA of Gly-T in air (**Figure 4.7**) with a comparable initial decomposition followed by a second step change which corresponded to the combustion of residual organics and reached completion at *ca*. 550 °C. The small mass loss prior to the first decomposition event likely corresponds to water, again underscoring the moisture adsorbing propensity of the dried material. When factoring in the initial gain due to buoyancy (see), the measured mass that remained following combustion was virtually zero (**Figure 4.7** insets) and fell close to experimental error (± 0.1 wt. %), thus indicating the absence of any thermally stable inorganic matter (e.g. salts).

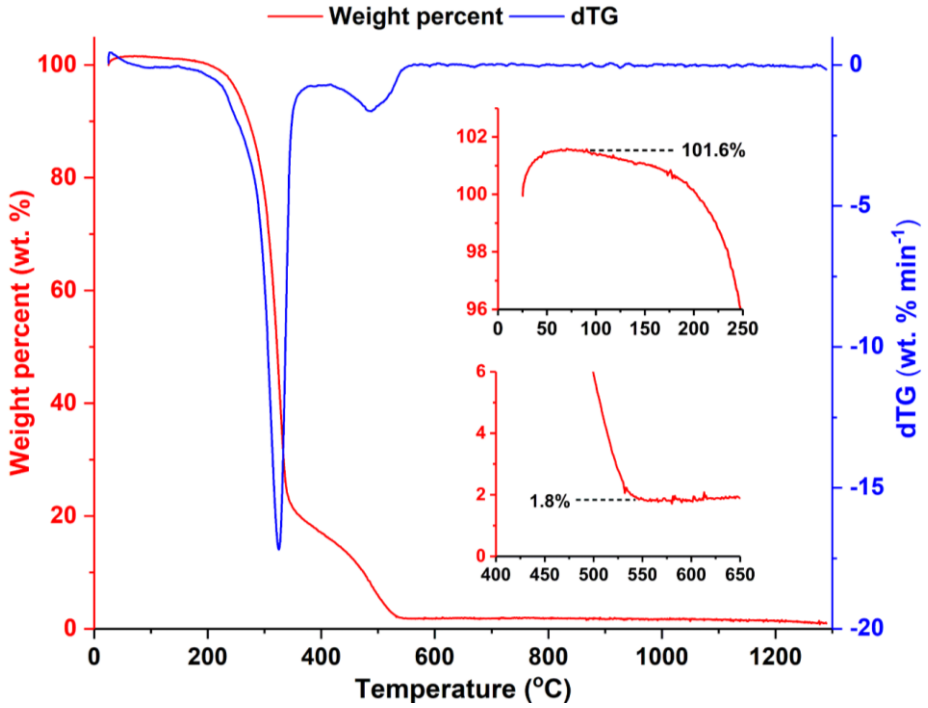

Figure 4.7: High-temperature TGA of Gly-T (T = 25 – 1300 °C, 10 K min-1, air:N_2, 80:20). Originally in colour.

The lack of crystallinity was further confirmed by cyclic DSC (- 80 to 80 °C, 5 K min^{-1}, **Figure 4.8**) wherein it was only possible to observe a reproducible glass transition during the second heat cycle that was again immediately followed by a similar (albeit less intense) relaxation endotherm. During the first heat cycle it was also possible to observe a very weak and broad endothermic peak centred at *ca*. 55 °C. The nature of this signal is not obvious although the associated enthalpy (~ 0.5 J g^{-1}) is far too low to originate from any significant melting, suggesting that it may instead correspond to some type of relaxation within the amorphous fluid or even minimal dissolution of Gly-T components within a small amount of adsorbed moisture. Interestingly, these values are somewhat comparable to those which have been reported for several monosaccharides (*ca*. 36, 38 and 31 °C for glucose, galactose and mannose respectively) and considerably lower than that of archetypal glucose-based disaccharides such as sucrose (62 °C), maltose (92 °C) or trehalose (107 °C).[275] This is not in-keeping with the common trend of increasing T_g with molecular mass amongst structurally similar carbohydrates and suggests that the glycerol moiety improves plasticity. However, this

assertion can only be fully appraised once purer anhydrous glycoin is tested as the small carbohydrate impurities (fructose, glucose etc.) or residual water may have also contributed to plasticisation of the vitrified melt.

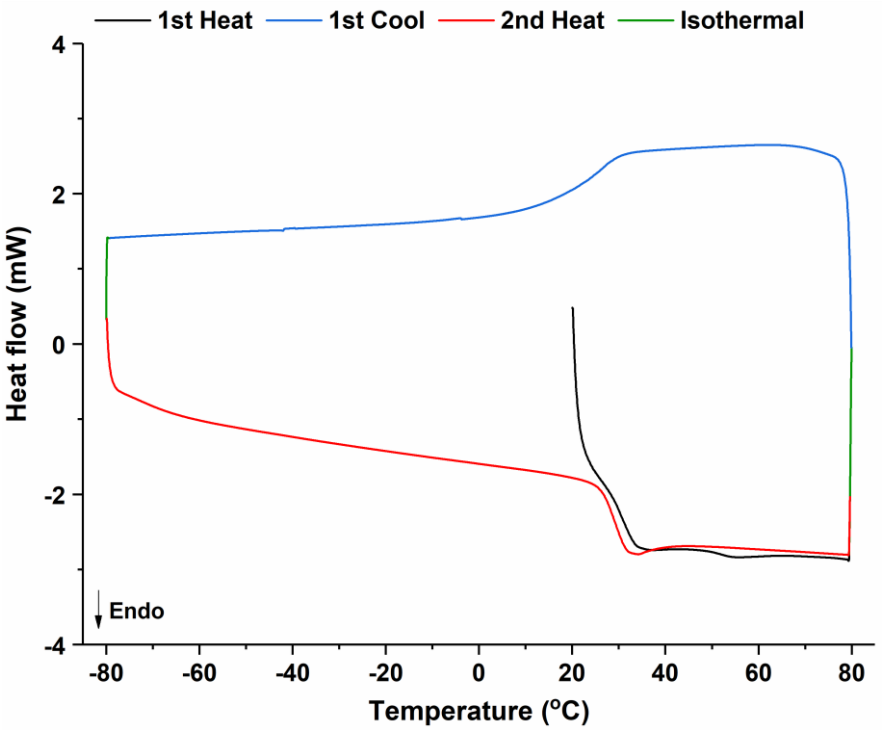

Figure 4.8: DSC of Gly-T (- 80 to 80 °C at 5 K min^{-1}) showing the first heating (black), first cooling (blue) and second heating (red) cycles. Originally in colour.

Unfortunately, on account of the aforementioned hygroscopicity, it was not possible to perform any further complimentary analyses (e.g. pXRD) due to unavoidable exposure to ambient humidity during measurement. This was exemplified in the ATR-FTIR spectrum of Gly-T (see **Appendix Figure B.2**) wherein a weak band manifesting at *ca.* 1650 cm^{-1} can be assigned to the scissoring deformation mode of residual water. The presence of this signal, coupled with the amorphous nature of the sample is also consistent with the generally broad form (indicating a lack of regular vibrational levels) of the characteristic carbohydrate bands centred at approximately 3300 (O-H

stretch), 2900 (C-H stretch), 1450 - 1200 (C-H bending) and 1150 - 1015 (C-O stretch, C-C stretch etc.) cm^{-1}.

During initial attempts to induce crystal growth, it became apparent that Gly-T displayed a remarkable complete miscibility (visually assessed according to pellucidity) with common anhydrous alcohols; MeOH, EtOH and iPrOH which are often employed as antisolvents for carbohydrates (e.g. D-glucose solubility is < 24/2/0.7 g L^{-1} in MeOH/EtOH/iPrOH at 22 ^{o}C).[276] Further investigations indicated that this solubility only extended to polar protic solvents in that addition of a second polar aprotic (acetone/ethyl acetate/acetonitrile) or an apolar (hexane/heptane) liquid resulted in solute precipitation (indicated by visible turbidity). However, crystallisation experiments using antisolvent approaches or via basic temperature manipulations (e.g. ice cooling) were ultimately unsuccessful and led to the formation of an amorphous solid or fluid depending on the relative amount of residual water and or anti-/solvent ratios. The high stability of the amorphous Gly-T matrix is noteworthy from a confectionery (and general food) perspective and suggests that the material could be employed as a crystal growth inhibitor for metastable ingredients which readily crystallise under ambient conditions, namely amorphous saccharides. A recent patent has described the use of various glycosides for the inhibition of sucrose crystallisation yet none of the examples given appear to contain glycerol as the aglycone moiety.[277]

The aforementioned crystallisation studies suggested that the ability for a liquid to participate in hydrogen bond donation rather than polarity, is necessary for facilitating dissolution of glycoin. More pertinent to confectionery applications was the complete miscibility of Gly-T with water (also a strong H-bond donor), resulting in the formation of homogenous ‘solutions’ over virtually the entire concentration range. This behaviour is reminiscent of glycerol, which is also difficult to crystallise under relatively ambient conditions (i.e. without significant supercooling/seeding) and is completely soluble in both water and lower alcohols.[278]

Given the miscibility of Gly-T with water, a series of aqueous mixtures ranging from ~ 2 to 94 wt. % were prepared either via simple dilution of the as-received Glycoin® Natural solution ($\leq$ 62.0 wt. %) or Gly-T (> 62 wt. %). In the case of mixtures that were $\geq$ 80 wt. %, brief, moderate (*ca*. 60 ^{o}C for 10 mins) heating with stirring (within sealed glass vials) was applied in order to ensure complete homogenisation. T_g analysis of solutions that were < 70 wt. % could not be evaluated as they fell below the lower temperature limit of the instrument (– 80 ^{o}C). This is demonstrated in the case of the 'as-received' solution (~ 62 wt. %, scan rate = 10 K min^{-1}) wherein the presence of an amorphous phase can be inferred from the lack of any crystallisation exotherm during cooling and via the sequential exo- and endotherms that signify cold crystallisation and subsequent melting during reheating (**Figure 4.9**). Similar supercooling and cold crystallisation have been reported in other aqueous solutions containing high concentrations polar organic compounds including citric acid and sucrose.[279, 280]

Unsurprisingly, increasing the concentration of Gly-T resulted in an increased T_g, which ranged from *ca*. – 74.4 to -6.8 ^{o}C for ~ 70 to 94 wt. % solutions (**Figure 4.10** and **Table 4.1)**, wherein a single glass transition was the only noteworthy signal within the corresponding thermograms (full traces are shown in **Appendix Figure B.3**). This indicated that all were homogenous mixtures given that phase separation should have resulted in the formation of multiple glassy phases of different concentrations (i.e. one would be freeze concentrated/diluted with respect to the other) which should display non-equivalent T_g.

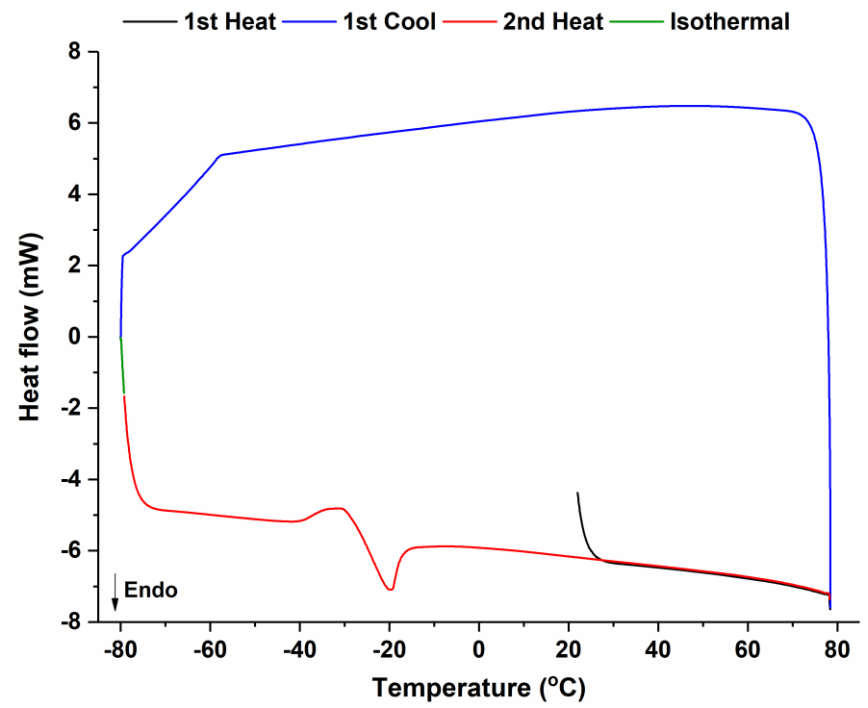

Figure 4.9: DSC thermogram of as-received Glycoin® natural solution showing first heating (black), first cooling (blue) and second heating (red) cycles (recorded using a scan rate of 10 K min^{-1}). Originally in colour.

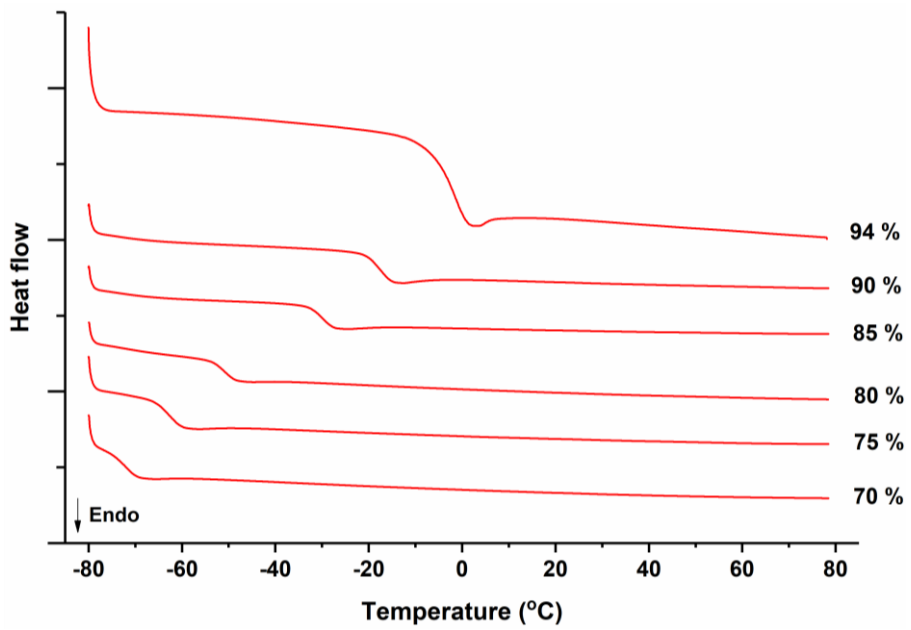

Figure 4.10: Second heat cycles for aqueous Gly-T solutions of approximately (from bottom to top) 70, 75, 80, 85, 90 and 94 wt. % (from – 80 to 80 °C at 5 K min^{-1}). Large *y*-axis tick marks correspond to 5 mW. Originally in colour.

Table 4.1: T_g data for Gly-T and aqueous solutions thereof at varying concentrations.

Gly-T concentration (wt. %)	T_g (°C)	
	Onset	Midpoint
69.9	- 74.4	-71.7
74.9	- 65.8	- 62.8
80.1	- 53.7	- 50.9
85.0	- 32.8	- 29.8
90.0	- 20.9	- 17.3
94.3	- 6.8	- 2.1
'anhydrous'	26.1	29.2

The T_g of carbohydrate-water matrices ($T_{g,mix}$) can often be well described by the Gordon-Taylor equation (**Equation 4.1**), as has been demonstrated in the case of various polyols and mono- or di-saccharides:[275, 281]

$$T_{g,mix} = \frac{w_s T_{g,s} + k_{GT} w_w T_{g,w}}{w_s + k_{GT} w_w} \qquad \textbf{Equation 4.1}$$

Where w_i is the mass fraction of component i, the subscripts s, w and mix denote the solute, water and mixture respectively and k_{GT} is a system-dependent empirical constant which essentially describes the sensitivity of the amorphous solute matrix to water plasticisation. Roos has previously suggested that k_{GT} is linearly related to the anhydrous T_g (onset) of the molten carbohydrates/polyols and can be well-described (R^2 = 0.920) via the regression equation (**Equation 4.2**):[275]

$$k_{GT} = 0.0293\, T_{g,s} + 3.61 \qquad \textbf{Equation 4.2}$$

Employing this relation for anhydrous Gly-T (onset = 26.1 °C) gives k_{GT} = 4.37 which when used in **Equation 4.1** gives a good, albeit systematic underprediction of the experimental T_g (by *ca.* 5 K). This can be improved by lowering k_{GT}, for instance setting k_{GT} = 4.00 provides a very accurate

description of the experimental data as shown in **Figure 4.11a**. Consistent with the previous analyses of neat Gly-T, the measured T_g values of the aqueous amorphous phase most closely resemble those containing a smaller monosaccharide. This is highlighted via comparison with Gordon-Taylor plots for other common free sugars using experimental data from the literature (**Figure 4.11b**).[275] For most single confectionery ingredients, the minimal a_w that can be achieved is primarily influenced by the solubility viz. x_s which is sufficiently low in most cases that $x_w >> x_s$ and results in only high to moderate a_w values at saturation (at 25 ^oC), as shown in **Figure 4.12**.[78, 89, 282-284]

In the case of glycoin, the target a_w range for aqueous confectionery can be readily approached at *ca*. 70 - 90 wt. % which is not possible for most of the other solutes due to their limited solubilities. Aside from glycerol, only fructose could be considered remotely comparable in terms of being able to sufficiently lower a_w as a single solute. On a wt. % basis both glycerol and fructose are more effective than glycoin at reducing a_w (**Figure 4.12a**), primarily through the colligative effect due to their lower molecular masses. Yet glycoin is more potent than both on a molar basis and is instead more comparable to sucrose (see **Figure 4.12b**).

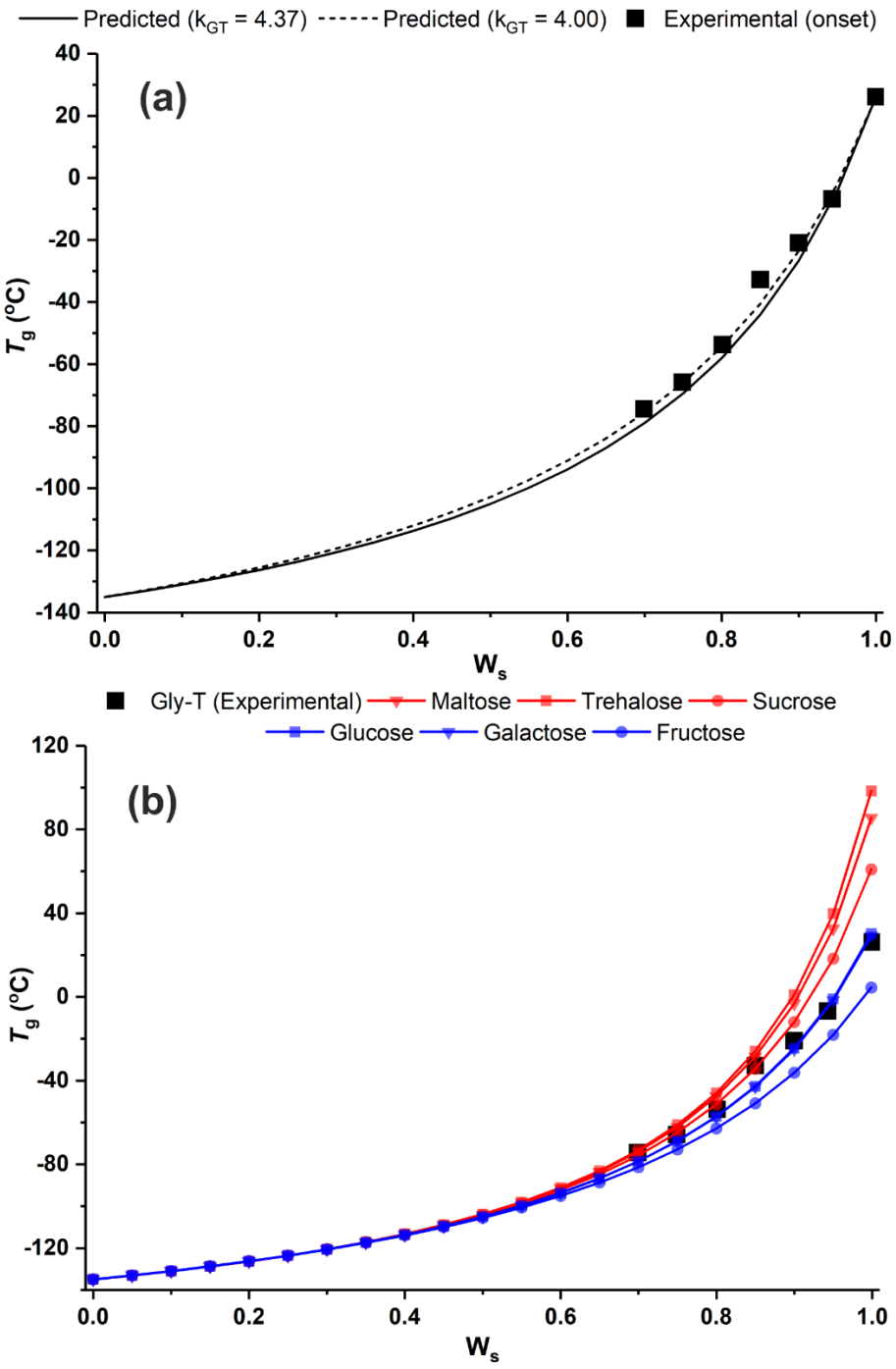

Figure 4.11: (**a**) Experimental and predicted T_g of aqueous Gly-T solutions as a function of solute mass fraction calculated using **Equation 4.1**, (**b**) comparison of experimental T_g of aqueous Gly-T solutions with various common mono- (blue) and di-saccharides (red) (data taken from Roos).[275] Originally in colour.

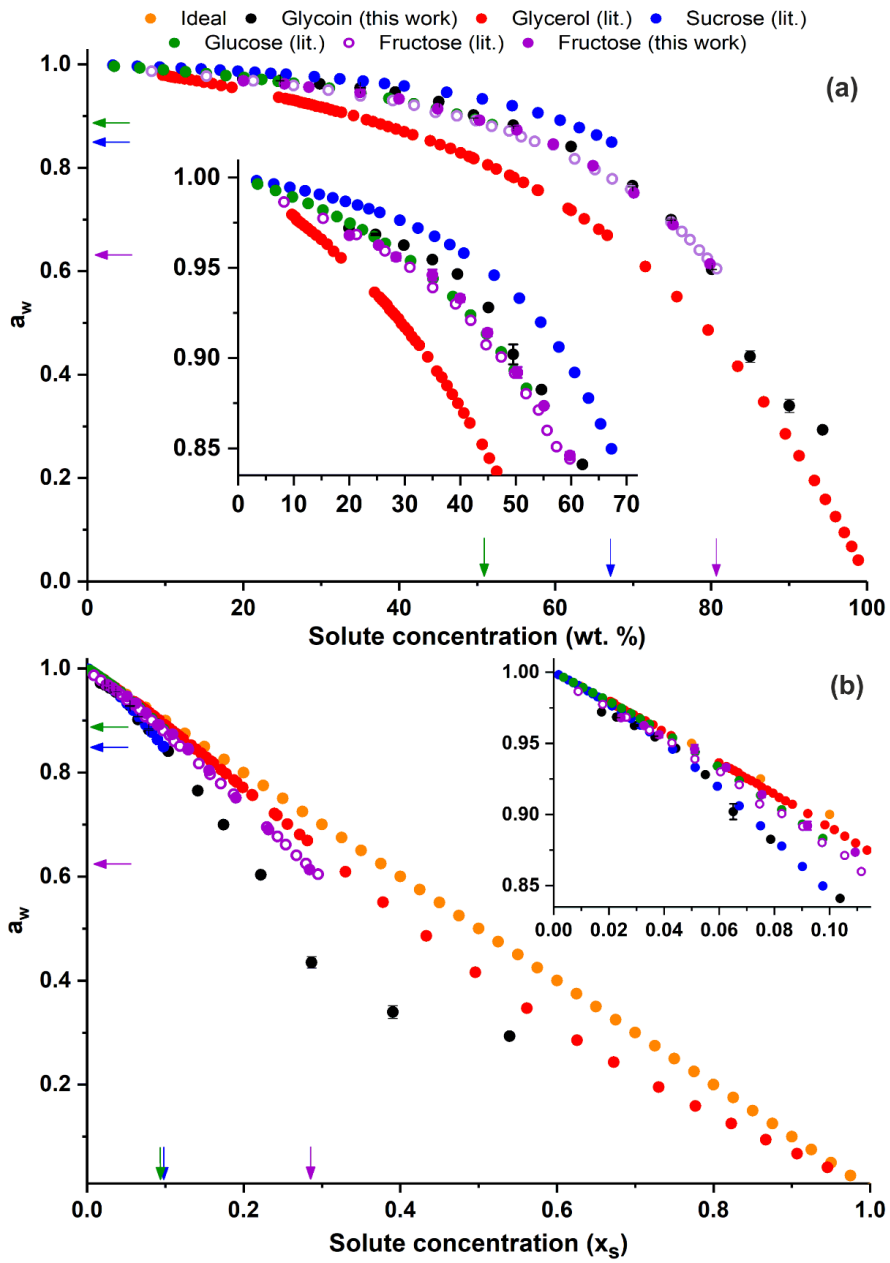

Figure 4.12: Experimental a_w (25 °C) of aqueous glycoin and comparison with selected confectionery solutes as a function of solute concentration either represented as wt. % (**a**) or x_s (**b**). Literature data is taken from Scatchard *et al*. (sucrose),[282] Baeza *et al*. (fructose),[89] Bonner and Breazeale (glucose)[283] and Rudakov and Sergievskii (glycerol),[284] respectively. Solubility limits (represented by coloured arrows) are taken from Ergun *et al*.[78] Error bars represent $\pm$ 1 standard dev. Originally in colour.

In a parallel experiment, an isopiestic moisture sorption 'isotherm' (n.b. the temperature was not strictly regulated but was maintained at *ca*. 21 $\pm$ 1 ^{o}C) was constructed via equilibration (inferred via a plateau in moisture adsorption – see **Appendix Figure B.4**) of Gly-T over saturated salt slurries of known a_w (**Figure 4.13**) for 69 days. Despite the significant error displayed by several samples, there is generally good agreement between the mean values obtained through this method and those from the commercial a_w meter, especially when considering the small discrepancy in temperature. It can be seen that even under conditions of very low a_w (i.e. low RH), glycoin displays some propensity towards moisture adsorption which becomes increasingly significant at intermediate levels. This is consistent with visual observations of its considerable hygroscopicity under ambient conditions. This behaviour is similar to glycerol but notably different to that of structurally similar crystalline solids (when accounting for hydrate formation) which instead, adsorb only a minimal amount of water (*ca*. 0.01 – 0.10 wt. % dry basis)[285-287] prior to reaching a characteristic deliquescent a_w (equal to that of the supersaturated solution) which manifests as an inflection point on the isotherm.

It should be noted that a limited study of the moisture de-/sorption properties of mixed α-glucosyl glycerol (containing glycoin but predominantly the 1-*O*-isomers) was conducted by Takenaka and Uchiyama,[257] who reported a change of *ca*. + 7 wt. % upon increasing RH from 60 to 75 % and a change of - 6 wt. % when decreasing RH from 60 to 35 %. Both results are considerably lower than those found in the present work (*ca*. + 13 wt. % (60 to 75 % RH) or - 17 wt. % (60 to 35% RH)), which is likely a reflection of the limited equilibration time (8 versus the 69 days used in this study) and non-equivalent composition of the analyte used by Takenaka and Uchiyama, whilst the initial water content at 60% RH was also undisclosed by the authors.

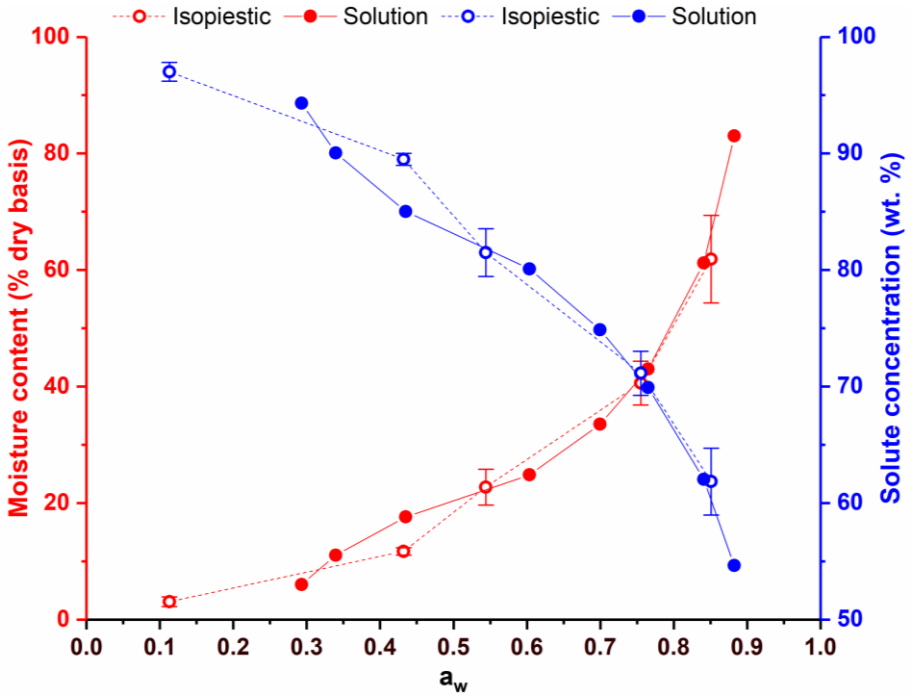

Figure 4.13: Isopiestic moisture sorption isotherm of glycoin after 69 days equilibration (red) compared with direct a_w measurements made using aqueous glycoin solutions (blue) with lines added to aid visual representation. Error bars represent $\pm$ 1 standard dev. Originally in colour.

All of the aqueous glycoin solutions displayed negative deviations from ideal behaviour (i.e. $a_w < x_w$) and especially at large solute concentrations. This is visualised through a plot of concentration against the activity coefficient of water, y_w (**Figure 4.14**). As described in **Chapter 1** and **Chapter 3**, the non-ideal solution behaviour is generally described through the Norrish constant, K_N which is obtained via a plot ln y_w vs. x_s^2. When compared to archetypal confectionary solutes, the K_N determined via linear regression for glycoin up to 85 wt. % (using the solution a_w data) was - 5.77 ($R^2 = 0.995$) (**Figure 4.15**), which falls close to that of common disaccharides (e.g. trehalose ≈ 6.6, sucrose ≈ 6.0 - 6.5).[89, 242, 288] This is consistent with earlier conclusions (see **Chapter 3**) and other studies that have concluded that a_w lowering in aqueous sugars/sugar alcohols is predominantly influenced by solute size when controlling for structural similarity.[246, 289-291] The aforementioned findings underscore the potential of glycoin as an a_w lowering agent as it displays a combination

of potency (approaching that of sucrose) with a relatively low molecular mass and almost unparalleled solubility.

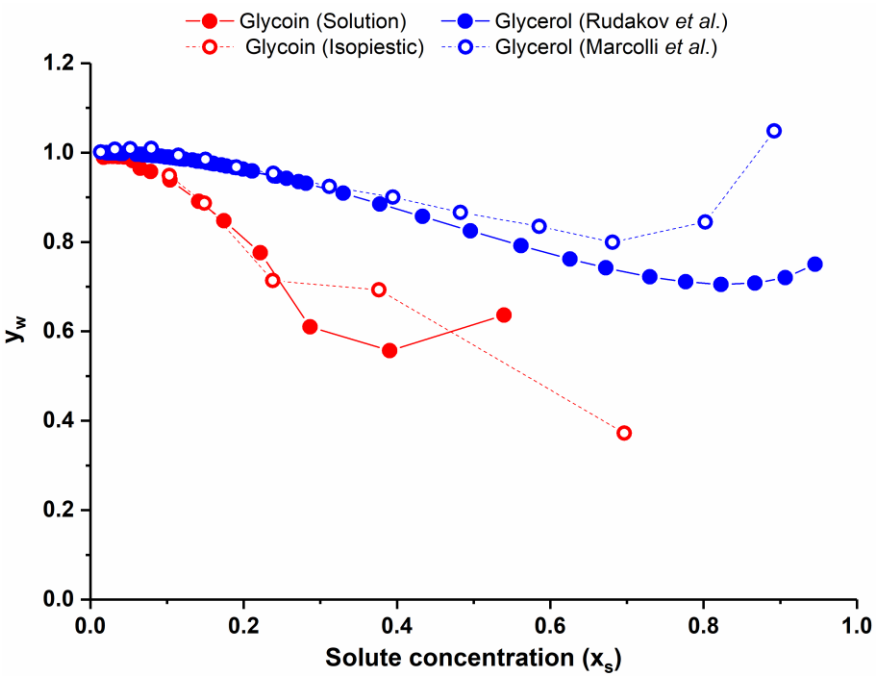

Figure 4.14: Variation in the activity coefficient of water (y_w) with solute mol fraction (x_s) for aqueous solutions of glycoin (red) and glycerol (blue - data is taken from Rudakov *et al*. and Marcolli *et al*).[284, 292] Lines have been added to aid visualise representation. Originally in colour.

As has been noted previously (see **Chapter 3**), application of the Norrish equation using a single value of K_N cannot offer an accurate description of the solution a_w over the entire concentration range. The data presented in **Figure 4.14** indicates that this is also the case for the glycoin-water system wherein y_w may actually reach a minimum at $x_s \approx 0.3$ - 0 .5 (*ca*. 85 - 95 wt. %), although this was not reproduced using the isopiestic data which instead decreased monotonically with increased x_s. This reduction ultimately results in the lowering of K_N with the overall fit found to be increasingly poor when the data points for 90 and 94 wt. % mixtures were included (**Figure 4.15a**). It is interesting to note that a y_w minimum has been reported for the sucrose-water system according

to a meta-analysis of the data (at $x_s \approx 0.5$, 95 wt. %)[193] and also appears to manifest in aqueous solutions of glycerol at $x_s \approx 0.7$ - 0.8 according to multiple published data sets (**Figure 4.14**).[284, 292] Yet this must be verified for the glycoin-water system by further repeat measurements under highly controlled (humidity) conditions.

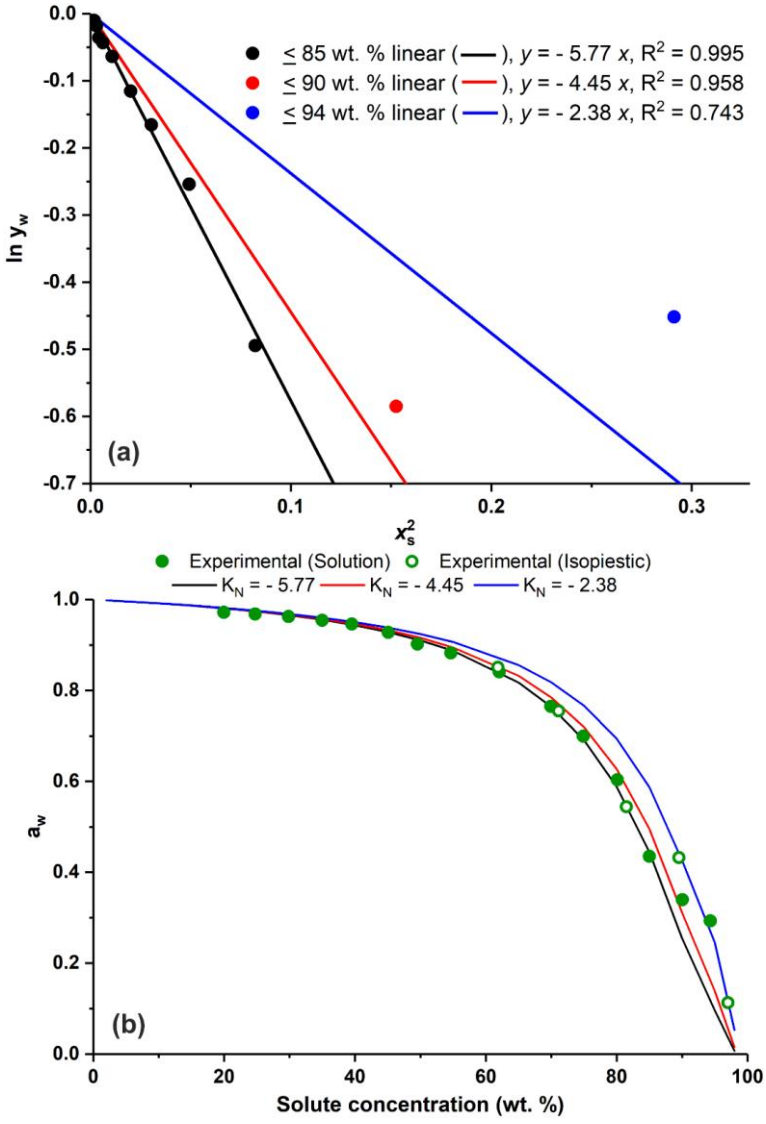

Figure 4.15: Determination of the Norrish constant (K_N) via linear plots of ln y_w vs. x_s^2 for aqueous glycoin solutions up to *ca*. 85 (black points), 90 (black and red points) and 94 wt. % (black, red and blue points) (**a**) and comparison of predicted a_w with experimental data (**b**). Originally in colour.

4.3. Summary

The natural osmolyte 2-O-α-D-glucopyranosyl glycerol a.k.a. glycoin was identified as a possible replacement humectant/plasticiser for common confectionery sugars owing to obvious structural similarities and various attractive confectionery-relevant properties (low digestibility/cariogenicity, sweet taste). Given the surprising lack of information in the literature regarding the influence of glycoin on physicochemical properties of interest (namely a_w and T_g), an experimental investigation was undertaken in order to assess performance as a potential sugar substitute. Initial characterisation (via LC-MS and NMR) validated the high enantiopurity and concentration of glycoin within a commercial aqueous solution (Glycoin natural®). The presence of impurities (most likely carbohydrate-/derivatives) could also be detected albeit in seemingly low amounts, although exact quantification was not possible at owing to the complex mix of species within the analyte. Following either simple water dilution or dehydration and subsequent dilution of the resulting 'anhydrous' glycoin, it was possible to prepare a range of binary water-glycoin mixtures that were subsequently analysed for both T_g (via DSC) and a_w (using a commercial a_w meter) determination. Surprisingly, anhydrous glycoin was found to remain amorphous throughout experimentation and could not be crystallised using basic temperature and solvent manipulations unlike most common confectionery solutes (sucrose, glucose, fructose etc). Notably, it was also completely miscible with common polar protic liquids (including water) but immiscible with aprotics akin to glycerol, although the reasons for this remain unclear at this time.

Due to the aforementioned miscibility with water, binary aqueous solutions of glycoin as the sole solute could be prepared across virtually the entire concentration range (20 to 94 wt. %). Solutions underwent supercooling to form homogeneous glasses at $\geq$ 70 wt. % glycoin, displaying T_g values that were most comparable to monosaccharides when modelled using the Gordon-Taylor equation ($k_{GT} \approx 4.00$) whilst T_g determination for less concentrated solutions ($\leq$ 62 wt. %) was impeded due to cold crystallisation during re-heating. The T_g of the anhydrous material (onset = 26.1 °C, midpoint = 29.2 °C) was also more in-keeping with that of a monosaccharide, implying that the glycerol aglycone moiety may have some

plasticising influence within the amorphous matrix although this must be confirmed using purified glycoin within a more controlled and moisture-free environment. In terms of humectancy, the a_w lowering ability (assessed using both an a_w meter and via an isopiestic moisture sorption study) of glycoin was compared to that of fructose, glucose, glycerol and sucrose and could be well described by the Norrish equation using K_N = - 5.77 up to 85 wt. %. On a weight-by-weight basis, the behaviour of glycoin was found to be very similar to fructose/glucose and superior to sucrose in the low-to-medium concentration range (< 80 wt. %) although it is notable that the minimum attainable a_w of the binary glycoin-water solution is appears to be far lower. On a molecule-by-molecule basis, the performance of glycoin was superior to lower molecular weight solutes (glucose, fructose and glycerol) and only marginally lower than the larger disaccharide sucrose. This is consistent with the hypothesis that a_w suppression by sugars is predominantly a function of solute size (**Chapter 3**). Taken together with the relatively low T_g values, the results indicate that glycoin could be effectively employed as a 'drop-in' type replacement for common confectionery sugars which motivated subsequent application within a model aqueous confectionery system (**Chapter 7**).

Chapter 5: Clean, food-grade extraction of the natural osmolyte floridoside and identification of unforeseen crystal forms thereof

Aspects of the work presented in this chapter have been published in: **A. J. Maneffa**, A. C. Whitwood, A. S. Whitehouse, H. Powell, J. H. Clark, and A. S. Matharu, Unforeseen crystal forms of the natural osmolyte floridoside, 2020, *Communications Chemistry*, **3**:128

The overarching goal of this Chapter is to investigate **Aim 2b** as described previously within section **1.4**. In particular, it seeks to evaluate the suitability of the natural osmolyte 2-*O*-α-D-galactopyranosyl glycerol (floridoside) as a replacement humectant and plasticiser for common confectionery sugars. The Chapter is divided into three principal sections:

(i) **Section 5.1**: Offers a brief overview of floridoside as a natural osmolyte with specific reference to its utilisation as a promising functional biomolecule/food ingredient and its existence within natural biomasses.

(ii) **Section 5.2**: Investigates the extraction of floridoside from the natural bioaccumulator *Palmaria palmata* and subsequently provides detailed characterisation of 'clean' floridoside-rich extracts using a variety of thermal and spectroscopic techniques, including analysis of T_g and a_w lowering capacity.

(iii) **Section 5.3**: Presents the unambiguous identification of two previously unheralded crystal forms of floridoside which are comprehensively analysed using a range of different methods and in particular, single crystal X-ray diffraction which provide some rationalisation of their disparate physicochemical properties.

5.1. Preamble

As discussed in **Chapter 1**, floridoside (2-α-*O*-D-galactopyranosyl glycerol, **Figure 5.1**) was identified as a target natural humectant due to its ubiquity as an osmolyte within most species of *Rhodophyta* macroalgae. It has already been shown in **Chapter 4** that its C4 epimer glycoin exhibits excellent a_w lowering capabilities whilst also having a relatively low T_g for a molecule of its size, making it a promising drop-in replacement for sugar-based humectants/plasticisers. According to the KB analysis presented in **Chapter 3**, it would be expected that the same should hold true for floridoside given their virtually identical size and high structural similarity.

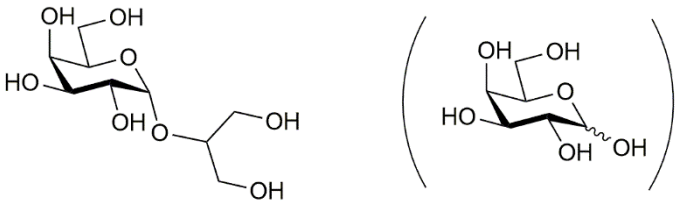

Figure 5.1: Skeletal structural formulae of floridoside compared with that of its parent monosaccharide galactose.

The presence of floridoside in nature was first formally recognised in 1930 by Colin and Gueguen who initially isolated it from the red macroalga *Palmaria palma*ta.[293] Early work on the compound quickly recognised its importance in osmotic acclimation, yet there is now an emergent picture of floridoside as a multifunctional biomolecule. Indeed, it has now been implicated as an important regulator of *inter alia* transient carbon storage/polysaccharide biosynthesis and the mitigation of oxidative stress, heat shock and dessication.[294-297] Given this multifunctionality, it is unsurprising that floridoside has attracted interest from both academia and industry for use across a wide variety of applications

including; neuroinflammatory supression,[298] antibiotic potentiation,[299] cosmetics[300] and nutraceuticals.[301, 302]

Additionally, there have also been previous works that describing the use of floridoside within the context of foodstuffs. For instance, it has been patented as an antifreeze agent for beef and touted as a potential "sweetener" owing to a purported low Maillard reactivity and lack of cariogenicity.[303, 304] The food safety of floridoside is inferred from the considerable precedence for consumption of floridoside-containing biomass e.g. Nori (*Porphyra tenera*) (which can contain up to 10 dry wt. % floridoside), which constitutes a significant part of the traditional East Asian diet.[305] It is also noteworthy that various red algae within which floridoside is naturally accumulated are permitted for use as "flavour enhancers" under the US Food and Drug Administration and appear to be GRAS.[306] However, despite this academic and commercial interest, there have been no published studies that examine the relevant physicochemical properties, namely a_w and T_g of either floridoside or its aqueous solutions to the best of this author's knowledge.

In addition to attractive functional properties, a particularly promising aspect of floridoside utilisation as a 'natural' humectant/plasticiser is its abundance within a variety of natural *Rhodophyta* macroalgae. Macroalgae or seaweeds represent an ideal source of food ingredients as they themselves are generally considered as healthy 'functional foods' or 'nutraceuticals' and are already cultivated at scale, with global production (all types) estimated at close to 30 million tonnes.[307] As mentioned in **Chapter 1**, the harvest of several genera of the *Rhodophyta* e.g., *Gracilaria* and *Porphyra* already exceeds one million tons (wet basis)[129] whilst the floridoside content within certain species can reach up to *ca*. 25 wt. % (dry basis) depending on growth conditions.[130] One of the most prominent sources is *Palmaria palmata*, commonly referred to as dulse, which is extensively distributed across the Northern Atlantic Ocean and widely consumed within the Western world.[308] Due to the increasing interest in floridoside and its often

high intercellular accumulation, many studies have described the extraction of the title compound from various *Rhodophyta* including for instance; Simon-Colin *et al*. (*Palmaria palmata*), Courtois *et al.* (*Mastocarpus stellatus*), Li *et al*. (*Laurencia undulata*) and Rødde *et al*. (*Palmaria palmata*).[309-312] However, given that the objective of those studies often focussed on obtaining material of high purity (e.g. for single crystal determination or biological trials), they were generally very poor yielding and involved a multitude of purification steps that employed vast quantities of highly problematic auxiliaries (e.g. $CHCl_3$, CH_2Cl_2 , acids etc.). As the aim of the present study is to ultimately collect floridoside in sufficient quantities so as to evaluate a_w and T_g in addition to potential application within model confections, a high yielding 'clean' process that is capable of producing it at scale ($\geq$ 100g) in as pure a form as possible must first be established.

5.2. Results and Discussion

5.2.1. Identification and characterisation of food-grade, floridoside-rich extracts from *Palmaria palmata*

Given that previous work in the literature had identified the red macroalga *Palmaria palmata* as a high intracellular accumulator of floridoside, coupled with the fact that it is widely available within the UK, efforts were initially focussed on investigating the extraction of the title compound from the aforementioned biomass. Following partial drying under reduced pressure (24 h, 50 °C, 20 mbar), the biomass (shown in **Figure 5.2a**) was found to contain approximately 12 wt. % ash according to TGA (**Figure 5.2b**) based on mass loss > 600 °C, of which ~ 80 % was volatilised prior to reaching the maximum operating temperature (1300 °C). ICP-OES analysis indicated that the most abundant metal-/loids present within the biomass included namely K, followed by Na and to a lesser extent S, Ca and P (**Appendix Table C.1**). Separate elemental microanalysis detected a significant quantity of Cl (3.58 wt. %) along with the expected C (35.28 wt. %), H (5.36 wt. %) and N (2.22 wt. %). Surprisingly, a small amount of F (0.22 wt. %) was also detected which may originate from several organofluorine compounds that have previously been identified in *Palmaria palmata*.[313] The high K, Na and Cl content

can be attributed to KCl and NaCl, both of which (and especially the former) are known to be the major inorganic constituents of dulse.[130]

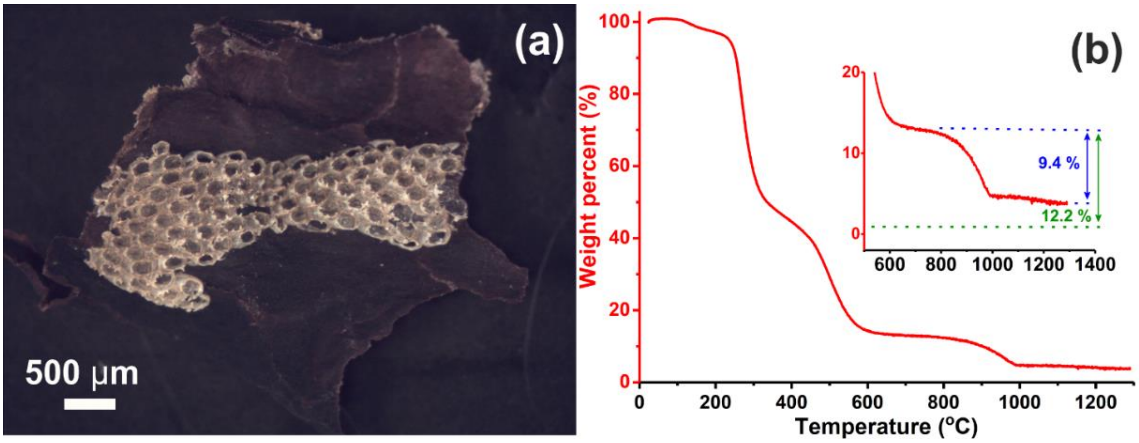

Figure 5.2: Optical microgram (**a**) and TGA (**b**, T = 24 - 1300 °C, 10 K min^{-1}, N_2: air 20:100 mL min^{-1}) of as-received *Palmaria palmata* biomass. Originally in colour.

Initially water was chosen as the extracting solvent on account of its high polarity (and thus hypothesised solubilising power of floridoside) coupled with attractive 'green' and 'clean label' credentials. The extraction process involved simply stirring dried ground and sieved biomass in neat refluxing water for 24 h, with the resulting filtrate concentrated via heating *in vacuo* to yield a glassy brown and hygroscopic solid (**Figure 5.3a**). The spent macroalgae (which was visibly softer and less structurally rigid following extraction, **Figure 5.3b**) was also dried *in vacuo*. The dried, hygroscopic extract was found to be amorphous according to DSC analysis, exhibiting a clear glass transition with T_g (midpoint) ≈ 47 °C and a comparative lack of any other notable signals (**Figure 5.3c**). High-temperature TGA indicated that the extract was constituted of a significant amount of the thermally stable inorganic matter which persisted following decomposition of the organic fraction (cf. mass loss at ~ 200 – 550 °C) before undergoing volatilisation starting at *ca*. 550 °C (**Figure 5.3d**). This was further corroborated by a comparative lack of C (23.12 wt. %) and H (4.21 wt. %) content within the water

extract with respect to the untreated biomass. There was also a measurable N content (0.93 wt. %) which suggested that partial free amino acid/peptide/protein extraction from the biomass had also occurred.

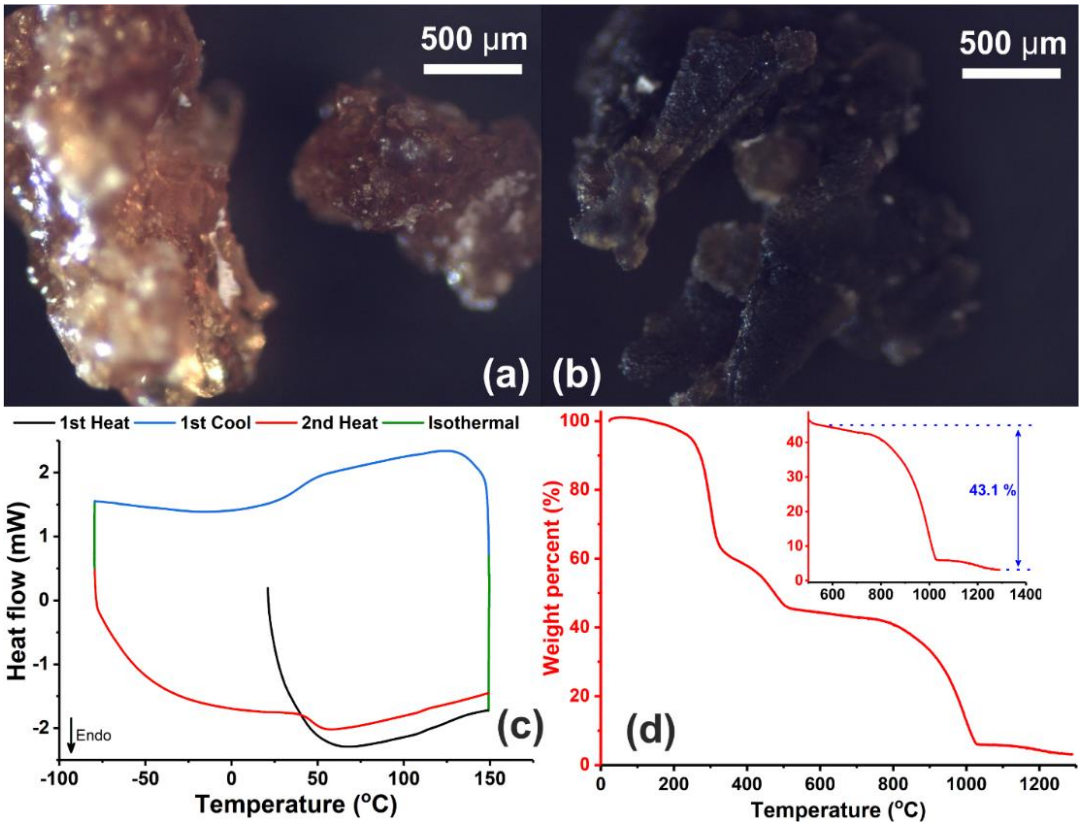

Figure 5.3: Optical micrographs of the dried H_2O extract (**a**) and residual (**b**) *Palmaria palmata* following refluxing water extraction with corresponding DSC (**c**) and TGA (**d**) traces of the former. Originally in colour.

The organic contents of the extract were characterised via ^{1}H NMR spectroscopy which indicated the presence of multiple species on account of the number and complexity of observable signals (**Figure 5.4**). Aside from the dominant signal corresponding to the residual protic solvent at 4.75 ppm, it can be seen that most of the others manifest within the 3.5 – 5.5 ppm region, indicative of moderately deshielded protons. It is likely that these originate from other small molecular weight osmolytes such as taurine and isethionic acid which have also been recently identified by Kulshreshtha *et al*. in the

aqueous EtOH extracts of other red macroalgae.[314] There are also clusters of peaks at comparatively lower frequencies (1.0 - 2.5 ppm) which likely originate from methyl/methylene protons belonging to amino acids, triglycerides etc. whereas virtually no significantly downfield-shifted signals can be observed (aside from a small singlet at ~ 8.50 ppm), indicating the absence of phenolics/aldehyde moieties.

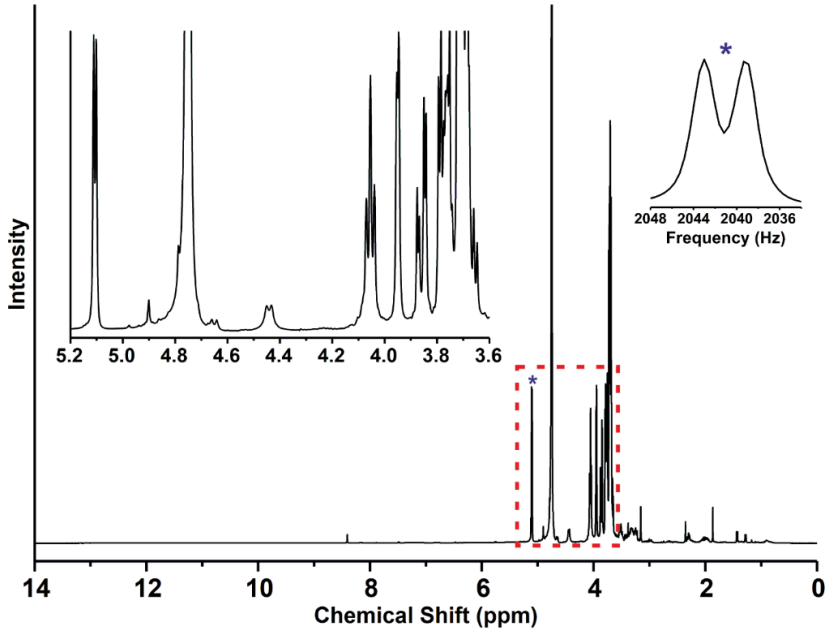

Figure 5.4: ^{1}H NMR (400 Hz) spectrum of refluxing water extract of *Palmaria palmata* recorded in D_2O (referenced with respect to HOD at 4.75 ppm). Originally in colour.

Satisfyingly, signals corresponding to floridoside – such as the relatively intense doublet and triplet at *ca*. 5.10 and 4.10 ppm respectively were in-keeping with the values quoted in the literature and highlighted the high relative concentration of the target molecule within the extract.[297] In particular, the former signal, which originates from the anomeric proton, displays a relatively small coupling constant ($^{3}J_{H1,H2}$ = 3.8 Hz) and is diagnostic of an α-substituted pyranose (cf. glycoin – see **Chapter 4**). This was further corroborated by ^{13}C NMR spectroscopy, wherein nine prominent signals could be readily observed (**Appendix Figure C.1**) along with one further discernible (albeit far less intense) peak at

approximately 100.5 ppm. This likely corresponds to an anomeric carbon of another saccharide and would be consistent with the detectable protons in the anomeric region of the ^{1}H spectrum (4.4 – 5.9 ppm).

The significant salt content (presumably KCl/NaCl) in the extract was not surprising given its relative abundance within the as-received biomass and significant solubility of the principal species in water (33.7/27.6 wt. % for KCl/NaCl in water at 80 °C respectively).[315] Unfortunately, significant amounts of such components (which are often perceived as salty and bitter/metallic tasting) would be incompatible with the organoleptic profile that is general required for confectionery products. Therefore, the use of water as an extractant was not extended further although it had however, been useful in highlighting the presence of floridoside within the macroalgal biomass and seemingly at a high concentration relative to the other water-soluble species.

On account of the aforementioned issues, it was hypothesised that ethanol would be more suitable as an extraction solvent given the comparatively limited solubility of major salt species even at refluxing temperature (< 0.1 wt. % for KCl/NaCl at 75 °C within the binary salt-ethanol system).[315] Importantly, ethanol is one of only a few solvents that are currently certified as food-grade and of GRAS status,[316] whilst it is also considered a benchmark 'green' option from a more general perspective.[317] In order to prevent potential water trituration during the extraction process, a rigorous pre-drying of the biomass via vacuum oven treatment was carried out beforehand. As the aim was to maximise the quantity of extracted floridoside in order to provide sufficient quantities for later testing, Soxhlet extraction was chosen as the most appropriate technique because the solvent is constantly recycled throughout the process which prevents the solution saturation of any extracted solutes and maximises yield.[318]

Following several preliminary experiments, an optimised extraction procedure (outlined in section **2.2.3.2**) which involved extracting *ca*. 80g of vacuum-oven dried, ground and sieved (125 – 250 μm) biomass using approximately 900 mL pure EtOH (biomass:solvent ~ 1:11 w/v) for 24 hours was developed. Following extraction, two powdered solids; an off-white material (*ca*. 2 – 3 % dry yield) collected directly after the extraction and a second cream/sandy-coloured material (*ca*. 15 – 20 wt. % dry yield) collected after a series of simple preparative steps were obtained. Both of the solids were then subsequently submitted for a variety of thermal and spectroscopic analyses.

Both extracts were readily soluble in water/D_2O and initially characterised using ^{1}H NMR. At comparable concentrations (*ca*. 40 mg mL^{-1}), there were virtually no observable signals in the first extract (when normalised with respect to the HOD signal at 4.75 ppm), indicating that it was devoid of (non-exchangeable) protons (**Figure 5.5a**) and thus, predominantly inorganic in nature. Conversely, the spectrum recorded for the second extract was consistent with that of floridoside and seemingly in remarkable purity given that the previous additional signals which had been present in the hot water extract were virtually non-existent (**Figure 5.5b**). The corresponding ^{13}C spectrum and signal assignments are provided in **Appendix Figure C.2** and **Appendix Table C.2**, respectively. This purity was further corroborated by polarimetry, with the average recorded value of $[\alpha]_D^{20}$ (c 1.00, H_2O) = + 160 ° in good agreement with those provided in the literature (*ca*. + 164 °).[319, 320]

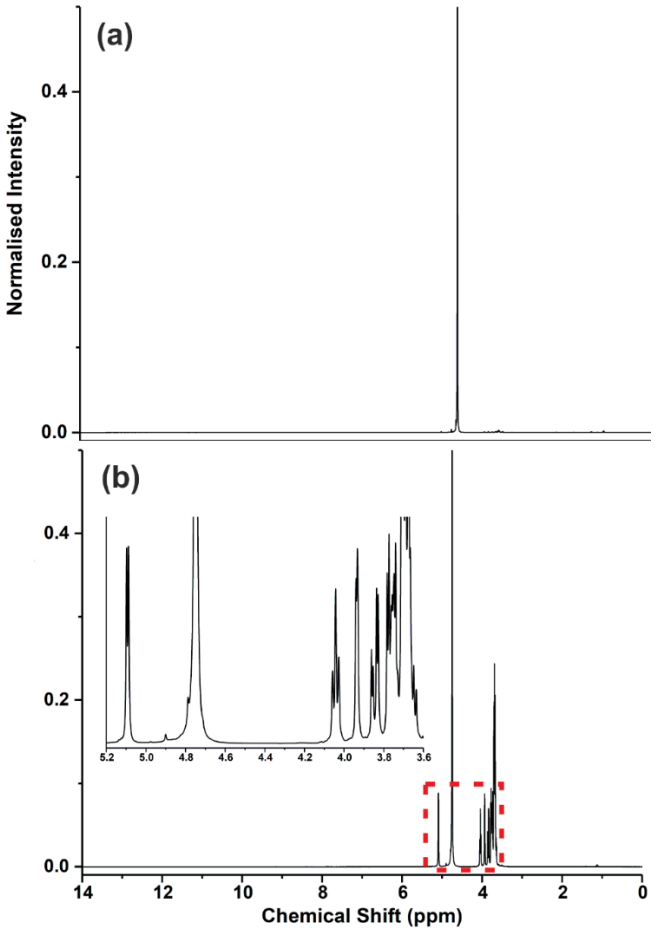

Figure 5.5: ^{1}H NMR (400 MHz) spectra of a typical first (**a**) and second (**b**) extract obtained following ethanol Soxhlet extraction of *Palmaria palmata* (referenced and normalised with respect to HOD at 4.75 ppm). Originally in colour.

Subsequent pXRD analysis confirmed that the inorganic extracts were primarily constituted of crystalline KCl on account of sharp intense peaks at 2Θ = 28.5, 40.4 and 50.1 ° and also crystalline NaCl according to several further signals, namely at 2Θ = 31.5, 45.4 ° but no other common seawater minerals (**Figure 5.6**).

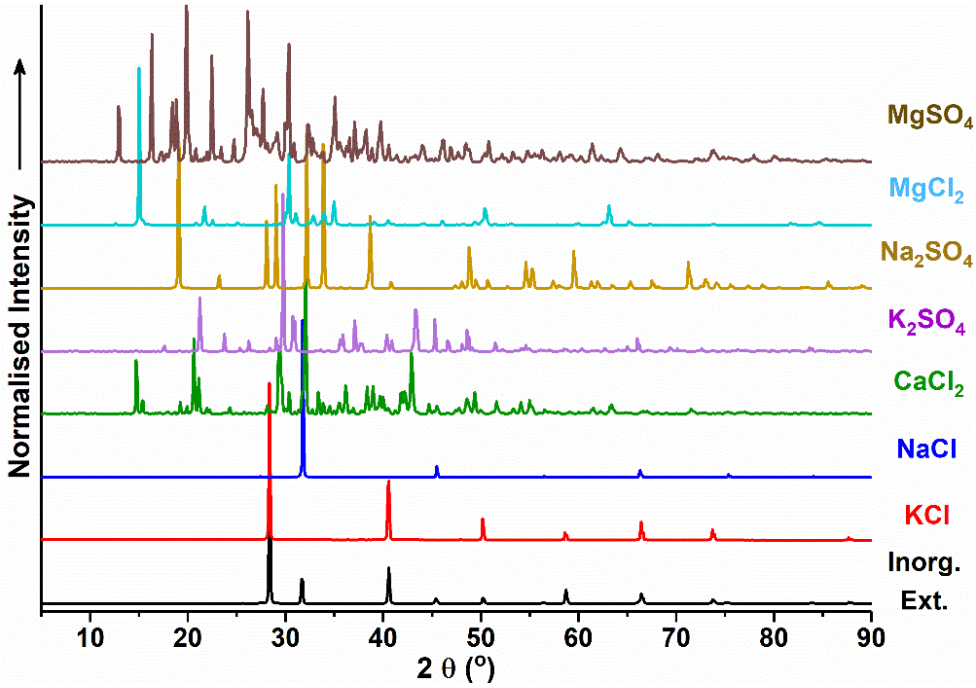

Figure 5.6: pXRD pattern for a typical inorganic extract alongside those of KCl, NaCl and other common seawater minerals. Arrow indicates direction of increasing normalised intensity. Originally in colour.

Indeed, an artificial blend of KCl and NaCl prepared via ethanol-induced precipitation of the two salts from an initial 1:1 w/w aqueous solution gave a good approximation of the corresponding pXRD pattern and TGA trace (**Figure 5.7**) with the major decomposition occurring at 750 – 1200 °C, which was found to be intermediate between that exhibited by the individual salts. It should be noted that although the initial concentrations of both inorganic species within solution were equal, the precipitated mixture is likely to be enriched in KCl due to its comparatively lower solubility (with respect to NaCl) in the EtOH-water system,[321] although this is yet to be confirmed. In a similar vein, a higher relative quantity of KCl within the Soxhlet extracts would be intuitive given its poorer solubility in pure EtOH and greater initial concentration within the biomass, resulting in preferential precipitation out of the collated solution within the solvent reservoir of the Soxhlet apparatus.

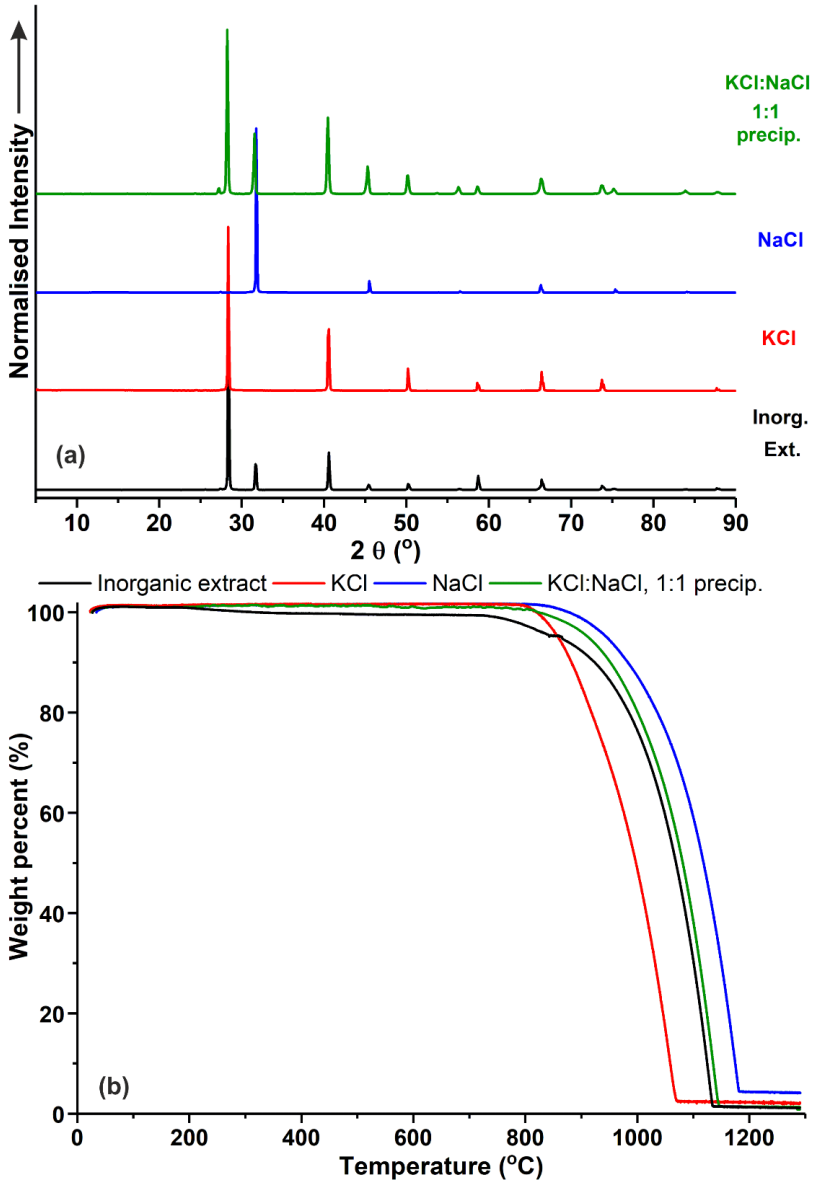

Figure 5.7: Comparison of (**a**) pXRD pattern and TGA trace (10 °C, min-1, 80:20 air:N_2), arrow indicates direction of increasing normalised intensity (**b**) of a typical inorganic extract with those recorded for an artificial KCl/NaCl mixture and neat KCl/NaCl. Originally in colour.

The procedure outlined in **Figure 2.1** represented a very reproducible method of obtaining an organic material with high floridoside purity as highlighted previously in the relevant NMR spectra. TGA indicated that these extracts also contained a small amount of KCl/NaCl on account of the characteristic decomposition at > 700 °C. In general, TGA of the organic extracts were found to follow two common

thermal events that are attributed to (i) the thermal decomposition of floridoside (200 – 320 °C) and (ii) combustion of the char produced therefrom (320 – 600 °C). Realising this and assuming that; (i) the extracts were completely devoid of volatiles (all were dried prior using a vacuum oven for 5 hrs at 80 °C/20 mbar prior to analysis) and (ii) floridoside was the sole organic constituent (cf. NMR), it was possible to simply estimate the floridoside content according to mass lost up to < 600 °C (when accounting for buoyancy, which initially resulted in an increase over 100 wt. % – cf.). Using this approach, floridoside was found to consistently represent *ca*. 90 – 95 wt. % of total extract (as highlighted in **Figure 5.8**). It should be noted that very slow crystallisation (sans stirring) from the amorphous syrup occasionally (albeit in a time inefficient and sporadic manner) led to the production of highly 'pure' floridoside (~ 99 wt. %), which was found to have a C and H content of 42.09 and 7.07 wt. % respectively - close to that calculated for pure floridoside (C = 42.52, H = 7.14, O = 50.34 wt. % based on $C_9H_{18}O_8$). Satisfyingly, the TGA method outlined above was found to be in good agreement with results of elemental microanalysis as shown in Table 5.1.

Table 5.1: Elemental microanalytical results of ground (125 – 250 μm), vacuum-oven dried *Palmaria palmata* biomass before (Entry 1) and after (Entry 2) ethanol Soxhlet extraction and typical organic extracts containing 93.8 (3a) and 99.0 (4a) wt. % according to TGA (3b and 4b).[a]

Species	**Elemental content (wt. %)**					
	1	**2**	**3a**	**3b[a]**	**4a**	**4b[a]**
C	35.33	36.89	39.92	39.88	42.14	42.09
H	5.35	5.09	6.50	6.69	7.00	7.07
N	2.21	3.17	ND	-	ND	-
Cl	3.58	NA	3.40	NA	NA	NA

[a]Estimated assuming that mass loss < 600 °C is attributable solely to floridoside. ND = Not detected. NA = Not analysed.

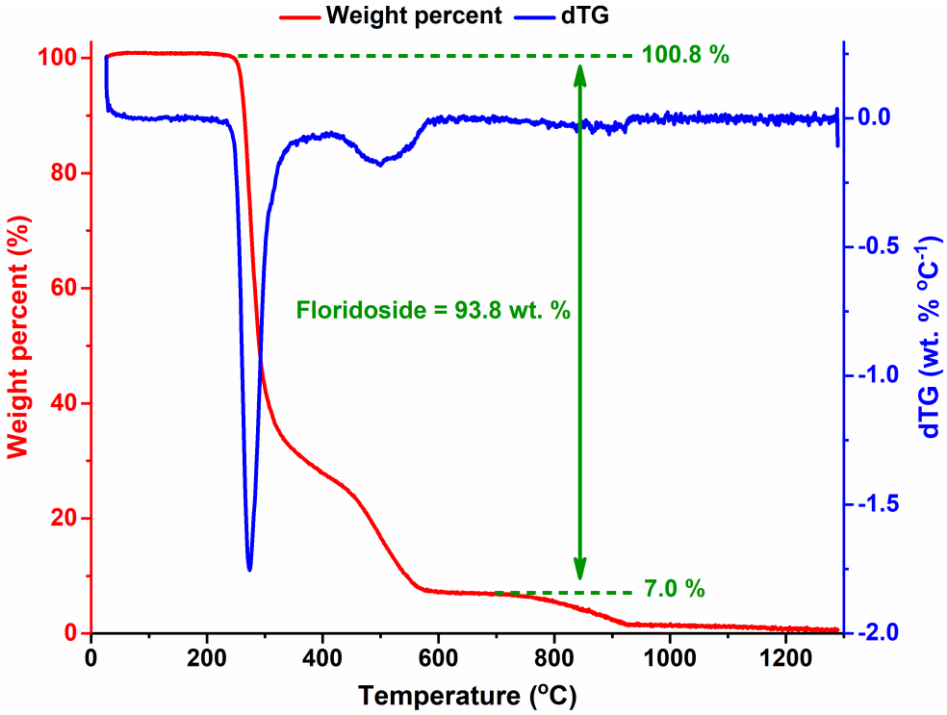

Figure 5.8: TGA and dTG (T = 25 – 1300 °C, 10 °C min^{-1}, air:N_2, 80:20) traces of a typical organic extract containing *ca*. 93.8 wt. % floridoside obtained via ethanol Soxhlet extraction of *Palmaria palmata*. Originally in colour.

Taking into account the estimated floridoside content within the organic extracts, the overall isolated floridoside yield using the ethanol Soxhlet extraction approach is calculated to be between 15 – 20 wt. % of biomass (dry basis) which is very high in terms of natural product extraction. This fact, coupled with the facile nature and green credentials of the methodology presented herein demonstrates a highly promising, food grade and 'clean' route to bio-based floridoside which offers up new opportunities for further research and development that have otherwise been stifled by an acute lack of readily available substrate.[297]

Because the nature of the Soxhlet extraction method maintains a maximal concentration gradient with respect to the analyte throughout the experiment, it is conceivable that the results of this work may represent a 'best-case' scenario in terms of floridoside extraction directly from the biomass. However,

as the overall aim was ultimately to collect enough so as to enable subsequent medium lab scale experiments (~ 100g), no further attempts to optimise the extraction method (e.g. via biomass particle size, solvent and biomass loadings, time etc.). Additionally, it is also pertinent to note that the extraction yield will ultimately be limited by the *in-vivo* floridoside accumulation within the macroalgae which itself is known to vary depending on a multitude of factors (temperature, salinity, nitrogen content, sunlight etc.) and should be the most important future consideration for optimising floridoside production via this approach.[311]

Unlike the hot water extract, the organic fraction obtained via ethanol Soxhlet extraction was found to be crystalline according to DSC, with the purest material exhibiting a sharp melting endotherm at $T_m \approx$ 139 ºC which became increasingly depressed and broadened with increasing salt content (**Figure 5.9a**). In all cases, the molten phases underwent supercooling and exhibited T_g values of *ca*. 31 ºC during the second heating cycle (**Figure 5.9b**). It is interesting to note that these values are very close to those recorded for Gly-T (**Chapter 4**) and also of other comparatively smaller monosaccharides (glucose/galactose). This is again suggestive of a plasticising role of the glycerol moiety within the amorphous melt (potentially via reduced packing/increased free volume etc.) and promising for application as a confectionery plasticiser. Notably, the melting point of the high purity sample was considerably greater than the ranges quoted in most of the literature 127 – 129 ºC,[320] with that reported by Craigie *et al.* being closer but still somewhat low (132 – 134 ºC), although the authors provided no further characterisation or comment regarding this result.[322]

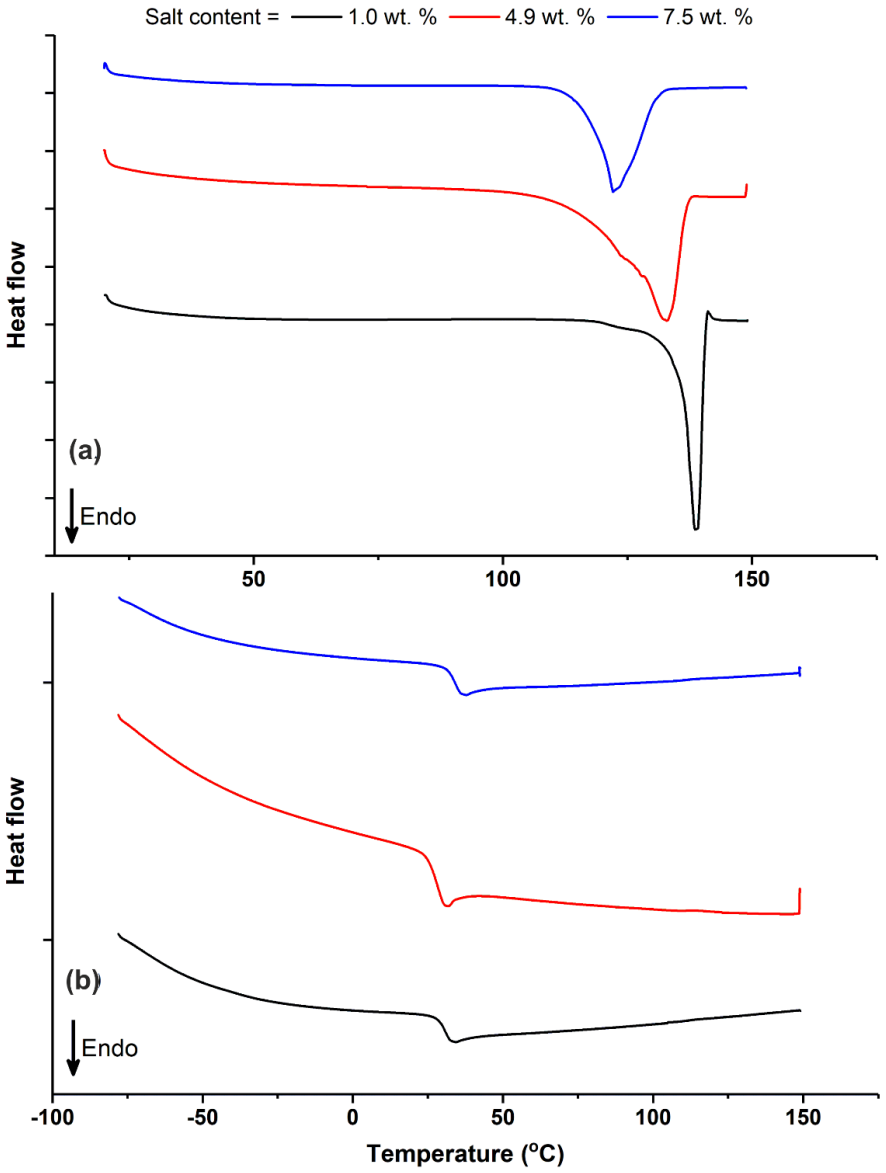

Figure 5.9: First (**a**) and second (**b**) heat cycles of floridoside-rich organic extracts with varying salt contents obtained via ethanol Soxhlet extraction of *Palmaria palmata*. Tick marks along the *y*-axes correspond to 5 mW. Originally in colour.

The crystalline nature of the organic extracts was also borne out by pXRD analysis, wherein myriad of new signals were visible alongside those originating from KCl/NaCl (**Figure 5.10**) but surprisingly, very different to that simulated using single crystal data for crystalline floridoside (Flor-Cry) isolated by Vonthron-Senecheau *et al*. (which was identical to that published earlier by Simon-Colin and co-

workers).[312, 323] For instance, it can be seen that prominent peaks at 2Θ = 7.4 and 19.6 ° are absent whereas otherwise unheralded signals at 14.0, 15.3 and 20.6 ° are instead visible. This was highly indicative of a seemingly novel crystal form (i.e. polymorph) of floridoside which instigated a more thorough subsequent investigation (section **5.2.2**). Given that the molecular packing within such non-equivalent crystal lattices is often quite disparate, this can often lead to notable differences in the thermal stability of the individual polymorphs as has been reported in D-sorbitol for instance, which exhibit melting point differences of > 10 °C.[324] This would explain why the observed melting point range was somewhat higher than those given in the literature which have historically been very comparable to the values provided by Simon-Colin *et al*. and Vonthron-Senecheau *et al*. for the corresponding crystal form described therein.[312, 323]

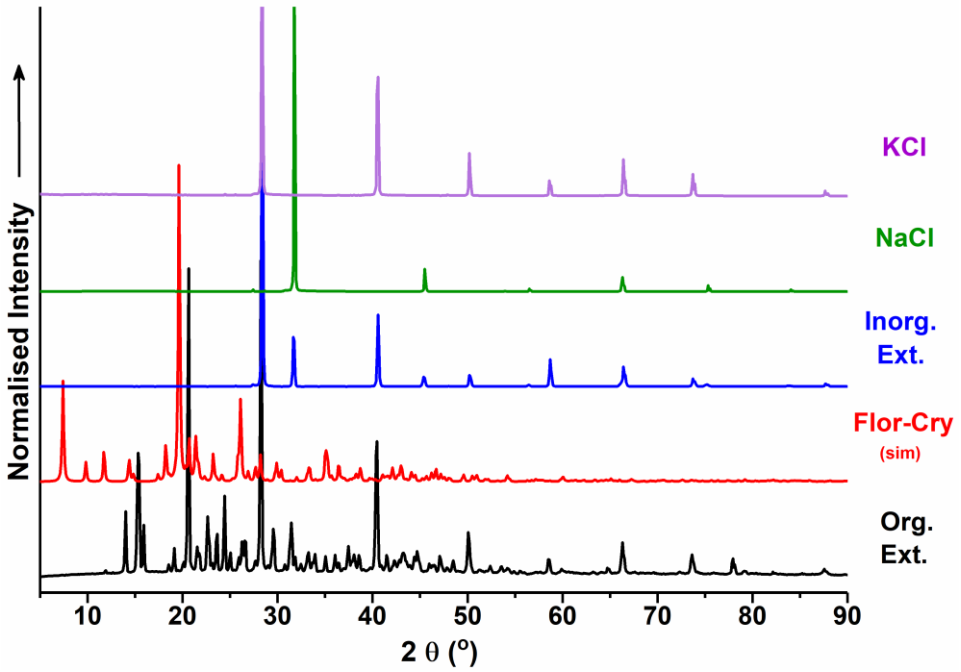

Figure 5.10: pXRD spectrum of typical organic extract compared with selected other spectra including that which was simulated for floridoside using the single crystal data of Vonthron-Senecheau *et al*.[323] Arrow indicates direction of increasing normalised intensity. Originally in colour.

The corresponding FTIR spectra were virtually identical for all of the isolated organic extracts (an example is shown in **Figure 5.11**), irrespective of the salt content. As KCl and NaCl are IR transparent (see red trace in **Figure 5.11**), the origin of the observable signals is attributable solely to floridoside. Indeed, the series of bands at > 3200 (O-H stretching) 2800 – 3050 (C-H stretching), 1200 – 1400 (C-H/O-H bending) and 950 – 1200 cm^{-1} (C-O-C/C-C stretching etc.) are in-keeping with the structural features of the floridoside molecule.

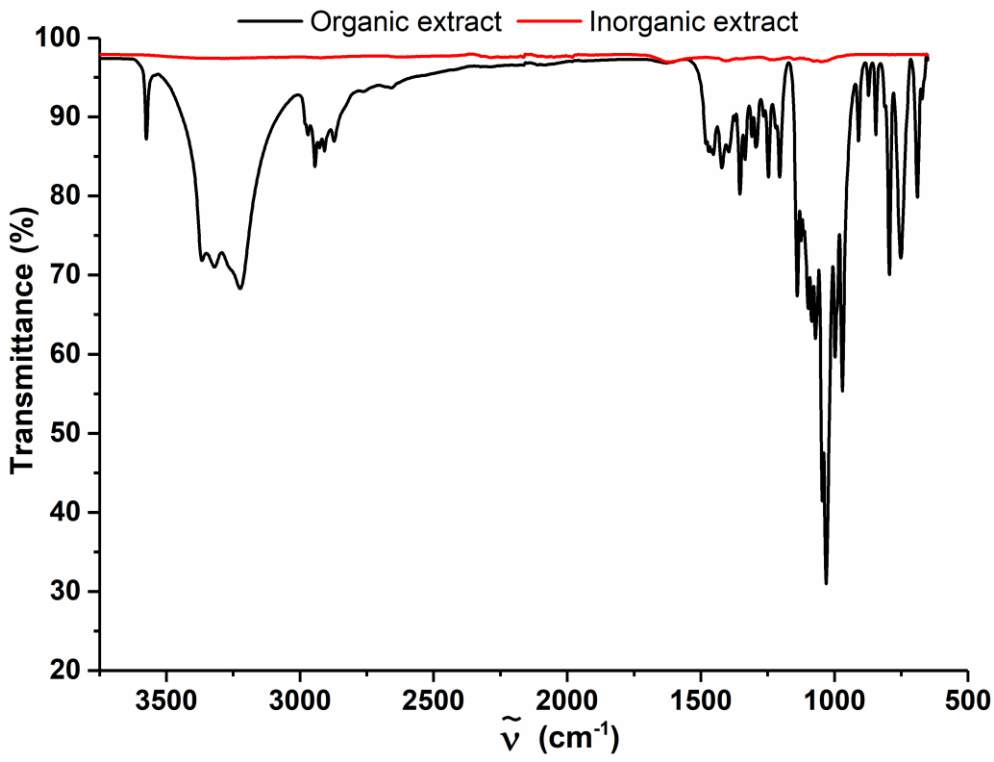

Figure 5.11: Mid (650 – 3750 cm^{-1}) ATR-FTIR spectra of a typical organic and inorganic extract obtained following ethanol Soxhlet extraction. Originally in colour.

Surprisingly, upon dissolution in water, the sandy coloured organic extract (*ca*. 92.5 wt. % floridoside, **Figure 5.12a**) gave rise to initially pale-yellow solutions which darkened to a brown appearance upon progressive concentration (**Figure 5.12b**). This is indicative of the presence of pigment/s co-extracted concomitantly alongside the floridoside. The a_w of the solutions was measured and compared with those

containing common confectionery solutes (sucrose and fructose). Owing to a limited quantity of material only one such extract could be investigated in this way, with the sample chosen having a median-level of salt content (*ca*. 7.5 wt. %) so as to provide a reasonable representation of the typical extract composition.

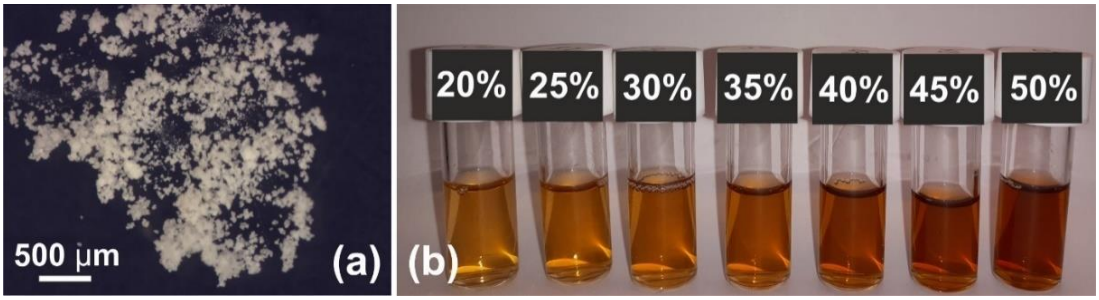

Figure 5.12: Visual appearance of a typical floridoside-rich organic extract (*ca*. 92.5 wt. %) (**a**) and following dissolution in water at 20 – 50 wt. % (**b**). Originally in colour.

A plot of the measured a_w as a function of solute concentration is shown in **Figure 5.13** wherein it can be seen that the floridoside-rich extract displayed a very comparable a_w lowering ability to that of the preeminent confectionery solute fructose on a weight basis. This is in part due to the presence of KCl/NaCl, which are both known to strongly reduce a_w even at relatively low solute concentrations due to ion dissociation.[282, 325] Theoretically, a greater suppression in a_w should be attainable using an extract with a greater relative salt content, although this would obviously be detrimental in terms of the organoleptic character. The solubility limit of the extract (58.8 wt. % at 21 °C based of KF titration) is considerably lower than that of fructose (*ca*. 80 wt. % at 25 °C), which somewhat limits the lowest a_w (predicted to be 0.832 using a fitted cubic polynomial – see **Appendix Figure C.3**) that could be achieved in a thermodynamically stable manner (i.e. no supersaturation). According to DSC analysis, all of the solutions had T_g values below the lowest temperature limit of the instrument (- 80 °C) as no signals corresponding to a glass transition could be observed during cyclic cooling/heating.

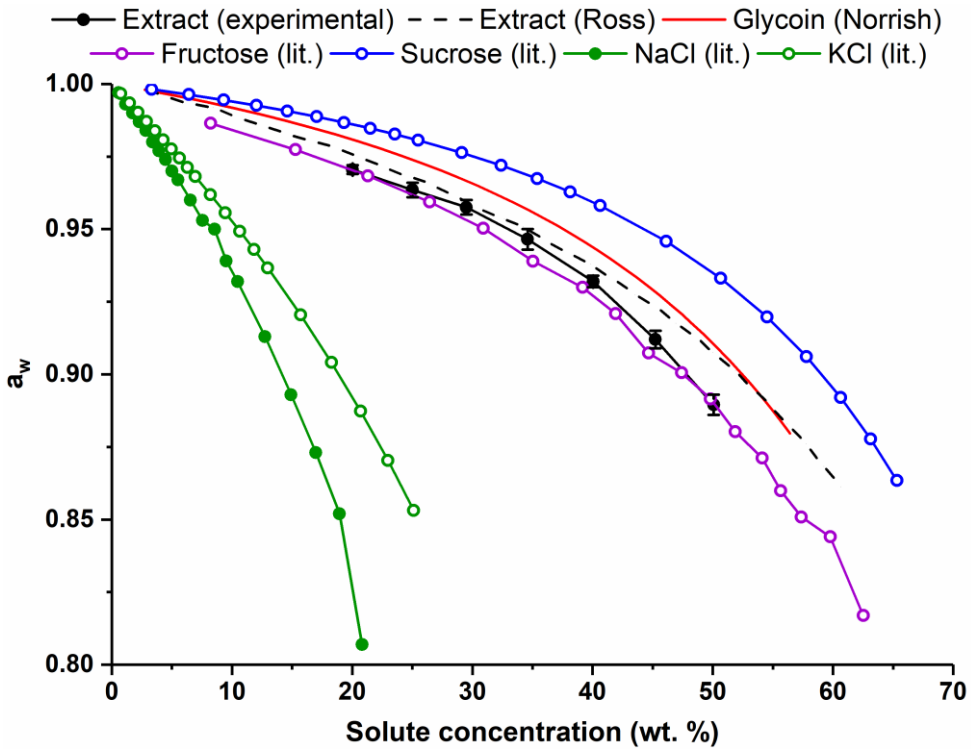

Figure 5.13: Influence of solute concentration (wt. %) on a_w using experimental a_w data (lines + points) from this work (extract) or literature; Scatchard *et al*. (sucrose/KCl),[282] Baeza *et al*. (fructose)[89] and Chirife and Resnik (NaCl)[325] and predicted a_w using the Norrish and Ross equations (lines only). Error bars represent $\pm$ 1 standard dev. Originally in colour.

The measured a_w of the extract was also compared with that predicted by the preeminent Ross equation (**Equation 1.9**), which simply considers that the a_w of the mixed solution is a product of the a_w of each individual solution containing the same amount of that solute. It been reported to display good accuracy up to the saturation limit of most mixed solute systems.[326] The composition of the extract was approximated as 0.93:0.035:0.035 (mass fraction) floridoside:KCl:NaCl according to the relevant TGA/CHN data. As it was not possible to purify sufficient amounts of floridoside, its individual contribution to a_w lowering at the various concentrations was instead estimated using the Norrish constant determined previously for glycoin (**Chapter 4**) over the concentration range that is of interest here (K_N = - 5.77). This is reasonable given the high degree of structural similarity between the two

solutes (see **Chapter 3)**, as exemplified by several free monosaccharide sugars for which the K_N values are essentially identical (K_N = - 2.25/-2.24/-2.25 for glucose/galactose/fructose).[21] Using K_N = - 5.77, along with literature a_w data for the binary KCl-water (Scatchard *et al.*)[282] and NaCl-water (Chirife and Resnik)[325] the estimation given by the Ross equation is shown alongside the experimentally measured a_w in **Figure 5.13**. The curves for the fructose-water (Baeza *et al.*)[89] and sucrose-water systems (Scatchard *et al.*)[282] are also shown for comparison.

Interestingly, the Ross equation appears to be quite accurate up to moderate concentrations of the extract, only overestimating a_w by approximately 0.05 yet for the 45 and 50 wt. % samples, the extent of overestimation increases to *ca*. 0.015. Because of the mixed nature of the sample, it is not possible to fully account for this discrepancy at the present, but at least three possible explanations may be operative. The first is that the K_N value of - 5.77 determined for glycoin (which was not the pure glucosyl glycerol) may simply be lower than the true value for floridoside. The second is that the concentration of NaCl within the sample may be higher than the 0.035 mass fraction used to calculate the Ross prediction (NaCl lowers a_w more effectively than KCl on a wt. % basis). The third is that it is indicative of some deeper solvation behaviour whereby the interaction between the salt species, floridoside and water results in a progressively less ideal solution. According to the KB analysis presented in **Chapter 3**, the greatest values of K_N were found for solutes that exhibited large solute self-exclusion and moderate to high hydration. Applying this logic here would suggest that past some concentration threshold around 40 wt. %, there is a change in the overall solution structure which results in a greater degree of overall solute self-exclusion and/or hydration. This is counterintuitive as the increasing addition of solute would have been expected to lead to greater solute-solute interaction and perhaps reduce the overall amount of solute-water interaction (at least within the immediate vicinity of the solute) due to greater competition between solute molecules for water. This suggests that further measurements are required in order to confirm the veracity of data presented in **Figure 5.13**, ideally via systematic variation of constituent concentration within the extract. In any case, given the promising

a_w and anhydrous T_g results, a mixture of organic extracts collated via several repeats of the procedure outlined in **Figure 2.1** (totalling around 100g of *ca*. 95 wt. % floridoside extract) was subsequently tested for application within a model aqueous confectionery system (see **Chapter 7**).

5.2.2. Identification and characterisation of unforeseen floridoside polymorphs and possible implications for food-relevant applications

As discussed in section **5.2.1**, pXRD analysis had indicated that the floridoside-rich organic extracts obtained via ethanol Soxhlet extraction of *Palmaria palmata* were constituted by a previously unheralded polymorph which displayed an obviously different diffraction pattern to that simulated for the only currently known crystal form.[312, 323] This also appeared to be consistent with the notably higher melting point (approximately + 10 ºC compared to the literature) that was recorded for the relative 'pure' floridoside sample produced via the same approach. Given this, it was therefore reasonable to assume that further crystalline forms of floridoside may also exist and that knowledge of such entities could be critical in terms of optimising any potential product/process involving floridoside as individual polymorphs can exhibit very disparate, food relevant physicochemical behaviours (e.g. solubility rate/hygroscopicity) cf. D-glucose and D-lactose.[286, 327]

During early work with the *Palmaria palmata* biomass, it was noted that there was a pale pink crystalline material on some of the as-received biomass surface (**Figure 5.14a**) – referred to herein as untreated crystalline material or UCM, which could be simply removed via careful mechanical scraping (**Figure 5.14b**). This solid was found to be readily soluble in (deuterated) water with the corresponding ^{1}H NMR spectrum (**Appendix Figure C.4**) being identical to that of the organic Soxhlet extracts and thus, also consistent with floridoside again in seemingly remarkable purity. Subsequent STA (N_2, 50 mL min^{-1}, 5 ºC min^{-1}) identified a single concerted endothermic mass loss event (of 5.9 wt. %) and accompanying broad endotherm which occurred over a range of approximately 60 – 95 ºC (**Figure**

5.14c) - far too low to originate from floridoside which instead decomposed starting *ca*. 200 °C, corroborating the findings of the previous work with the organic Soxhlet extracts.

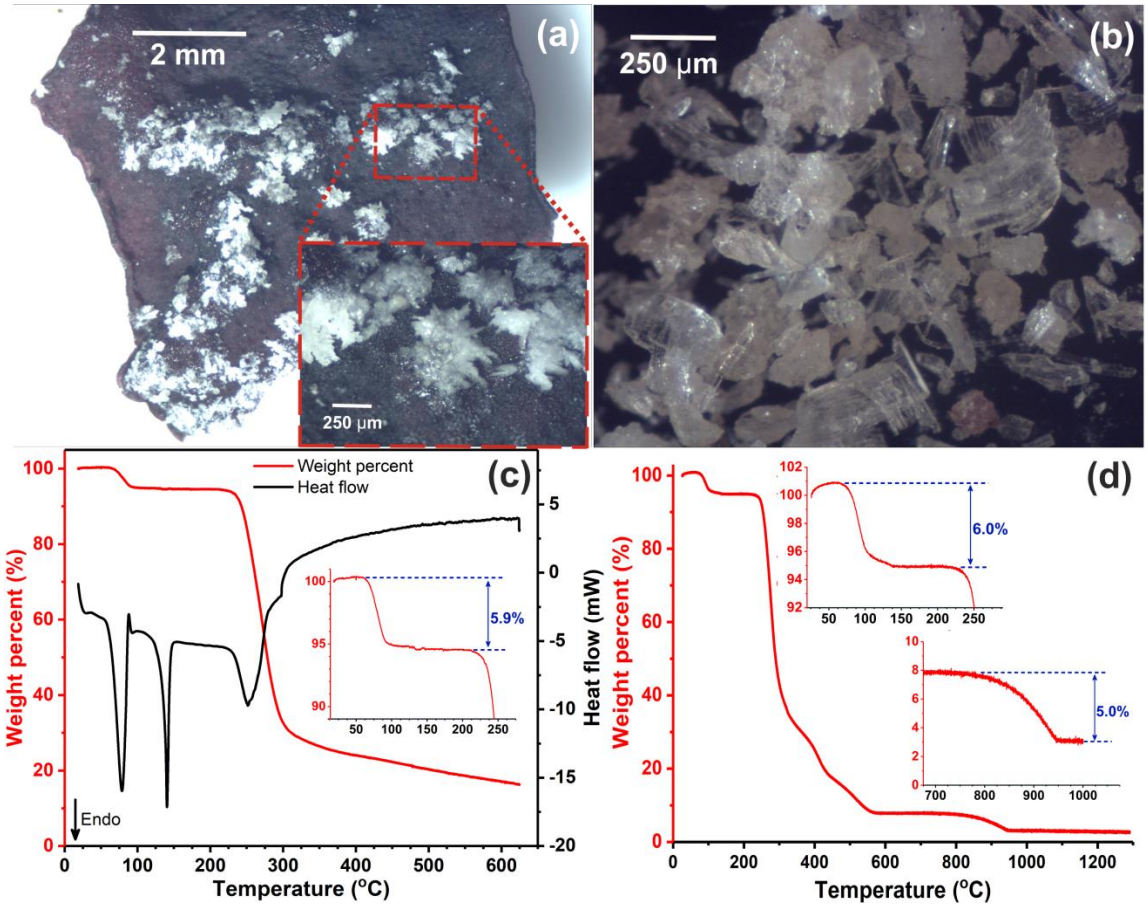

Figure 5.14: Optical micrographs of the *Palmaria palmata* surface (**a**) and obtained UCM following mechanical removal (**b**) with corresponding STA (**c**) and TGA (**d**) traces thereof. Originally in colour.

Interestingly, the initial endotherm was followed by a second sharper signal at *ca*. 140 °C, which was quite comparable to that of the high purity floridoside extract (cf. **Figure 5.9a**). In addition to this, the UCM also exhibited the characteristic mass loss at > 700 °C during high temperature TGA (Air:N_2 100:20 mL min^{-1} at 5 °C min^{-1}, (**Figure 5.14d**)) indicating the presence of inorganic salts which were presumed to be KCl/NaCl based on previous characterisation as presented in section **5.2.1**. It is not

currently clear exactly how such crystals may have formed, although one possible explanation could be that they originate from an internal exudate released by the organism (as has been reported to occur in *Palmaria palmata*).[328] This could have subsequently combined with the inorganic species (KCl/NaCl) either from the sea or again internally (perhaps exuded in a similar manner) and crystallised upon initial dehydration (5 min at 70 ºC followed by 80 min at 40 ºC under vacuum) following harvesting.

In order to elucidate the identity of the fugacious constituent, TGIR analysis (N_2, 10 ºC min^{-1}) was conducted on the UCM with the results presented in **Figure 5.15**. It can be seen that initially (bottom trace in **Figure 5.15b**), the only notable signal in the FTIR trace is that originating from the asymmetric C=O stretch of CO_2 at *ca*. 2330 – 2360 cm^{-1} which is present as an impurity within the system (probably as air) and independent of the sample. It should be noted that data collected < 850 cm^{-1} wherein the bending modes of CO_2 would be expected to manifest (typically ~ 600 – 800 cm^{-1}) are not shown given a high noise to signal ratio which prevented accurate assignment in this region. A series of new signals beginning at *ca*. 700s and reaching a maximum at 836s (see **Figure 5.15c**) can be seen immediately following the mass loss at 60 – 90 ºC. The strong series of bands at 3600 – 3200 cm^{-1} and 1500 – 1900 cm^{-1} (red trace in **Figure 5.15b**) are consistent with the O-H stretching and bending modes of water vapour, which then virtually disappeared after approximately 900s. The later intense signals at > 2700 cm^{-1} (green trace in **Figure 5.15b**) which followed the thermal decomposition of floridoside are consistent with pyrolysis products, exhibiting characteristic bands at *ca*. 2900 (C-H stretch), 1650 – 1750 (C=O stretch) and 1000 – 1500 cm^{-1} (C-H bend, C-O stretch, H-O bend etc).

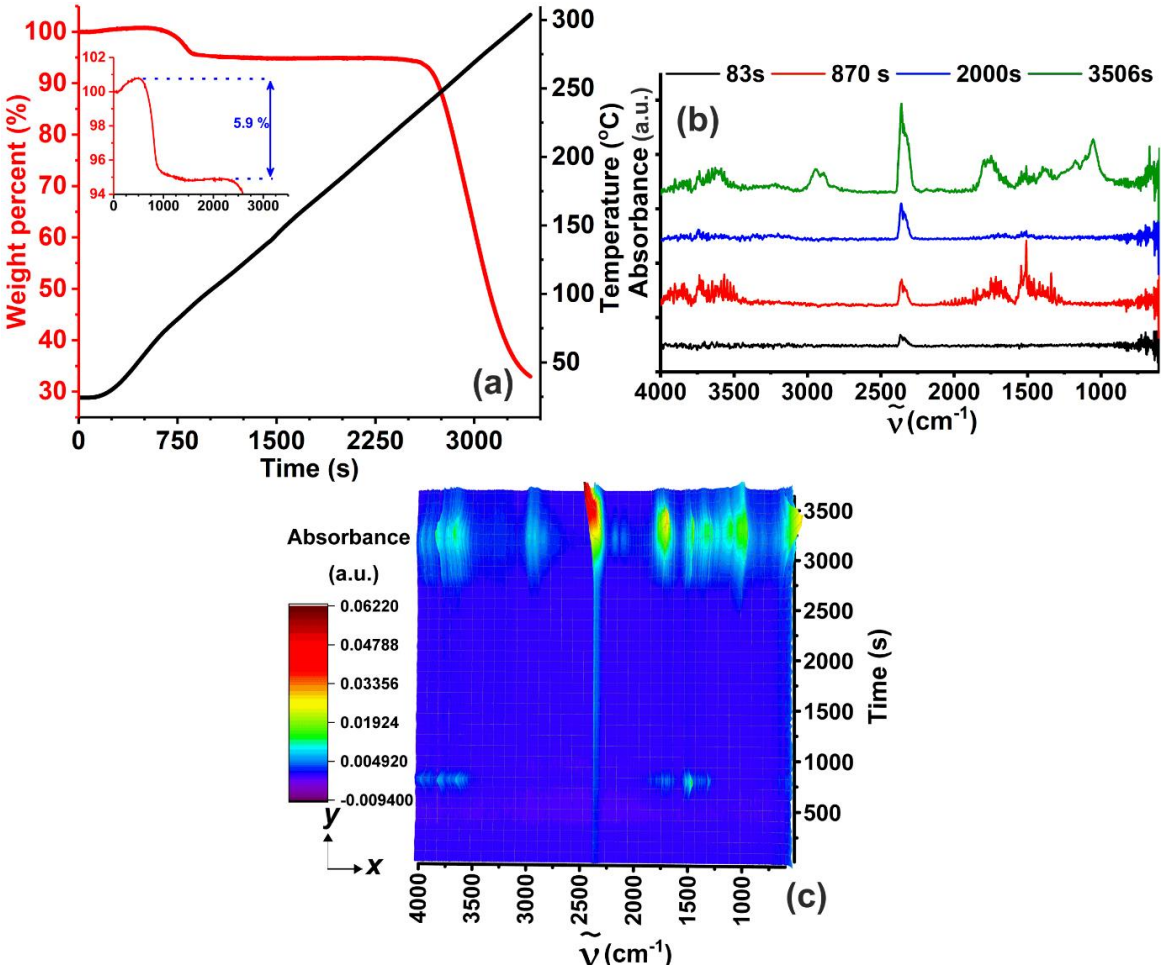

Figure 5.15: Corresponding TGA (**a**) and selected FTIR traces (**b**) for TGIR analysis of UCM for which the complete time-resolved FTIR data is also included (**c**). Originally in colour.

Given that the volatile was water and attributing the mass loss at < 150 °C (5.9 wt. %) and 150 - 700 °C (86.6 wt. %) to water and floridoside respectively, a simple mass balance indicated a close to 1:1 stoichiometry of the two components (6.1 wt. % calculated). This, coupled with the concerted nature of the dehydration event was in-keeping with the UCM being constituted of a monohydrated form of floridoside. This was unexpected as no hydrated variant of floridoside has been formally reported to the best of the author's knowledge, although it is worth noting that brief mention of such a species does appear to have been made in passing during early work by Colin and co-workers (at least according to a machine translation of the original French texts).[293, 329] It is not particularly surprising however, when

considering that various closely related polyhydroxyl pyranoses e.g. D-glucose, D-trehalose and D-lactose are all well-known hydrate formers.[327, 330, 331] In a further experiment, moderate thermal treatment of UCM under vacuum (80 ºC, 3h, 20 mbar) yielded a visibly similar crystalline material (UCM-T, **Figure 5.16a**) with an identical NMR spectrum (**Appendix Figure C.4c/d**) which no longer exhibited the initial dehydration event but that retained the endotherm at *ca*. 136 ºC upon heating during STA (**Figure 5.16b**) and also the mass losses beginning at *ca*. 200 and 700 ºC that were consistent with the presence of floridoside and salt respectively (**Figure 5.16c**). This indicated that dehydration of the monohydrate could lead to the formation of anhydrous floridoside which was hypothesised to be the same from as that identified within the ethanol Soxhlet extracts on account of the relatively high melting point.

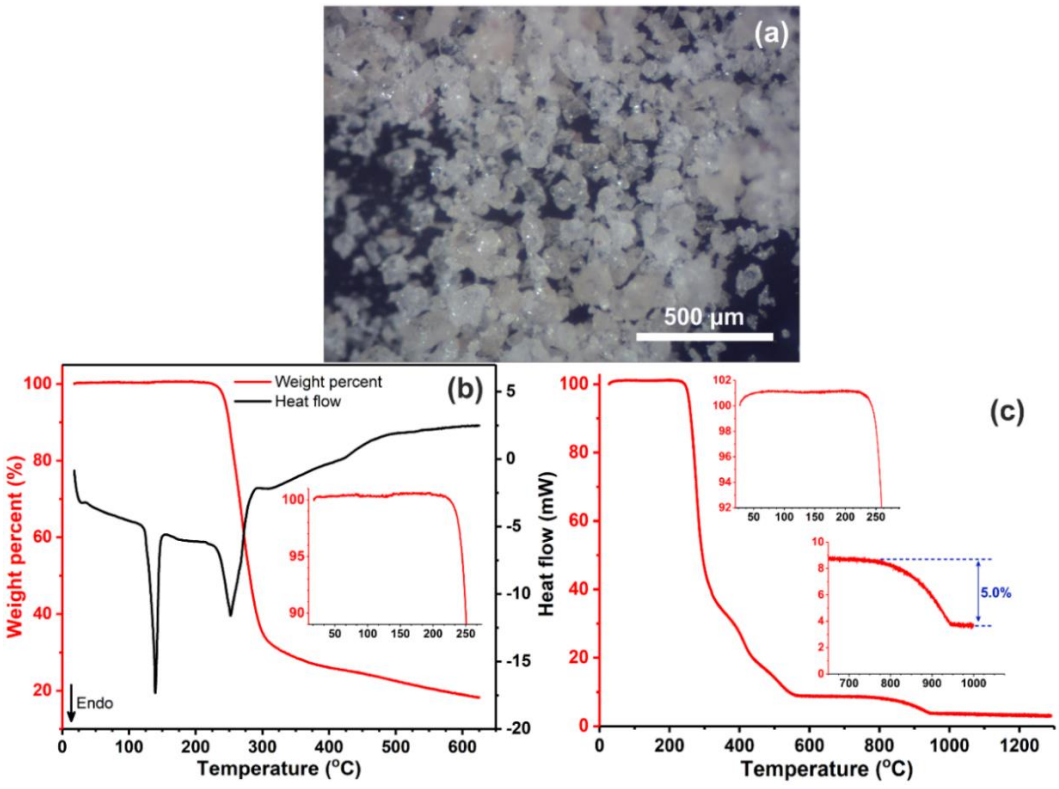

Figure 5.16: Optical micrograph of the UCM-T (**a**) and with corresponding STA (**b**) and TGA (**c**) traces thereof. Originally in colour.

p-XRD was also conducted on UCM and UCM-T and provided conclusive evidence that both materials were clearly different to that simulated for the only previously reported crystal form (referred to herein as Form I, F_I) based on the structure deposited by Vonthron-Sénécheau *et al.*) (**Figure 5.17**).[323] It can be seen that as expected, the pattern for UCM-T is the same as that of the organic Soxhlet extract (cf. **Figure 5.10**) displaying intense signals at 2Θ = 14.0, 15.3 and 20. 6 °. The corresponding trace for UCM is very different to both that and F_I with the major peaks instead occurring at 2Θ = 15.5 and 16.9 °. This was proof that UCM and UCM-T were primarily constituted of two unreported forms of crystalline floridoside; a monohydrated variant (F_h) in UCM and a second anhydrous dimorph (F_{II}) in UCM-T.

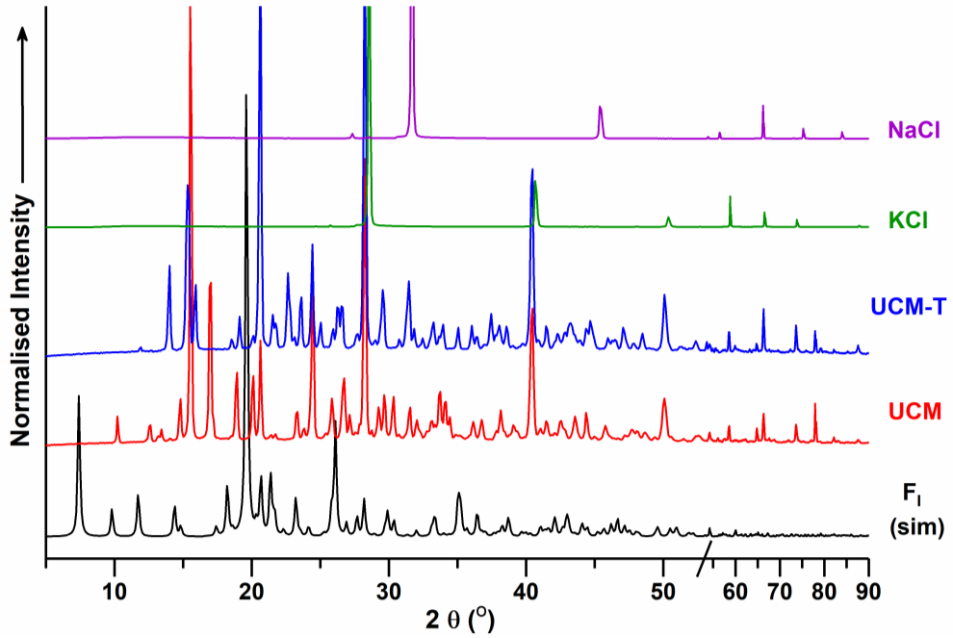

Figure 5.17: Comparison of pXRD spectra recorded for UCM and UCM-T with that simulated for F_I (using the single crystal data of Vonthron-Sénécheau *et al.*),[323] and experimental traces for KCl and NaCl. Arrow indicates direction of increasing normalised intensity. Originally in colour.

Following this discovery, attention was subsequently focussed on further investigation of the deformation of UCM (F_h) given that STA and pXRD had indicated that F_{II} could be formed upon simple

heating past the dehydration event (*ca*. 60 – 90 ºC). Instead of performing experiments in an open system, both the UCM and UCM-T were analysed via cyclic DSC which involved heating/cooling within a hermetically sealed aluminium pan. In the case of former analyte, the initial endotherm manifested over a similar, albeit narrower temperature range (n.b. also with significantly less associated enthalpy given that water vaporisation was prevented) and was immediately followed by an exothermic deviation beginning at *ca*. 87.5 ºC and then a second, broader signal from 93 to 118 ºC (**Figure 5.18a**).

As in the previous STA experiments, the UCM-T exhibited only one endotherm at approximately 115 – 142 ºC (**Figure 5.18b**). In a similar fashion to the floridoside-rich Soxhlet extracts, the amorphous melts of both UCM and UCM were found to undergo supercooling with T_g = -12.4 and 30.1 ºC, respectively with the latter being very comparable to the those found for the Soxhlet extracts (see **Figure 5.9b**).The precipitous drop in T_g is consistent with the presence of water, which acts as a potent plasticiser of carbohydrate glasses and has been reported to supress T_g by up to 10 ºC wt. %$^{-1}$ (calculated to be ~ 7 K wt. %$^{-1}$ based on a water content of *ca*. 6 wt. %).[332] In a further experiment, UCM was heated to a temperature of 90 ºC within the sealed pan (this sample is referred to as UCM-90 herein) prior to cooling after which, no obvious T_g could be observed even at - 80 ºC (**Figure 5.18c**) indicating the comparative absence of any melting. Interestingly, when UCM-90 was subjected to STA the endotherm at 60 – 90 ºC no longer manifested, with the mass loss resulting from water vaporisation instead proceeding in a gradual manner and over a much broader temperature range beginning at approximately 30 ºC (**Figure 5.18d**).

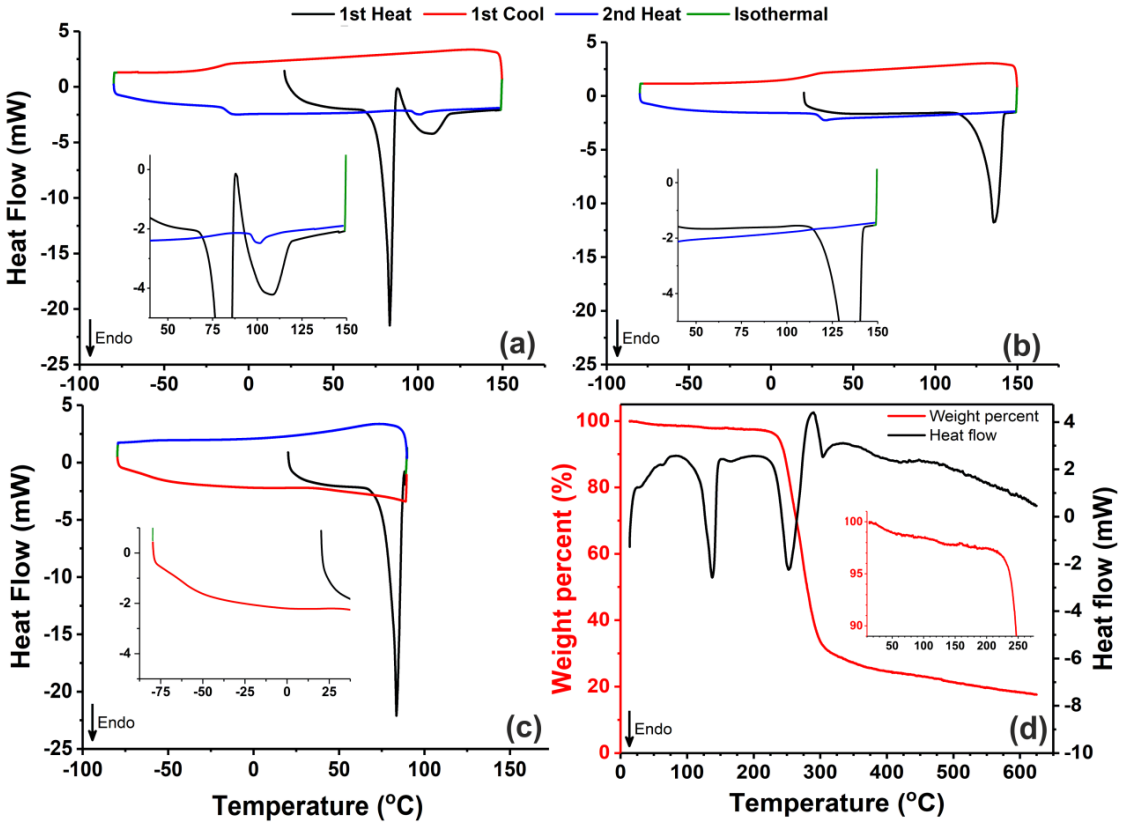

Figure 5.18: DSC of UCM (**a**) and UCM-T (**b**) and UCM-90 (**c**) showing the first heating, first cooling and second heating cycles along with the STA trace of UCM-90 (**d**). Originally in colour.

ATR-FTIR analyses (**Figure 5.19**) of the three materials proved to be illuminating, with the spectrum of UCM being observably very different to those of UCM-T and UCM-90 (and indeed all of the organic Soxhlet extracts cf. **Figure 5.11**), which instead were virtually identical. It is interesting to note that the band corresponding to the OH bending deformation of water is shifted towards a higher wavenumber and takes a considerably sharper form in UCM (1672 cm^{-1}) with respect to UCM-90 (1645 cm^{-1}). This indicates a stronger H-bonding environment as a greater amount of energy is required to induce bending if an O-H bond is more rigidly fixed via H-bonding to the floridoside hydroxyls.[333]

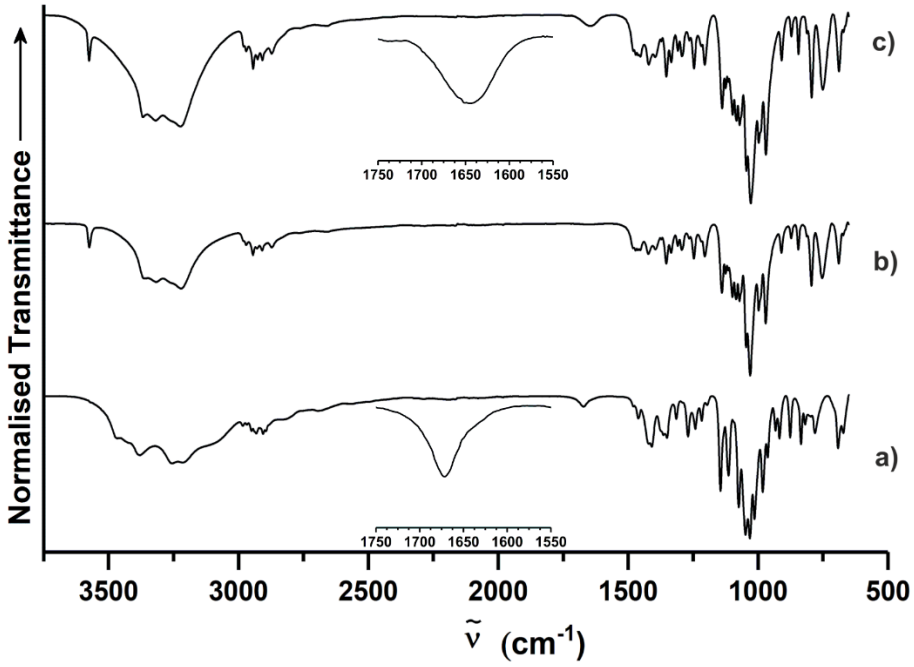

Figure 5.19: ATR-FTIR spectra of UCM, UCM-T and UCM-90 with zoomed insets magnifying the 1550-1750 cm^{-1} region for UCM and UCM-90. Arrow indicates the direction of increasing transmittance.

Considering all of the aforementioned results, it appears as though the initial endotherm in UCM corresponds to the deformation of the monohydrated crystal species (F_h) which results in the concomitant release of the crystalline water and anhydrous floridoside. In the open system (i.e. STA/TGA), this water freely vapourises, leaving only anhydrous floridoside which can be inferred to be F_{II} given that melting occurred at *ca*. 140 °C. Conversely, the water released upon the thermal deformation of F_h within the pressurised DSC pan cannot vaporise and is instead liquified where its presence ultimately results in the suppression of the melting event at *ca*. 110 °C in the UCM (**Figure 5.18a**). The exotherm that follows the initial F_h deformation is somewhat difficult to interpret given that it could conceivably correspond to multiple possible events including; (i) cold crystallisation of floridoside from a partially amorphous matrix (formed during F_h deformation), (ii) dissolution of a small amount of amorphous floridoside in the liquified water (e.g. the dissolution of amorphous lactose has

been reported as exothermic for instance)[334] or (iii) a crystal-crystal transition of one form of anhydrous floridoside dimorph to the other.

In an attempt to better resolve this sequence of events, variable-temperautre (25 to 150 ºC) XRD (VTXRD) was performed on both UCM and UCM-T (**Figure 5.20**). It should be noted that due to experimental limitations, well-resolved data could only be collected at relatively small diffraction angles ($2\Theta \leq 24^{o}$) by holding and irradiating samples at set temperautres (in *ca*. 2 ºC intervals) for an extended period (45/60s temperature equilibration/irradiation respectively) and hence, some differences with respect to the DSC could be expected. In the case of UCM (**Figure 5.20a/b**) it can be seen that as expected, the main peaks corresponding to F_h are readily observable up until *ca*. 81 ºC at which point a previously unheralded peak at $2\Theta = 14.0^{o}$ indicates the presence of F_{II} although this signal then dissapeared upon further heating to 83 ºC (n.b. all signals corresponding to KCl/NaCl manifest at $2\Theta > 24^{o}$). At this stage, F_h seemingly reappeared according to the significant peak at 15.2^{o} although the lack of other signals is indicative of a loss of general crystallinity by this temperature. There is an apparent shift that occurred between 88 and 90 ºC (end of red traces/start of blue traces in **Figure 5.20a**) which resulted in development of a weak trimodal series of signals at $2\Theta = 14.8/15.2/15.9^{o}$ and concomitantly, a further prominent singular peak at 20.5^{o} (see pattern recorded for 98 ºC in **Figure 5.20b**) which together persisted until 112 ºC then later at 117 ºC and are most consistent with F_{II}. Interestingly, a small and then extremely intense peak at $2\Theta = 19.0^{o}$ which likely belongs to F_I (or very shifted F_{II}) could be observed at 110 and 115 ºC, respectively and is indicative of a seemingly 'frustrated' liquid crystalline-type phase within UCM in which the various polymorphic species appear to spontaneously form and then rapdily disappear again. At $\geq$ 120 ºC, all signals progressively vanished and completely so by 129 ºC, signifying the presence of a purely liquid melt. In the case of UCM-T (**Figure 5.20c/d**), the characteristic peaks at $2\Theta = 14.8/15.2/15.9^{o}$ and 20. 5^{o} dominate the spectra until 124 ºC at which point, the latter signal becomes extremely intense whilst the others briefly diminish before reverting back to the earlier pattern recorded at 127 ºC. This is attributed to the onset

of melting, which initially results in some sort of crystallographic readjustment followed by a progressive reduction in signal intensity up to 137 °C and then complete formation of the isotropic liquid melt thereafter.

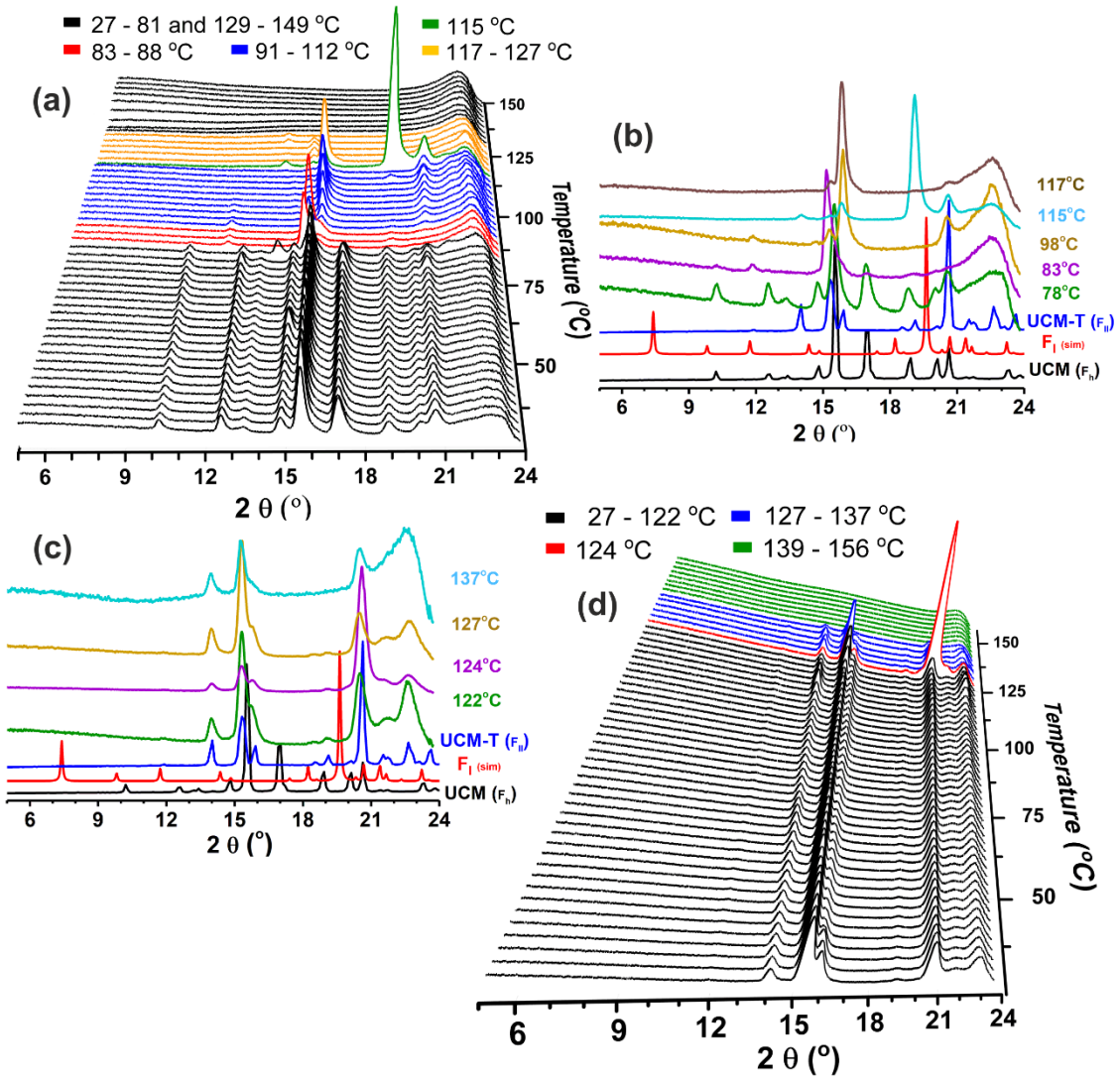

Figure 5.20: Temperature-resolved (**a** and **c**) and selected (**b** and **d**) VTXRD patterns of UCM (top) and UCM-T (bottom) respectively. Originally in colour

Given the high purity of UCM (cf. NMR/TGA), it was hypothesised that this material could be used to prepare single floridoside crystals. After some initial experiments, it was found that EtOH and

particularly MeOH could both be used (in conjunction with EtOAc as an antisolvent in some instances) to produce all three of the different crystalline forms. The best results (i.e. higher crystal quality/yield, greater reproducibility) were obtained with the latter solvent which is likely a reflection of its superior ability to dissolve floridoside (visually evaluated). It is hypothesised that this enhanced solubility provided a more facile route to achieving higher degrees of supersaturation and hence, subsequent crystallisation from the hot solution following cooling/antisolvent addition etc.

The typical approach consisted of boiling UCM in MeOH (initial concentrations of *ca*. 25 mg mL^{-1}) and hot (vacuum) filtration of the resulting suspensions followed by either storage or further treatment of the filtrate. F_{II} could be consistently produced via prolonged boiling (for several minutes) of UCM before hot filtration and natural cooling in sealed vials for 1 – 7 days. This process generally resulted in the preparation of transparent, colourless crystals which adopted either well-formed cuboid-like or higher polyhedral morphologies (**Figure 5.21a/b**).

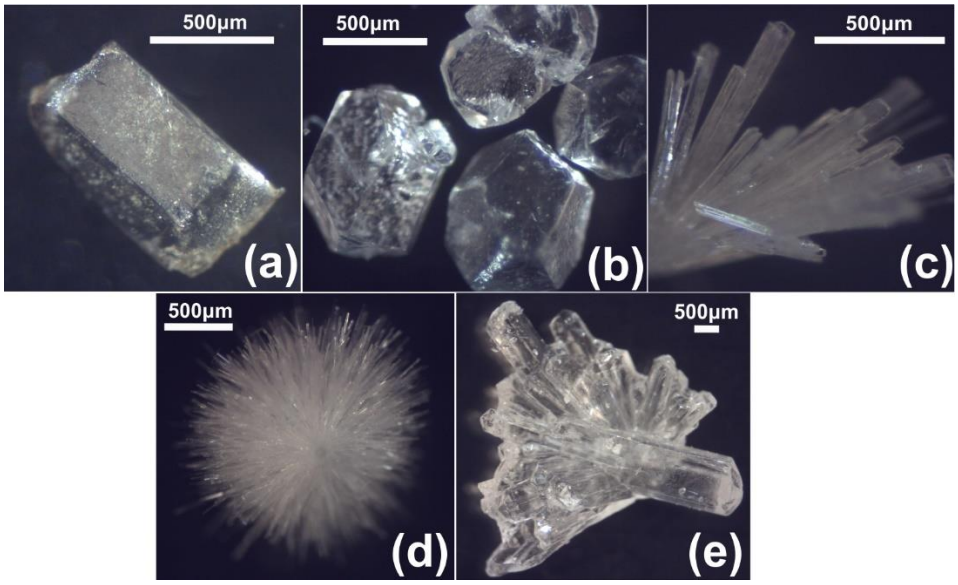

Figure 5.21: Optical micrographs of the three crystalline floridoside polymorphs; F_{II} (**a** and **b**), F_I (**c** and **d**) and F_h (**e**).

Conversely, the most reliable method of F_I production involved the addition of an excess quantity of EtOAc (as an antisolvent) to the supersaturated MeOH filtrate. Interestingly, lower quantities of excess EtOAc (MeOH filtrate:EtOAc ≈ 1:3 v/v) often resulted in the formation of relatively large needle clusters (**Figure 5.21c**) which grew concomitantly with F_{II} whereas greater concentrations of EtOAc (approximately 1:5 v/v) led to fine spherulitic aggregates as the sole crystal system (**Figure 5.21d**), which were collected rapidly (< 3h) in order to limit any potential solvent-mediated polymorphic transition. In the latter case, the addition of antisolvent was actually sufficient so as to induce visible turbidity, indicating a particularly high-degree of supersaturation and thus, acute driving force towards crystallisation. Further addition of antisolvent past this point resulted in the formation of visually non-crystalline, globular material which is likely to have been amorphous in nature and was not investigated further.

Of the three different crystal forms, F_h proved the most difficult to prepare in reproducible manner with large and often twinned crystals (**Figure 5.21e**) occasionally being formed following partial evaporation of the MeOH filtrate (typically under a fume hood). In some instances, this approach also resulted in the absence of any crystal growth, indicating that subtle differences in the concentrations of individual crystallisation liquor components had significant influence on the crystallisation process. This has been reported for other water-soluble solutes from water-alcohol solutions.[335] It is obvious that at least some quantity of water would have to be present within the system in order to form the monohydrate, although excessive amounts would likely prevent any crystallisation owing to the considerable solubility of floridoside in water (*ca*. 54 wt. % for F_{II} according to KF titration). It is also worth mentioning that some residual water from the UCM could have remained within the filtrate following boiling given the zeotropic nature of the methanol-water system and thus, anticipated predominance of MeOH within the evolved vapour. Additionally, it can be expected that moisture absorption by the concentrated and air-exposed MeOH-floridoside solutions may be significant given that the equilibrium water contents of

even neat MeOH have been reported to be high at moderate ambient humidities (*ca*. 11/18 wt. % H_2O at 25.3/39.5 % RH).[336]

The newly identified crystal structures of F_h, F_{II} and F_I are shown in **Figure 5.22** (the F_I structure has been generated using the CCDC data deposited by Vonthron-Senecheau *et al*.) with full crystal and structural data being provided in **Appendix Table C.3**. All three crystals are orthorhombic and belong to the $P2_12_12_1$ space group with each unit cell comprising four floridoside molecules in addition to four H_2O molecules in the case of F_h confirming unequivocally that it is a stoichiometric monohydrate.

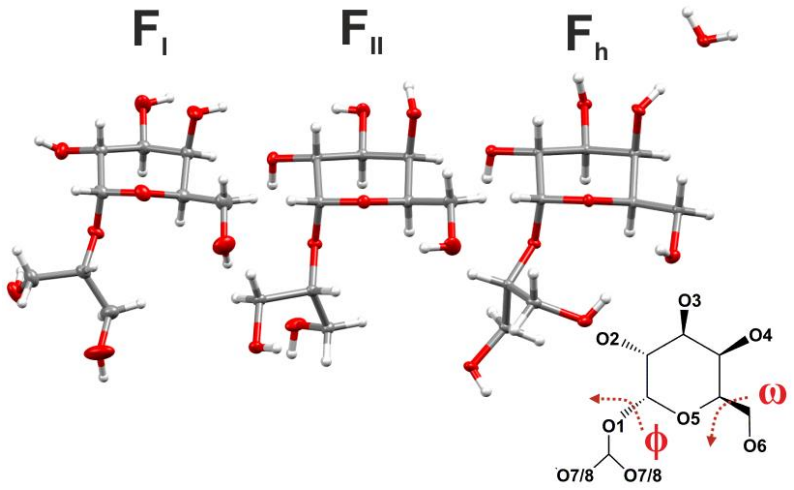

Figure 5.22: Thermal ellipsoid representations for F_I, F_{II} and F_h at the 50 % probability level wherein hydrogens are drawn with arbitrary radii. Torsion angles ω and ϕ are also depicted to aid visualisation. Originally in colour.

From inspection of **Figure 5.22**, it can be seen that in each of the three forms, the central pyranose rings exist in the $^4C_1$ conformation and also that all three are *gauche-trans* rotamers with respect to the C_5-C_6 bond, with O_6-C_6-C_5-O_5 torsion (ω) angles of 58 – 68 °. Conversely, the orientation of the glycosidic bond (as described through the ϕ angle, i.e. O_5-C_1-O_1-C_7) is somewhat different across the crystals, with F_{II} (63.39) and F_I (73.89) displaying comparatively smaller angles with respect to F_h (91.02) wherein the greater space appear to allow a terminal glycerol hydroxyl to rotate such that it can engage in strong

H-bond donation to O_6. The unit cell axes (**Figure 5.23**) of both F_{II} (a = 8.54811(10) Å, b = 9.19251(10) Å, c = 14.34851(17) Å) and F_h (a = 8.22038(16) Å, b = 11.2533(3) Å, c = 12.9852(2) Å) display relatively comparable lengths with respect to F_I, wherein one axis is markedly longer and another noticeably short (a = 4.88440(10) Å, b = 9.7259(3) Å, c = 23.8754(6) Å) on account of an almost head-to-tail arrangement of molecules which results in a very high aspect ratio.

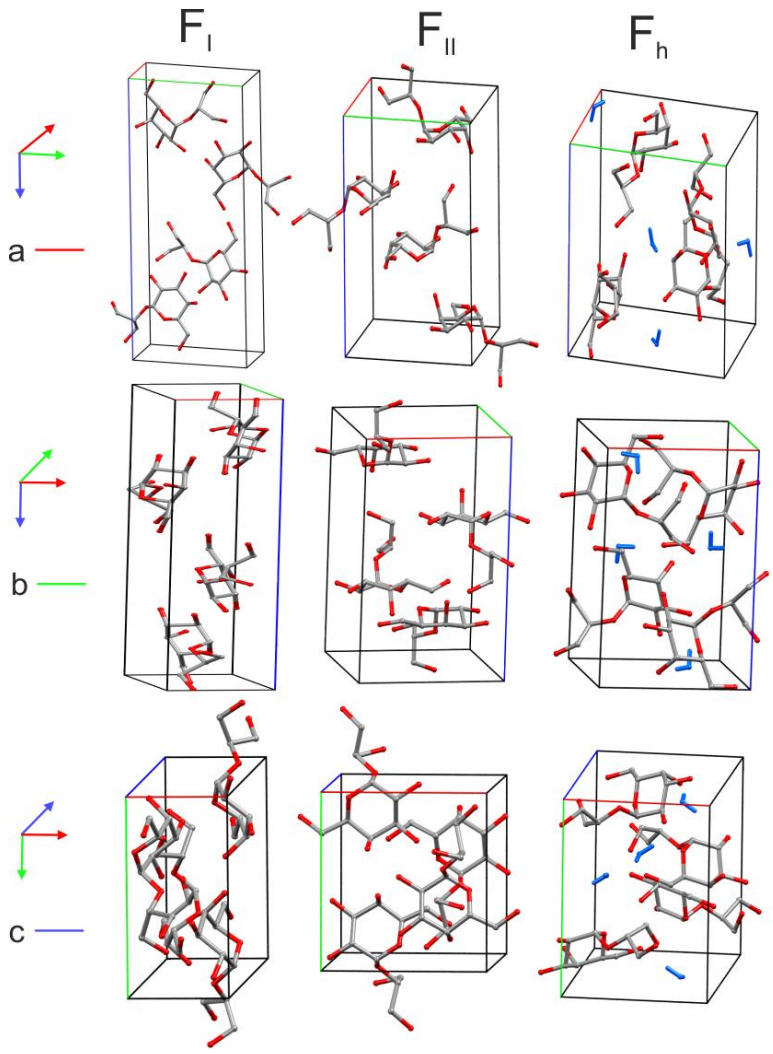

Figure 5.23: Unit cells of (from first to third column; F_I, F_{II} and F_h viewed along the (from top to bottom) a-,b- or c axes (red, green or blue cuboid edges). Hydrogen atoms, except those belonging to H_2O (coloured blue) in F_h are omitted for clarity. Originally in colour.

Unsurprisingly, due to the presence of the six hydroxyl groups belonging to each floridoside molecule (in addition to the H_2O for F_h), each crystal lattice is comprised of myriad of hydrogen bonds, both between (i.e. intermolecular) and within individual (i.e. intramolecular) molecules. In order to search for differences in the H-bonding profiles, a relatively lenient (albeit arbitrary) definition was applied with the maximum distance and minimum angle between the OH donor hydrogen and acceptor (R_1-O-R_2) being set to $\leq$ 3 Å and $\geq$ 90 º respectively. If the definition was extended past this point or modified so as to include C-H donors, then the number of possible contacts rapidly became overly cumbersome and unrealistic in some instances (illustrative examples are provided in **Appendix Figure C.5**).

It is notable that the same limits appear to have been previously established independently by Steiner and Saenger through a comprehensive study of fifteen non-ionic carbohydrates,[337] from which the authors concluded that discrimination between H-/non-bonding regions become very difficult outside the aforementioned boundaries. Using this approach, H-bonds could be generally described in one of two ways; (1) comparatively 'strong' contacts, displaying lengths and angles of $\leq$ 2.20 Å and $\geq$ 140 º respectively or (2) 'weaker' contacts which were > 2.20 Å and < 140 º (and presumably more ambiguous with respect to their actual existence). The results are summarised in **Figure 5.24**. An interesting note is that under these criteria, the water molecule in F_h actually appears to (unrealistically) make five hydrogen bonds with the neighbouring floridoside molecules (**Appendix Figure C.6**), which indicates that the limits for H-bonding are likely to be overly inclusive. Three of the five bonds are classified as 'strong' ($\leq$ 2.00 Å, $\geq$ 175.10 º), in-keeping with the higher energy of the water O-H bending vibration ($\tilde{\nu} \approx 1672$ cm^{-1}) of crystalline F_h (**Figure 5.25**) and UCM compared to that of liquified water within the UCM-90 sample as highlighted previously.

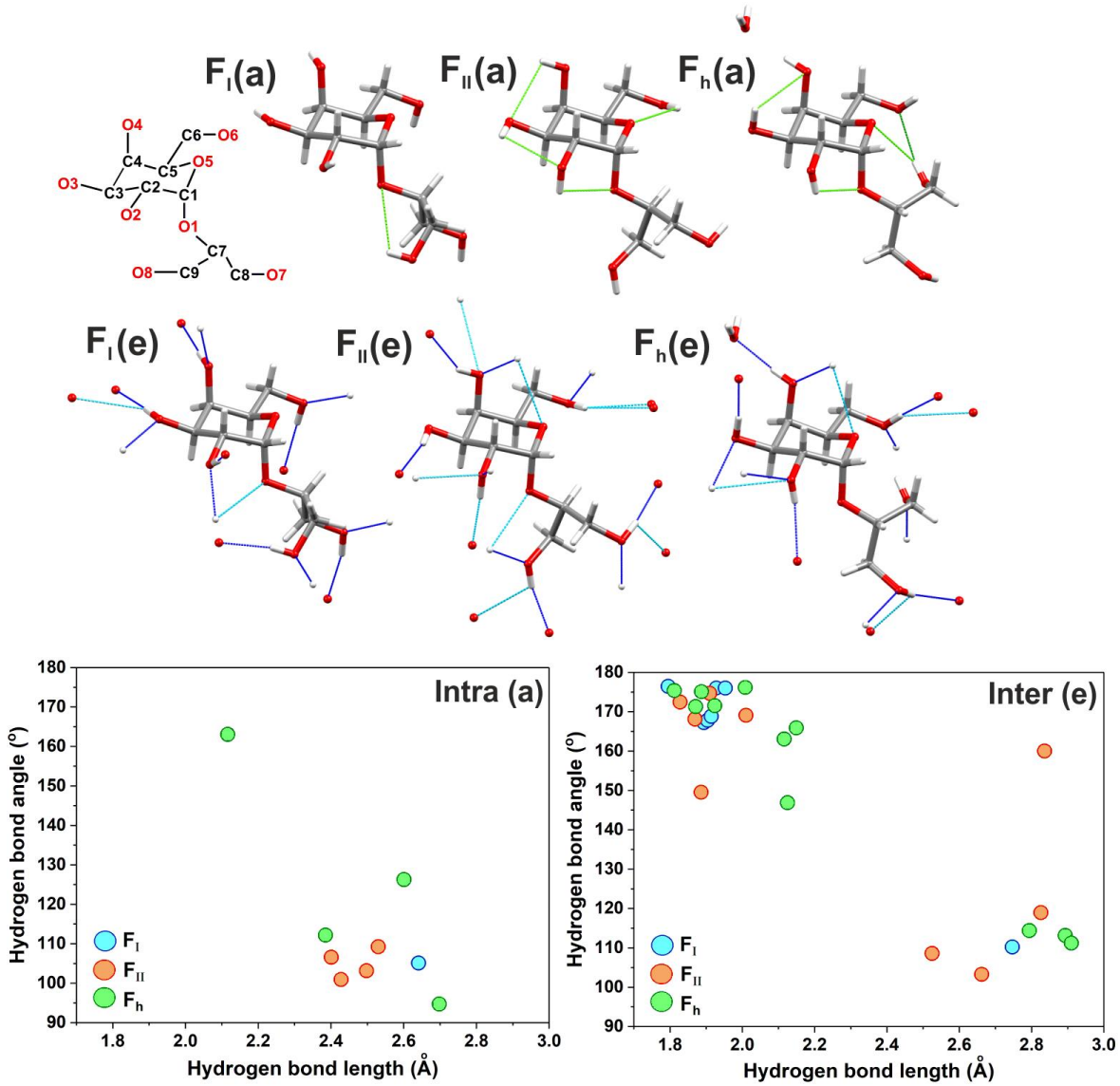

Figure 5.24: Hydrogen-bonds calculated (using Mercury) from single-crystal structures of F_I, F_{II} and F_h showing 'close' (donor: OH, acceptor: O, $\leq$ 2.20 Å, $\geq$ 90 °, navy line) and 'far' (donor: OH, acceptor: O, 2.21 – 3.00 Å, $\geq$ 90 °, cyan line) intermolecular or intramolecular (donor: OH, acceptor: O, $\leq$ 3.00 Å, $\geq$ 90 °) (H-bonds for F_I, F_{II} and F_h are represented by blue, red and green circles respectively). Originally in colour.

It is also notable that the IR spectrum F_{II} (and UCM-T) contains a sharp band at *ca*. 3576 cm^{-1} which is indicative of the isolation of a single hydroxyl group. Under the enacted criteria, all of the hydroxyls in F_{II} (and indeed also the other two forms) apparently participate in H-bond donation and acceptance, which again suggests that they may be excessively lenient (F_{II} (a)/(e) in **Figure 5.24**). Of these, the

isolated hydroxyl should most likely be O_3-H or O_6-H given that the rest display H-bonds for both donation and acceptance that fall into the 'strong' classification. O_3-H actually acts a donor to O_6 i.e. O_3-H···O_6 for which the relevant contact would also be considered as strong (2.010 Å, 169.08 °). Hence, according to the classical interpretation where strong H-bond donation would result in the elongation and weakening of the O_3-H bond, the corresponding stretching modes should display an effective lowering in vibrational energy.

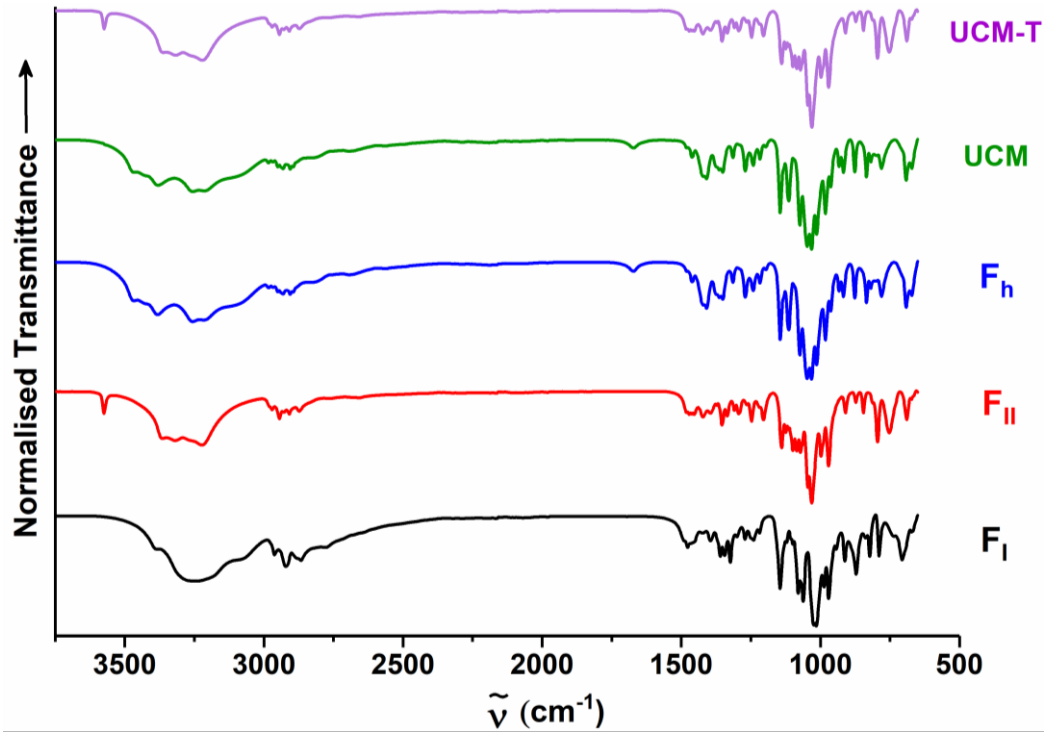

Figure 5.25: ATR-FTIR spectra (650 – 3750 cm^{-1}) of pure crystalline F_I, F_{II} and F_h and comparison with UCM/-T. Originally in colour.

Because the isolated band actually manifests at a high relative frequency, this suggests that O_6-H is therefore the most plausible hydroxyl given that the contacts for which it partakes in as a donor appear to be considerably 'weaker' (distance (Å)/angle (°) of 2.498/103.15, 2.662/103.28 and 2.836/160.01) in nature and thus, more questionable as to their actual manifestation within the crystal. However, this

hypothesis should be investigated further using computational calculations which would also ideally incorporate other considerations that were outside of the current scope (e.g. C-H donation).

Unsurprisingly, these spectroscopic differences also manifested in the (DRIFT) NIR spectra of the various species wherein the first overtone of the isolated hydroxyl in F_{II} can be readily observed at 6987 cm^{-1} (**Figure 5.26**). Similarly, obvious differentiation between F_h and F_I can be made for instance, by the presence of the strong signal at 5140 cm^{-1} in the former, which should correspond to the OH combination bands of water. The ability to easily discriminate between the various forms via this technique is particularly encouraging as NIR is often the analytical method of choice during on-line process monitoring in the food and pharmaceutical industries as it is quick, facile and non-invasive in nature.[338]

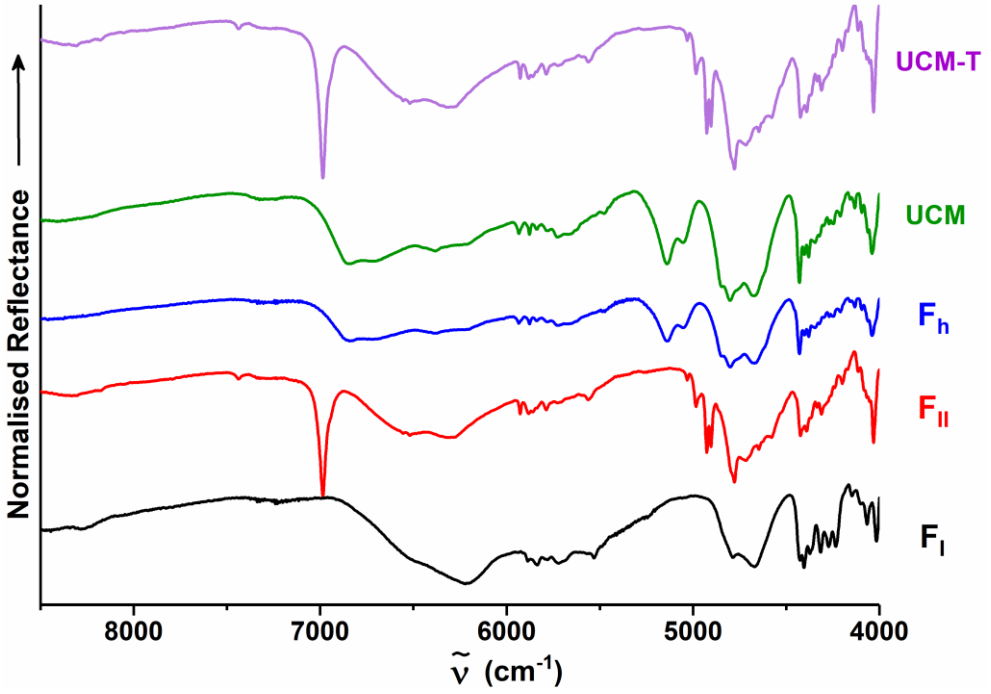

Figure 5.26: (DRIFT) NIR (4000 – 8500 cm^{-1}) spectra of neat, crystalline F_I, F_{II}, F_h and also UCM/-T. Arrow indicates the direction of increasing reflectance. Originally in colour.

A more general inspection of **Figure 5.24** indicates that F_{II} exhibits a greater overall number and variation in its H-bonding profile with respect to F_I, containing many bi-/trifurcated configurations (both intra/intermolecular). Conversely, as has been mentioned previously by Vonthron-Sénécheau *et al.*, all hydroxyls in F_I are involved in both strong intermolecular hydrogen bond donation and acceptance (**F_I (e)** in **Figure 5.24**) but form only one weak intramolecular bond and comparatively few bifurcated contacts.[323] It is hypothesised that this may contribute to the comparatively greater thermal stability of F_{II} with respect to F_I according to both DSC and hot-stage optical microscopy (Figure 5.27), wherein the former and latter were found to display a $T_{max} \approx 142$ and 130 ºC respectively (i.e. $\Delta T_{max} \approx 12$ ºC).

It can also be seen that the T_g of the pure anhydrous floridoside appears to be very comparable to that recorded previously for the floridoside-rich organic extracts and also that of glycoin (**Chapter 4:**). Within the corresponding DSC trace of F_I (Figure 5.27**a**), there is a significant exotherm which occurs at approximately 133 ºC immediately after the melting endotherm. This is then followed by a second melting endotherm at *ca*. 140.5 ºC which was consistent with that found for pure F_{II} (Figure 5.27**b**). This series of events is noteworthy in that it appears to indicate a monotropic relationship between the two anhydrous floridoside crystals, whereby the irreversible transition from the lower (F_I) to higher (F_{II}) stability form manifests as an exothermic event which occurs either through a solid-solid or liquid-solid process close to or above the fusion *T* of the former.[339] It should be noted that neither crystallisation or a solid-solid transition could not be observed during hot stage microscopy (a full series of micrographs taken between 45 – 139 ºC are presented in **Appendix Figure C.7**), although this is not unexpected given the kinetic nature of such events.

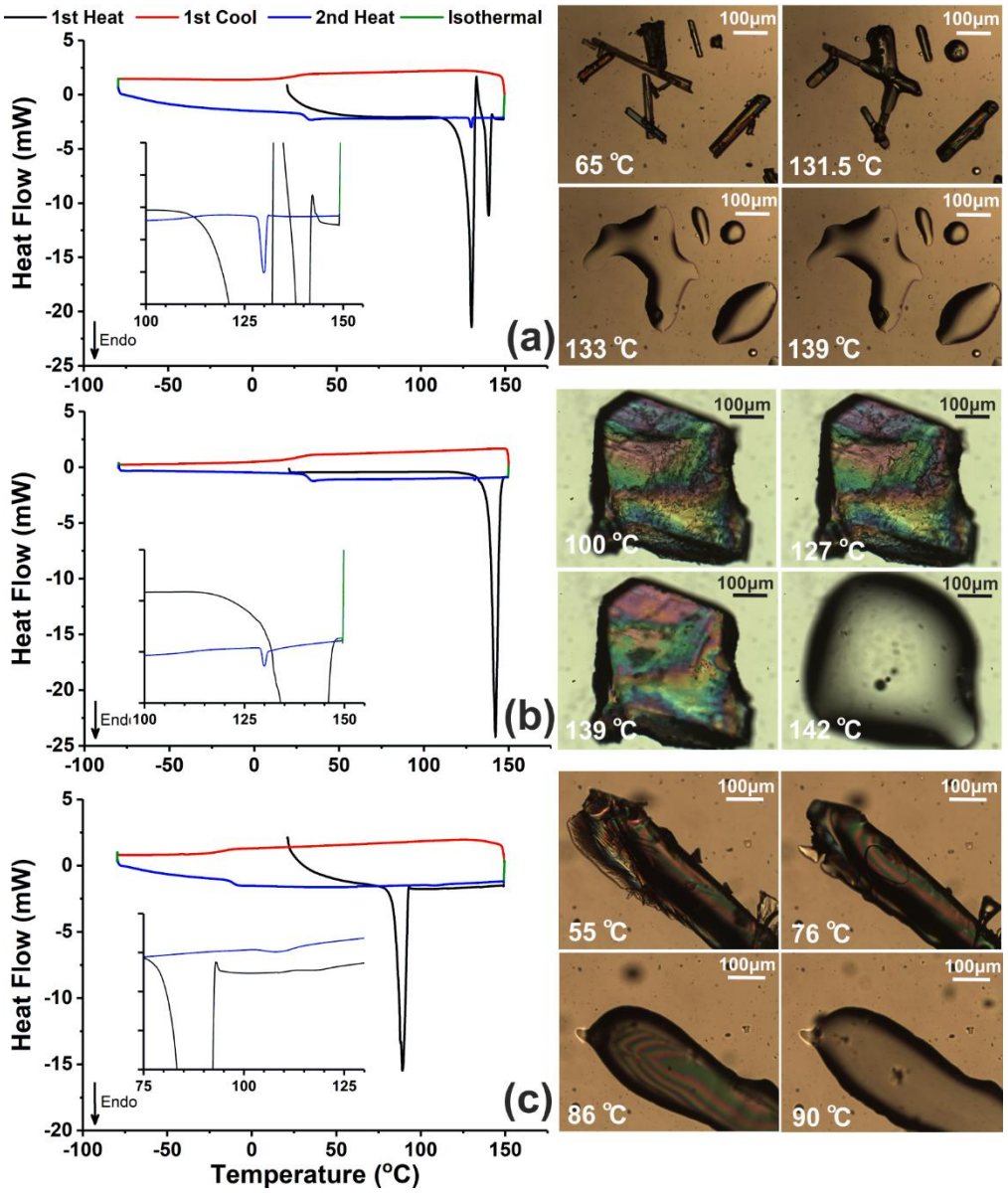

Figure 5.27: Cyclic DSC (including inset zoomed traces of melting endotherms) and hot stage micrographs of crystalline F_I (**a**), F_{II} (**b**) and F_h (**c**). Inset *y*-axis ticks correspond to 0.5 mW. Originally in colour.

In addition to DSC/hot stage microscopy, the monotropic transition of F_I to F_{II} was also studied using VTXRD (**Figure 5.28a/b**) as was the deformation of F_h (**Figure 5.28c/d**), with both of the experimental patterns (in addition to that recorded for F_{II} – see **Appendix Figure C.8**) all displaying an excellent

match to those simulated using the corresponding single crystal data. Concerning the crystalline F_I sample, it appears as though there was a small contamination with F_{II} (perhaps during concomitant crystal growth) although F_I was still the predominant form as evidenced by the strong characteristic peaks at $2\Theta = 7.4$ and 19.4 °.

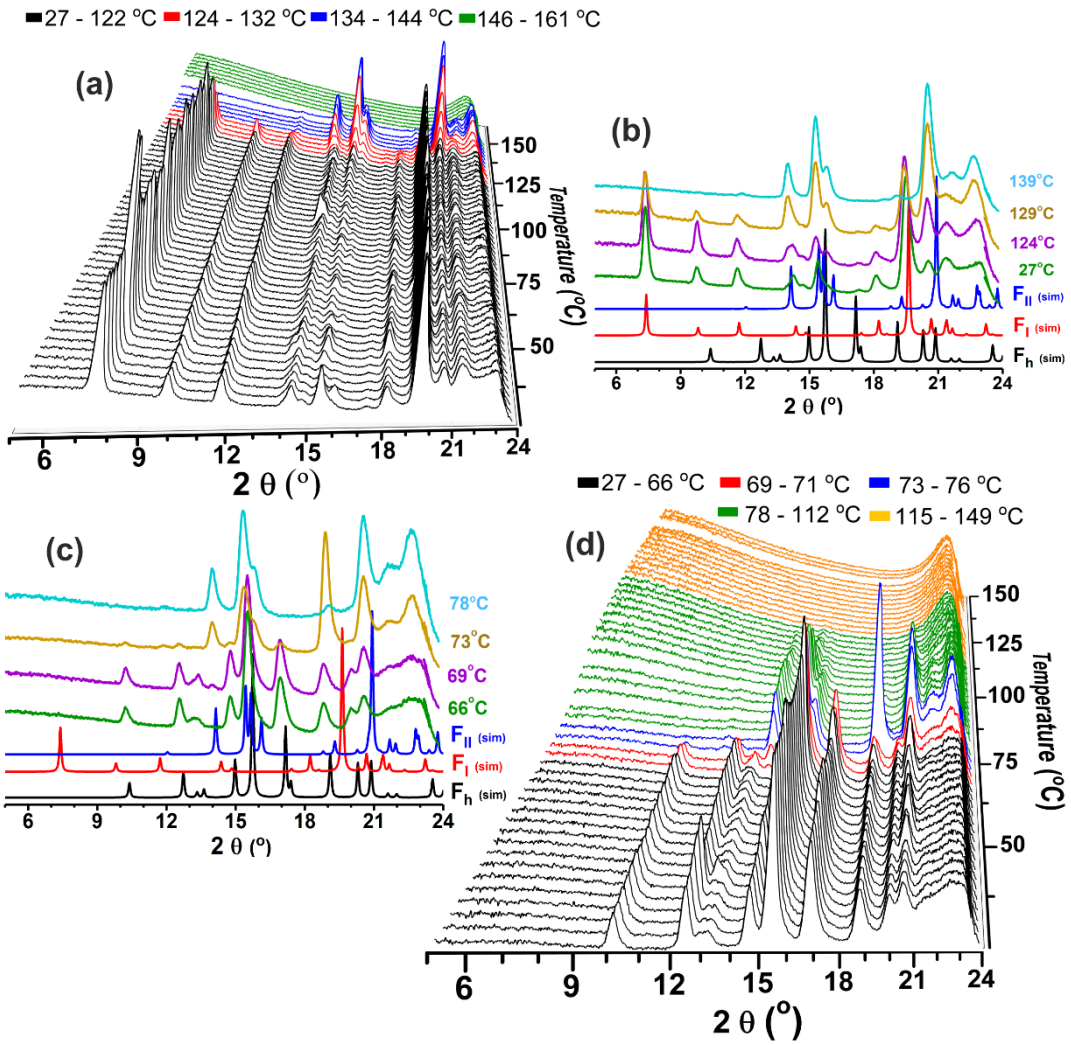

Figure 5.28: Temperature-resolved (**a** and **c**) and selected (**b** and **d**) VTXRD traces of pure, ground crystalline F_I (top) and F_h (bottom) respectively.

The recorded patterns remain largely unchanged up until approximately 124 °C at which point, there is a notable development of the peak at 20. 5 °, consistent with the initial evolution of F_{II}. Over the next ~

10 ºC, F_I is steadily converted into F_{II} as highlighted by the simultaneous diminution of the low angle signals (< 12 º) and growing intensity of the trimodal cluster at 14.0, 15.2, 15.8 º and aforementioned peak at 20.5 º. By 134 ºC there is a complete conversion into F_{II}, which persists up until *ca*. 144 ºC before abruptly melting, in good general agreement with the results of the other thermal analyses. This was also true of the corresponding VTXRD recorded for F_{II} wherein no detectable signals could be observed above approximately 142 ºC (**Appendix Figure C.8**).

In the case of F_h deformation, the process appeared to initiate at approximately 69 ºC (**Figure 5.28c/d**) whereby the weak peak at 2Θ = 14.0 º is indicative of the initial development of F_{II}. By 73 ºC, the signals at 10.2, 12.6 and 13.1/13.3 º and concomitant evolution of prominent peaks at 18.9 and 20.6 º signified the transition from F_h to the anhydrous F_I and F_{II} respectively. The F_I that was formed during this process then appeared to rapidly morph into F_{II} given the almost complete disappearance of the peak at 18.9 º by 78 ºC after which point, F_{II} persisted through further heating albeit with progressively diminishing intensity until approximately 115 ºC before melting. Interestingly, this order of events is somewhat different to those which occurred during the deformation of UCM which also contained crystalline F_h. This suggests that the exact nature of the transition is highly dependent on experimental conditions (heating rate/holding time etc.) and also that the other constituents (KCl/NaCl) had some type of directing effect on the sequence of the mesophases that were observed.

The particle size also appears to be influential in terms of F_h deformation, whereby the lower number of defects in the whole crystal relative to the ground F_h sample/UCM resulted in almost complete melting on account of the single prominent endotherm/T_g in **Figure 5.28c** and formation of isotropic liquid during hot stage microscopy from 35 to 135 ºC (see **Appendix Figure C.9**). In this case it is hypothesised that the movement of water throughout the solid matrix is slowed inside the large and comparatively well-formed single F_h crystal which prevents an expedient rearrangement of the lattice that is required for the formation of the anhydrous polymorphs and results in structural collapse leading

to the observed amorphous phase. Therefore, the particle size of F_h should be considered during any potential processing as it may otherwise lead to unwanted dehydration/amorphisation and further undesirable phenomena (e.g. increased hygroscopicity in the latter case).

Concerning anthropocentric use of floridoside, the identification and characterisation of metastable and hydrated crystalline species is noteworthy given that individual polymorphs and hydrates often exhibit very disparate physicochemical behaviours as exemplified by other carbohydrates such as D-glucose and D-lactose.[286, 327] The metastable crystal of a polymorphic pair often displays a comparatively faster dissolution rate but greater hygroscopicity for instance, indicating that controlled crystal engineering towards either F_I, F_{II} and/or F_h should facilitate more optimised floridoside-containing products/processes that can be tailored towards an individual end application.

In addition to anthropocentric applications, the identification and characterisation of a hydrated form of floridoside could shed some light on its internal accumulation as a method for regulating the *in-vivo* concentration and distribution of water in most *Rhodophyta* and particularly within floridoside-rich intracellular domains such as the cytoplasm.[340] Formation of a hydrate would be an effective means by which either water or floridoside could be sequestered from the intracellular matrix during transitions of low to high or high to low moisture/humidity (a_w) respectively. In the former case, it could help to preserve anhydrobiosis via conversion of any water vapour absorbed at low to medium humidity values into the hydrated form, thereby localising it and maintaining an otherwise anhydrous bulk. It should be noted that stabilisation of a completely anhydrous system via maintenance of a vitrified matrix (as has been suggested for trehalose)[341] by floridoside is somewhat implausible, given its relatively low T_g (32 ^oC) but could instead proceed through a water replacement type mechanism (i.e. direct H-bonding with macromolecules). Conversely, if the external a_w/humidity/temperature is rapidly decreased then hydrate crystallisation will result in the removal of an equimolar quantity of water and floridoside, maintaining

a relatively dilute solution with high a_w, which may be necessary for homoeostasis in some instances. Indeed, this is somewhat analogous to crystallisation within honey, whereby the formation of crystalline glucose monohydrate effectively releases net water molecules (previously solvating it) into solution which results in an overall increase in a_w.[210] This may explain why floridoside upregulation has recently been implicated as a drought mitigation mechanism within *Pyropia haitanensis* upon desiccation (i.e. low humidity/a_w) during low tide.[296] Concerning the comparison with trehalose dihydrate, it has been suggested that the potential to reversibly un-/load water via connected, structured channels within the crystalline lattice is likely the cause of its superior functionality.[330, 342] Inspection of the F_h lattice suggests however, that this is not the case for floridoside on account of the large distance that exists between neighbouring water molecules ($\geq$ 6.56 Å O···O) and that a different molecular level mechanism must exist.

5.3. Summary

Following identification of the natural osmolyte, 2-α-*O*-D-galactopyranosyl glycerol a.k.a. floridoside as a promising humectant/plasticiser candidate (**Chapter 1**) initial work focussed on its extraction directly from *Palmaria palmata* biomass using water as the only solvent in the process. This approach was found to yield an extract which was relatively rich in floridoside (according to NMR analysis) yet ultimately unviable from a confectionery application perspective because of a prohibitively high salt content (> 40 wt. %) which was inferred to be a mixture of KCl/NaCl based on the results of ICP and elemental microanalysis. EtOH was subsequently employed as an extraction solvent given its comparatively lower solubilising power of the aforementioned salts and was found (via Soxhlet extraction) to produce floridoside-rich extracts (> 90 wt. %) in high yields (15 – 20 % of the starting dry biomass) at an appreciable scale (> 10 g) and in a facile and reproducible manner.

The a_w lowering capacity of one such floridoside-rich extract (*ca*. 92.5 wt. %) was evaluated via preparation of a series of aqueous solutions (20 – 50 wt. %) and was found to be superior to sucrose and glycoin and very similar to fructose on a weight-by-weight basis which can in part, be attributed to the presence of the divalent salt constituents (NaCl/KCl). However, the lowest a_w that can be attained using solely the extract as a humectant is likely to be inferior to that using the aforementioned solutes due to a comparatively limited solubility (58.8 wt. % of the according to KF titration). Highly pure floridoside (*ca*. 99 wt. % according to TGA/CHN) produced via the EtOH Soxhlet approach was found to have a T_g (midpoint) of approximately 31 ^oC which was close to both that measured for glycoin (**Chapter 4**) and literature values for various monosaccharides (glucose and galactose) and is again indicative of plasticisation by the glycerol moiety. The presence of salt appeared to have limited effect on the T_g although it may have contributed to a reduction in and broadening of the melting temperature. On account of the aforementioned a_w and T_g results, a collated floridoside-rich extract (94.9 wt. % according to TGA) obtained via the EtOH Soxhlet extraction of *Palmara palmata* was subsequently trialled as a replacement humectant/plasticiser within a model aqueous confectionery system (**Chapter 7**).

Surprisingly, pXRD analysis of the organic Soxhlet extracts of *Palmaria palamata* suggested that they were constituted of a crystal form which was inconsistent with the only structure that had been reported in the literature. This instigated a further study which ultimately culminated in the identification, preparation and detailed characterisation (via a host of thermal and spectroscopic analyses) of the newly identified form (an anhydrous dimorph of the known crystal) along with a stoichiometric monohydrated crystal form also. Both of these newly identified crystals were found to exhibit quite disparate thermal and spectroscopic characteristics and possible reasons (e.g. differences in the intra/intermolecular hydrogen bonding profiles) for some of these discrepancies were offered whilst relevant implications for both commercial anthropocentric and natural *in-vivo* utility were also suggested.

Chapter 6: Preparation and characterisation of novel, food-grade eutectic mixtures as potential neoteric humectants and plasticisers

Aspects of the work reported in this chapter have been published in: **A. J. Maneffa**, A. B. Harrison, S. J. Radford, A. S. Whitehouse, J. H. Clark, and A. S. Matharu, Deep eutectic solvents based on natural ascorbic acid analogues and choline chloride, 2020, *ChemistryOpen*, **9**, 559–567.

This Chapter investigates **Aim 3** as discussed previously within section **1.4**. More specifically, it deals with the development of novel, food-grade 'deep' eutectic mixtures based on naturally-occurring lactones and choline chloride. It consists of two main sections:

(i) **Section 6.1**: Initial screening of mixtures containing non-sugar, food-grade components for stable (deep) eutectic formation and subsequent selection of the most promising candidates.

(ii) **Section 6.2**: Detailed physicochemical characterisation (DSC, a_w, rheology) of candidate eutectic mixtures selected as part of (i) in order to assess suitability as potential plasticisers and humectants.

6.1. Screening of eutectic mixtures using food-grade components

Initial work focussed on the screening of different mixtures comprising food-grade components in order to assess their ability to form eutectics that had relatively low melting temperatures which would ideally lie at or close to room-temperature and thus remain a stable liquid once stored at ambient temperature. This was because it was hypothesised that the formation of an amorphous, liquid substance could have significant benefits from a practical standpoint (e.g. easier storage, handling, more versatility in application etc) and would allow for accurate appraisal of important physicochemical properties of interest (T_g, a_w and viscosity). The method employed for DES preparation involved simply weighing different ratios of the individual components, before briefly combining them and then heating, typically to 100 ^oC, whereby the formation of a liquid was evaluated visually. This protocol was chosen on

account of its simplicity relative to other methods, which can require initial dissolution in water followed by subsequent removal via reduced pressure/freeze-drying for instance.[343]

Many of the 'deep' eutectics described in the literature that have been utilised within food-relevant applications contain sugars or sugar alcohols as one of the components. Because the overall aim of this thesis was to develop novel sugar-reduced humectants/plasticisers that were not based on currently used sugars or sugar replacement strategies (sugar alcohols), such compounds were not considered any further within the screening stage. Similarly, other popular components which were deemed problematic from either a chemical compatibility and/or sensorial perspective such as common organic acids (citric acid, malic acid etc.) or urea-based amides were also not considered.

According to the literature, the most common component used to form water miscible DES and NADES is choline chloride (ChCl, **Figure 6.1**). Whilst ChCl cannot currently be considered as a natural molecule per se, its constituent choline cation is contained with various natural phospholipids and is considered an essential nutrient which is required for a multitude of homeostatic functions (cell-membrane signalling, lipid transport, neurotransmitter synthesis etc).[344] ChCl has an approved GRAS status by the FDA and is already an established food ingredient and dietary supplement for both adults and infants and has also been patented as a key ingredient within nutraceuticals.[345-347] There may be future scope to extract natural choline-rich materials from natural sources given that 'free' choline (i.e. not that which simply constitutes phospholipids etc.) has been identified within extracts from *Moraceae* (fig/mulberry family) and red algae for instance,[348, 349] however this aspect was not explored any further within the current thesis.

Within typical DES, ChCl plays the role of a 'hydrogen bond acceptor' and is often successfully combined with a 'hydrogen bond donor' (HBD) species (e.g. sugars, organic acids), leading to strongly

non-ideal melting behaviour which is indicative of the formation of strong and favourable interactions between the components within eutectic phase that are otherwise absent in the native crystalline components. In these systems, the non-ideality is primarily considered to be a manifestation of charge delocalisation between the choline cation and chloride anion that constitute ChCl which in turn, is a result of strong hydrogen bonding between the added HBD and Cl^-.[132, 133]

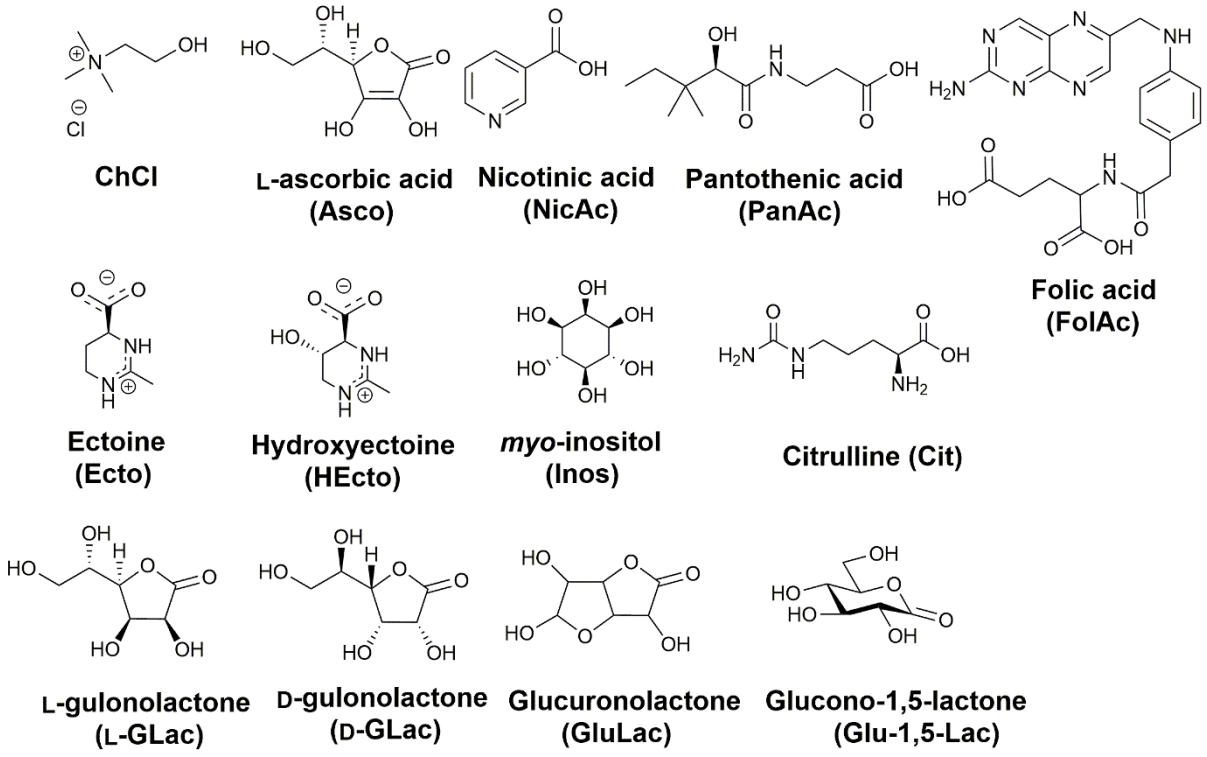

Figure 6.1: Food-grade components tested within the eutectic screening process.

Given that ChCl is a dietary supplement and vitamin, it was hypothesised that a eutectic mixture formed using it and a second vitamin HBD component would make for an attractive nutritional yet highly functional food-grade additive. To this end, a series of mixtures containing ChCl and different vitamins containing at least one and, in most cases, several HBD functionalities (OHs and NHs); nicotinic acid (NicAc, Vitamin B3), pantothenic acid (PanAc, Vitamin B5), L-ascorbic acid (Asco, Vitamin C) and

folic acid (FolAc, Vitamin B9) were screened for eutectic formation. In addition to the aforementioned compounds, several natural, non-sugar osmolytes that were highlighted previously in **Chapter 3** (hydroxyectoine, ectoine and myo-inositol) were also screened as HBDs (**Figure 6.1**). In order to reduce the number of screening experiments required and considering that for most eutectic mixtures containing ChCl the reported eutectic points tend to be around an equimolar ratio, each of the HBD:ChCl systems were prepared and tested at three different molar compositions, 2:1, 1:1 and 1:2. A summary of the DES experiment conducted within this thesis is provided in **Table 2.2**.

In general, most of the components completely failed to liquefy and either remained visually unchanged (PanAc:ChCl, NicAc:ChCl and Cit:ChCl, Ecto:ChCl, HEcto:ChCl) or degraded following heating (FolAc:ChCl). In the case of the Inos:ChCl system, all mixtures visibly softened upon reaching 100 ^{o}C yet no obvious liquid phase could be formed even after further heating to 140 ^{o}C (**Figure 6.2a - c**).

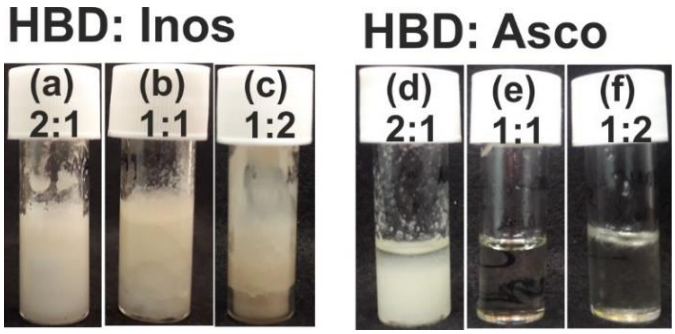

Figure 6.2: Visible appearance of Inos:ChCl and Asco:ChCl mixtures at different molar ratios (2:1, 1:1, 1:2) following $\geq$ 7 days storage at room temperature. Originally in colour.

Conversely, all of the Asco:ChCl mixtures were found to at least partially liquefy following only several minutes heating at 100 ^{o}C, with the 1:1 mixture forming a clear liquid that was devoid of any solid matter. The same was also true of the 1:2 system, which was converted into a clear liquid following

approximately 1h heating/stirring at 100 ºC, whilst full liquefaction was not observed in the 2:1 mixture even following prolonged heating (> 2 h). Notably, the 1:1 mixture was found to be stable for at least seven days upon storage at room temperature with both the 2:1 and 1:2 mixtures exhibiting some degree of recrystallisation during the same period (**Figure 6.2d-f**).

The inability of most of the mixtures to liquefy can in large part, be attributed to their relatively high fusion temperatures and enthalpies. Indeed, for a typical crystalline solid (denoted *i*) within a simple binary mixture comprising two components that are completely immiscible in the solid phases but miscible in the liquid phase (i.e. they form a 'homogeneous' melt but crystallise into two distinct solids) their solid-liquid equilibria (SLE) can often be effectively approximated according to a Schröder-van Laar model (**Equation 6.1**):[350-352]

$$\ln x_i\, y_i = \frac{\Delta H_{m,i}}{R}\left(\frac{1}{T_{m,i}} - \frac{1}{T}\right) \qquad \textbf{Equation 6.1}$$

Where x_i, $\Delta H_{m,i}$, $T_{m,i}$ refer to the mole fraction, molar enthalpy of fusion and fusion temperature of species *i* with *R* and *T* denoting the universal gas constant (8.314 J K^{-1} mol^{-1}) and temperature at which the solid and liquid phase of *i* are in equilibrium (i.e. the melting temperature). In order to account for/quantify any potential non-ideal eutectic melting behaviour, **Equation 6.1** also incorporates an activity coefficient term, y_i, which, if the temperature chosen describes a phase boundary (liquidus or solidus), can be calculated if the aforementioned properties of a component are known. A summary of $\Delta H_{m,i}$, $T_{m,i}$ for the various components of the mixtures examined herein have been taken (where possible) from the literature and are summarised in **Table 6.1.**

Table 6.1: Summary of thermal properties ($T_{m,i}$ and $\Delta H_{m,i}$) of components used within the initial DES screening.

Compound	$T_{m,i}$ (°C / K)	$\Delta H_{m,i}$ (kJ mol^{-1})	Ref.
Choline chloride (ChCl)	323.8 / 597.0	4.3	Fernandez *et al*.[353]
Pantothenic acid (PanAc)	ND	ND	-
Ectoine (Ect)	237.8 / 511.0	16.0	Held *et al*.[113]
Folic acid (FolAc)	250.0 / 523.2	29.6	Wysoczanska *et al*.[354]
Hydroxyectoine (HyEct)	476.8 / 750.0	12.2	Held *et al*.[113]
L-ascorbic acid (Asco)	193.8 / 467.0	45.3	Corvis *et al*.[355]
L-citrulline (Cit)	ND	ND	-
Myo-inositol (Inos)	223.7 / 496.9	47.9	Barone *et al*.[356]
Nicotinic acid (NicAc)	236.8 / 509.9	60.8	Haneef and Chadha[357]

ND = Not determined

It should be noted that strictly speaking, for components that undergo a solid-solid transition (i.e. display polymorphism) during heating/cooling e.g. ChCl, an additional term should be included in **Equation 6.1**. However, this has previously been indicated to have only a small impact on the SLE in many cases.[352] Rearranging **Equation 6.1**, the ideal melting curves (wherein y_i = 1) for either the HBD component or ChCl (using the experimental transition data measured in this work), respectively can be constructed via **Equation 6.2**:

$$T = \frac{1}{\left(\frac{1}{T_{m,i}} - \frac{\ln x_i y_i R}{\Delta H_{m,i}}\right)} \qquad \textbf{Equation 6.2}$$

The ideal solidus is predicted as the point at which the two melting liquidus curves intersect and is demonstrated for both the NicAc:ChCl and Asco:ChCl systems in **Figure 6.3a** and **Figure 6.3b**, respectively. In both cases, it can be seen that the predicted solidus temperatures fall above the uppermost operating temperature (140 °C or 413 K), which is consistent with the complete lack of melting observed in most of the systems. A lack of any notable non-ideal depression in the SLE

behaviour can also be inferred from the absence of any observable melting i.e. y_i must be close to or above 1 in these systems. Conversely, for the Asco:ChCl mixture, the predicted solidus lies at approximately 423 K and x_{ChCl} = 0.70 (*ca*. Asco:ChCl 1:2.3), which is also above the experimentally accessible temperature. However, as some melting was observed this demonstrates that the actual measured solidus falls considerably below the predicted one. This is indicative of a non-ideal melting point depression wherein $y < 1$ (for at least one but not necessarily both components), which has been suggested by some aficionados to be the appropriate definition for the 'deep' designation within the deep eutectic mixture/solvent descriptor.[144]

On account of the success of Asco to generate stable, relatively low melting eutectics with ChCl, it was hypothesised that other structurally similar components may also be capable of forming non-sugar 'deep' eutectic mixtures. In nature, two lactone species; Glucuronolactone (GluLac) and L-Gulonolactone (L-GLac) (shown in **Figure 6.1**) are both intermediates in the biosynthesis of Asco.[358] GluLac is already a common ingredient within sports drinks and has been implicated as a stimulant for natural *in-vivo* defence mechanisms against undesirable tumour promoters and carcinogens.[359] The two aforementioned species in addition to the enantiomer of L-GLac, D-gulonolactone (D-GLac) and a fourth lactone HBD, glucono-1,5-lactone (Glu-1-5-Lac) (see **Figure 6.1**) (itself a natural compound of the human body and an established food additive),[360, 361] were all screened for eutectic melt formation with ChCl.

Satisfyingly, all of the mixtures containing the four lactones and ChCl were found to at least partially liquefy at each of the three molar ratios (2:1, 1:1, 1:2) with the 1:1 mixtures all once again exhibiting complete liquefaction under experimental conditions (Glu-1,5-Lac was only tested at the 1:1 ratio due to a lack of material availability). This observation suggested that the eutectic ratio for the

aforementioned mixtures lay around a 1:1 ratio, which was further explored by subsequent testing of mixtures at 1.5:1 and 1:1.5 ratios for the GluLac, L-GLac and D-GLac systems.

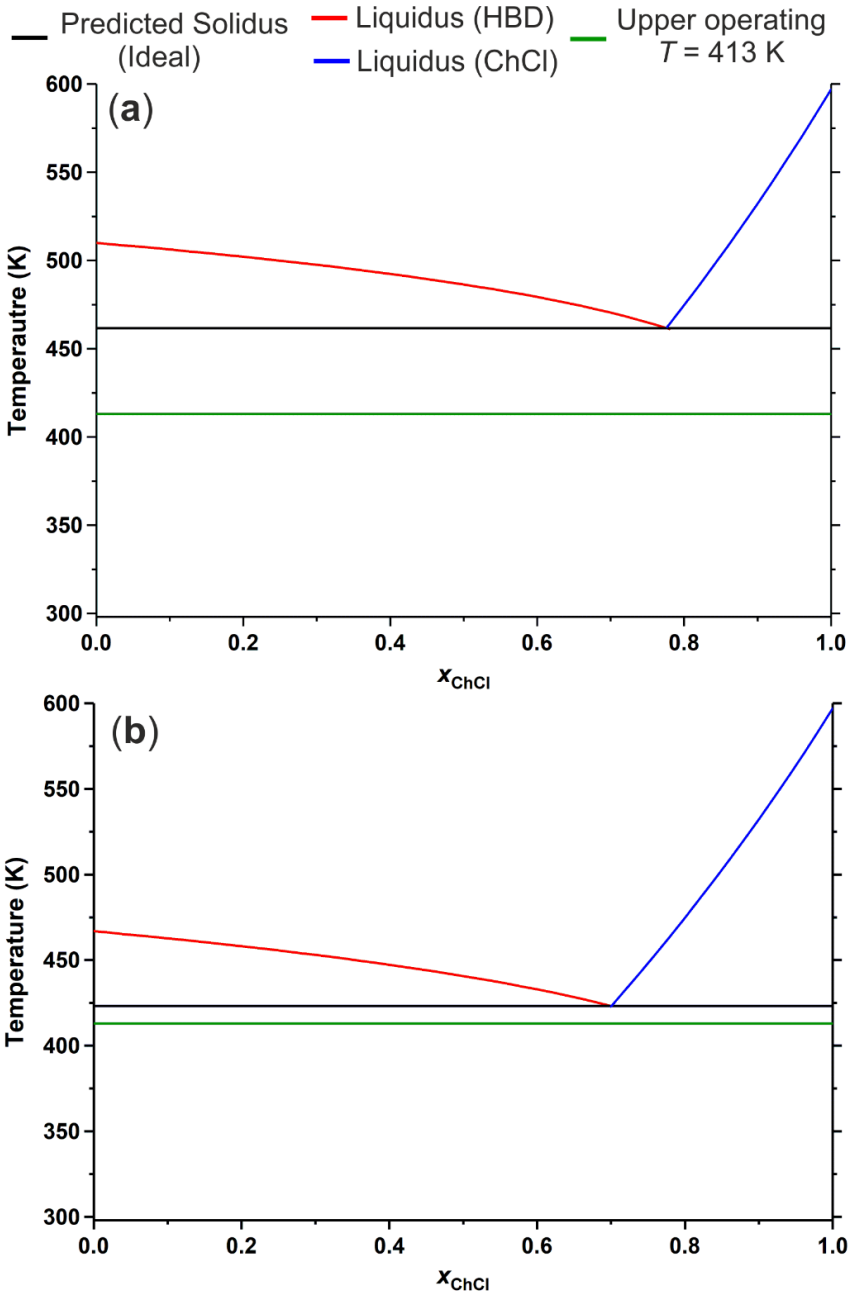

Figure 6.3: Ideal SLE phase diagrams for mixtures of (**a**) NicAc:ChCl and (**b**) Asco:ChCl predicted using Equation 6.2. Originally in colour.

The experimental SLE behaviour was very similar across each of the lactone:ChCl mixtures, with the 1:1 and 1:1.5 blends being the only compositions to produce a completely liquid melt. An upper operating temperature limit was set at 110 ^{o}C as continued heating above this value resulted in an observable darkening of the liquid phase, which likely signified the onset of degradation. Again, the eutectic melts were found to be highly metastable and could be stored for in excess of seven days at room temperature before any recrystallisation was observed (**Figure 6.4**).

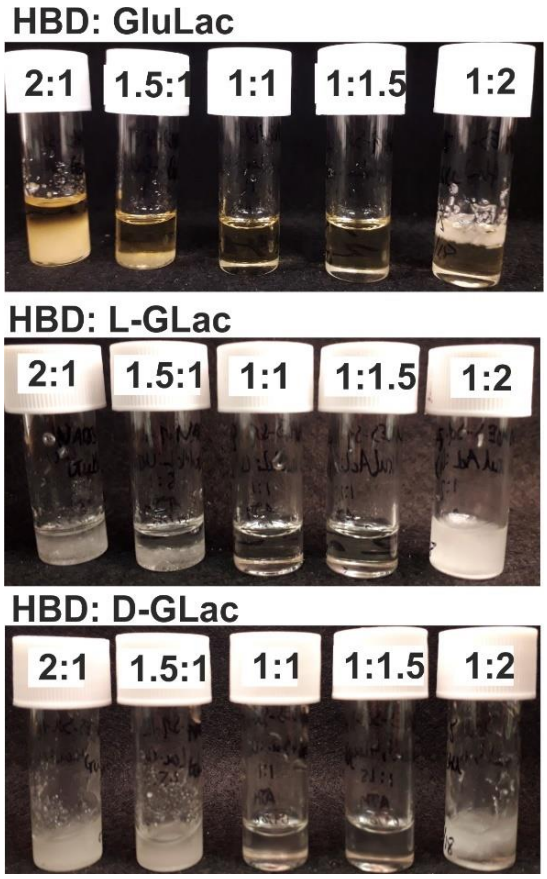

Figure 6.4: Visible appearance of GluLac:ChCl, L-GLac:ChCl and D-GLac:ChCl (bottom) mixtures at different molar ratios (2:1, 1.5:1, 1:1, 1:1.5, 1:2) following $\geq$ 7 days storage at room temperature. Originally in colour.

It should be noted that during the undertaking of this work, the Asco:ChCl DES has now been reported independently by others - first by Liu *et al*. in a patent and a subsequent paper outlining its application as a protective antioxidant and potential food additive and secondly by Silva *et al*. who also employed it as an antioxidant.[362-364] A eutectic melt formed using Glu-1,5-Lac and citric acid for the production of polyesters has been described by de Jongh *et al*. whilst a short-lived mixture containing both Glu-1,5-Lac and ChCl was formed during *in-situ* oxidation of a glucose:ChCl DES but was highlighted only in passing.[365, 366] Therefore, the DES based on the aforementioned lactones appear to be novel to the best of this author's knowledge and as such, were characterised in comparatively greater detail (section **6.2**) in order to assess potential applicability as 'proof-of-concept' humectants/plasticisers.

6.2. Physicochemical characterisation of food-grade eutectic mixtures based on natural L-ascorbic acid analogues

Initial characterisation of the lactone-based DES involved the application of DSC/STA in order to more closely probe their thermal properties. $\Delta H_{m,i}$ and/or $T_{m,i}$ for GluLac, L-GLac, D-GLac and Glu-1,5-Lac were all determined experimentally as highlighted in **Figure 6.5**. The melting points of L- and D-GLac were found to be very similar (T_{max} = 186/185 ^{o}C) to those provided in the literature (186/186 ^{o}C respectively),[367] whilst the values of $\Delta H_{fus,i}$ were around 3 to 4 kJ mol^{-1} lower. For GluLac, the melting endotherm actually appears to be somewhat bimodal, exhibiting two maxima at *ca*. 168.2 and 171.8 ^{o}C (lit. = 176 - 178 ^{o}C).[368] The origin of this behaviour is not currently clear although it could correspond to the presence of a minor impurity or the initial stages of degradation which appeared to begin almost concomitantly with melting endotherm according to STA (**Appendix Figure D.2a**), as has been reported for Asco.[355] It appears to at least partly correspond to a phase change from solid to liquid given that the presence of a molten liquid following heating could be inferred from a glass transition at *ca*. 12 ^{o}C that manifested during the second heat scan of cyclic DSC (**Appendix Figure D.2b**). In the case of L-GLac, D-GLac or Glu-1,5 the melting endotherms could be more clearly resolved from any decomposition events (see **Appendix Figure D.2c-e**).

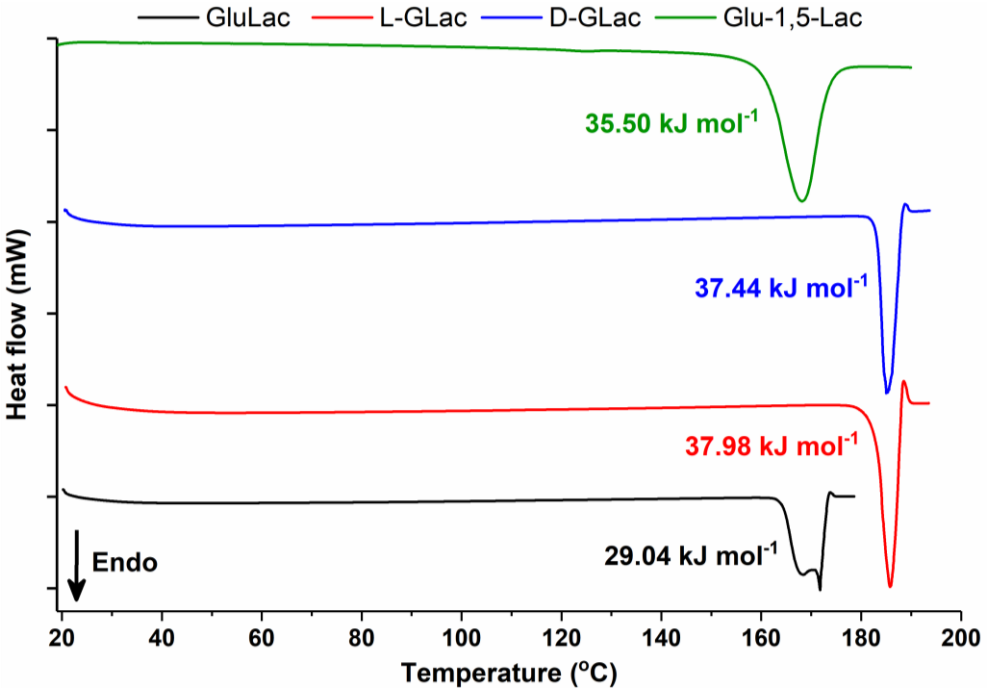

Figure 6.5: Overlay of first heat cycles (3 °C min^{-1}) for pure GluLac (7.2 mg), L-GLac (7.0 mg), D-GLac (6.6 mg) and Glu-1,5-Lac (5 °C min^{-1}, 9.9 mg) along with the corresponding $\Delta H_{m,i}$ associated with each endotherm. *y*-axis tick marks correspond to 10 mW. Originally in colour.

In an attempt to fully characterise the SLE phase diagrams of novel lactone:ChCl eutectics, the mixtures that were previously found to fully liquefy during the initial screen were subjected to more detailed DSC analysis. The first heating scans for the 1:1 and 1:1.5 lactone:ChCl mixtures are shown in **Figure 6.6** wherein clear endothermic deviations from the baselines following initiation equilibration (to approximately 20 °C) and beginning at *ca*. 28 - 30 °C can be seen in all cases (full *in-situ* traces are shown in **Appendix Figure D.3**). Such signals were not present in the corresponding thermograms in any of the individual lactones (cf. **Figure 6.5**) or ChCl (**Figure 6.6a**) and either absent or considerably less observable in the second heat cycles. These events were attributed to the onset of eutectic melting and can thus be considered the solidus temperatures of the respective systems, as corroborated by the fact that they manifested at similar temperatures independent of composition (Table 6.2). The solidi were estimated as the temperature at which two tangent lines corresponding to the baseline and the

initial endothermic deviation respectively were found to intersect (demonstrated graphically in **Appendix Figure D.4**).

It can be seen that the solidus temperatures measured in this way were all found to be very comparable, which is attributed to the high structural similarity of the individual starting components and thus, the extent/nature of the interactions that must occur within the DES. Yet the extent of and enthalpy change associated with the eutectic melting appeared to be somewhat variable across the different mixtures (note the magnitude of the *y*-axes). This is probably due to a combination of sample mass, system dependent properties (e.g. the energy input related to breaking the native crystal lattices vs. that released via formation of new inter/intra molecular contacts) and the extent to which the individual components could be brought into contact with each other within the 40 μL sample pans through very limited manual mixing prior to loading. However, the onset of eutectic melting should be an intensive property and theoretically only require minimal contact between the two components.

Table 6.2: Solidi of lactone:ChCl mixtures estimated from the first heating cycles using DSC.

System	**Solidus temperature (ºC / K)[a]**
GluLac:ChCl, 1:1	27.9 / 301.1
GluLac:ChCl, 1:1.5	29.1 / 302.3
L-GLac:ChCl, 1:1	29.6 / 302.8
L-GLac:ChCl, 1:1.5	28.7/ 301.9
D-GLac:ChCl, 1:1	29.2/ 302.4
D-GLac:ChCl, 1:1.5	28.8/ 302.0
Glu-1,5-Lac:ChCl, 1:1	29.2/ 302.4

[a]Determined using a heating rate of 3 ºC min^{-1}.

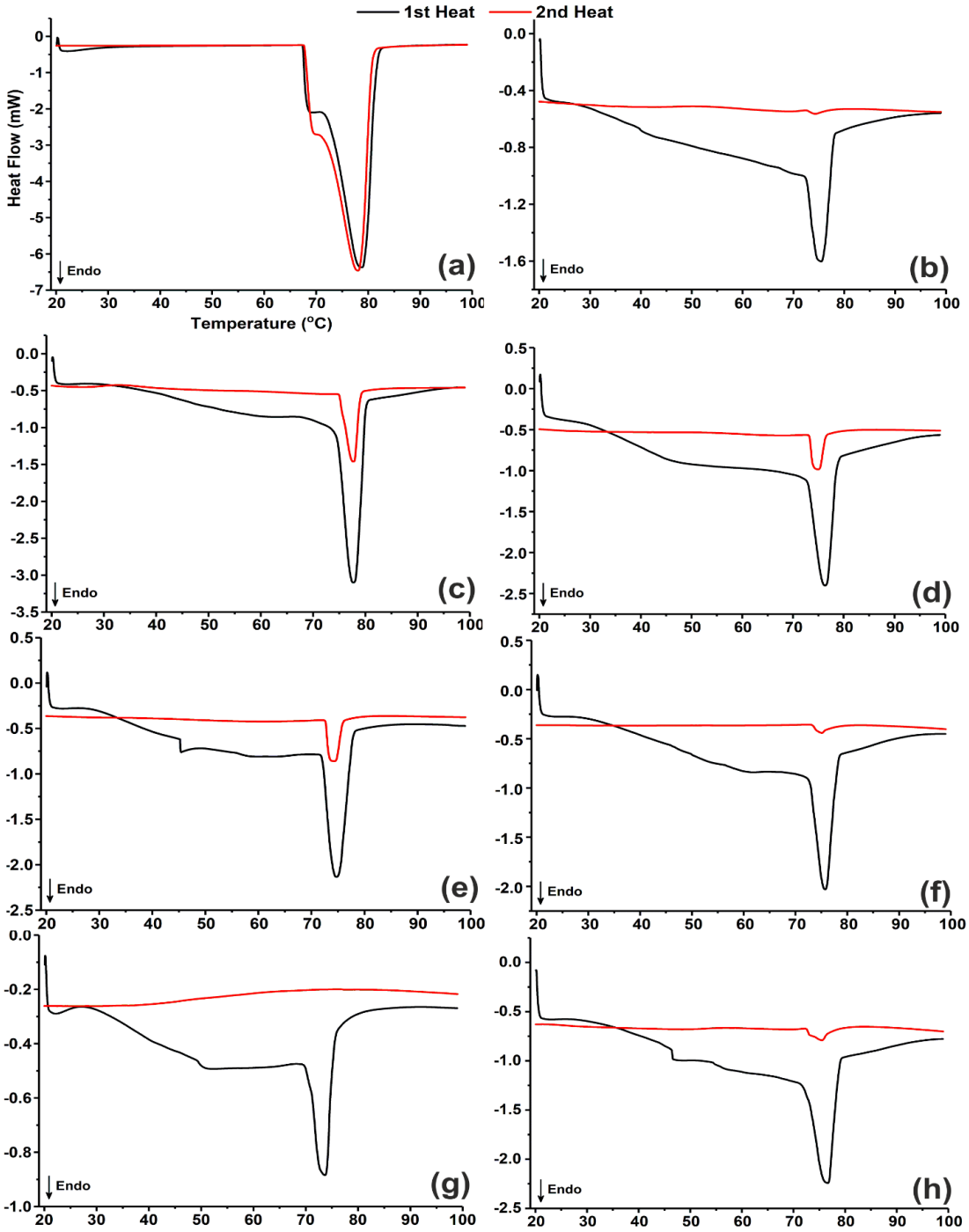

Figure 6.6: DSC thermograms showing the 1st and 2nd heat cycles (3 °C min^{-1}) of (**a**) neat ChCl (8.7 mg) and solid mixtures of (**b**) 1:1 GluLac:ChCl (5.0:3.8 mg), (**c**) 1:1.5 GluLac:ChCl (3.8:4.4 mg), (**d**) 1:1 L-GLac:ChCl (4.9:4.1 mg), (**e**) 1:1.5 L-GLac:ChCl (3.3:4.1 mg), (**f**) 1:1 D-GLac:ChCl (4.5:3.5 mg), (**g**) 1:1.5 D-GLac:ChCl (2.5:3.0 mg) and (**h**) 1:1 Glu-1,5-Lac:ChCl (5.7:4.3 mg). Originally in colour.

Interestingly, it was not possible to discern any obvious baseline deviations within the corresponding thermograms of the Asco-based DES, suggesting that the solidus may lie around or below the equilibration temperature that was used (20 ^{o}C). Silva *et al*. reported that a liquid DES with a composition of 1:2 Asco:ChCl remained following < 8 hours storage at 'room' temperature although this value was not disclosed, whereas the 1:1 and 2:1 mixtures were found to be molten at 40 ^{o}C but yielded pasty solids when left to cool (n.b. the 1:1.5 does not appear to have been analysed).[363] Liu *et al.* suggested that homogenous liquids could be obtained via heating mixtures of Asco:ChCl there were between 1:1.2 to 2.5 at starting at 60 ^{o}C yet no detailed information regarding their formation or storage stability was forthcoming.[362] Despite the marginally higher $\Delta H_{m,i}$, $T_{m,i}$ of Asco with respect to the other lactones, a lower eutectic temperature may reflect its greater acidity (due to extra stabilisation of (partial) negative charge within the conjugated system) which in turn should lead to an enhanced strength of interactions with ChCl (e.g. charge delocalisation of the Cl^{-}) within the DES phase.

Inspection of **Figure 6.6** highlights the consistent presence of a significant endothermic maxima that manifested at *ca*. 70 – 80 (**Figure 6.6a**) and 74 - 77 ^{o}C (**Figure 6.6b – 3h**) but which was otherwise completely absent in the traces of the individual lactones. This signal corresponds to the aforementioned solid-solid transition of the so-called α to β form of ChCl which is reversible upon cooling in the case of neat ChCl that was measured to have a transition enthalpy of *ca*. 15 kJ mol^{-1} which is reasonably close to that reported by Crespo *et al*. (17.2 kJ mol^{-1}) (**Appendix Figure D.1**).[352] Naturally, the absolute enthalpy associated with the transition is an extensive property and thus would be expected to increase/decrease with higher/lower concentrations of ChCl. This is consistent with the diminution of the peak corresponding to the transition that can be observed when comparing the first and second heat cycles in **Figure 6.6** as the ChCl becomes progressively consumed into the liquid phase. Given that the transition occurred concomitantly with eutectic melting, it was not possible to accurately measure $\Delta H_{m,mix}$ and therefore construct a phase diagram via the common Tammann plot approach (a plot of $\Delta H_{m,mix}$ as a function of composition) for any of the ChCl-containing mixtures.

It is interesting to note that many of the ChCl-containing DES which are described in the literature are commonly prepared via heating at temperatures that are slightly above the aforementioned dimorphic transition temperature (typically 80 °C). Earlier single crystal XRD studies have suggested that upon transition from the α to β dimorph, the oxygen of the hydroxyl group assumes a closer position to the cationic nitrogen and further from Cl^-, possibly resulting in comparatively weaker interaction of the latter with both of the two former entities.[369] If charge delocalisation from Cl^- to the second component can be considered as a key interaction that leads to a 'deep' eutectic depression in ChCl-based DES, it follows that the β form could lend itself to more ready DES formation given that the Cl^- is already less complexed to the choline functional groups within the native crystal.

Due to the hygroscopicity of ChCl, a small amount of water was likely present within each system during DSC analysis which may have somewhat inadvertently reduced the measured solidus temperatures. It has been reported that the presence of around 10 wt. % water resulted in the depression of T_{eu} by 30 °C in the urea:ChCl, 2:1 DES,[370] whereas Silva *et al*. found that addition of 3 and 9 wt. % H_2O could suppress the T_{eu} of mannose:ChCl and xylose:ChCl respectively to 25 °C, representing a drop of at least > 20 °C (although the compositions of the sugar:ChCl mixtures containing water were not disclosed).[371] KF analysis indicated that the preformed DES had a water content of 0.9 – 1.2 wt. % (corresponding to a mole fraction of *ca*. 0.08) even though they were prepared using components that had been dried *in vacuo* (> 2 h, 80 °C, *ca*. 20 mbar) prior to use and stored in a desiccator following preparation. In spite of this, full prevention of moisture absorption was not technically feasible in the present study owing to a lack of available preventative measures (e.g. glovebox). It should also be noted that although water content could not be measured for the *in-situ* DSC experiments, the difference between the two experimental sets is anticipated to be relatively small given that they were exposed to the same external environment (i. e. ambient air) for similar lengths of time (approximately 1 – 2 minutes). Similarly, KF analysis could not be used to determine the water content of the Asco DES due to the unavoidable reduction of iodine by ascorbic acid, necessitating estimation via STA (**Appendix**

Figure D.5) which yielded values of 1.4 and 1.6 wt. % for the 1:1 and 1:1.5 mixtures respectively (presuming that the water content was equal to the mass lost < 150 °C cf. broad endotherm).

Unsurprisingly, given the minimal concentration of water the measured a_w of the DES was also found to be extremely low (**Table 6.3**) at < 0.050, with similar results having recently been reported for the urea:ChCl 2:1 DES.[372] This may be beneficial in dry comestible products that are very sensitive to even low a_w and which cannot be used within composite products with almost all currently available aqueous humectant mixtures. It is however problematic from a hygroscopicity standpoint, as evidenced by the fact that all of the DES displayed a high propensity (visually assessed) to pick up moisture from ambient air, although this issue is already extensively encountered in the confectionery for most amorphous sugar-based products.

Table 6.3: Measured a_w values of several lactone-DES (~ 1 wt. % water) at 25 °C.

System	a_w (± 0.003)
GluLac:ChCl, 1:1	0.032
L-GLac:ChCl, 1:1	0.048
Glu-1,5-Lac,ChCl, 1:1	0.031

Interestingly, the moisture absorption at room temperature appeared to result in the partial crystallisation of the DES in some instances, which has not been documented in similar mixtures (e.g. sugars plus ChCl) to the best of the author's knowledge. It remains uncertain whether this phenomenon is localised to the DES surface where the water was initially absorbed (and presumably facilitated sufficient molecular mobility so as to enable aggregation and nucleation of the individual components) or if it signifies an incompatibility of the lactone-DES with water at a medium concentration level and hence, must be studied more thoroughly moving forward. Similarly, the influence of the order of water addition should also be investigated given that such an occurrence was not documented by the very

similar sugar/ChCl/water or Asco/ChCl mixtures that were described by Silva *et al*. and Liu *et al*. respectively.[362, 371] One final caveat that should be considered upon water addition is the potential for hydrolysis of the lactones into the corresponding acids (particularly during DES preparation at elevated temperatures), which would presumably alter the composition of inter-molecular/atomic interactions within the mixtures.

In order to verify that the initial components had not undergone degradation or reaction during DES preparation which been reported for instance in the case of ChCl and carboxylic acids,[373, 374] each of the preformed systems was compared with the pure crystalline constituents via solution-state ^{1}H NMR. In all cases, the spectra appeared to be virtually identical, as shown in **Figure 6.7** for the L-GLac:ChCl DES (spectra of the other DES are presented in **Appendix Figure D.6**) with the relative peak intensities being the only notable discrepancies and which were to be expected given the varying quantities of the lactone and ChCl present in each sample. The omnipresent peak at 2.50 ppm originates from the non-deuterated solvent (i.e. DMSO) and was used as an internal reference whilst the signal at *ca*. 3.38 ppm corresponds to residual water (HOD) and overlaps with the peak of the methylene group neighbouring the nitrogen in ChCl (peak number 2) in some spectra.

Within the analyte solution, L- and D-GLac appeared to primarily adopt the 1,4-furano-γ form, with the other low intensity signals that are visible in the spectra corresponding to the less abundant 1,5-pyrano-δ lactone isomers. The opposite was true for Glu-1,5-Lac (**Appendix Figure D.6c**) which existed almost exclusively in the latter form when present as the sole solute although some 1-4 lactone could be observed for the mixed DES sample. Both findings are in good agreement with previous reports in the literature.[375] The lack of any significantly downfield signals (> 6.50 ppm) indicated that hydrolysis of the lactones to the corresponding carboxylic acids did not occur during preparation and also that GluLac (**Appendix Figure D.6a**) was present as the bicyclic structure as opposed to the potential monocyclic

aldehyde. It is currently unclear as to which form/s of the lactone structures actually exist within the liquid DES themselves and this could be probed further (e.g. via magic angle NMR) in order to gain additional information concerning the potential intra/intermolecular contacts that presumably underpin their formation. From the standpoint of the present study, preservation of the starting constituents which are well-characterised, food-grade ingredients is important as decomposition towards potentially hazardous by-products would prove highly problematic for applications involving direct human consumption.

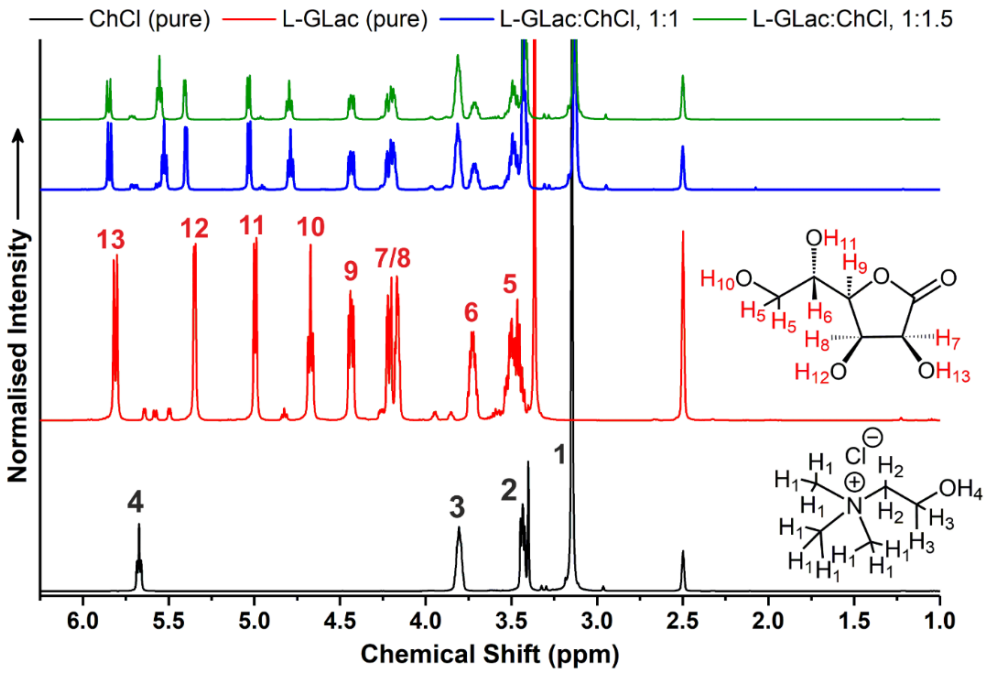

Figure 6.7: Comparative ^{1}H NMR (400 MHz, D_6-DMSO) spectra of crystalline ChCl and L-GLac with the 1:1 and 1:1.5 L-GLac:ChCl DES. Originally in colour.

In principle, the eutectic melting of a mixture should be fully reversible and yield the corresponding solidified components once the temperature is taken below the liquidus/solidus. This would serve as potential method of confirming the solidus temperatures measured previously. However, this process was found to occur prohibitively slowly according to visual observations, with samples and especially

those that were presumed to be closest to the eutectic composition (1:1 and 1:1.5) remaining partially liquid even following storage under ambient conditions for several months. This is ascribed to limited molecular mobility within the viscous melt. Efforts to expedite freezing through rapid and deep cooling of preformed DES via DSC were unsuccessful and instead revealed that all of the melts, in which the aforementioned dimorphic transition could not be detected (and thus indicating the absence of crystalline ChCl), had a strong propensity to supercool as evidenced by readily discernible glass transitions at – 55 to - 40 ºC (**Figure 6.8**).

The measured T_g values (midpoint) of the 1:1.5 lactone:ChCl DES were consistently lower than those of the corresponding 1:1 mixtures by approximately 5 to 10 ºC, possibly due to the aforementioned hygroscopicity of ChCl that may have resulted in a marginally higher amount of water being incorporated into the mixtures and hence a reduction in T_g given the potent plasticising power of water. In any case, the values are still very comparable or even lower than common aqueous confectionery systems, which this author considers remarkable given that they contain virtually no water and an extremely low a_w. The combination of extremely low a_w and T_g that can be achieved with these eutectic mixtures are particularly exciting from a functionality perspective given that in the current paradigm of available food systems, it is very difficult to achieve a high level of product fluidity/plasticity whilst maintaining a minimal a_w.

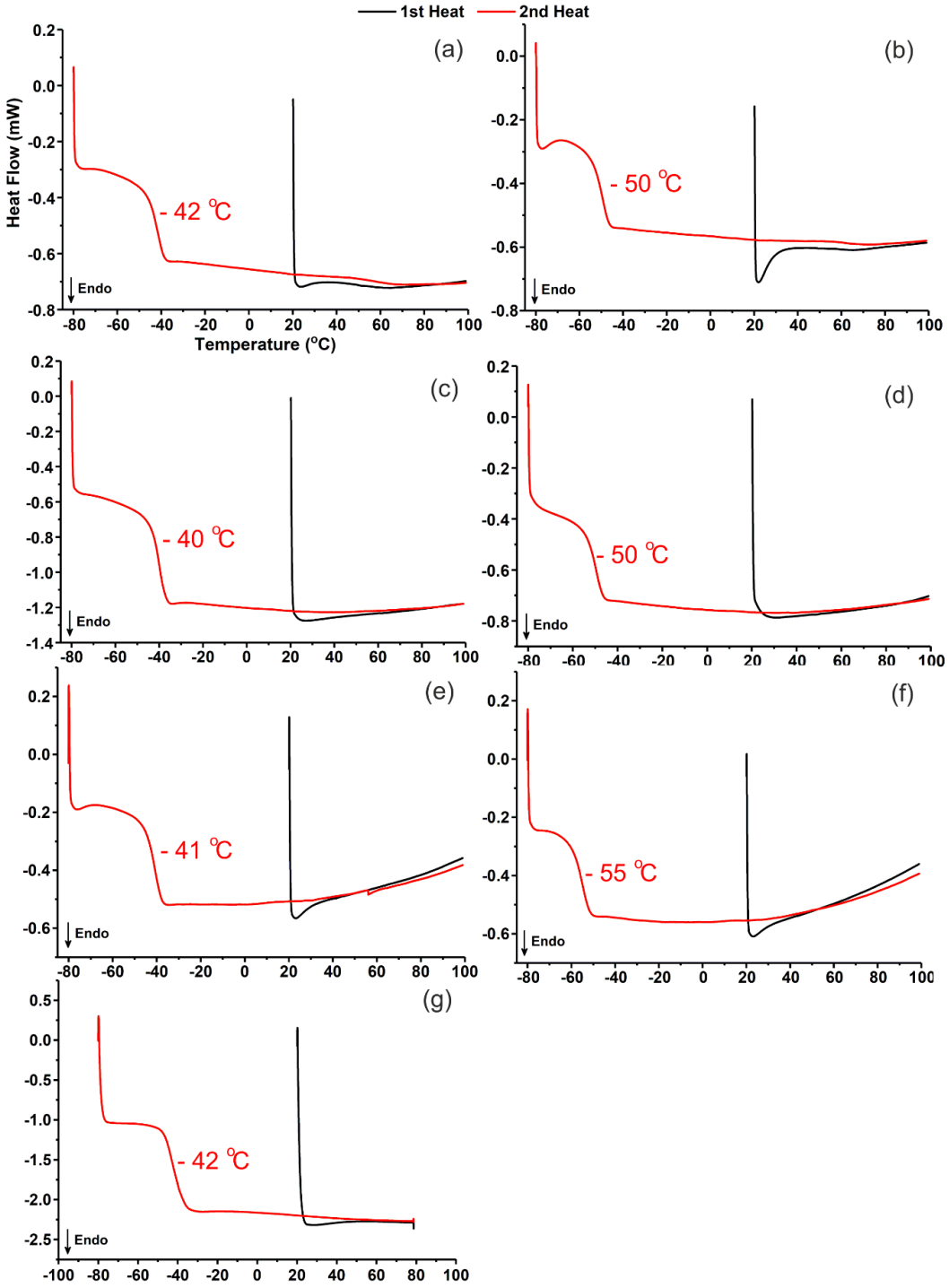

Figure 6.8: DSC thermograms showing the first and second heat cycles (3 °C min^{-1}) of preformed DES; (**a**) 1:1 GluLac:ChCl (10.4 mg), (**b**) 1:1.5 GluLac:ChCl (10.0 mg), (**c**) 1:1 L-GLac:ChCl (16.4 mg), (**d**) 1:1.5 L-GLac:ChCl (10.4 mg), (**e**) 1:1 D-GLac:ChCl (10.7 mg), (**f**) 1:1.5 D-GLac:ChCl (9.3 mg) and (**g**) 1:1 Glu-1,5-Lac:ChCl (9.8 mg – n.b. heated to a maximum of 80 °C at a rate of 10 °C min^{-1}).

An interesting recent theoretical development in food polymer science has suggested that the T_g of many common biopolymer-based food matrices, which like hydrophilic DES are constituted by an overarching hydrogen bonding network can be considered primarily as a reflection of the average number of OHs group per molecule, with a higher number of hydroxyls resulting in increased T_g.[30] A similar mechanism within the DES would be in-keeping with the lower glass transitions that are observed moving from 1:1 to 1:1.5 lactone:ChCl mixtures given that the latter component only has a single OH moiety to act as both a H-bond donor and acceptor (although Cl^- also likely acts an acceptor) whereas the lactones have three or four (at least in the native crystals) which are spatially well distributed and presumably partake in extensive and multi-directional hydrogen bonding throughout the fluid.

Also noteworthy in the preformed samples was the lack of observable cold crystallisation, which has been reported to occur in vitrified mixtures of ChCl and other polyhydroxyls (e.g. sugars)[376] and suggests that the lactone DES systems could have excellent utility in cryopreservation, wherein the avoidance of crystallisation is necessary for ensuring sufficient protection of labile substances that could otherwise suffer irreversible damage.[377] It should be noted that given the kinetic nature of crystallisation from the melts, it is likely that such an event would be highly dependent on the rate of heating as was found for the devitrification of the ChCl:Urea DES.[378] Therefore, future investigations along these lines are necessary for a more comprehensive evaluation of potential cryopreservation or low temperature applications using the lactone-DES.

In addition to the preformed materials, similar glass transitions were also visible starting in the second heat cycles of the *in-situ* experiments (**Appendix Figure D.7**) although they were notably weaker even following four cycles of heating/cooling, indicating that full eutectic formation could not be achieved, most likely due to a lack of sufficient mixing. The lower T_g (*ca*. 5 ^oC on average) values in the *in-situ*

samples could possibly be the result of a marginally higher water content than the preformed analogues. It was also possible to observe exotherms (sometimes multiple) during the cooling cycles (**Appendix Figure D.7**) although their origin is ambiguous as they could correspond to various events including the crystallisation of the aforementioned hypothetical ice melting, melt crystallisation of one of the eutectic components and/or transition of crystalline ChCl β dimorph back to α (the presence of which is inferred from the subsequent endotherms at *ca*. 75 °C). Given that they occurred in a somewhat sporadic manner with small and variable associated energies, the exotherms were not considered to be indicative of a liquidus/solidus phase boundary. Interestingly, the only reproducible signals in this regard appeared consistently at close to 0 °C (exemplified for Glu-1,5-Lac:ChCl, 1:1 in **Figure 6.9**), irrespective of the lactone identity. These are tentatively attributed to a concurrent event of ice melting and subsequent cold crystallisation/dimorphism (resulting from an increased molecular mobility afforded via plasticisation by the released liquid water) of a small quantity of the DES components and most likely ChCl, although this should be confirmed using a second complementary technique e.g. DSC-microscopy.

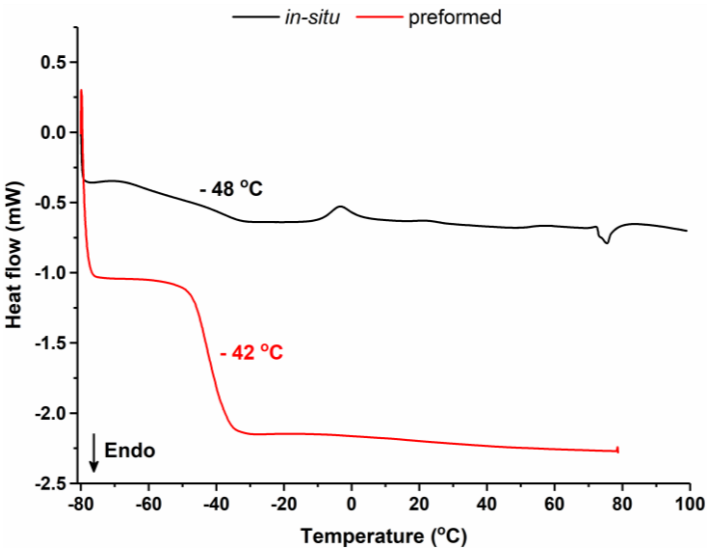

Figure 6.9: Comparison of DSC thermograms showing the second heat cycles of *in-situ* prepared (10.0 mg) and preformed (9.8 mg) Glu-1,5-Lac:ChCl DES.

Using the average solidus temperatures presented in Table 6.2, we can infer that significant negative deviations from ideal SLE were realised in all systems as highlighted by comparison with the corresponding ideal melting behaviour for GluLac:ChCl (**Figure 6.10**) in which x_{eu} and T_{eu} are predicted to occur at 0.64 (≈ 1:1.8 GluLac:ChCl) and 121 °C respectively (phase diagrams for the other DES are shown in **Appendix Figure D.8**). However, as the 1:1 and 1:1.5 GluLac:ChCl mixtures were the only compositions found to fully liquify and much more readily than 1: ≥ 2 GluLac:ChCl under the typically operating temperature (373 K/100 °C) according to the visual observations, the most realistic eutectic point is likely to be closer to x_{ChCl} = 0.50 - 0.60.

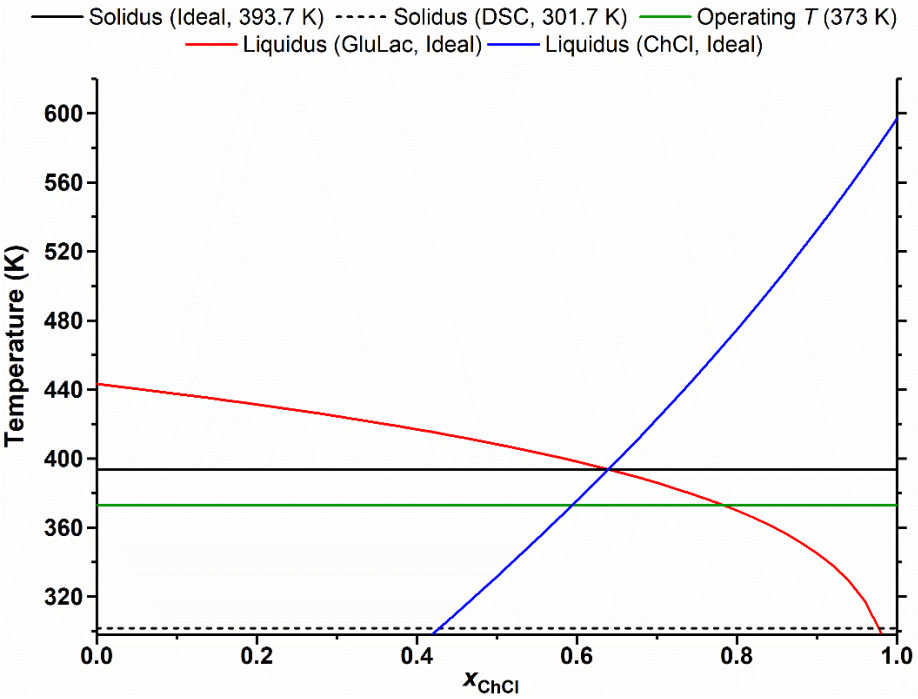

Figure 6.10: Theoretical solid-liquid phase diagram of the GluLac:ChCl mixture and comparison with the experimental solidus as measured via DSC.

Equation 6.1 can be rearranged to solve for y_i through **Equation 6.3**:

$$y_i = \frac{e^{\left[\frac{\Delta H_{m,i}}{R}\left(\frac{1}{T_{m,i}} - \frac{1}{T}\right)\right]}}{x_i} \qquad \textbf{Equation 6.3}$$

Solving **Equation 6.3** for the GluLac:ChCl system with T_{eu} = 301.7 K (28.5 °C) gives y_i (calculated for the component with the highest ideal liquidus boundary, in this case GluLac) as 0.049 or 0.062 for x_{ChCl} = 0.50 or 0.60 respectively. As both give y_i << 1, the GluLac:ChCl system can be considered to be a true 'deep' eutectic mixture. Such non-ideal melting behaviour appears to be a general hallmark of mixtures containing ChCl and polyhydroxyls including various sugars (y_i = 0.031 or 0.562 for sucrose or mannose) but also for aliphatic hydroxycarboxylic acids.[371, 379] A summary of y_i calculated based on the experimental solidi and a eutectic composition of either x_{ChCl} = 0.50 or 0.60 for the various lactone-DES is presented in **Table 6.4**. According to **Equation 6.3**, greater values of $\Delta H_{m,i}$ and/or $T_{m,i}$ should result in an increase of the solidus/liquidus temperatures, which accounts for the comparatively higher/lower values of y_i in the case of GluLac/L-GLac respectively (i.e. smaller/greater deviations from ideality are required to achieve the same solidus temperature).

Table 6.4: Summary of SLE phase behaviour of lactone:ChCl DES based on predicted and experimental solidi.

DES	**Predicted SLE**		**Experimental SLE**		
	x_{eu} (x_{ChCl})	T_{eu} (K)	$y_{Lactone}$ (x_{ChCl} = 0.5)	$y_{Lactone}$ (x_{ChCl} = 0.6)	T_{eu} (K)[a]
GluLac:ChCl	0.64	393.7	0.049	0.062	301.7
L-GLac:ChCl	0.68	412.1	0.012	0.014	302.4
D-GLac:ChC	0.68	411.0	0.013	0.016	302.2
Glu-1,5-Lac:ChCl	0.65	398.5	0.023	0.019	302.4

[a]Represents the average T_{eu} calculated for the 1:1 and 1:1.5 systems.

As indicated previously, all of the preformed DES were found to be relatively (meta) stable fluids that were devoid of crystalline starting components for $\geq$ 7 days storage (within a desiccator) at room temperature following preparation. Given that the rheology of a fluid is an important parameter from both a processing and product quality perspective, this was examined for all of lactone-DES and compared to the Asco-based systems. Due to the propensity of the DES to absorb moisture, a coating layer of immiscible, low viscosity silicone oil was immediately applied to the edge of each sample following loading onto the rheometer. As shown in **Figure 6.11**, all of the eutectics were found to be viscous fluids that exhibited virtually Newtonian flow behaviour (i.e. independence of viscosity on rate of shear) when subjected to a dynamic shear rate sweep from 20 to 500 s^{-1} operating at 20 to 60 ^{o}C. The measured viscosities were broadly similar across the three non-Asco containing DES whereas both the Asco systems were higher at all temperatures and noticeably so at 20/30 ^{o}C.

All systems exhibited an inverse relationship between viscosity and temperature which was found to follow an exponential type function that could be very well described via an Arrhenius model (**Equation 6.4**), yielding excellent fits (**Figure 6.12**, $R^2 \geq 0.997$) and for which the relevant model parameters are summarised in **Table 6.5**:

$$\eta = \eta_0 \, e^{\frac{E_a}{RT}} \qquad \textbf{Equation 6.4}$$

Here, η, R and T are the measured viscosity (recorded at a shear rate of 50 s^{-1} in all cases), gas constant (8.314 J K mol^{-1}) and system temperature respectively, whereas η_0 and E_a, the pre-exponential factor and activation energy which vary depending on the system. It should be noted that Liu *et al.* reported that the viscosity of Asco:ChCl, 1:2 DES as 12.5 mPas at 25 ^{o}C which is over three orders of magnitude lower than that found here (~ 46 Pas calculated for 1:1.5 via **Equation 6.4** at 25 ^{o}C),[340] although those authors did not provide any information regarding water concentration. The values presented here are

instead within an order of magnitude with those published by Silva *et al.* for the same 1:2 mixture (*ca.* 17 Pas at 20 ^{o}C)[363] yet no experimental details concerning the water content were given and the measured viscosities were obtained using a relatively fast temperature sweep (2 ^{o}C min^{-1}) which may have resulted in significant thermal lag between the actual/measured temperature.

Within **Equation 6.4**, the E_a can be considered to reflect the energy barrier that must be overcome for a molecule/group of molecules to move from one occupancy within a fluid to a second, that is prerequisite for viscous flow of the material to occur. Indeed, the viscosity of DES has historically been rationalised through the conceptually related hole theory which suggests that it results from a disparity between the large radii of the constituents (especially if multiple species associate to form a quasi-single entity) and the small average void size existing within the liquid matrix.[380] Inspecting the rheological traces, the most obvious trend is that the measured viscosities of the 1:1.5 DES were consistent lower than the corresponding 1:1 mixture which could, in part be attributed to a marginally higher water content in the former as indicated previously by the lower measured T_g values. It may also indicate that the strength and/or overall extent of the interactions that manifested within the liquids containing higher concentrations of lactones were greater and ultimately more resistant to flow.

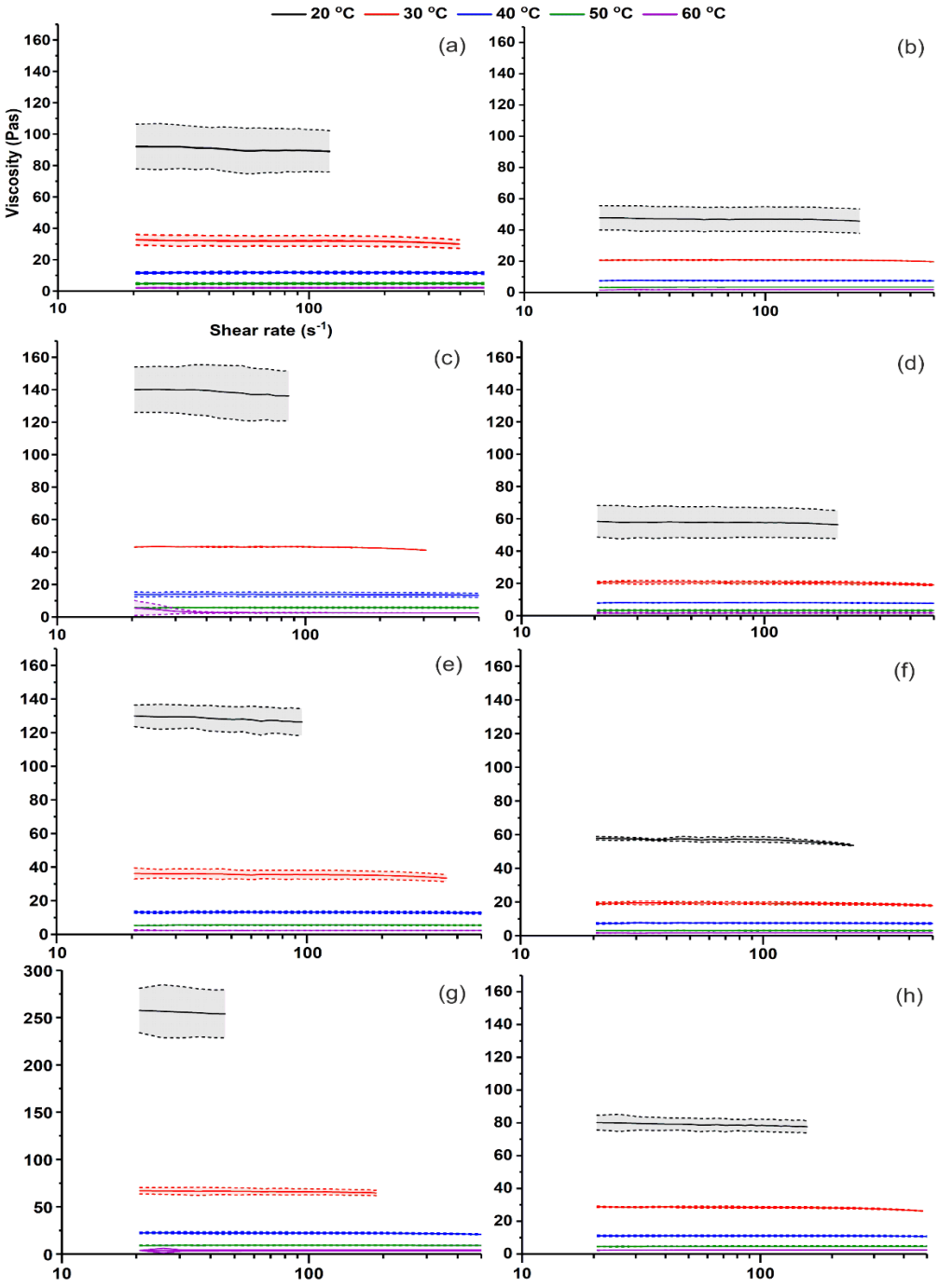

Figure 6.11: Viscosity of lactone DES measured as a function of temperature (20 – 60 °C) and shear rate (20 – 500 s^{-1}); (**a**) GluLac:ChCl, 1:1, (**b**) GluLac:ChCl, 1:1.5, (**c**) L-GLac:ChCl, 1:1, (**d**) L-GLac:ChCl, 1:1.5 (**e**) D-GLac:ChCl, 1:1, (**f**) D-GLac:ChCl, 1:1.5, (**g**) Asco:ChCl, 1:1 and (**h**) Asco:ChCl, 1:1.5. The solid lines and shaded areas/dashed lines represent the average of at least two replicate and $\pm$ 1 standard deviation respectively. Originally in colour.

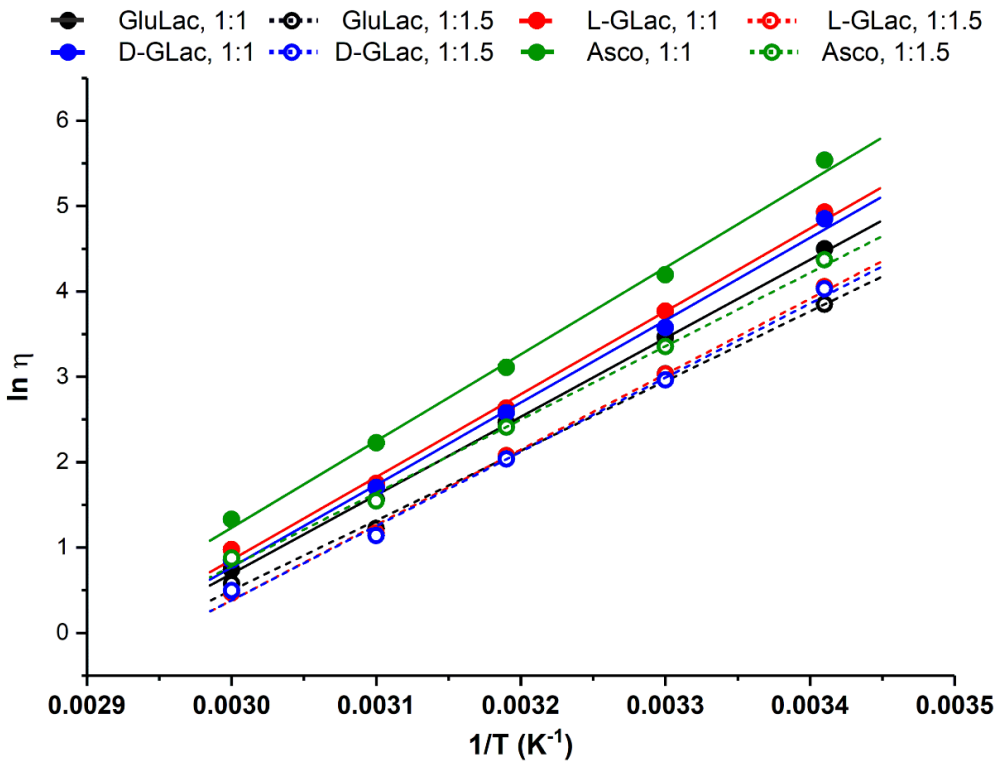

Figure 6.12: Arrhenius plots of lactone- and Asco-DES using viscosity measured at 50 s^{-1} where solid (1:1 HBD:ChCl) or dashed (1:1.5 HBD:ChCl) lines correspond to linear fits thereof. Originally in colour.

Table 6.5: Model parameters of the Arrhenius equation **(Equation 6.4)** for lactone and Asco DES.

System	R^2	E_a (kJ mol^{-1})	η_0 (Pas)
GluLac:ChCl, 1:1	1.000	76.50	2.057×10^{-12}
GluLac:ChCl, 1:1.5	0.998	67.92	3.742×10^{-11}
L-GLac:ChCl, 1:1	0.997	80.71	5.295×10^{-13}
L-GLac:ChCl, 1:1.5	0.999	73.45	4.521×10^{-12}
D-GLac:ChCl, 1:1	0.997	80.22	5.787×10^{-13}
D-GLac:ChCl, 1:1.5	0.998	72.27	6.927×10^{-12}
Asco:ChCl, 1:1	0.997	84.44	2.0110×10^{-13}
Asco:ChCl, 1:1.5	0.998	71.48	1.3695×10^{-11}

Intuitively this can be rationalised by the ability of the lactone species to partake in comparatively greater number of intermolecular interactions than ChCl, and especially those of relatively high energies such as H-bonds which would be highly penalising to break from an energetic standpoint. In this vein, the viscosity of other DES comprising the polyhydroxyl glycerol and ChCl was also found to decrease with increasing ChCl content which was attributed to a disruption of intermolecular forces, namely H-bonding by the salt.[381] Similar arguments would also explain why the Asco-DES, which are otherwise structurally identical to L-/D-GLac aside from the alkene moiety were found to exhibit the highest viscosity, as the greater acidity resulting from the conjugated 2-3-enediol/lactone carbonyl should strengthen any interactions involving C_3-OH in particular. Yet this hypothesis needs to be investigated more thoroughly via alternative methods e.g. molecular simulations. From a more general confectionery perspective, the measured viscosities are broadly similar to those encountered for instance in aqueous syrup binders based on glucose syrups of moderate *DE* (*ca*. 40 - 60) and median to high water contents (*ca*. 15 - 20 wt. %),[54] although it is notable that this can be achieved in the absence of water.

6.3. Summary

Taking inspiration from the potential role of natural 'deep eutectic' mixtures in providing humectancy and plasticisation *in-vivo* in addition to the increasing precedent for their use within food relevant applications (particularly as plasticisers for starch) (**Chapter 1**), a series of novel food-grade, eutectic mixtures formed using naturally-occurring lactones and the nutritional supplement, choline chloride were prepared following initial screening involving other vitamin-based constituents. These mixtures were found to liquefy at close to room temperature, exhibiting solidus temperatures of around 30 °C (as determined via DSC) and also to remain stable molten fluids for at least 7 days storage at room temperature. Comparison with ideal SLE that were constructed using measured $\Delta H_{m,i}$ and $T_{m,i}$ confirmed that all of the experimentally measured solidi represented 'deep' eutectic melting point depressions albeit in the presence of a small amount of unavoidable absorbed moisture (*ca*. 1 wt. % according to KF titration). Subsequent NMR analysis indicated that the starting components were

preserved during the preparation step and that undesirable thermal/chemical degradation had not taken place.

Importantly, the measured a_w of the DES was found to be extremely low in all cases, which is primarily a reflection of the absence of water within the mixtures. Even without this moisture, all of the systems exhibited very low glass transition temperatures (- 40 to – 55 ^oC) which were comparable to sugar-containing DES that have been described previously within the literature. This combination of extremely low a_w and T_g indicated that they could potentially act as efficient humectants/plasticisers within a model aqueous confectionery system (which was subsequently investigated further in **Chapter 7**). Rheological studies confirmed that all of the DES were viscous fluids which exhibited Newtonian flow behaviour when subjected to low to moderate shear rates (< 500 s^{-1}) and whose dependence on temperature could be very well-described using the Arrhenius model. Both the viscosity and T_g were found to be strongly influenced by the choline chloride content yet largely unaffected by the identity of the lactone constituent. Interestingly, all of the novel lactone DES exhibited lower viscosity (reduced activation energy) than their corresponding L-ascorbic acid analogues which is tentatively hypothesised to reflect stronger interactions within the ascorbic acid-choline chloride mixtures resulting from the comparatively greater acidity of ascorbic acid.

Chapter 7: Evaluation of novel nature-inspired humectants and plasticisers within a model aqueous confectionery filling

This Chapter investigates **Aim 4** as discussed previously within section **1.4**. More specifically, it deals with the evaluation of the novel humectants/plasticisers that were developed in **Chapter 4**, **Chapter 5** and **Chapter 6** within a model aqueous confectionery filling based on a low 'added' sugar glucose syrup. This Chapter comprises two main sections:

(i) **Section 7.1**: Introduces the materials that are to be used in the preparation of the model aqueous confectionery fillings and in particular, highlights the properties of Mylose 351® glucose syrup (MYL) that will be used therein.

(ii) **Section 7.2**: Initially describes the characterisation of MYL before evaluating the ability of glycoin, a floridoside-rich extract and the GluLac:ChCl, 1:1 deep eutectic mixture to provide humectancy and plasticisation within a model, MYL-based confection. The influence of these novel additives on the physicochemical properties of interest (a_w, T_g and viscosity) will be compared to that of two common confectionery solutes; glycerol and D-fructose in order to assess their suitability as drop-in sugar replacers.

7.1. Preamble

Given that the overall aim of this thesis was to develop a solution for potential real-world applications, the candidate 'drop-in' humectant/plasticiser species described previously in **Chapter 4**, **Chapter 5** and **Chapter 6** namely; glycoin, floridoside (extracted from *Palmaria palmata*) and the GluLac:ChCl (1:1) DES were applied within a model aqueous confectionery system wherein the performance of the new materials could be compared to those of two archetypal ingredients, glycerol and fructose (summarised in **Figure 7.1**).

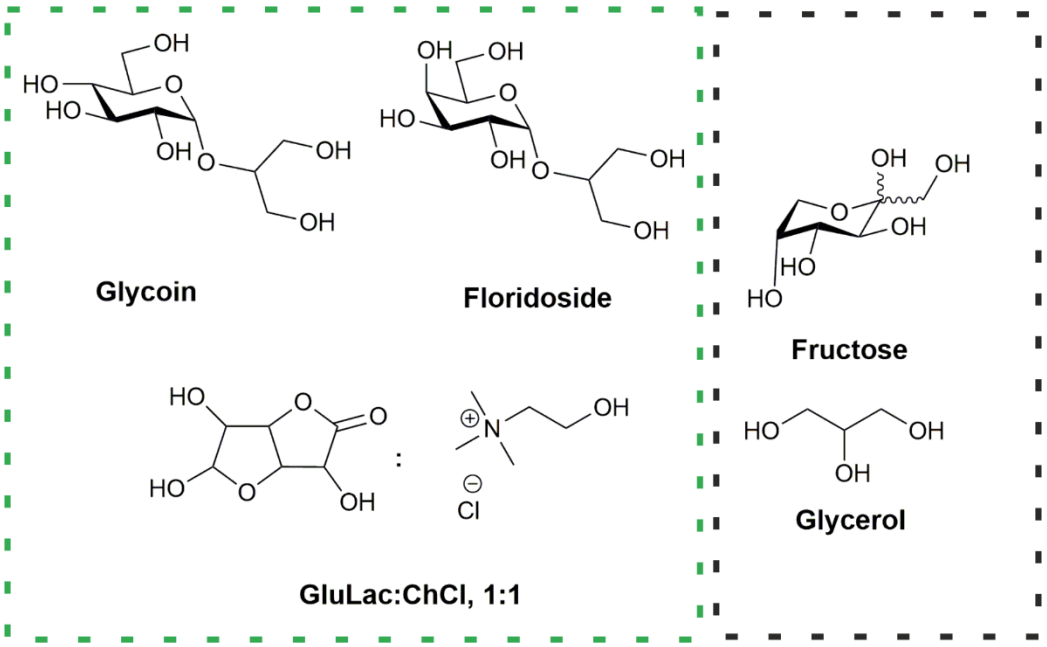

Figure 7.1: Candidate (green border) and benchmark (black border) humectant/plasticiser species selected for bench scale studies in this work. Originally in colour.

On account of its ubiquity in virtually all aqueous confectionery fillings (**1.1**), glucose syrup was selected as the base ingredient with which the candidate humectants would be formulated in order to create a representative 'model' aqueous confectionery filling. The syrup chosen for the present studies was Mylose 351® (MYL), a relatively new ingredient introduced by Tereos Starch and Sweeteners that is particularly attractive for the preparation of sugar-reduced comestibles due to uniquely low levels of D-maltose and D-glucose i.e. 'free 'sugars which constitute only 9 – 14 wt. % of the overall solids.[382] Instead, it comprises D-maltotetraose (α-D-glucopyranosyl-(1→4)-α-D-glucopyranosyl-(1→4)-α-D-glucopyranosyl-(1→4)-α-D-glucopyranose) and to a lesser extent D-maltotriose (α-D-glucopyranosyl-(1→4)-α-D-glucopyranosyl-(1→4)-α-D-glucopyranose) as the dominant α-D-1,4 glucose species. These species are thought to be digested considerably more slowly than the common mono- and di-saccharides, something which is ultimately beneficial for health (although this is disputed by some).[44, 383] Because of this, MYL has received recent attention as a low 'added' sugar option within various baked products (cookies, cakes, muffins etc.)[384-386] yet there does not appear to be any published work

concerning its application within aqueous confections to the best of the author's knowledge. From a physicochemical perspective, the relatively high concentration of larger oligomeric species should result in a significant increase in T_g/viscosity but only a modest reduction in a_w, making the successful utilisation of MYL more challenging with respect to traditional 'free' sugar-rich syrups. It was hypothesised that this would make it particularly sensitive to the addition of an external humectant/plasticiser and provide a useful gauge for performance evaluation of the novel additives. Yet the composition of MYL would first have to analysed in order to ensure that this is the case.

7.2. Results and Discussion

Initial work focussed on characterisation of the as-received MYL to confirm that it was compositionally in-keeping with the manufacturer's specifications. HPLC analysis (**Appendix Figure E.1**) indicated the presence of multiple species, with glucose and maltose being readily discernible based on characteristic retention times (according to an in-house database compiled at the GCCE). As the solutes contained within the syrup represent a homologous series, it is expected that the mode by which they interact with the stationary phase is to be similar and thus, that the separation mechanism would be primarily based on size. This appeared to be the case for the MYL sample, with the glucose eluting last (t_R = 14.7 min) followed by maltose (t_R = 12.8 min) and then a seemingly broad collection of signals which contained within it a noticeably sharp peak that elicited by-far the greatest response and was attributed to maltotetraose at t_R = 11.4 min. Unfortunately, attempts to better resolve this mixed fraction (e.g. through the modification of eluent flow rate, column temperature etc.) were ultimately unsuccessful, but the results had indicated the high relative concentration of an oligomeric constituent with respect to glucose/maltose which was in-line with hypothetical expectations.

In addition to HPLC, MALDI-TOF-MS was also employed to further characterise the as-received syrup and in particular, to gain a more complete understanding of the range of oligomeric species that were

present within it. The corresponding fragmentation pattern for MYL is shown in **Figure 7.2** wherein it can be seen that there is a series of signal clusters whose base peaks are separated by *ca*. 162.1 m/z which corresponds to the (singly charged) mass of a hexose monomer and is therefore diagnostic of mixed hexo-oligosaccharides. Each of these base peaks corresponds to the sodiated oligomer and although the results are not strictly quantitative, it is notable that by far the most intense signal (excluding those originating from the 2,5-dihydroxbenzoic acid matrix at < 500 m/z – see **Appendix Figure E.2**) is that which corresponds to maltotetraose at m/z = 689.14 (calculated M_r = 689.21 $gmol^{-1}$ based on $C_{24}H_{42}O_{21}Na$).

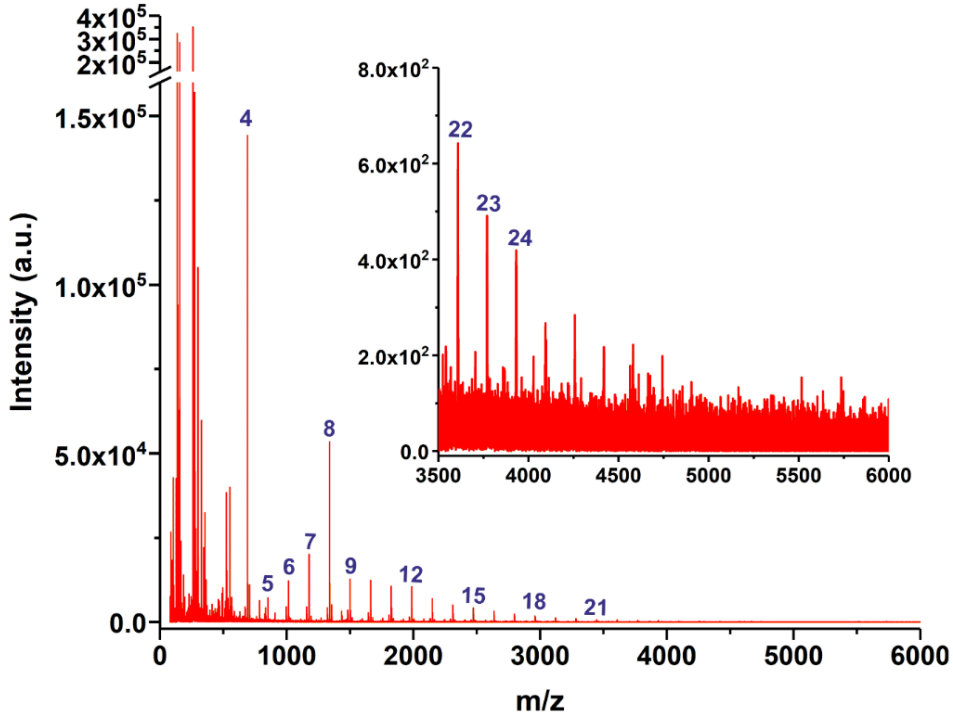

Figure 7.2: MALDI-TOF-MS spectrum for as-received Mylose 351 syrup solids with zoomed inset magnifying the m/z = 3500 – 6000 region. Blue numbers refer to degree of polymerisation. Originally in colour.

Surprisingly, the signal at m/z = 1337.42 which corresponds to maltooctose is also relative intense which may originate from the production process employed to manufacture MYL (i.e. selective hydrolysis of larger oligomers) or the gas-phase dimerisation of maltotetraose. It is also interesting to note the presence of relatively large species up to approximately m/z ≈ 4000 or degree of polymerisation ≈ 23 (that were distinguishable from the background noise – see **Figure 7.2** insert), which would otherwise not have been detected via HPLC but could conceivably have a non-negligible effect on the physicochemical properties of the syrup mixture given their considerable size.

Due to constraints to both time and availability of materials it was decided that the additive concentration be fixed at 10 wt. % syrup solids (9.1 wt. % wet basis) in all cases except for a control experiment containing only MYL (see section **2.2.5**). This corresponded to six different experimental sets, within which a series (> 6) of samples with differing a_w/T_g would be produced in order to cover different areas of the confectionery 'space' via boiling to different cook temperatures. The floridoside-rich extract that was used to prepare the model confections consisted of a collated sample (referred to herein as FLO) and contained 94.9 wt. % floridoside (F_{II} cf. FTIR) based on TGA method of analysis outlined in **Chapter 5** (see **Appendix Figure E.3**) and which was consistent with the results of microanalysis (measured (calc. based on 94.9 wt. %): C = 40.34 (40.35), H = 6.77 (6.77), Cl = 2.45 wt. %). As the Mylose was found to readily form a 'skin' (i.e. dehydrated glass) especially under elevated conditions, this prevented accurate monitoring of the cook temperature due to unavoidable temperature gradients that developed within the cooking vessel. However, by sampling several ($\geq$ 6) aliquots according to visual observations still provided sample sets that covered an acceptable a_w/T_g range (as is shown later).

To ensure that degradation had not occurred over the course of sample preparation through either thermally or chemically induced decomposition of the starting ingredients, HPLC analysis was

conducted on each additive system both at the beginning (i.e. following initial homogenisation) and end of the boil-off experiments. This is critical given that any hydrolysis of larger glucooligomers into smaller constituent molecules would likely lead to a simultaneous decrease in the a_w primarily via a colligative effect and also T_g given the relative increase in small plasticising species (preventing accurate performance evaluation of any added humectant/plasticisers) in addition to an undesirable increase in 'free' sugars. Furthermore, in terms of health and safety the conversion of well-characterised starting materials (that are either of GRAS status or hypothesised to be safe for consumption) into unknown and potentially harmful compounds would be highly problematic. An example set of HPLC results are shown in **Figure 7.3** for the MYL-DES system, where peaks originating from the DES components (**Figure 7.3a**) and MYL (**Appendix Figure E.4**) are clearly visible in the mixed additive system produced at the end of the boil-off (**Figure 7.3b**) with no obvious additional signals/change in relative peak intensities resulting from degradation etc. This was also found to be the case for all of the model systems (see **Appendix Figure E.4**).

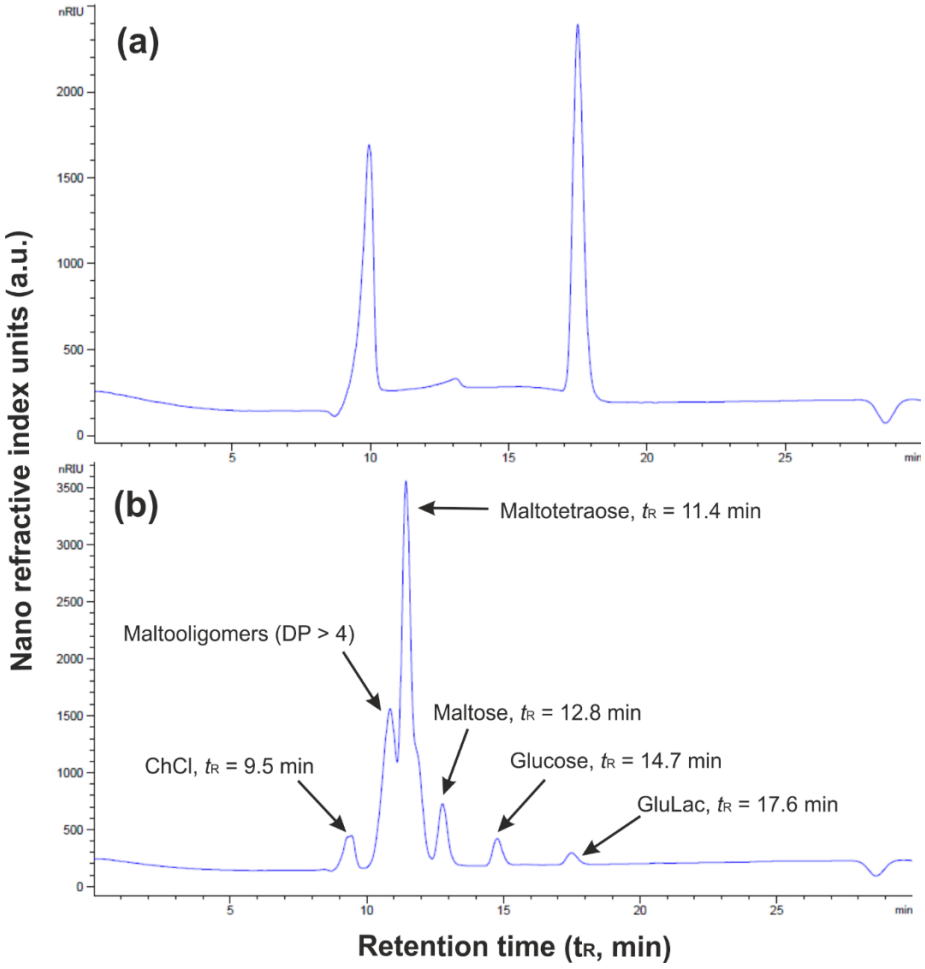

Figure 7.3: HPLC chromatographs of (**a**) GluLac:ChCl, 1:1 DES and (**b**) model confection prepared therewith following final boil-off. Originally in colour.

As is typical in confectionery preparation, the water content was found to be inversely correlated with a_w and could be reduced via boiling in order to bring about the desired reduction in a_w to a target range of *ca*. 0.40 - 0.65 which corresponded to approximately 8 – 15 wt. % water, as summarised in **Figure 7.4**. In most systems it can be seen that despite a lack of rigorous temperature regulation, aliquot samples covering a large range of water contents (i.e. boiling points) could be obtained with the only exception being MYL-DES for which, most were taken over a relatively narrow range in the low water/a_w region. It should also be noted that although each data point generally represents the average of at least two duplicates, only a single measurement could be recorded for several samples owing to time/resource

constraints. If a_w is plotted as a function of water content, the data more or less collapses onto a single curve, irrespective of either the identity or even presence of an added humectant/plasticiser (**Figure 7.4**). This is indicative of a compensatory effect within the confections whereby the larger solute molecules (namely those comprising MYL) have an individually greater a_w reducing power (i.e. they decrease y_w to a greater extent) compared to the smaller additives (especially GLE) which instead lower a_w predominantly through a colligative mechanism (i.e. comparatively greater x_w reduction). At the relatively low level of plasticiser addition used here, the concentration of each added species is actually considerably lower than either water or MYL, whose interplay is therefore expected be the dominant influence on a_w across all of the mixtures.

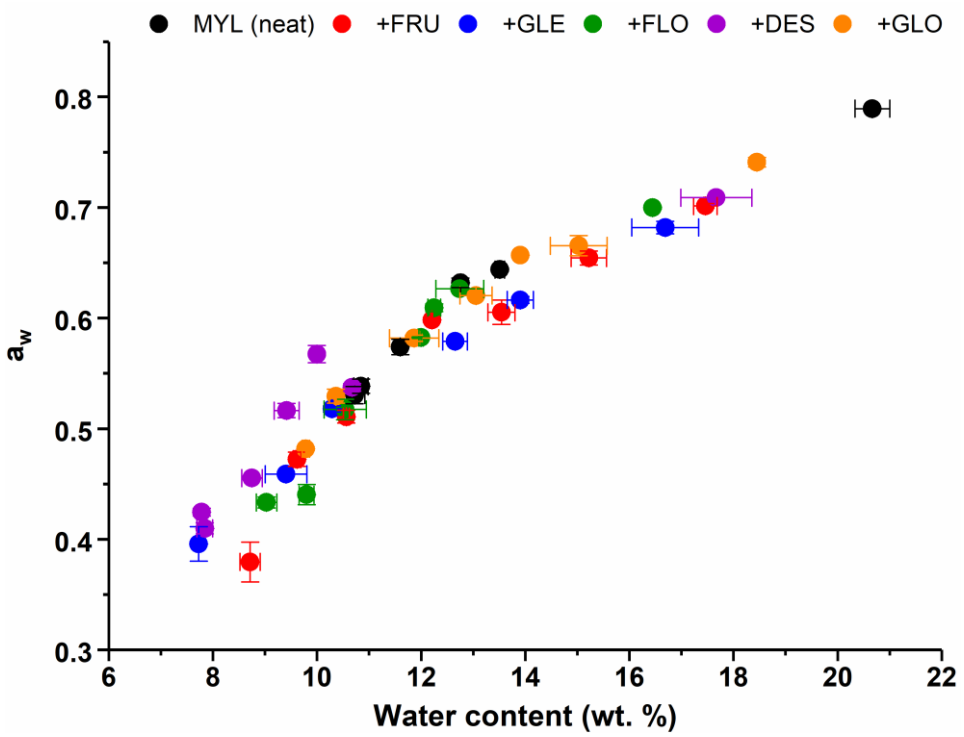

Figure 7.4: Change in a_w of model confections as a function of water content (wt. %). Error bars represent $\pm$ 1 standard deviation. Originally in colour.

An interesting note is that the confections prepared with DES actually appear to display slightly elevated a_w values compared to the other systems at equivalent water contents which is counter to what may have been expected given their (partially) dissociative nature. Dissociation should have resulted in an increase in the effective number of solute entities (i.e. molecules and ions) and thus decreased a_w on a purely colligative basis. As this was in fact not observed, it suggests that the ChCl ions contained within the confectionery matrix primarily exist in an associated, ion pair-type state and may have even facilitated the association of non-ChCl molecules reducing the effective number of solute entities even further. More extensive probing of the inter-solute or solute-solvents interactions would be very challenging owing to the shear breadth of species present within the amorphous matrices and is outside of the scope of this thesis.

Because of the highly viscous and even glassy nature of many of samples, it is questionable as to whether equilibration of the partial water vapour pressure (and also temperature) of the matrix, headspace and measuring device was attained within the timeframe of the measurement (*ca*. 60 minutes). As this condition is a prerequisite within the formal definition of a_w (i.e. it is an equilibrium measurement) the values given above should strictly be considered relative a_w which describes a pseudo steady-state type scenario.[387] Additionally, it has been argued that even the very act of transferring such material from storage container to measuring device (exposing the sample to the external environment) can have a non-trivial influence of the measured value of a_w which should therefore be considered an 'apparent' value. This can be corrected if the sample is appropriately heated (this was not possible with the a_w meter used in the present work).[388] In light of this, it would be useful to confirm the accuracy of the values presented herein through a second, potentially more rigorous approach such as an isopiestic-type methodology which has been employed previously in the literature.[389, 390] However, this was not possible in the present study due to time constraints. Additionally, the procedure used here is however, more representative of a real-world system where confections are produced via direct formulation, boiling and cooling before subsequent use/analysis.

All of the model confections in addition to neat MYL were found to be amorphous according to DSC analysis, exhibiting characteristic glass transitions according to the endothermic baseline shift in heat flow which could be readily observed in each case (n.b. T_g herein refers to the onset temperature recorded during the second heating scan). In all cases, the measured T_g of the MYL+ additive system was reduced with respect to pure MYL, which exhibited vitrification at close to ambient temperatures even at ~ 11 wt. % water (in **Figure 7.5**).

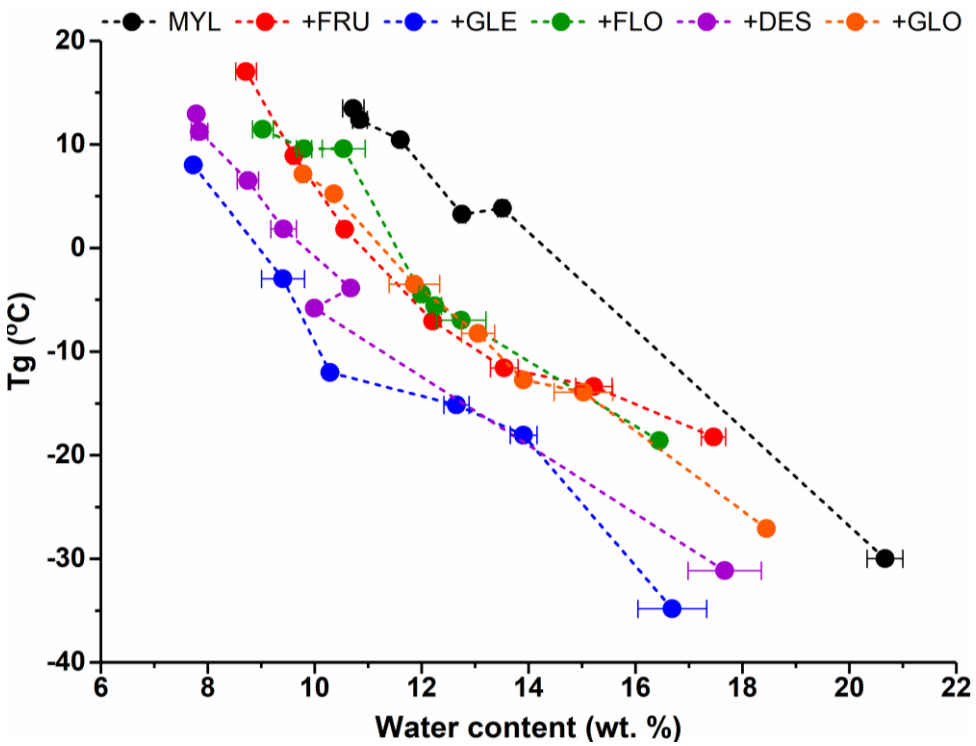

Figure 7.5: Change in T_g (onset) of model confections as a function of water content (wt. %). Error bars represent $\pm$ 1 standard deviation. Lines are added to aid visualisation. Originally in colour.

The extent to which T_g depression occurred was highly dependent on the identity of the added plasticiser. GLE appeared to be the most efficacious in terms of T_g reduction, whereby the apparent T_g/water 'curve' is left-shifted to the greatest extent with respect to the pure MYL system and that

measured T_g was suppressed by ~ 20 ºC at the same wt. % (i.e. the curve was effectively shifted by *ca*. 4.0 – 5.0 wt. % water). The second most effective plasticiser was DES which shifted the curve by approximately 3.5 – 4.0 wt. % or 10 – 15 ºC. FRU, FLO and GLO all behaved very similarly in that T_g was consistently reduced by around 10 ºC compared to pure MYL almost irrespective of which of the three was used.

In mixed confectionery-type systems which comprise constituents that are highly dissimilar in nature (e.g. significant size disparities) it is not uncommon for microscopic phase separation or inhomogeneities within the amorphous matrix to exist due to the development of localised domains containing non-equivalent compositions.[391] These microdomains, which are relatively enriched in either the biopolymer or plasticising species and can manifest as multiple measurable T_g values or a broadened T_g range. This has been reported in for instance, mixtures of starch/polyols, maltodextrins/glucose or maltose and amylopectin/sugars.[392, 393] In the present study, all of the model confections were found to exhibit a single and well-resolved T_g, wherein the difference between the onset and endpoint T_g remained constantly < 20 ºC, irrespective of additive presence/identity or final a_w. This is exemplified in the case of the MYL+FLO model confections as shown in **Figure 7.6** (the T_g ranges for the other model confections are presented in **Appendix Figure E.5**).

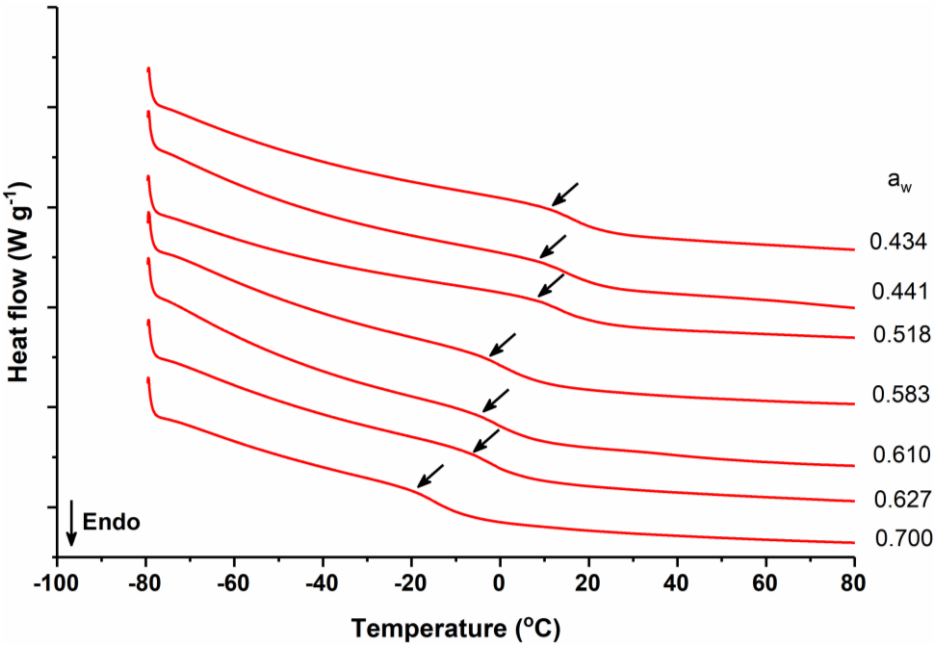

Figure 7.6: Second heat cycles of model MYL+FLO confections at varying a_w, large *y*-axis tick marks correspond to 0.2 W g^{-1}. Arrows indicate onset of T_g. Originally in colour.

As mentioned briefly in **Chapter 1**, the fundamental basis by which the plasticisation of polymeric/oligomeric carbohydrates matrices actually manifests is still not fully understood but generally attributed to an increase in free volume following the addition of small molecules e.g. water and sugars. An interesting recent development in this area has instead suggested that the T_g in mixtures of biopolymers (including maltooligomers), sugars/polyols and water ($T_{g,mix}$) can be directly related to the inverse average number of OH groups per molecule within the mixture ($\frac{n}{n_{OH,mix}}$) via the following equation (**Equation 7.1**):[30]

$$T_{g,mix} = \left[2\left(T^{\infty}_{g,gluco} - T_{g,w}\right)\left(\frac{1}{2} - \frac{n}{n_{OH,mix}}\right)\right] + T_{g,w} \quad \textbf{Equation 7.1}$$

Here, $T_{g,w}$ and $T^{\infty}_{g,gluco}$ are the glass transition temperatures of pure water (139 K) and a hypothetical infinitely long chain of α-(1→4)-linked glucopyranose for which a value of 450 K was found to

accurately describe mixtures based on glucooligmers (i.e. glucose syrups).[30] This assumes that the mixtures obeys an ideal mixing relation which assumes that the final T_g of a mixture is simply equal to the T_g of each individual component weighted by their mass fraction.

In the same work, it was also shown that $n_{OH,mix}/n$ could be computed using **Equation 7.2**:[30]

$$\frac{n_{OH,mix}}{n} = \frac{\left(m_w \frac{n_{OH,w}}{M_{r,w}}\right) + \left(m_p \frac{n_{OH,p}}{Mr,p}\right) + (m_{MYL}\, N_{MYL})}{\left(\frac{m_w}{M_{r,w}}\right) + \left(\frac{m_p}{M_{r,p}}\right) + \left(\frac{m_{MYL}}{M_{r,MYL}}\right)} \qquad \textbf{Equation 7.2}$$

Where $n_{OH,i}/n$, m_i and M_i correspond to the average number of OH groups per molecule, mass fraction and molecular mass of species *i* with *w*, *p* and *MYL* and *mix* subscripts referring to water, plasticiser, MYL and the overall mixed confection respectively. N_{MYL} is a constant which accounts for the glucose-based biopolymeric/oligomeric component (in this case MYL) that is computed via $N_{MYL} = n_{GLU}/M_{GLU}$ where n_{GLU} and M_{GLU} are the number of OHs groups (3) and molecular mass (162 g mol^{-1}) per anhydroglucose monomer. A summary of $M_{r,i}$ and n_{OH} of each plasticiser is presented in **Table 7.1** wherein FLO and GLO have been considered pure and DES has been calculated using an intermediate mass between that of the individual components (GluLac, M_r = 176 g mol^{-1}, ChCl M_r = 140 g mol^{-1}) and assuming that GluLac has three hydroxyl groups as has been identified in the native crystal.[394]

Owing to the complex mixed nature of glucose syrups, it is extremely difficult to evaluate their exact composition and approximation is necessary. For MYL, using the *DE* value of 33 as quoted by the manufacturer and knowing that $M_{r,MYL} = \frac{M_{r,GLU}}{(DE/100)}$ (where $M_{r,GLU}$ = 180.15 g mol^{-1}), $M_{r,MYl}$ was calculated to be 545 g mol^{-1}. Then using this value, the DP_{MYL} could be calculated via: $DP = \frac{M_{r,MYL}}{M_{r,GLU}}$ which yielded

a value of *DP* = 3.36. These calculated values are very reasonable given that they fall between those computed for maltotriose (M_r = 504 g mol^{-1}, *DP* = 3) and maltotetraose (M_r = 667 gmol^{-1}, *DP* = 4) and are consistent with the results of HPLC/MALDI-TOF-MS analyses.

Table 7.1: Summary of parameters relevant to **Equation 7.2** for individual added plasticisers (and water) used within the model MYL confections.

Plasticiser	$M_{r,I}$ **(g mol^{-1})**	n_{OH}
Water	18	2
FRU	180	5
GLE	92	3
FLO[a]	254	6
DES	158[b]	2[b]
GLO[a]	254	6

[a]Considered pure. [b]Average based on 1:1 GluLac:ChCl.

The result of linearising **Equation 7.1** each confectionery mixture through a plot of $T_{g,mix} - T_{g,w}$ versus $1/2 - n/n_{OH,mix}$ is presented in **Figure 7.7**. It can be seen that virtually all of the data points converge onto a single line (R^2 = 0.998) with a gradient (i.e. $2T^{\infty}_{g,gluco} - T_{g.w}$) of 605 $\pm$ 4 K (see **Appendix Figure E.6**) which is very close to that which was found to describe other ternary food mixtures containing glucose oligomers, disaccharides and water ($2T^{\infty}_{g,gluco} - T_{g.w}$ = 622 K, included in **Figure 7.7**).[30]

Indeed, the average absolute deviation (AAD) between the predicted and experimental $T_{g,mix} - T_{g,w}$ for the entire dataset (*N* = 40) was found to be only 3.41 K according to **Equation 7.3**:

$$AAD = \frac{1}{N}\sum_{i=1}^{N}\left[\left(T_{g,mix}^{pred} - T_{g,w}\right) - \left(T_{g,mix}^{exp} - T_{g,w}\right)\right] \quad \textbf{Equation 7.3}$$

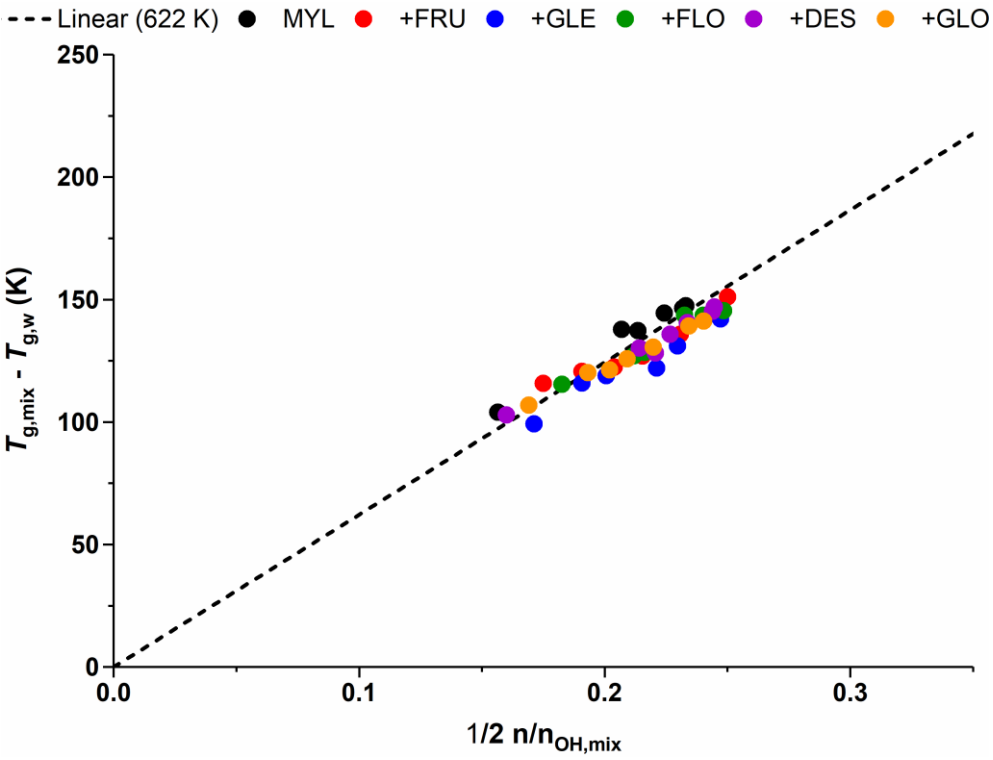

Figure 7.7: Experimental glass transition temperatures (onset) of model MYL-based confections ($T_{g,mix} - T_{g,w}$) shown as a function of the inverse number of OH groups per molecule ($1/2 - \mathrm{n/n_{OH,mix}}$). The dotted line represents ideal mixing behaviour reported previously by van der Sman, $2\left(T^{\infty}_{g,gluco} - T_{g.w}\right)$ = 622 K.[30] Originally in colour.

The correlation is especially good considering the error associated with the water contents and also the assumptions made during the calculation of $M_{r,MYL}$. These results provide further indication that there may be a universal link between plasticity and hydrogen bond density within amorphous confectionery matrices comprising glucooligomers, smaller humectants/plasticiser and water which can be accurately predicted through a simple heuristic model. According to the original author, the presence of water is hypothesised to be key in facilitating ideal mixing and minimising microscopic phase separation of ternary glucooligomer, sugars and water mixtures.[30] A lack of phase separation in the MYL confections was supported by the aforementioned DSC measurements, suggesting that matrix homogeneity was maintained at the moderate levels of plasticiser addition and water content used within this investigation.

Based on the n_{OH} estimated for the GluLac:ChCl, 1:1 DES (2), the plasticising effect of the DES would have been expected to be greater than glycerol and closer to that of water, which was not observed within the actual confections, although T_g suppression was superior to FRU/FLO/GLO (n_{OH} = 5/6) at comparable water concentrations (cf. **Figure 7.5**). One possible explanation is that GluLac undergoes tautomerism to the enol within the DES/confection which would result in a greater number of OH than accounted for in **Table 7.1**. Also, the model does not account for other polarised functional groups that could partake in hydrogen bonding (acceptance) such as the carbonyl/etheric moieties of GluLac. This suggests that the use of n_{OH} as a single universal descriptor of all glass transition related phenomena is an over simplification, as exemplified by comparing the disparate T_g values of acyclic polyols (sorbitol, mannitol etc.) and their cyclic analogues (monosaccharides) despite identical n_{OH}. Indeed, van der Sman apparently refined n_{OH} to account for such discrepancies via a so-called "effective" n_{OH} (i.e. n_{OH}^{eff}).[30] This was calculated for each solute by using **Equation 7.2** after replacing $T_{g,mix}$ with the T_g of pure anhydrous compound and with different values of the T_g^{∞} term depending on the class of compound in question. It was suggested that a higher n_{OH}^{eff} is indicative of a greater degree of intermolecular hydrogen bonding within the wider H-bonded network which for sugars, could be linked to the number of equatorial OHs. However, little supporting evidence for this claim was provided and the prediction using n_{OH}^{eff} was not superior to n_{OH}, yet requires more inputs and is less intuitive in the opinion of this author. The hypothesised importance of intermolecular H-bonding could however, provide some rationalisation of the comparatively low T_g values recorded for amorphous glycoin (**Chapter 4**) and floridoside (**Chapter 5**) as both contain an axially-locked glycerol group.

From a practical perspective, a synthesis of the a_w and T_g data for the model confections is presented in **Figure 7.8**. It can be seen that in all of the additives systems, the aforementioned curves are shifted to the right with respect of MYL, indicating that comparable values of a_w could be achieved whilst consistently maintaining T_g at *ca*. 10 or 20 °C (for GLE) lower than in the pure system. In contrast to

the T_g vs water graphs (**Figure 7.5**), the DES curve is closer to FRU/FLO/GLO group and further from GLE which is due to compensation for the comparably higher measured a_w as shown previously in **Figure 7.4**.

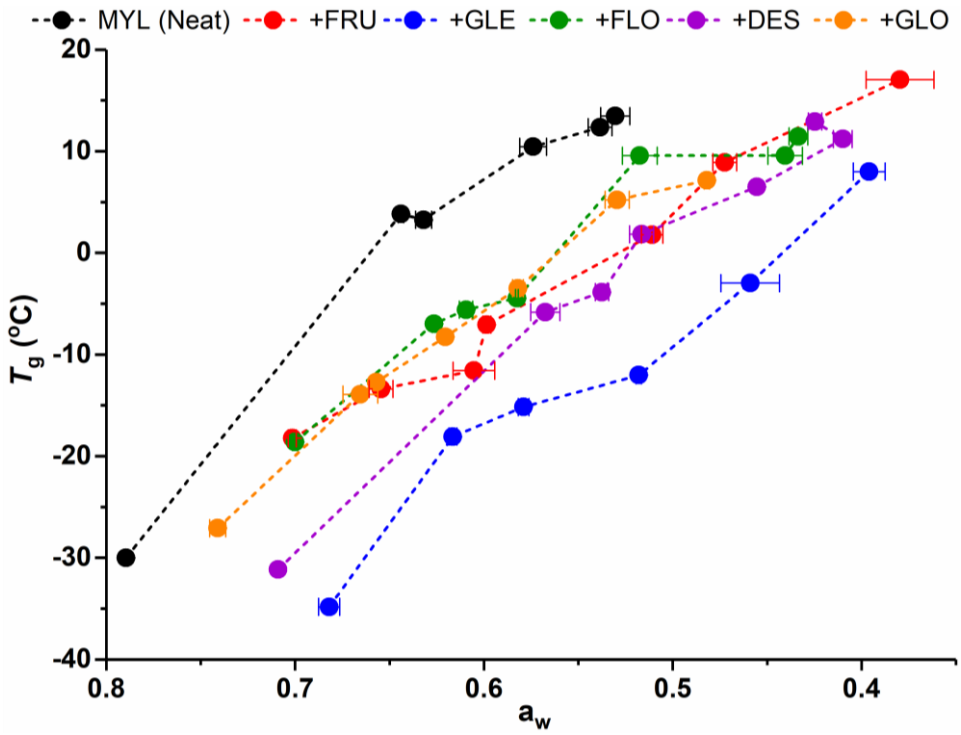

Figure 7.8: Plot of T_g (onset) versus a_w for model confections with lines added to aid visualisation. Error bars represent ± 1 standard derivation. Originally in colour.

Depending on the final application, the preferred a_w for an aqueous confectionery filling is typically in the range of 0.45 – 0.65 whilst it is necessary that they maintain a 'firm ball' or 'hard ball' type texture which loosely corresponds to T_g (onset) values of *ca.* - 5 and 5 °C respectively.[395] **Figure 7.8** highlights the fact whilst a hard ball-type consistency could be achieved even at $a_w \approx 0.50 – 0.55$ for the FRU/FLO/GLO/DES confections, unplasticised MYL would be unacceptably hard and brittle for many relevant applications (e.g. binder) given that the corresponding T_g values are around 15 °C. In this regard, it is satisfying to observe that all of the novel candidates perform very comparably with D-

fructose, which is considered to be the preeminent sugar-based humectant/plasticiser for confectionery applications. This suggests that all of the neoteric options presented herein could be promising 'drop-in' replacements for it or similar ingredients (e.g. D-glucose, invert sugar). If T_g is an effective representation of $n_{OH,mix}$ then the notable differences in measured a_w that are observed when moving from the left to right-hand side of **Figure 7.8** could reflect the fact that progressively fewer of the overall totality of hydroxyl groups within the mixture belong to a water molecule (i.e. x_w is reduced) even though the number of hydroxyls *per* molecule is effectively constant.

Linked to the glass transition, another important characteristic of the model confections that merited investigation was the rheological behaviour given that it can provide relevant information concerning the processing/handling and also key sensorial qualities of the product.[396] The rheology of the model confections was investigated under a controlled constant shear rate of 10 s^{-1}, primarily in order to investigate the influence of temperature on viscosity but also to probe for potential differences originating from the addition of the plasticiser species into the MYL matrix. Due to instrument limitations (of the maximum permissible torque and size of the measuring cone spindle – cf. **Equation 2.3**), the highest attainable shear stress in the rheology experiments was approximately 12233 Pa whereas the lower shear rate limit was capped at 0.500 s^{-1}. This in turn prevented probing of the viscosity within the vicinity of the glassy state (in which $\eta \approx 10^{10}$ - 10^{14} Pas) even at the lowest shear rate limit of 0.500 s^{-1} (n.b. $\eta = \tau/\dot{\gamma}$). Additionally, measurements performed under shear rate which approached this limit became consistently noisier (possibility due to small structural deformations that existed on the surface of the lower measuring plate) and prevented acquisition of repeatable measurements. It was found that the quality of the data could be improved by operating at higher shear rates, yet in order to best maximise the operational viscosity range, a shear rate of 10 s^{-1} was selected as a compromise between the opposing factors.

In all cases, the application of elevated initial temperatures (typically 80 but up to 120 °C) and equilibration thereat were required in order to induce initial flow of the confections (given that many samples were glassy under ambient conditions). This was followed by a cooling temperature sweep which proceeded at 0.1 °C s^{-1}. During initial experimentation, it was observed that samples subjected to these high temperatures were plagued by rapid dehydration and the subsequent formation of the aforementioned surface skin. This typically led to an often-inconsistent fluctuation in and overall higher measured viscosity, as demonstrated in **Figure 7.9** (note the consistent offset to higher viscosity at comparable *T*) and which has been reported previously in the literature for other glucose syrup systems.[397]

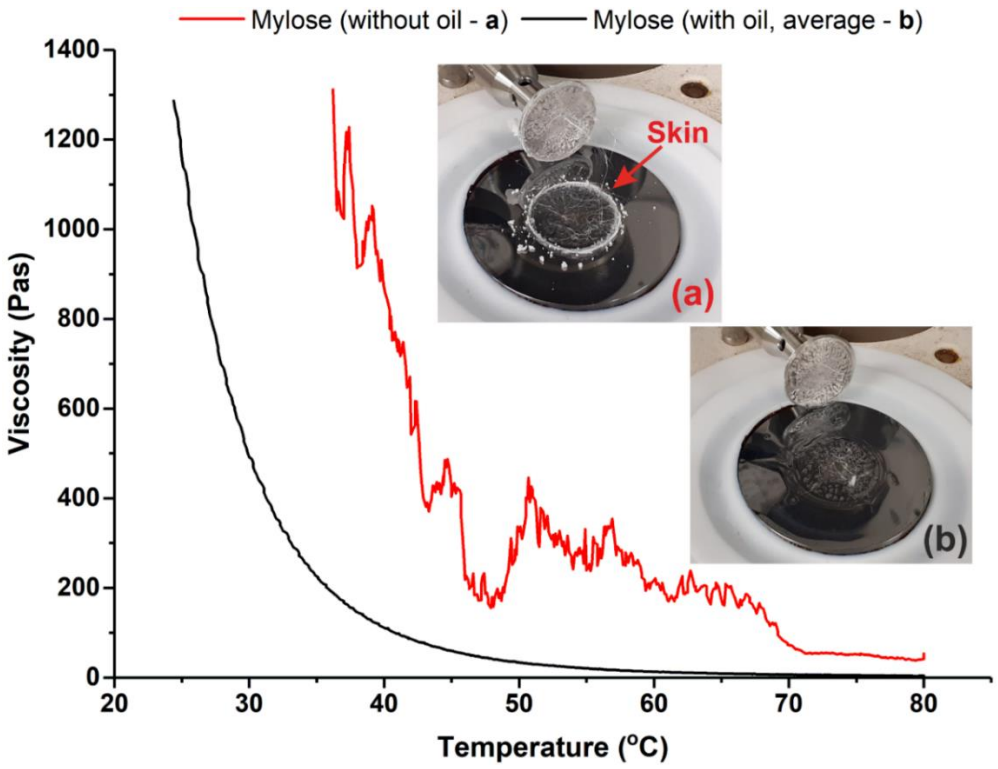

Figure 7.9: Visual appearance of MYL following rheological measurement both without (**a**) and with (**b**) the application of coating silicone oil shown alongside the corresponding rheological traces. Originally in colour.

In light of this, two different actions were taken in order to improve the general accuracy and reproducibility of the results. Firstly, an excess of sample was purposefully used so that the cone/plate gap was always slightly overfilled by molten material as mechanical removal of the heated excess sample could not be consistently replicated in a sufficiently expedient manner. Secondly, dehydration was minimised via application of a solvent trap and also an immiscible, low viscosity silicone oil (*ca*. 0.005 Pas) which was used to coat the surface of the fluid confections immediately following compression of the upper cone onto the sample. A similar mitigative strategy has also been employed recently by Dupas-Langlet *et al*. in their study on glucose oligomer/maltose blends.[389]

It is known that the use of excess sample can lead a slight decrease in measurement accuracy through a so-called 'edge effect' which originates from the dependence of the measured torque (effectively proportional to the viscosity) on the radius of the measuring cone that is assumed to be equal to the fluid analyte (which is not true during over/underfilling).[398] However, this was shown to be insignificant when a commercial reference standard of a comparable viscosity (*ca*. 115 Pa s at 20 °C) was tested under almost identical conditions (**Appendix Figure E.7**). It should be noted that the commercial standard displayed considerable erraticity in the measured viscosity at $\geq$ 85 °C, possibly because at the shear rate used (10 s^{-1}), the torque value fell close to or below the lowest detection limit of the rheometer. Finally, a blank run of solely the coating silicone oil without sample confirmed that there were no readily observable artefacts originating from the use of this auxiliary or the thermal expansion of the metal measuring components under the elevated experimental temperatures.

As expected, all samples were found to exhibit an inverse, exponential-type relationship between viscosity and temperature as shown in **Figure 7.10** and **Appendix Figure E.8** wherein the results represent the average of at least two replicates for which the final temperature reached at the end of the experiment did not deviate by more than 3 K. Even using this approach, it can be seen that there is a

noticeable error associated with the average plots of several of the systems – especially at higher viscosity values due to the aforementioned exponential character of the viscosity-temperature relationship ($\pm$ 1 standard deviation and limits thereof for each measurement are depicted by the shaded area and dashed lines respectively in **Figure 7.10**).

When controlling for temperature and a_w, the presence of plasticiser appeared to shift the viscosity curves as shown in **Figure 7.10** (MYL+GLO) to the left compared to the pure MYL confections i.e. the plasticised material had less resistance to flow at lower temperatures. As discussed in **1.1**, it is well known that the viscosity of such systems is highly dependent on the temperature above T_g.[399] This is demonstrated for the model confections by re-plotting the viscosity data as a function of the temperature $T_g + X$, the results of which are shown in either **Figure 7.11** (MYL, MYL+GLO) or **Appendix Figure E.9** (MYL+FRU/GLE/FLO/DES). This collapses the data into an almost single curve for most of the systems, where the exponential increase in consistently occurred at around X = 55 to 70 K, although some finer details may be masked somewhat by the aforementioned error spread. The only major divergence from this trend was exhibited for a few of the MYL+FLO samples (a_w = 0.441 and 0.434), for which the increase in viscosity occurred at approximately X = 65 to 80 K (**Appendix Figure E.9c**). Although it is not immediately apparent why this would be the case, it should be noted that these samples required the highest equilibration/initial temperatures (120 °C) in order to initiate flowability. This would make them the most susceptible to moisture loss during the course of experimentation which would lead to an increase in T_g/viscosity.

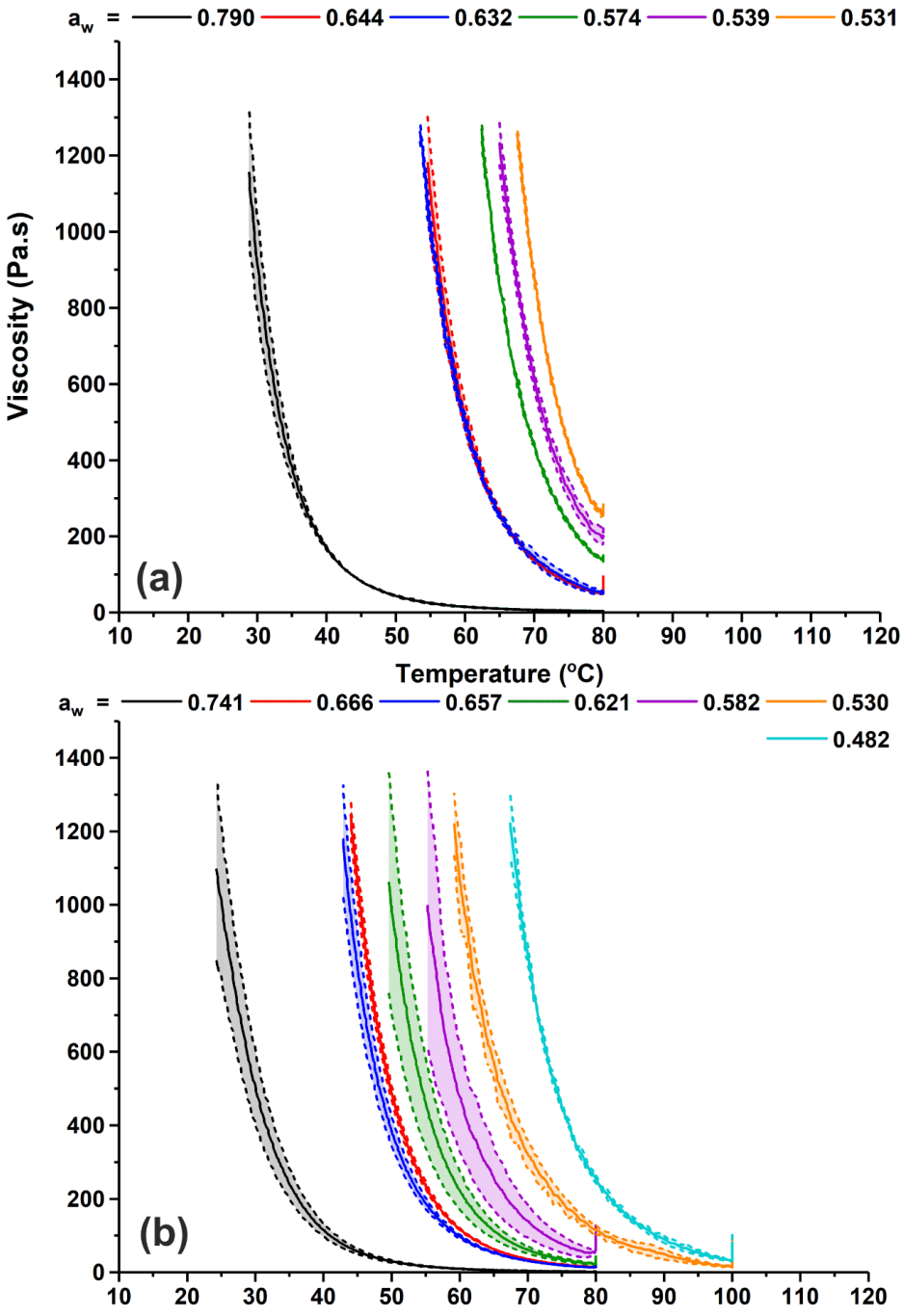

Figure 7.10: Viscosity of model confectionery systems based on (**a**) MYL and (**b**) MYL+GLO as a function of temperature at constant shear rate (10 s^{-1}). The shaded area and dashed lines of each curve represent ± 1 standard deviation and the limits thereof, respectively. Originally in colour.

As stated in **Chapter 1**, the exponential-type relationship between viscosity and T_g in amorphous confectionery matrices can typically be well-described using a modified version of the WLF model:[171]

$$log_{10}\left(\frac{\eta\,(T)}{\eta\,(T_g)}\right) = \frac{-C_1\,(T-T_g)}{C_2+(T-T_g)} \qquad \textbf{Equation 10}$$

To underscore the variability that can result from the exponential character of the relation, the WLF predicted viscosity (using the 'universal' constant values, C_1 = 17.44, C_2 = 51.66 K and $\eta\,(T_g)$ (onset) = 10^{12} Pas) is plotted in **Figure 7.12a** along with two further lines that are either plus (red) or minus (blue) the value of the AAD (3.4 K) determined previously based on the prediction using n_{OH}. It can be seen that these curves all fall within the common region (T_g + 55 to 70 K) that was generally found for the MYL/+ plasticiser matrices. The WLF prediction has also been compared with samples of intermediate a_w (*ca*. 0.570 - 0.600) from each of the different non-/plasticised model systems in **Figure 7.12b** (and **Appendix Figure E.9**). In this case, most of the experimental viscosity traces lie to the right of the WLF predicted curve, suggesting that the r.h.s. of **Equation 10** is actually less negative for most of the model confections.

A better fit can be achieved using for instance, C_2 = 56.0 K, which is plotted as the dashed black line in **Figure 7.12b** and better reproduces the viscosity measured at elevated temperatures ($\geq T_g$ + 85 K). At even higher temperatures ($T \approx T_g$ + 100 K) the viscosity often begins to diverge from the WLF model and exhibits increasingly Arrhenius-like behaviour.[168] It is known that the 'universal' constants often cannot accurately describe experimental data for oligomeric/polymeric food matrices and require modification in order to optimally fit the empirical results.[173, 389, 400] Although some connection to deeper physical meaning is lost through this fitting, it still remains of utility from a practical perspective for correlating other important product properties (e.g. a_w/plasticiser content) with viscosity/T_g which is crucial from both a manufacturing and quality control standpoint.

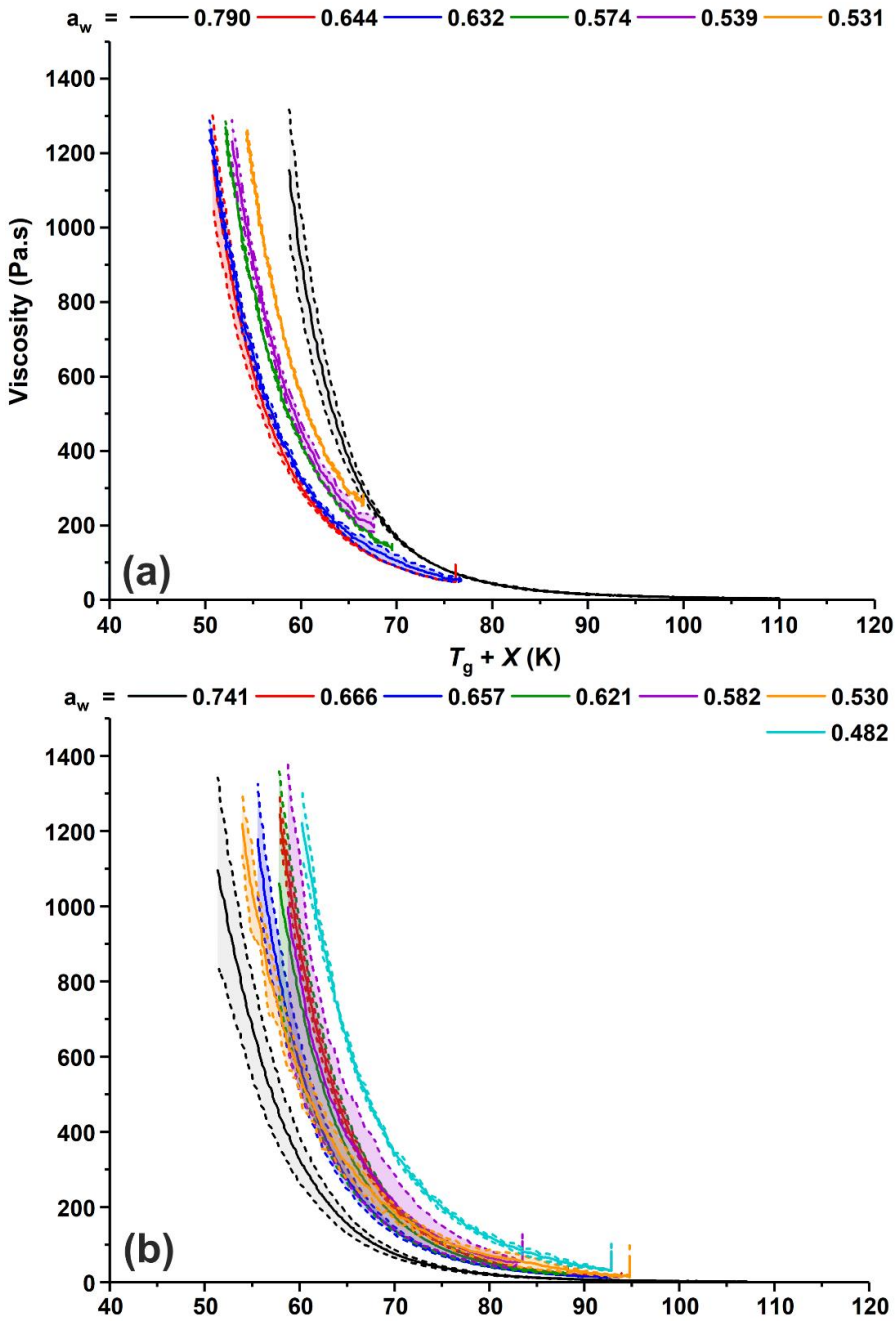

Figure 7.11: Viscosity of model confectionery systems based on (**a**) MYL and (**b**) MYL+GLO as a function of $T_g + X$ (K) at constant shear rate (10 s^{-1}). The shaded area and dashed lines of each curve represent $\pm$ 1 standard deviation and the limits thereof, respectively. Originally in colour.

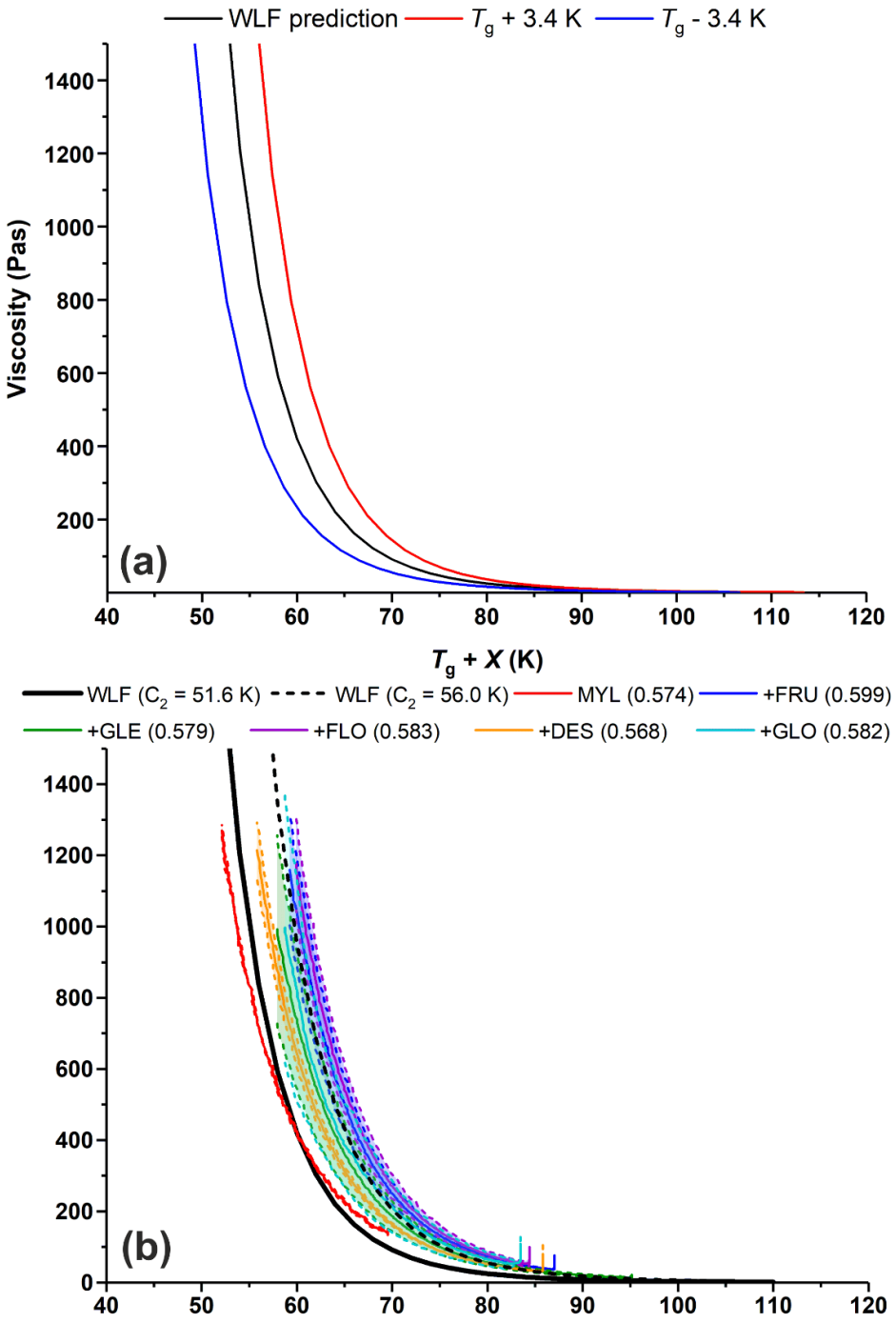

Figure 7.12: Viscosity predicted as a function of $T_g + X$ using the WLF equation (**Equation 10**) (**a**) with variable values of T_g ($\pm$ 3.4 K) and (**b**) compared to experimental viscosity of selected model confections (bracketed values refer to a_w) for which the shaded area and dashed lines of each curve represent $\pm$ 1 standard deviation and limits thereof, respectively. Originally in colour.

7.3. Summary

A series of model aqueous confections based on a low free sugar glucose syrup (Mylose 351) and covering an a_w range of *ca*. 0.5 – 0.7 were prepared using the neoteric humectants/plasticisers investigated within **Chapters 4** (glycoin), **5** (floridoside-rich extract derived directly from *Palmaria palmata*) and **6** (Glucuronolatone:choline chloride, 1:1 DES) and evaluated in terms of a_w and T_g against two archetypal confectionery ingredients; fructose and glycerol. Initial characterisation (via HPLC and MALDI-TOF-MS) of the base Mylose glucose syrup was consistent with the purportedly high concentration of maltotetraose and also highlighted the presence of significantly larger oligosaccharides (up to a degree of polymerisation of *ca*. 24) whilst HPLC was also used to confirm the integrity of the starting ingredients following confectionery formulation.

At 10 wt. % (with respect to the mass of the glucose syrup solids) addition of the humectant/plasticiser species, DSC analyses confirmed that all of the formulated confections were amorphous and also homogenous (no obvious phase separation) glasses based on single and relatively narrow measured T_g ranges. Unsurprisingly, both a_w and T_g were found to be inversely correlated with water content, with confections prepared at higher cook temperatures exhibiting the lowest a_w and greatest T_g values. Whilst glycerol was the most effective additive in terms of a_w and T_g reduction on a weight-by-weight basis, at equivalent a_w, the addition of each of the novel materials was found to suppress T_g by > 10 ºC compared to the control system containing no additive. This was similar to the degree of plasticisation offered by fructose, indicating that the newly developed additives may have potential as 'drop-in' humectants/plasticisers for use within low sugar aqueous confectionery fillings. The measured T_g values of all model confections were found to be linearly correlated with the average number of hydroxyl groups per molecule, in-keeping with recent studies in the literature. The temperature dependence of viscosity could be generally well-described by a slightly modified WLF model (C_1 = 17.44, C_2 = 56.00 K) and was highly correlated with the difference between the measurement and glass transition temperatures in almost all cases.

Chapter 8: Concluding remarks and future work

The overall aim of this thesis was to develop nature-inspired approaches for replacing the humectancy and plasticisation afforded by so-called 'free' confectionery sugars (and related solutes) within aqueous confectionery fillings as a response to the growing prevalence of dietary-related non-communicable diseases. Although the literature is replete with the application of various sugar replacement strategies including the use of polyols (sugar alcohols), natural syrups, fibres etc., such approaches are limited in either technical and/or physiological capacities, whilst general innovation in this area appears to have been limited over the preceding few decades. Other currently promising technologies that facilitate sugar reduction through alteration of solely physical properties e.g., via 'structuring' around an inert support or within an aerated amorphous matrix are ultimately ineffective within the aqueous confectionery systems of interest (syrups, caramels etc.) given the disruptive effect of relatively high levels of solvent water. As a response, through the identification of several knowledge gaps within the literature and subsequent application of a wide array of experimental techniques in addition to theory, this thesis has demonstrated that it is possible to better rationalise and ultimately replace the humectant/plasticising functionalities of common confectionery sugars, using judiciously selected natural compounds and novel, nature-inspired approaches. In the following, a synthesis of the main results and learning outcomes from each area explored within the thesis is provided whilst relevant limitations and recommendations for future work/directions are suggested thereafter.

8.1. Summary of main results

A molecular scale interpretation of 'water activity': One of the initial aims of the thesis was to provide a greater comprehension of the overarching concept of 'water activity' within aqueous sugar/polyol solutions on account of persistent ambiguity within the literature surrounding its origin on the molecular level. Given the fundamental importance of a_w within the context of aqueous confections, this confusion is likely to have hindered efforts towards the rationalisation of a_w reduction (and therefore

the development of substitute humectants), thus some amelioration appeared necessary. Via application of the statistical Kirkwood-Buff theory of solutions, it was demonstrated that the a_w of 'simple' binary, non-saturated solutions (i.e. water plus solute up to the solubility limit) should primarily be considered as a compensation between solute-solute (which ultimately increase a_w) and solute-water (which ultimately decrease a_w) interactions within solution, whilst water-water interactions play a comparatively minor role. This is inconsistent with two of the prevailing hypotheses which suggest that solution a_w is primarily a reflection of 'water structure' or a measure of 'free' water, but is qualitatively in agreement with a third that invokes the concept of competitive solute clustering and hydration.

In the case of common confectionery solutes such as sugars and polyols, there appears to be a broadly consistent solvation behaviour with the main differences in a_w lowering capability (on a molecule-by-molecule basis) stemming from excluded volume effects which in turn, are mainly a function of molecular size and less dependent on the stereochemistry of individual hydroxyl groups. Conversely, the high degree of a_w reduction bought about by several unheralded natural osmolytes (e.g. methylated glycines) can be attributed to strong self-exclusion within solution (i.e. overall clustering between solute molecules is lower) which presumably occurs through mainly steric effects. The results of this study contribute towards an improved understanding of the solvation behaviour and humectancy of both archetypal and perspective confectionery solutes, hopefully opening up greater opportunities for future innovation in this area.

Natural organic osmolytes as functional humectant and plasticisers for sugar replacement: According to a perceived knowledge gap in the existing literature, it was hypothesised that organic osmolytes could be utilised as 'drop-in' replacement humectants/plasticisers for confectionery sugars as they are of low molecular weight (necessary for optimal a_w/T_g reduction), relatively high solubility and natural-occurring (and therefore at least in principle, bio-derivable). Investigations in this work centred around two unheralded compounds; 2-*O*-α-D-glucopyranosyl glycerol (glycoin) and 2-*O*-α-D-

galactopyranosyl glycerol (floridoside). Both can be considered highly promising from a reduced-sugar confectionery perspective as they have been reported to display low digestibility, minimal cariogenicity but have a sweet or neutral taste. Yet their effects on a_w and T_g had not been documented, thus necessitating detailed experimental studies in order to validate them as promising sugar alternatives.

Glycoin (prepared from a commercially available solution) was surprisingly found to be fully miscible with water across the entire concentration range, enabling aqueous mixtures of very low a_w (< 0.5) to be prepared. Its capacity to reduce a_w was found to be superior (K_N = - 5.77 for $\leq$ 85 wt. %) to that of fructose (K_N = - 2.25) glycerol (K_N = - 1.16) and comparable to sucrose (K_N = - 6.47) on a molecule-by-molecule basis, whilst measured T_g values of the glycoin-water systems were instead very similar to those of some common confectionery monosaccharides (glucose and galactose). In the case of floridoside, relatively high purity (*ca*. 90 – 99 wt. %) extracts could be prepared in a facile manner directly from the natural bioaccumulator *Palmaria palmata* using only ethanol (a GRAS and food-grade solvent). One such extract (*ca*. 92.5 wt. % floridoside) was found to display an excellent a_w lowering behaviour that was very similar to fructose (on a weight-by-weight basis) up to the solubility limit, yet these results are likely to have been influenced by the presence of dissociating salts (KCl/NaCl) which were extracted concomitantly with the target compound. The T_g (midpoint) of anhydrous floridoside was measured to be *ca*. 31 ºC, which was very similar to that of glycoin (*ca*. 29 ºC) and quite comparable to literature values for galactose (38 ºC) and glucose (36 ºC) for instance. Taken together, the results of this work strongly indicated that both glycoin and floridoside would be very suitable replacement humectants and plasticisers for common mono- and disaccharides, motivating further validation within a model confectionery system.

During investigation, two previously unheralded forms of floridoside were discovered – a second anhydrous dimorph and a stoichiometric hydrate. Various spectroscopic and thermal analyses revealed clear physicochemical differences between the crystals, whose structures also exhibited obvious disparities on the atomic level. Recognition of the existence of different crystal forms is likely to be

important in the future development of floridoside as a commercial product and may also aid in furthering research regarding its role as an *in-vivo* osmolyte.

Development of novel 'deep' eutectic mixtures: Another gap in the literature had suggested that so-called 'deep' eutectic mixtures could potentially be utilised as a nature-inspired approach for controlling the plasticisation of starch, yet no works had examined their effect on glucose syrup (i.e. mixed starch hydrolysates), thus motivating further investigation. Initial work focussed on the screening of various non-sugar, food-grade components (predominantly vitamins) with the aim of finding mixtures that would form low melting temperature eutectics with the GRAS dietary supplement ChCl. Of the compounds tested, only L-ascorbic acid and several novel, natural lactone derivatives thereof were found to form (meta) stable melts upon moderate heating. Subsequent analyses indicated that these systems could be regarded as 'deep' eutectic fluids which all exhibited Newtonian flow behaviours that were broadly comparable to typical confectionery syrups. Interestingly, they were found to display very low T_g (*ca*. – 45 ºC) values whilst having minimal a_w (< 0.1), thus appearing to offer an exciting combination of a high degree of plasticity/fluidity with potent humectancy which is otherwise rare within the confectionery and wider food sector, thus prompting further evaluation within model system testing.

Application of neoteric humectants and plasticisers within a model, low-sugar aqueous confectionery system: Based on the investigations carried out in the earlier part of the thesis, glycoin floridoside and one of the novel deep eutectic mixtures (glucuronolactone:ChCl, 1:1) were applied within a model aqueous confectionery system based on low-sugar glucose syrup and their performance compared to two preeminent confectionery solutes; D-fructose and glycerol. Through a traditional formulation approach which consisted of ingredient premixing followed by water removal (via boil off) and subsequent cooling, confections that covered a commercially relevant range of a_w values (*ca*. 0.4 -

0.7) were prepared. The presence of the added humectant/plasticising species (at 10 wt. % with respect to the glucose syrup solids) consistently decreased T_g by 10 + °C with respect to the control experiment (no additive) of comparable a_w. Notably, all three of newly developed additives performed very similarly to D-fructose in terms of a_w and T_g reduction, yet glycerol consistently offered superior plasticisation (i.e. greatest T_g reduction when controlling for a_w). Interestingly, the experimental T_g values were found to be well correlated with the average number of hydroxyl groups per molecule (consistent with recent findings in the literature), whilst shear viscosities of the confections exhibited a common temperature dependence that was strongly related to the experimental temperature above T_g and could be well described using a slightly modified WLF equation. These preliminary results indicate that all three of the newly developed additives could serve as technically functional 'drop-in' replacement humectants/plasticisers for common sugars within aqueous confectionery, thus validating the original thesis hypothesis.

8.2. Recommendations for future work

There are various recommendations for future work to follow up on the results presented in this thesis and these have been provided below.

Water activity in confectionery relevant systems: Whilst this work focussed on investigating the molecular basis for water in 'simple' binary solutions, most common confections are multi-solute systems so expanding the field of study to include solutions of at least two solutes would be highly recommended. As significant amounts of empirical data (activity and volumetric measurements) would be required for such analyses, relatively dilute (and therefore high a_w) solutions in which there is no risk of spontaneous solute crystallisation (which would hinder measurement) would be a natural first step. Depending on the solutes selected it may however, be possible to access lower a_w mixtures in a thermodynamically stable manner through consideration of deliquescence lowering.[401] Due to an increased theoretical complexity (many more interaction terms that must be accounted for etc.), it is

recommended that future research along these lines be conducted in conjunction with experimental scattering techniques (small-angle X-ray neutron scattering) and also computational methods (e.g. molecular dynamic simulations). Both of these approaches have the potential benefit of providing detailed radial distribution functions (and thus, a more complete picture of local solvation behaviour) that are not possible to derive directly from Kirkwood-Buff interaction parameters alone. This would greatly help provide for a more complete understanding of the solvation behaviour within aqueous based confections, better facilitate identification of new candidate humectants and fundamentally aid in future efforts to develop sugar-reduced products.

Application of natural organic osmolytes: As real aqueous confections are mixtures containing multiple solutes, a key recommendation which may accelerate application in real sugar-reduced confectionery would be to investigate the physicochemical properties (namely T_g and a_w) of mixed aqueous solutions containing glycoin and/or floridoside in conjunction with other archetypal sugars/polyols as this was not possible in this work due to constraints to both time and materials. This would first require complete purification of both glycoin and floridoside and especially of the latter given that the a_w data presented herein is likely to have been strongly influenced by the presence of salts, thus limiting complete comprehension of its individual properties.

Whilst this work focussed on the study of floridoside and glycoin given their immediate availability in the short term, there are other structurally similar, saccharide-based osmolytes including isofloridoside (**a**), digeneaside (**b**) and firoin (**c**) which could also be expected to display comparable physicochemical properties and hence, are recommended as interesting targets for future work.[402, 403] In particular, salts such as digeneaside should make for excellent a_w reducing agents given an expected ionic dissociation within solution (and hence an increased van't Hoff factor).

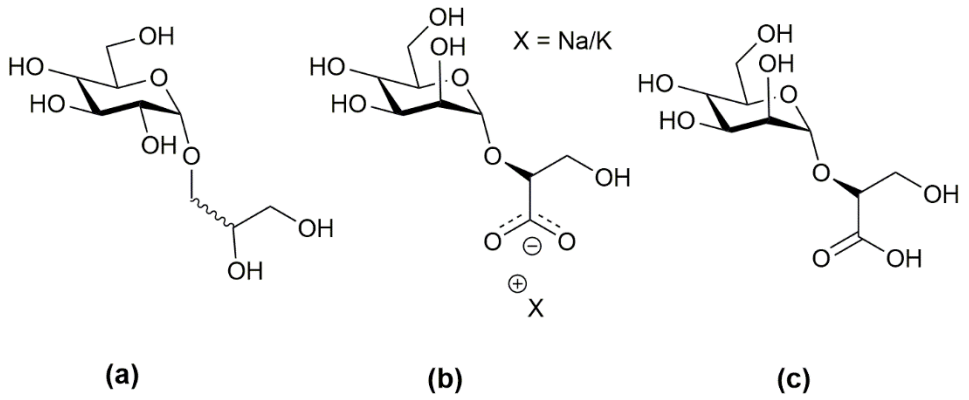

Figure 8.1: Other prominent saccharide-based osmolytes of the *Rhodophyta*; (**a**) isofloridoside, (**b**) digeneaside and (**c**) firoin.

Although this work has demonstrated that a solid-liquid extraction process using ethanol can yield large amount of floridoside in a facile, food-grade and somewhat 'clean' approach, Soxhlet extraction may not be feasible at an industrial scale. Therefore, to improve the viability of floridoside as a commercial sugar replacement strategy with a superior clean label reputation, it is recommended that other technologies such as subcritical (i.e. superheated/pressurised hot) water extraction also be investigated.[404] Similarly, glycoin is more likely to meet a desirable clean label mandate if it can be obtained directly from natural biomass. One such source that is recommended for investigation is *Spirulina platensis*, which is particularly attractive given that it can grow in brackish waters, is potentially available in large quantities and can bio-accumulate the target osmolyte at appreciable levels.[405]

In order to augment the commercial viability of floridoside as an industrial replacement for confectionery sugars it is recommended that floridoside extraction from red macroalgae is explored within the broader context of a biorefinery that also encompasses the production of other value-added chemicals, fuels and/or energy from the same single biomass source. For instance, there may be scope to use the spent and nitrogen-enriched (2.21 vs. 3.17 wt. % N before vs. after extraction) *Palmaria palmata* resulting from the floridoside extraction process for the production of functional protein/-

hydrolysates. It has recently been indicated that these extracts may have further functional food applications for the prevention and management of type 2 diabetes amongst other things.[406]

It is also recommended that future work should look to confirm the thermodynamic relationship of the two anhydrous floridoside dimorphs (e.g. via aqueous solubility or dissolution rate experiments) and also determine of the kinetics of F_h formation from anhydrous forms under real-world production/storage processing conditions. One particularly relevant characteristic of the different floridoside crystal forms that should be examined is their organoleptic profiles given that there are conflicting reports in the literature which indicate that floridoside elicits a sweet or neutral taste,[293, 329, 407] which would influence how it could be used within sugar-reduced confectionery moving forward. Hence, sensorial testing using human subjects is recommended. Linked to this, if the floridoside extracts prepared from *Palmaria palmata* are intended for human consumption, then it will be necessary to conduct a comprehensive characterisation of even trace compounds that were potentially not detectable using the current analytical techniques given the possible presence of problematic compounds such as the neurotoxic kainic acid, which has been reported previously to exist in *Palmaria palmata* of European origin.[408]

Outside of confectionery applications both glycoin and floridoside might have utility within other potential food and non-food applications such as; crystal inhibition, osmotic dehydration, cryopreservation, an osmotic draw solute for forward osmosis and an azeotrope breaker for polar a-/protic solvent mixtures (glycoin only).

Eutectic mixtures as novel humectants/plasticisers: Moving forward, although a novel food-grade eutectic mixture was demonstrated to act as an effective replacement humectant/plasticiser in an aqueous confectionery system on a technical level, it is unlikely that the lactone and ChCl based mixtures presented herein are suitable for application as wholly 'natural' ingredients within confectionery as the prospects of deriving ChCl from any type of natural resource remain very limited.

Therefore, it is imperative that further screening efforts are focussed on using solely bio-derivable components and especially those with low $\Delta H_{m,i}$ and/or $T_{m,i}$ as this should favour eutectic melting at lower temperatures that would be more suitable for room temperature applications. These future screening studies can be further expanded to examine the usage of minimal levels of intentional water addition in order to enable liquefaction whilst maintaining a low a_w.

Outside of direct food applications, it is recommended that future work could further examine the application of the novel lactone-DES presented within this thesis as an alternative to L-ascorbic acid DES which have already attracted interest from both the academic and industrial sectors. In particular, applications in which the presence of double bond of Asco might detrimental (e.g. reduction of disulphide-containing peptides and proteins)[409] should be sought.

Extending the investigation of model aqueous confections: Due to time and material constraints, it was only possible to test the novel humectants/plasticisers developed within this work at only a single level of addition within the model confectionery system. Therefore, a key recommendation is that these studies should be extended to examine the effects of even greater addition levels of the novel humectant/plasticiser used herein, even in the absence of any water given that the presence of the solvent has been implicated as a key for facilitating ideal mixing within amorphous sugar-based matrices.[30] In a similar vein, further future investigations should include the use of other more conventional and higher *DE* syrups given that they are still the most widely used products within the broader confectionery industry. In the case of floridoside and glycoin, it is recommended that model testing be expanded to include other areas of confectionery such as gelled confections and caramels.

Concerning further possible applications of eutectic mixtures in reduced-sugar confections, a key recommendation would be to compare the results of the pre-prepared mixture with those obtained via separate addition of the constituent components in order to ascertain whether there is any technological benefit to forming the eutectic mixture prior to addition into the confection. It is anticipated that the

greatest benefit of using pre-pared eutectics in confectionery applications may be in particularly low a_w systems, where the molten eutectic phase could act as a sufficiently plastic matrix even in the absence of water (and considerably more so than an anhydrous amorphous phase comprising only common sugars/polyols), thus future investigations along these lines are recommended.

Another recommendation is to perform more advanced rheological tests that were not possible within the present study owing to instrumental limitations such as oscillatory rheology for determination of properties including storage and loss moduli. Knowledge of such properties is likely to be important for various technological aspects (processing, storage etc) and could also provide deeper insights regarding interactions between constituent ingredients (particularly those involving the novel components introduced within this thesis) which are otherwise difficult to probe.

Appendix

Appendix A

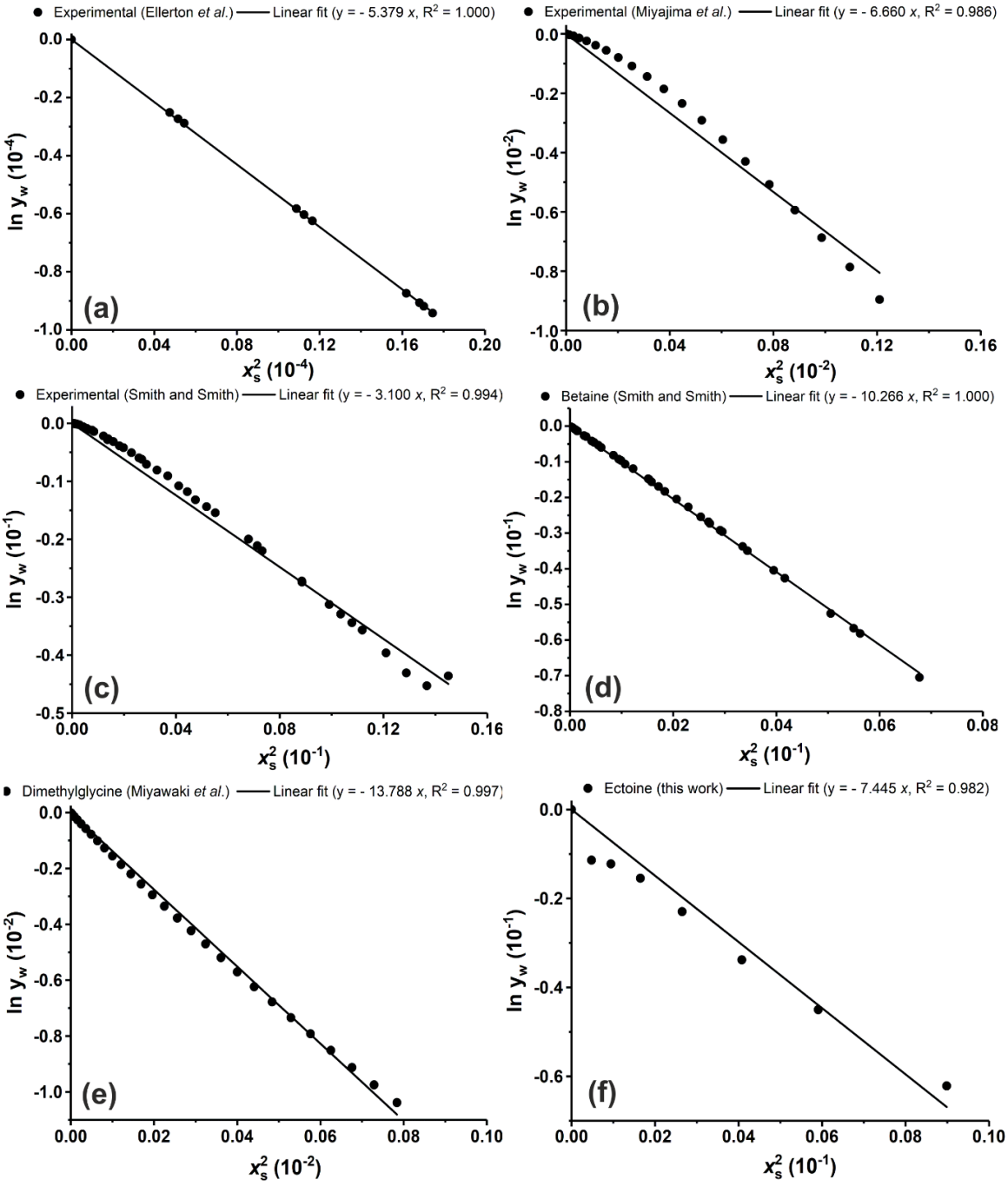

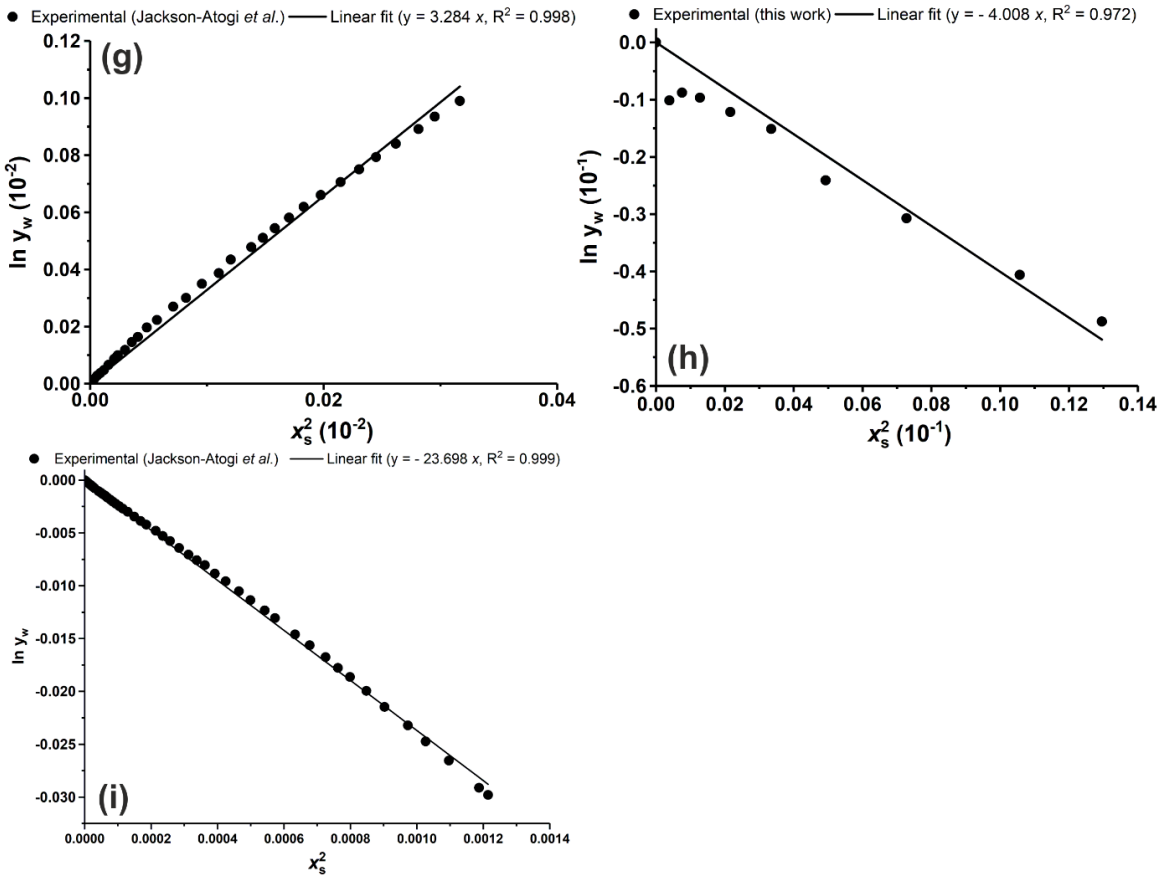

Appendix Figure A.1: Graphical determination of K_N for (**a**) raffinose,[241] (**b**) maltotriose,[240] (**c**) sarcosine,[248] (**d**) betaine,[248] (**e**) dimethylglycine,[249] (**f**) ectoine, (**g**) myo-inositol,[247] (**h**) hydroxyectoine and (**i**) α-GPC[247] via a plot of ln y_w vs. x_s^2 using experimental data taken from the literature or this work.

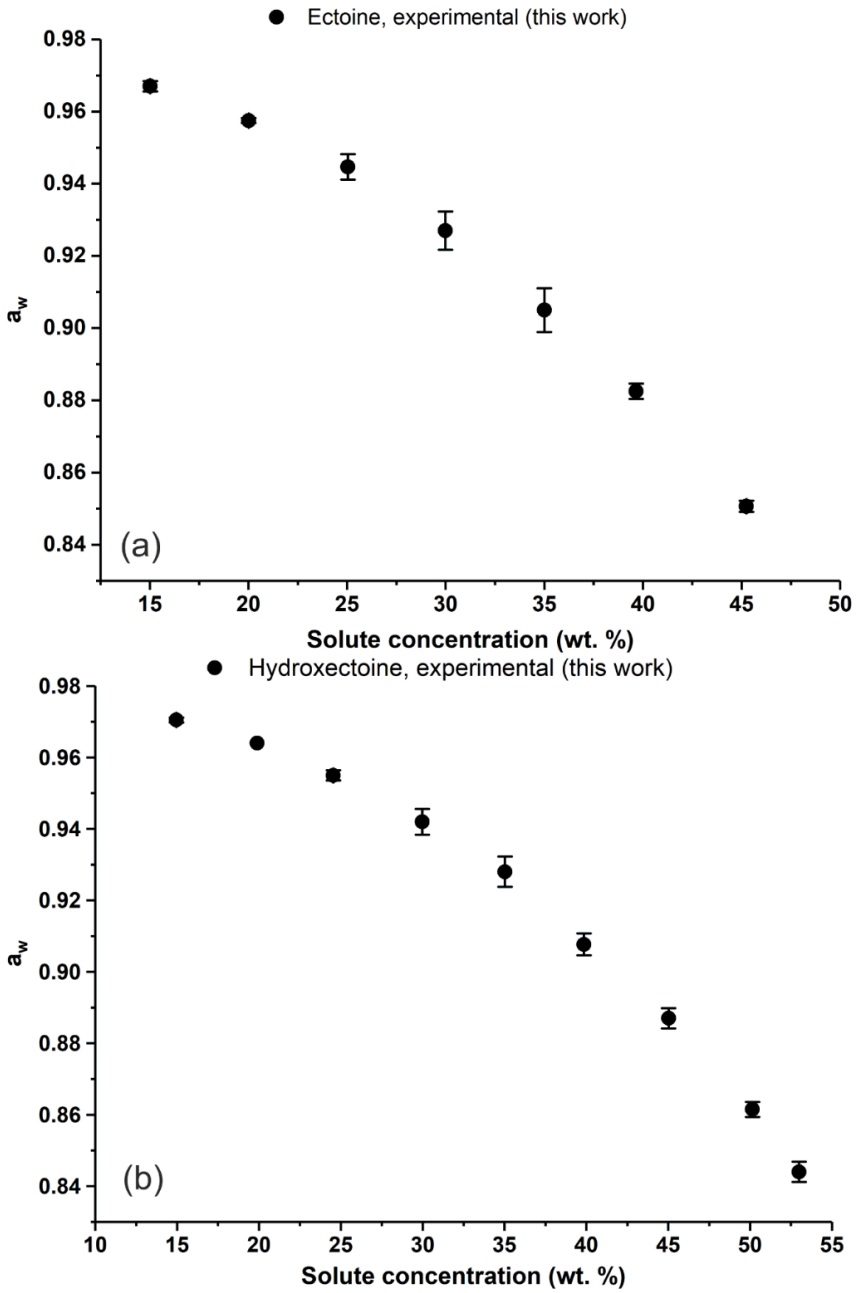

Appendix Figure A.2: Experimentally measured water activity (at 25 °C) as a function of solute concentration for (**a**) ectoine and (**b**) hydroxyectoine. Error bars represent $\pm$ 1 standard deviation.

Appendix Table A.1: Collated values of partial molar volumes (at infinite dilution), V_s^{∞} for various solutes studied in this work.

Solute	V_s^{∞}	**Ref.**
Raffinose	307.0	Cabani *et al*.[410]
Maltotriose	304.8	Cabani *et al*.[410]
Trehalose	206.9	Cabani *et al*.[410]
Lactose	209.1	Cabani *et al*.[410]
Sucrose	211.6	Cabani *et al*.[410]
Maltose	208.8	Cabani *et al*.[410]
Glucose	122.0	Cabani *et al*.[410]
Fructose	110.4	Cabani *et al*.[410]
Mannose	111.7	Cabani *et al*.[410]
Xylose	95.4	Cabani *et al*.[410]
Galactose	110.2	Cabani *et al*.[410]
Sorbitol	119.9	Cabani *et al*.[410]
Mannitol	119.3	Cabani *et al*.[410]
Xylitol	102.4	Cabani *et al*.[410]
Glycerol	71.0	Cabani *et al*.[410]
Erythritol	86.7	Cabani *et al*.[410]
Arabitol	103.3	Cabani *et al*.[410]
Ribitol	103.2	Cabani *et al*.[410]
Proline	82.2	Sirimulla *et al*.[411]
Alanine	60.4	Sirimulla *et al*.[411]
Glycine	43.2	Sirimulla *et al*.[411]
Sarcosine	62.5	Gheorghe *et al*.[412]
Dimethyglycine	81.2	Zhao[413]
Betaine	98.4	Pitkänen *et al*.[414]
α-GPC	182.8	Jackson-Atogi *et al*.[247]
myo-inositol	101.0	Jackson-Atogi *et al*.[247]

Appendix Equations A.1 – **A.3**: Note that the following equations were derived by Dr Seishi Shimizu (Department of Chemistry, University of York):

According to earlier KB theory, it is known that the dependence of the chemical potential of water μ_w on the mole fraction of solute x_s (at constant temperature and pressure) can be related to the KBIs G_{ww}, G_{sw} and G_{ss}through **Appendix Equation A.1**:[239]

$$\left(\frac{\partial \mu_w}{\partial x_s}\right)_{T,P} = -\frac{RT}{x_w}\frac{1}{1+x_s\, c_w\,(G_{ww}+G_{ss}-2G_{sw})} \qquad \textbf{Appendix Equation A.1}$$

At the limit of infinite dilution of x_s (denoted by the superscript ∞), the right-hand side of **Appendix Equation A1** can be re-evaluated as (**Appendix Equation A.2**):

$$\left(\frac{\partial \mu_w}{\partial x_s}\right)_{T,P} \approx -\frac{RT}{x_w}\left[1 - x_s\frac{G_{ww}^{\infty}+G_{ss}^{\infty}-2G_{sw}^{\infty}}{V_w^{\infty}}\right] \qquad \textbf{Appendix Equation A.2}$$

Where $V_w^{\infty}$is the partial molar volume of pure water (18.1 $cm^3\ mol^{-1}$). Rewriting **Appendix Equation 2** in terms of y_w gives (**Appendix Equation A.3**):

$$\left(\frac{\partial ln_{yw}}{\partial x_s}\right)_{T,P} = \frac{1}{RT}\left(\frac{\partial \mu_w}{\partial x_s}\right)_{T,P} + \frac{1}{x_w} \approx x_s\frac{G_{ww}^{\infty}+G_{ss}^{\infty}-2G_{sw}^{\infty}}{V_w^{\infty}} \qquad \textbf{Appendix Equation A.3}$$

Realising that $K_N = \frac{\ln y_w}{x_s^2}$, **Appendix Equation A.3** can be rewritten in terms of K_N (**Equation 3.4**):

$$K_N = \frac{1}{2V_w^{\infty}}\left(G_{ww}^{\infty} + G_{ss}^{\infty} - 2G_{sw}^{\infty}\right) \qquad \textbf{Equation 3.4}$$

Appendix B

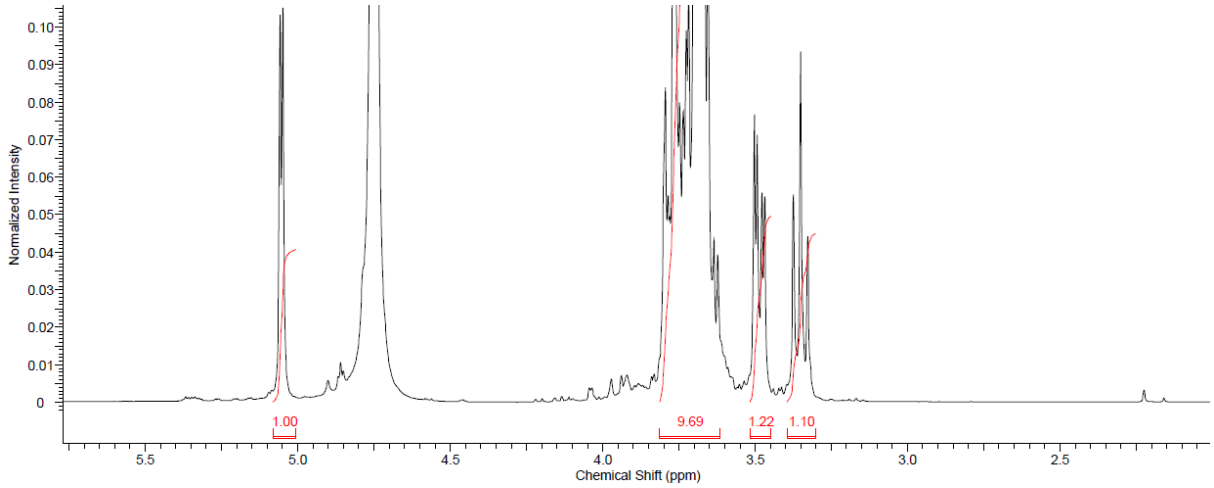

Appendix Figure B.1: Integration of primary signals in the ^{1}H NMR spectrum of glycoin (analysis conducted using ACD-NMR software). Originally in colour.

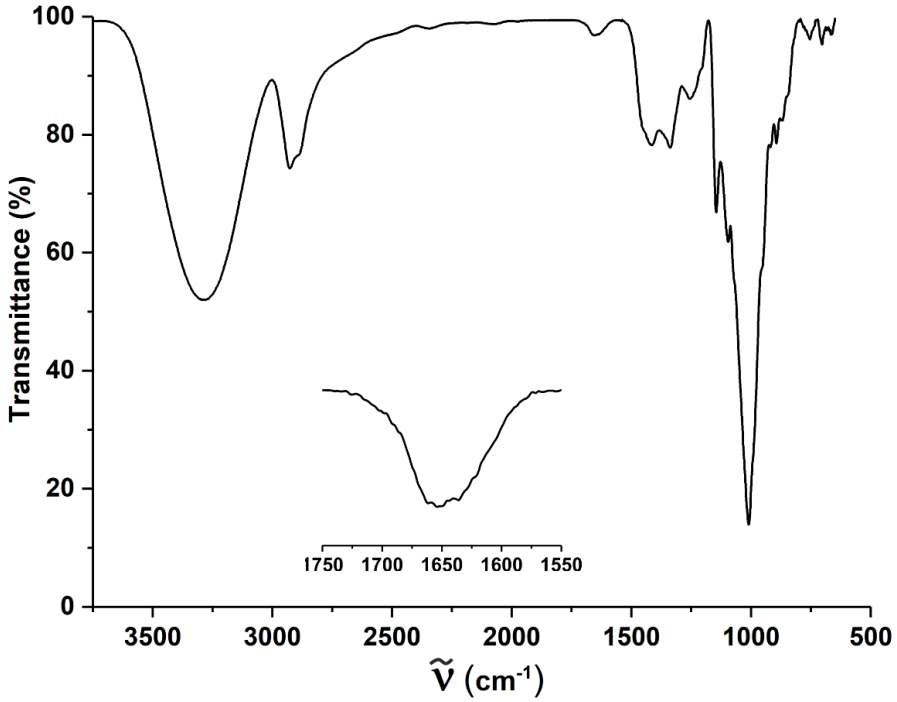

Appendix Figure B.2: ATR-FTIR of Gly-T (650 – 4000 cm^{-1}) following *ca*. 5 minutes after initial exposure to ambient humidity.

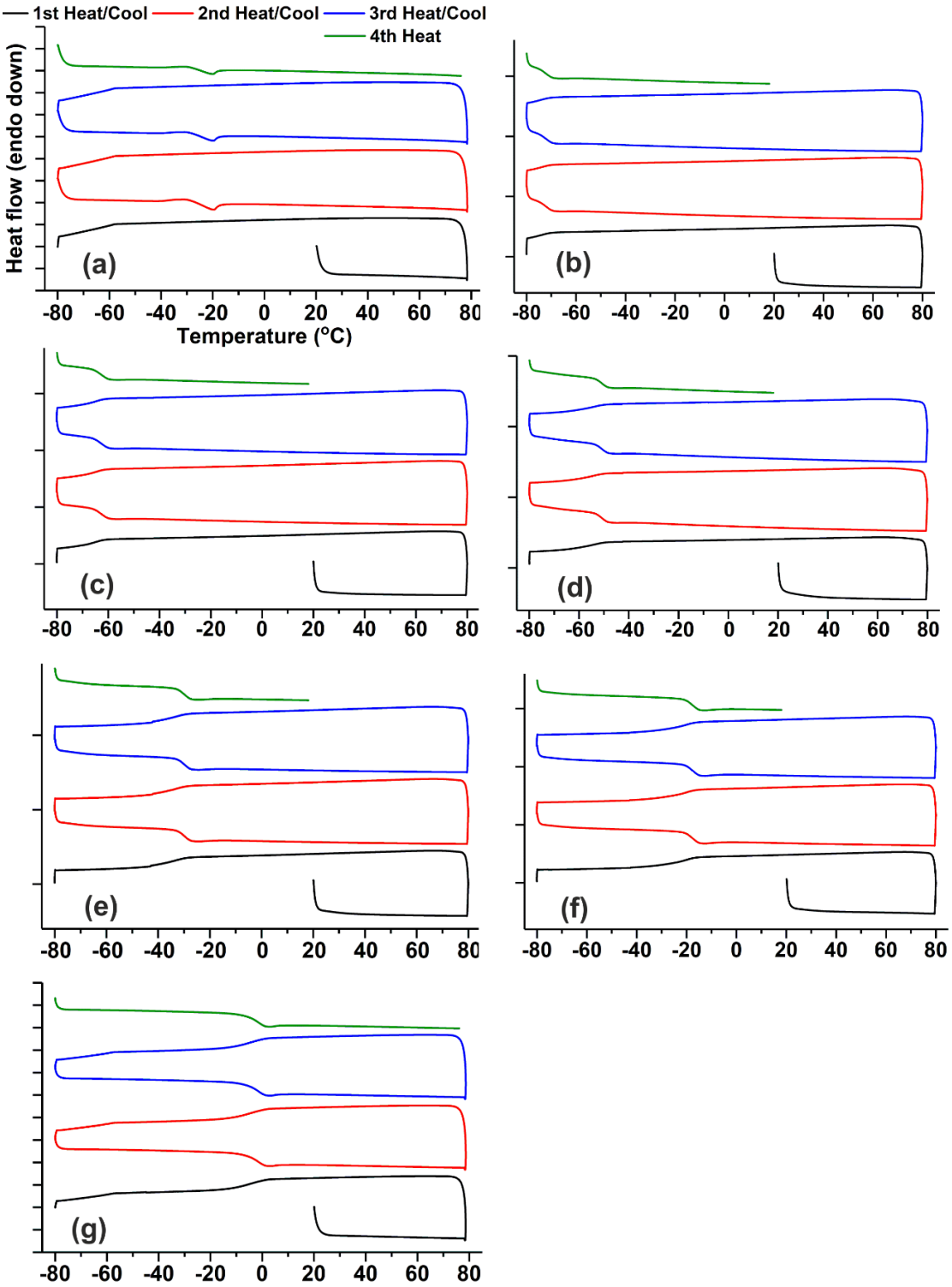

Appendix Figure B.3: Full DSC traces for Gly-T solutions of approximately 62 (**a**), 70 (**b**), 75 (**c**), 80 (**d**), 85 (**e**), 90 (**f**) and 94 (**g**) wt. % (heated to 80, cooled to – 80 and reheated to 80 °C (repeated twice further) at 5 K min^{-1}). Tick marks along the *y*-axes correspond to 5 mW. Originally in colour.

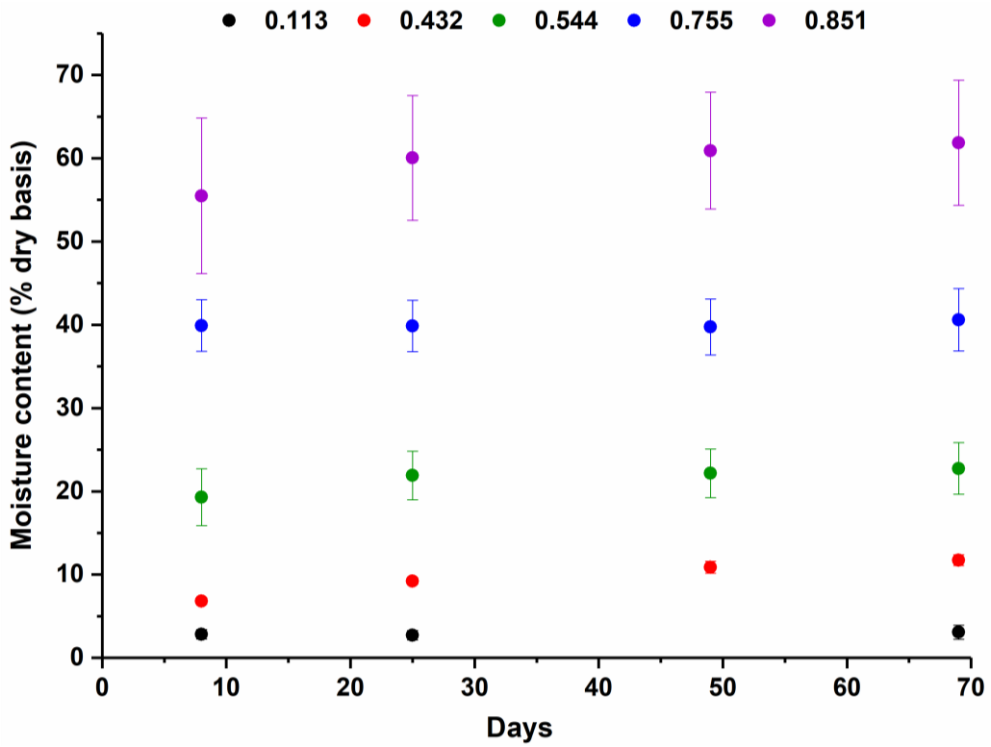

Appendix Figure B.4: Moisture adsorption of Gly-T at (from bottom to top) a_w = 0.113, 0.432, 0.544, 0.755 and 0.851 measured after 8, 25, 49 and 69 days equilibration at *ca*. 21 °C. (n.b. no measurement for a_w = 0.113 was recorded on the 49th day). Error bars represent ± 1 standard deviation. Originally in colour.

Appendix Table B.1: Concentration of constituent species in Glycoin® natural according to the Certificate of analysis (as determined via HPLC by bitop AG, Dortmund, Germany).

Species	Concentration (wt. %)[a]
2-*O*-α-D-glucopyranosyl glycerol	≥ 50
1-*O*-α-D-glucopyranosyl glycerol	≥ 7
D-glucose	≥ 3
D-fructose	≥ 5
D-sucrose	≥ 2
Glycerol	≥ 1

[a]The remaining mass corresponds to water.

Appendix Table B.2: ^{1}H and ^{13}C NMR assignments for glycoin recorded in D_2O at 25 °C. Atomic numbering corresponds to numerical labels presented in the structural formulae shown below the table. Originally in colour.

Carbon no.	**^{1}H: δ, ppm**	**^{13}C: δ, ppm**
1	5.05, (1H, d)	97.8
2	3.48, (1H, dd)	71.5
3	3.60 - 3.80, (1H, m)	72.9
4	3.35, (1H, t)	69.5
5	3.60 - 3.80, (1H, m)	72.0
6	3.60 - 3.80, (2H, m)	61.4
7	3.60 - 3.80, (1H, m)	78.8
8	3.60 - 3.80, (2H, m)	60.5/60.3
9	3.60 - 3.80, (2H, m)	60.5/60.3

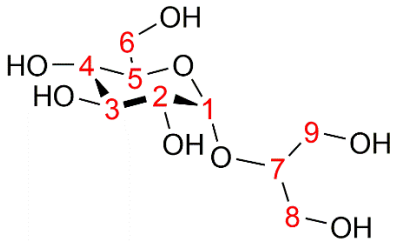

Appendix C

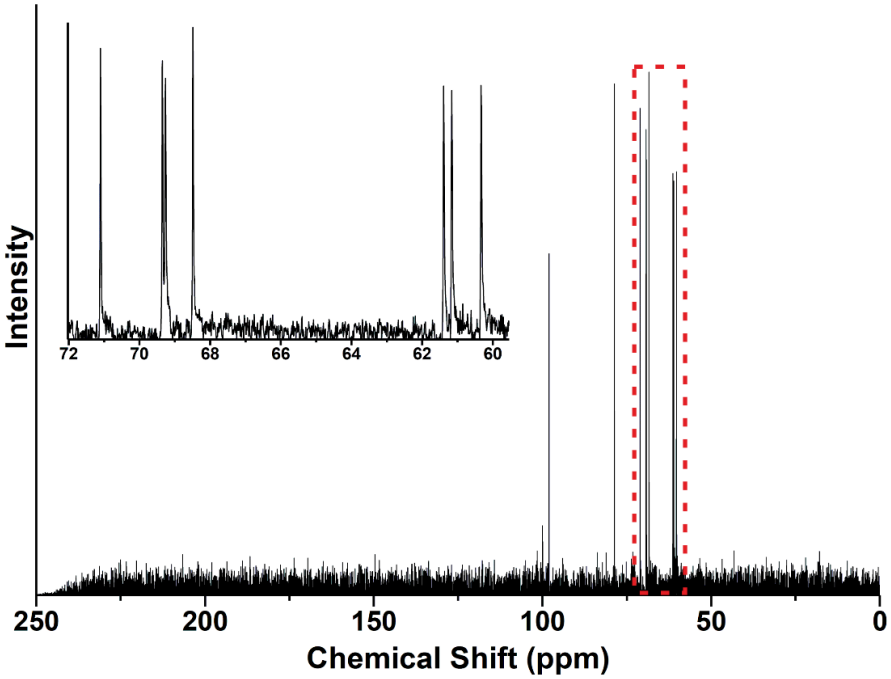

Appendix Figure C.1: ^{13}C NMR (101 Hz) spectrum of refluxing water extract of *Palmaria palmata* recorded in D_2O. Originally in colour.

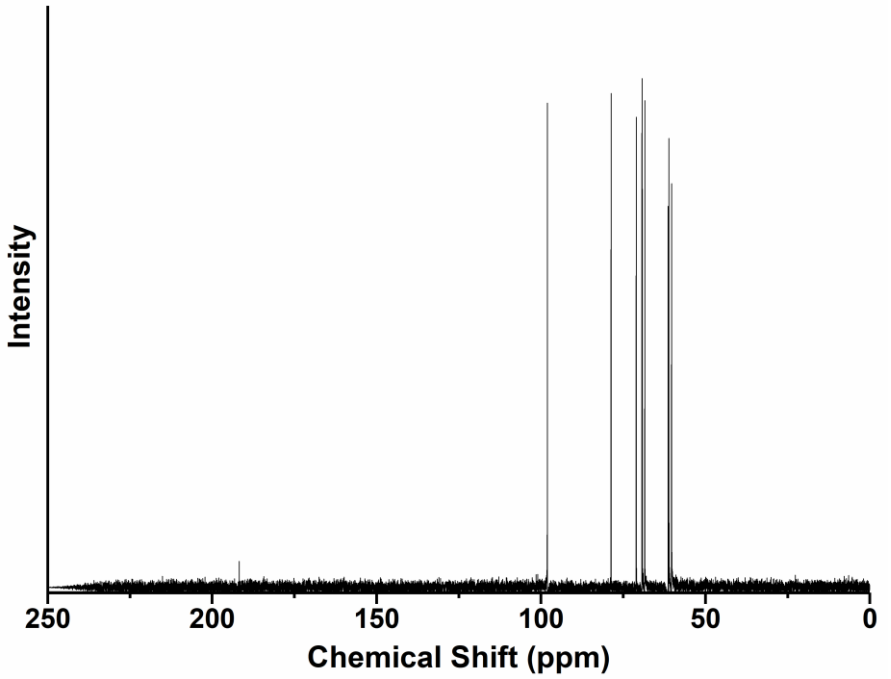

Appendix Figure C.2: ^{13}C NMR (101 Hz) spectrum of organic extract produced via ethanol Soxhlet extraction of *Palmaria palmata* recorded in D_2O.

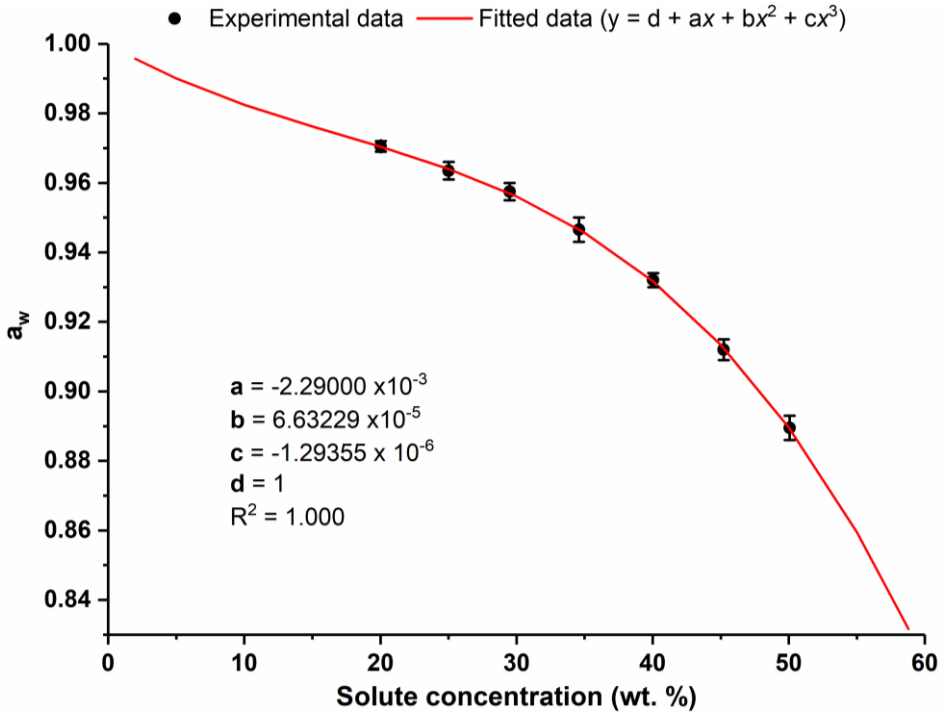

Appendix Figure C.3: Cubic polynomial fit of experimental a_w as a function of the concentration of floridoside-rich (*ca*. 92.5 wt. %) Soxhlet extract up to the aqueous solubility limit (≤ 58.8 wt. % according to KF titration). Originally in colour.

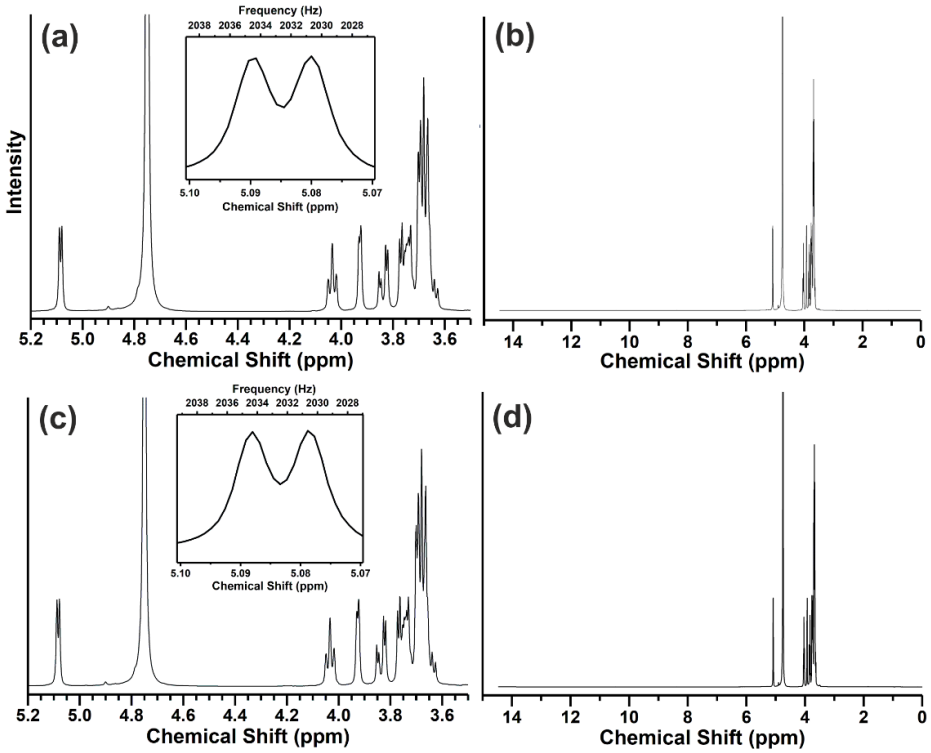

Appendix Figure C.4: ^{1}H (400 MHz) spectra of UCM (**a** and **b**) and UCM-T (**c** and **d**) recorded in D_2O at 25 °C and referenced with respect to HOD at 4.75 ppm.

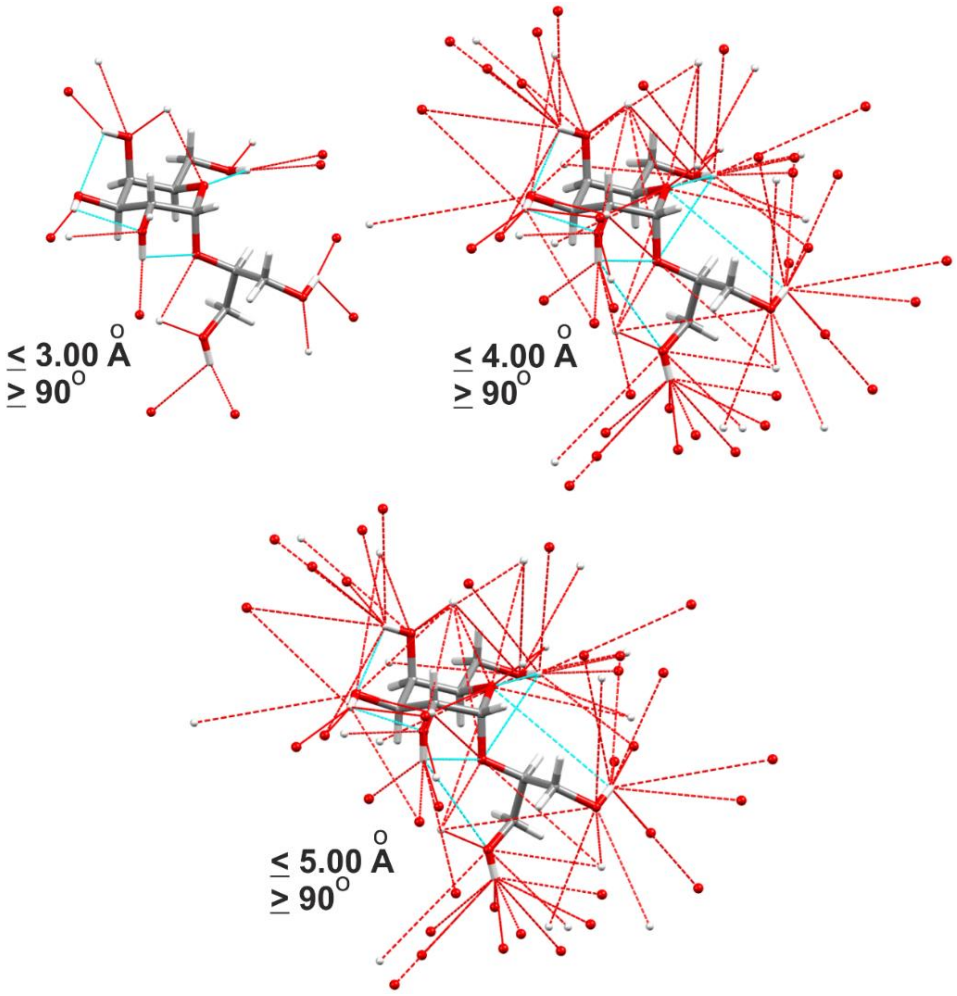

Appendix Figure C.5: H-bonds (dashed red line = intermolecular, dashed cyan line = intramolecular) formed by a floridoside molecule within crystalline F_{II} identified using a criteria of $\geq$ 90 ° and either $\leq$ 3.00, 4.00 or 5.00 Å. Originally in colour.

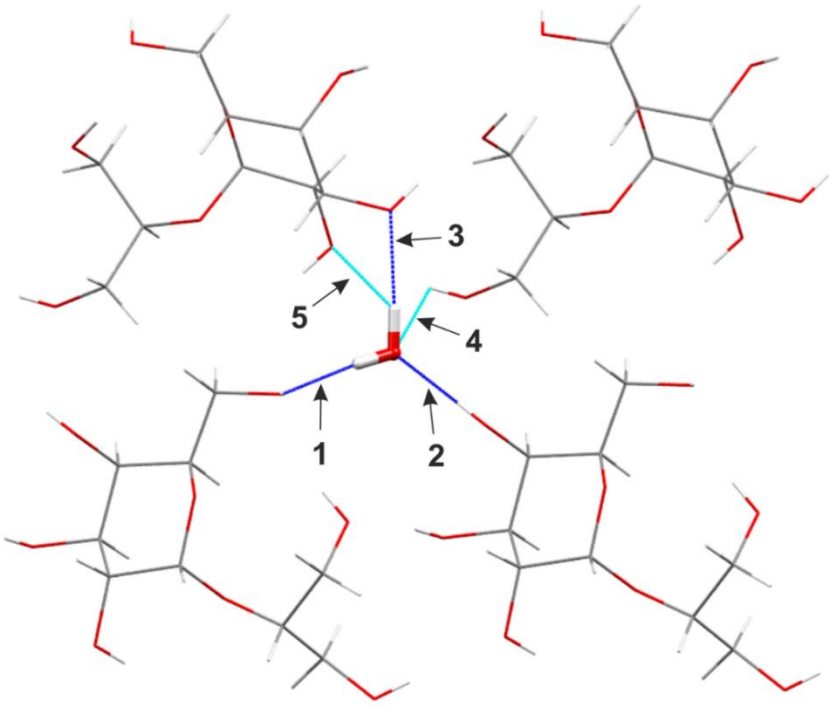

No.	Donor	Acceptor	Distance (Å)	Angle (°)
1	O(W)-**H**	O(6)	1.887	175.10
2	O(4)-**H**	O(W)	1.812	175.40
3	O(W)-**H**	O(3)	2.008	176.16
4	O(8)-**H**	O(W)	2.893	113.16
5	O(W)-**H**	O(2)	2.910	111.19

Appendix Figure C.6: Graphical and tabulated representation of hydrogen bonds found for the water (ball and stick) with the surrounding floridoside molecules (wireframe) in F_h as defined by the following criteria: < 3.00 Å (H···A) and > 90 ° (O-H···A), OH donor only, and > 1 bond separation between intramolecular donor/acceptor. The navy or cyan dashed lines indicate whether a H···A length is < 2.20 or 2.21 – 3.00 Å respectively and the bracketed numbers in the table denote the identity of the floridoside oxygen atom involved (w = water). Originally in colour.

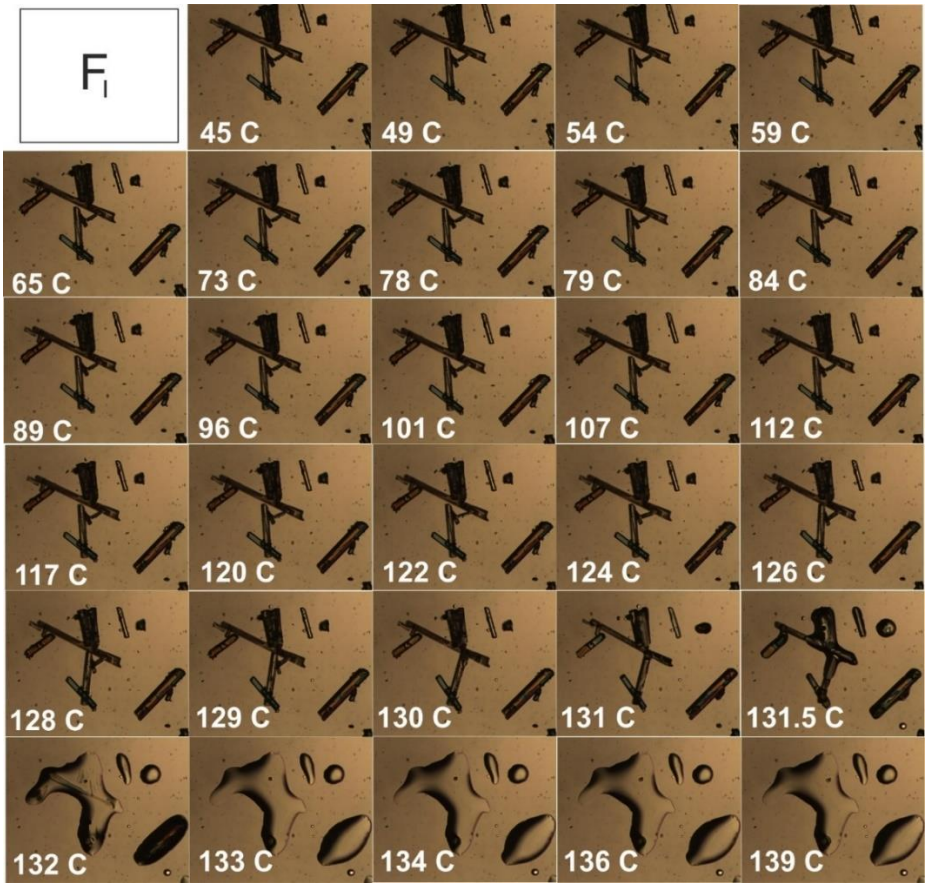

Appendix Figure C.7: Hot-stage micrographs of a single F_I crystal heated from 45 to 139 ^oC at a rate of 5 $^oC\ min^{-1}$. Originally in colour.

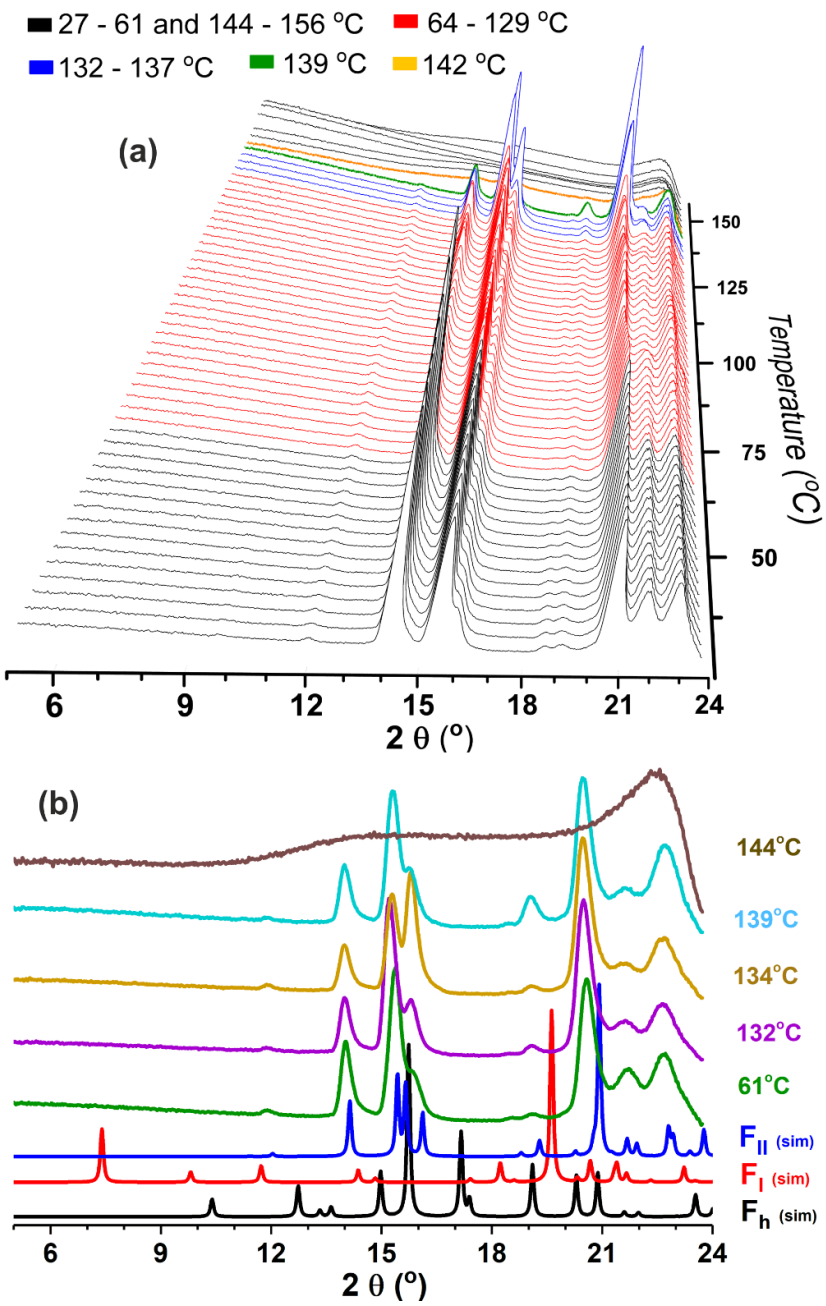

Appendix Figure C.8: Temperature-resolved (**a**) and selected (**b**) VTXRD traces of crystalline F_{II}. Originally in colour.

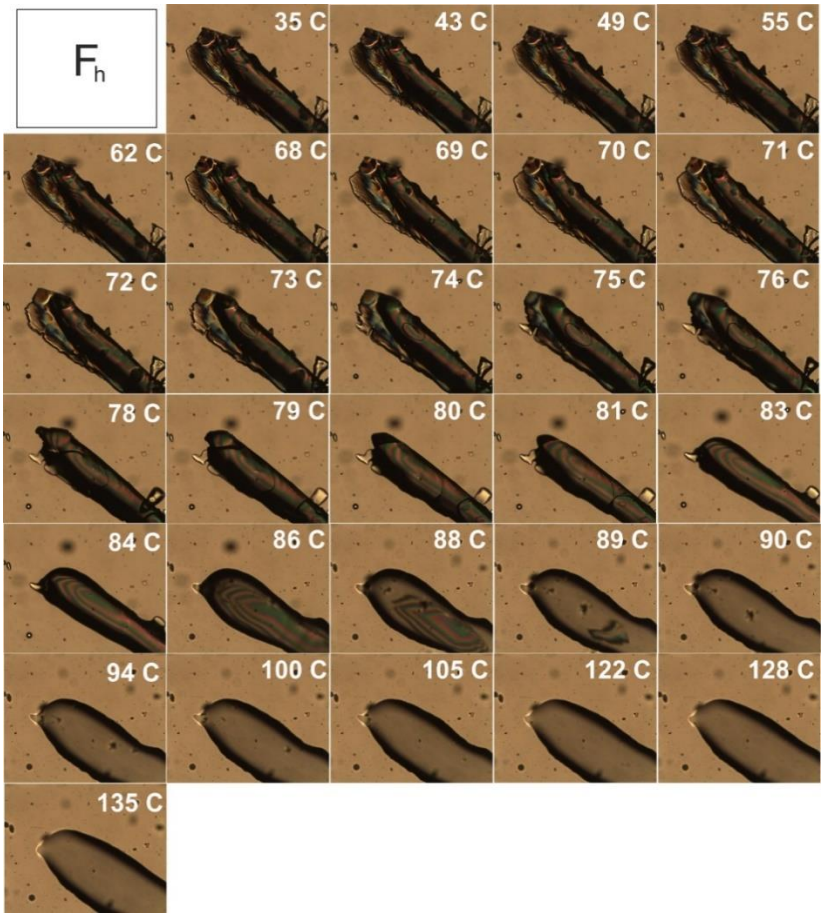

Appendix Figure C.9: Hot-stage micrographs of a single F_h crystal heated from 35 to 135 ^oC at a rate of 5 $^oC\ min^{-1}$. Originally in colour.

Appendix Table C.1: Major metal/-loid species (> 200 ppm) in vacuum oven dried *Palmaria palmata* according to ICP-OES analysis.

Species	Concentration (ppm)
K	24218
Na	6944
S	2092
Ca	1652
P	1073
Mg	661
Fe	280
Si	228

Appendix Table C.2: ^{1}H (400 MHz) and ^{13}C NMR (101 MHz) assignments for a typical organic extract recorded in D_2O at 25 °C. Atomic numbering corresponds to numerical labels presented in the structural formulae shown below the table. Originally in colour.

Carbon no.	**^{1}H: δ, ppm**	**^{13}C: δ, ppm**
1	5.10, (1H, d)	98.1
2	3.63 - 3.80, (1H, m)	68.5
3	3.85, (1H, dd)	69.4
4	3.94, (1H, d)	69.3
5	4.04 (1H, t)	71.1
6	3.63 - 3.80, (2H, m)	61.4/61.2/60.3
7	3.63 - 3.80, (1H, m)	78.7
8	3.63 - 3.80, (2H, m)	61.4/61.2/60.3
9	3.63 - 3.80, (2H, m)	61.4/61.2/60.3

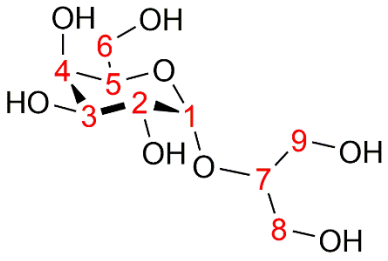

Appendix Table C.3: Summary of crystal and structural refinement data for F_h, F_{II}, and F_I (all refined by Dr Adrian Whitwood, University of York).

Polymorph Code	F_h	F_{II}	F_I
Empirical formula	$C_9H_{20}O_9$	$C_9H_{18}O_8$	$C_9H_{18}O_8$
Formula weight	272.25	254.23	254.23
Temperature/K	110.00(10)	110.00(10)	110.00(10)
Crystal system	orthorhombic	orthorhombic	orthorhombic
Space group	$P2_12_12_1$	$P2_12_12_1$	$P2_12_12_1$
a/Å	8.22038(16)	8.54811(10)	4.84791(13)
b/Å	11.2533(3)	9.19251(10)	9.7111(3)
c/Å	12.9852(2)	14.34851(17)	23.8172(7)
α/°	90	90	90
β/°	90	90	90
γ/°	90	90	90
Volume/Å^3	1201.22(4)	1127.49(2)	1121.28(5)
Z	4	4	4
ρ_{calc}g/cm^3	1.505	1.498	1.506
μ/mm^{-1}	1.185	1.154	1.160
F(000)	584.0	544.0	544.0
Crystal size/mm^3	0.236 × 0.114 × 0.025	0.275 × 0.153 × 0.136	0.2 × 0.102 × 0.072
Radiation/Å	CuKα (λ = 1.54184)	CuKα (λ = 1.54184)	CuKa (λ = 1.54184).
2Θ range for data collection/°	10.402 to 134.146	11.432 to 133.962	7.424 to 134.06
Index ranges	$-9 \le h \le 9$, $-13 \le k \le 13$, $-15 \le l \le 8$	$-10 \le h \le 10$, $-10 \le k \le 10$, $-17 \le l \le 16$	$-5 \le h \le 2$, $-11 \le k \le 10$, $-28 \le l \le 28$
Reflections collected	8062	10041	2553
Independent reflections	2155 [R_{int} = 0.0235, R_{sigma} = 0.0199]	2012 [Rint = 0.0222, Rsigma = 0.0151]	1727 [Rint = 0.0186, Rsigma = 0.0330]
Data/restraints/parameters	2155/0/196	2012/0/179	1727/0/226
Goodness-of-fit on F^2	1.044	1.036	1.048
Final R indexes [I>=2σ (I)]	R_1 = 0.0221, wR_2 = 0.0545	R1 = 0.0215, wR2 = 0.0550	R_1 = 0.0259, wR_2 = 0.0587
Final R indexes [all data]	R_1 = 0.0234, wR_2 = 0.0554	R1 = 0.0223, wR2 = 0.0556	R_1 = 0.0294, wR_2 = 0.0609
Largest diff. peak/hole / e Å^{-3}	0.18/-0.14	0.23/-0.16	0.22/-0.15
Flack parameter	-0.02(8)	-0.02(6)	0.19(16)

Appendix D

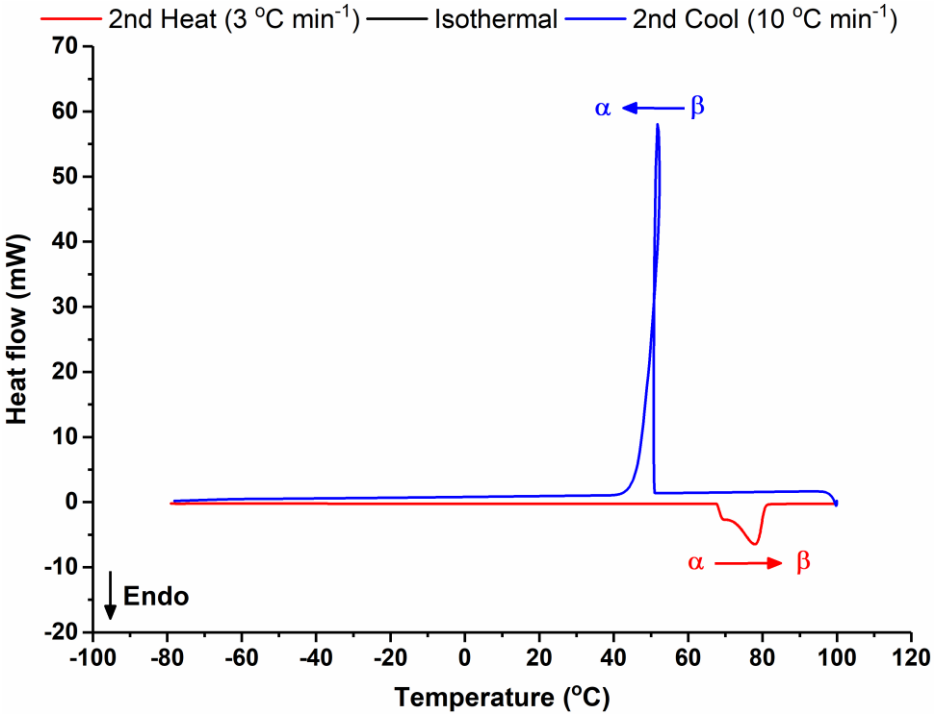

Appendix Figure D.1: Second heating (red) and cooling (blue) DSC thermograms recorded for crystalline ChCl (8.7 mg) at a scan rate of 3 and 10 °C min^{-1}, respectively. Originally in colour.

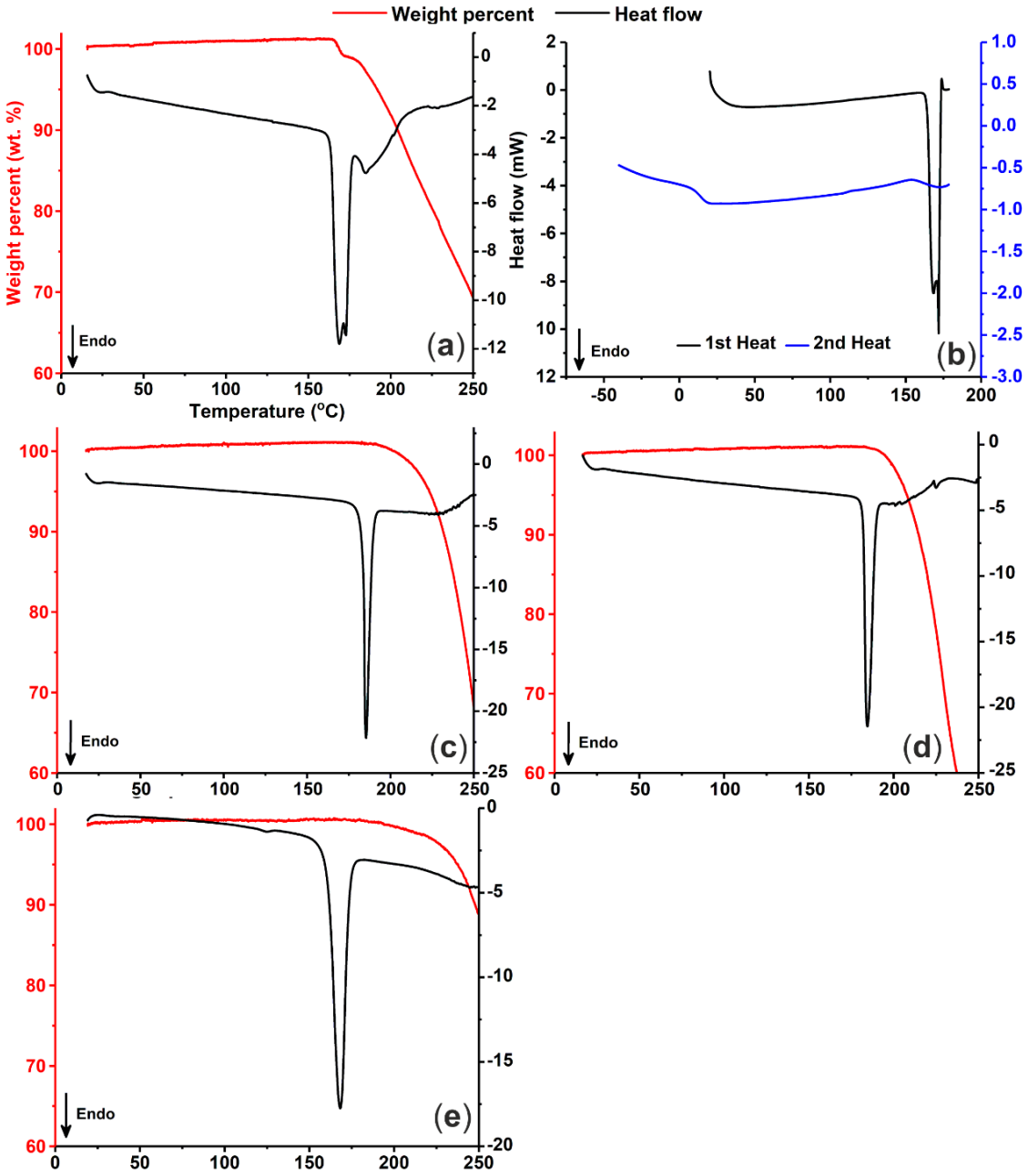

Appendix Figure D.2: STA (3 or 5 °C min^{-1}, 50 mL min^{-1} N_2) of selected DES components; (**a**) GluLac (8.6 mg), (**c**) L-GLac (8.7 mg), (**d**) D-GLac (8.7 mg), (**e**) Glu-1,5-Lac (9.9 mg) and DSC (3 °C min^{-1}) of (**b**) GluLac (7.2 mg) in a hermetically sealed pan. Originally in colour.

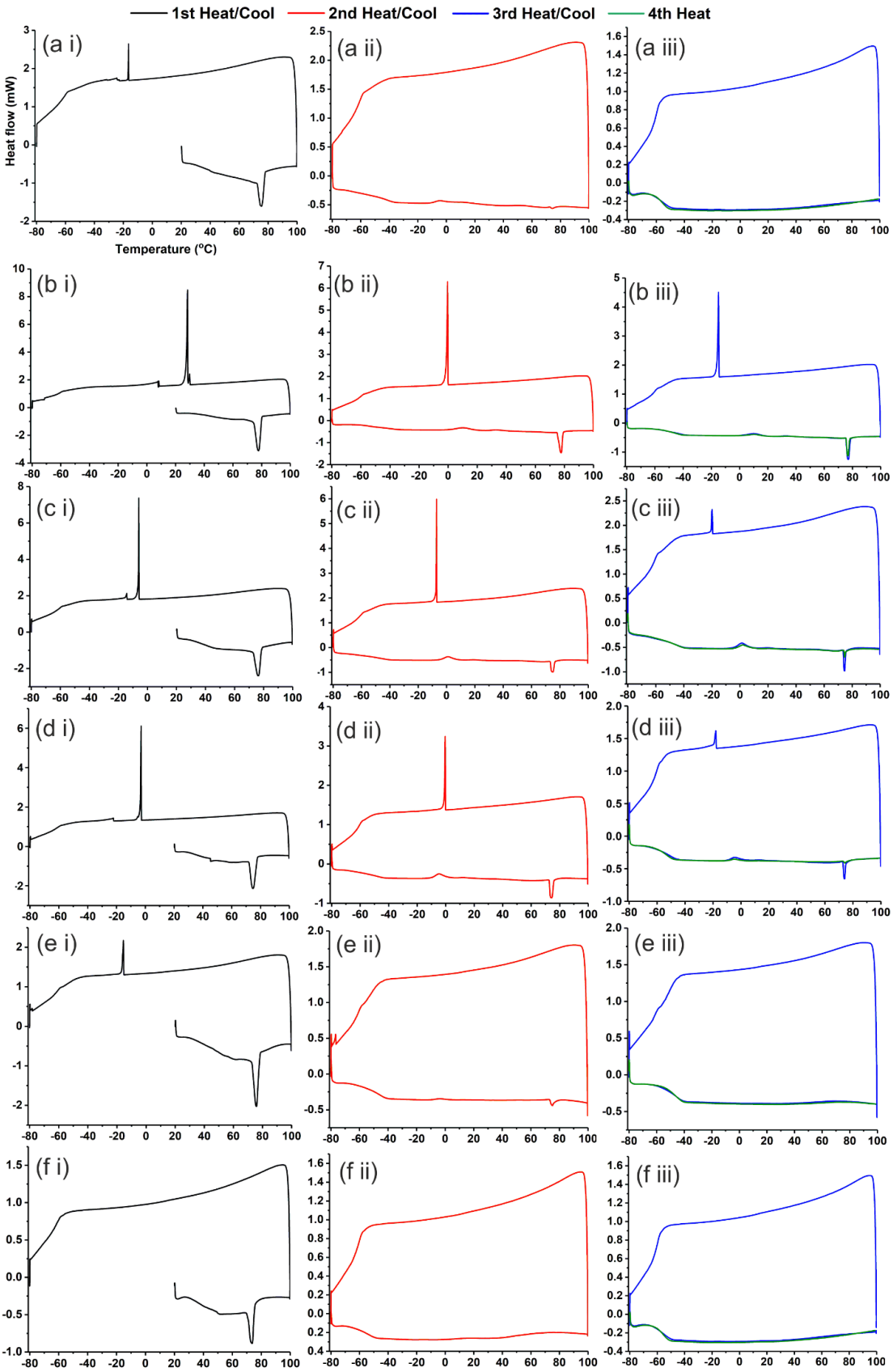
1st Heat/Cool
2nd Heat/Cool
3rd Heat/Cool
4th Heat
(a i)
(a ii)
(a iii)
(b i)
(b ii)
(b iii)
(c i)
(c ii)
(c iii)
(d i)
(d ii)
(d iii)
(e i)
(e ii)
(e iii)
(f i)
(f ii)
(f iii)
Heat flow (mW)
Temperature (°C)

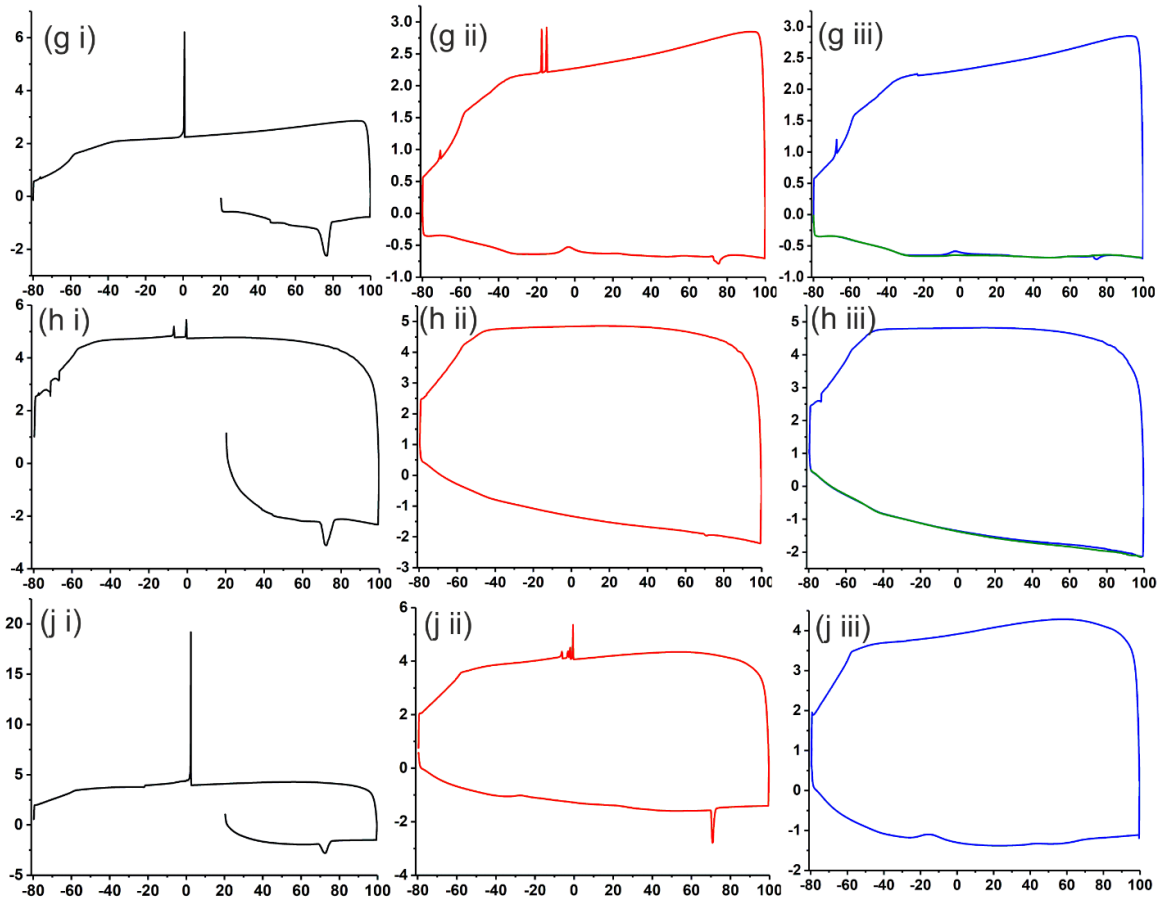

Appendix Figure D.3: First (**i**), second (**ii**) and third/fourth (**iii**) heating and cooling cycles for *in-situ* DES; (**a**) GluLac:ChCl, 1:1 (5.0:3.8 mg), (**b**) GluLac:ChCl, 1:1.5 (3.8:4.4 mg), (**c**) L-GLac:ChCl, 1:1 (4.9:4.1 mg), (**d**) L-GLac:ChCl, 1:1.5 (3.3:4.0 mg), (**e**) D-GLac:ChCl, 1:1 (4.5:3.5 mg), (**f**) D-GLac:ChCl, 1:1.5 (2.5:3.0 mg), (**g**) Glu-1,5-Lac:ChCl, 1:1 (5.7:4.3 mg), (**h**) Asco:ChCl, 1:1 (5.8:4.5 mg), (**j**) Asco:ChCl, 1:1.5 (4.3:5.7 mg). Originally in colour.

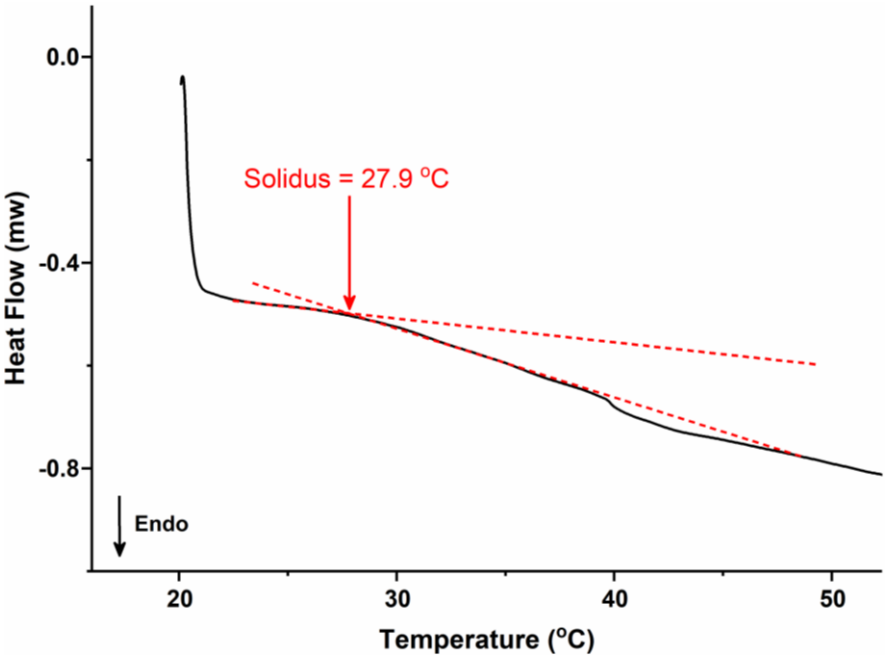

Appendix Figure D.4: Graphical estimation of solidus temperature in the lactone-ChCl DES as exemplified using the DSC thermogram recorded for the first cycle heat of the GluLac:ChCl, 1:1 solid mixture (3 °C min^{-1}). Originally in colour.

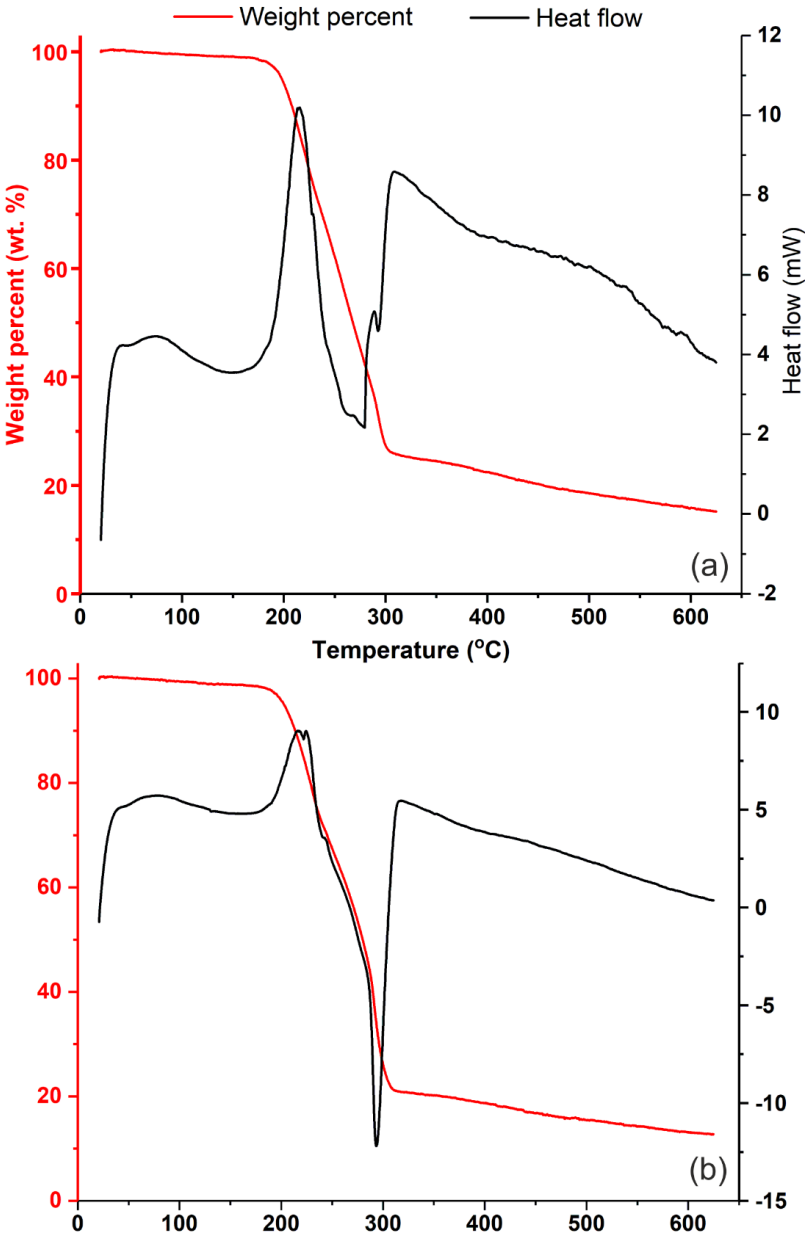

Appendix Figure D.5: STA (10 °C min^{-1}, 50 mL min^{-1} N_2) of (**a**) 1:1 and (**b**) 1:1.5 Asco:ChCl DES. Originally in colour.

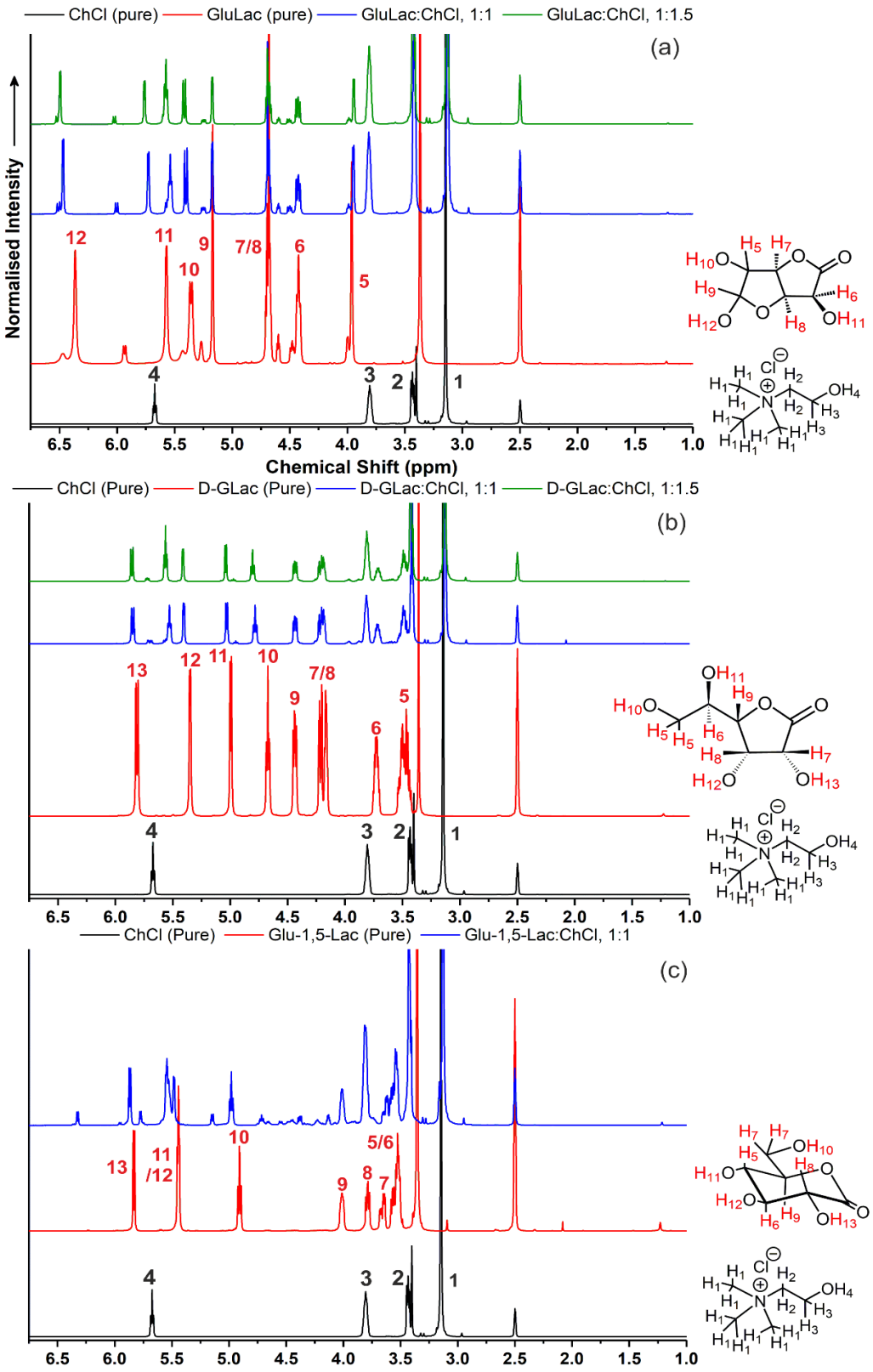

Appendix Figure D.6: Comparison of ^{1}H NMR spectra recorded for (**a**) GluLac:ChCl, (**b**) D-GLac:ChCl and (**c**) Glu-1,5-lac:ChCl DES. Originally in colour.

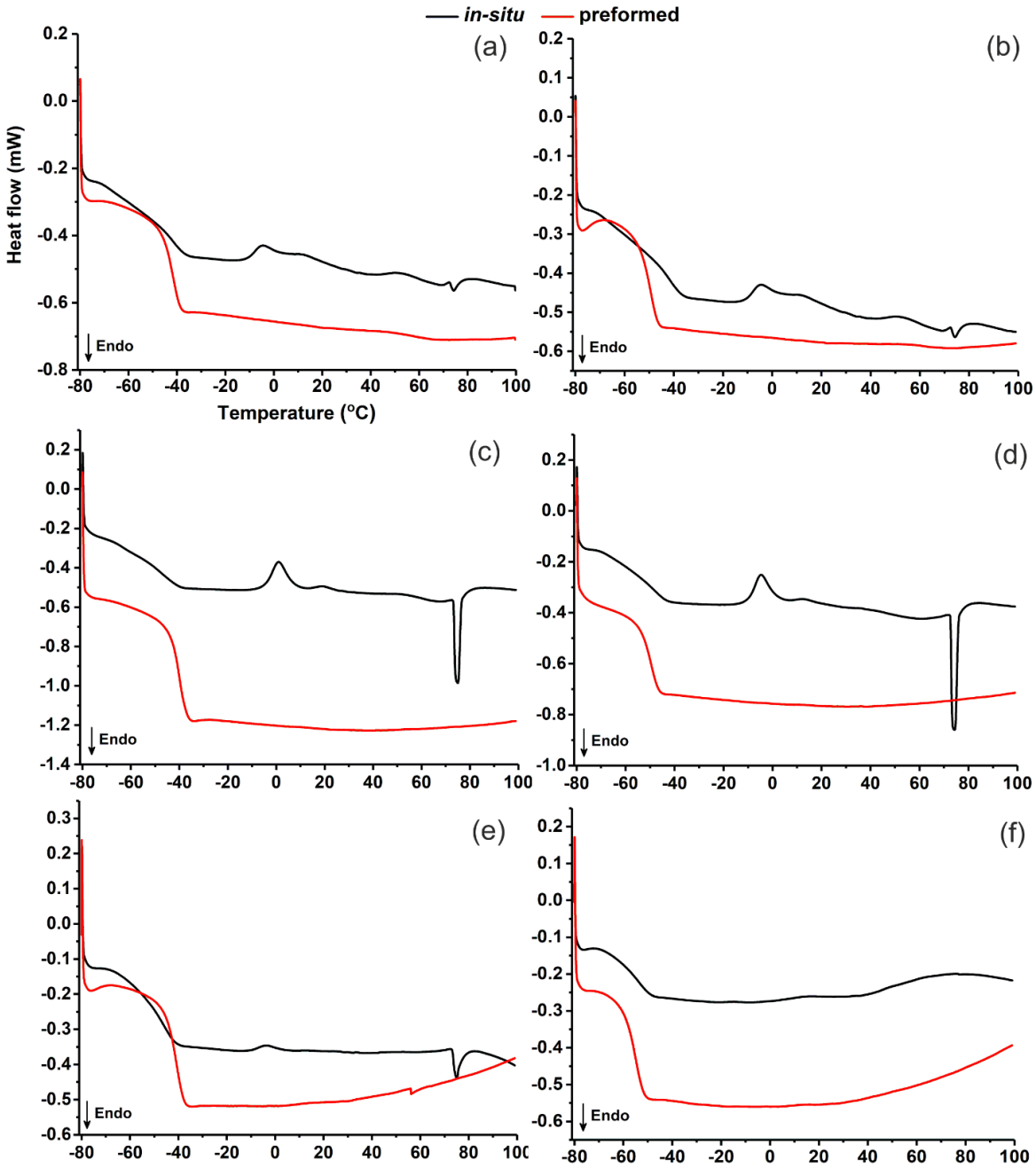

Appendix Figure D.7: Comparative DSC (3 °C min^{-1}) of *in-situ*/preformed DES during the second heat cycle; (**a**) GluLac:ChCl, 1:1 (8.8/10.4 mg), (**b**) GluLac:ChCl, 1:1.5 (8.2/10.0 mg), (**c**) L-GLac:ChCl, 1:1 (9.0/16.4 mg), (**d**)) L-GLac:ChCl, 1:1.5 (7.4/10.4 mg), (**e**)) D-

GLac:ChCl, 1:1 (8.0/10.7 mg) and (**f**)) D-GLac:ChCl, 1:1.5 (5.5/9.3 mg). Originally in colour.

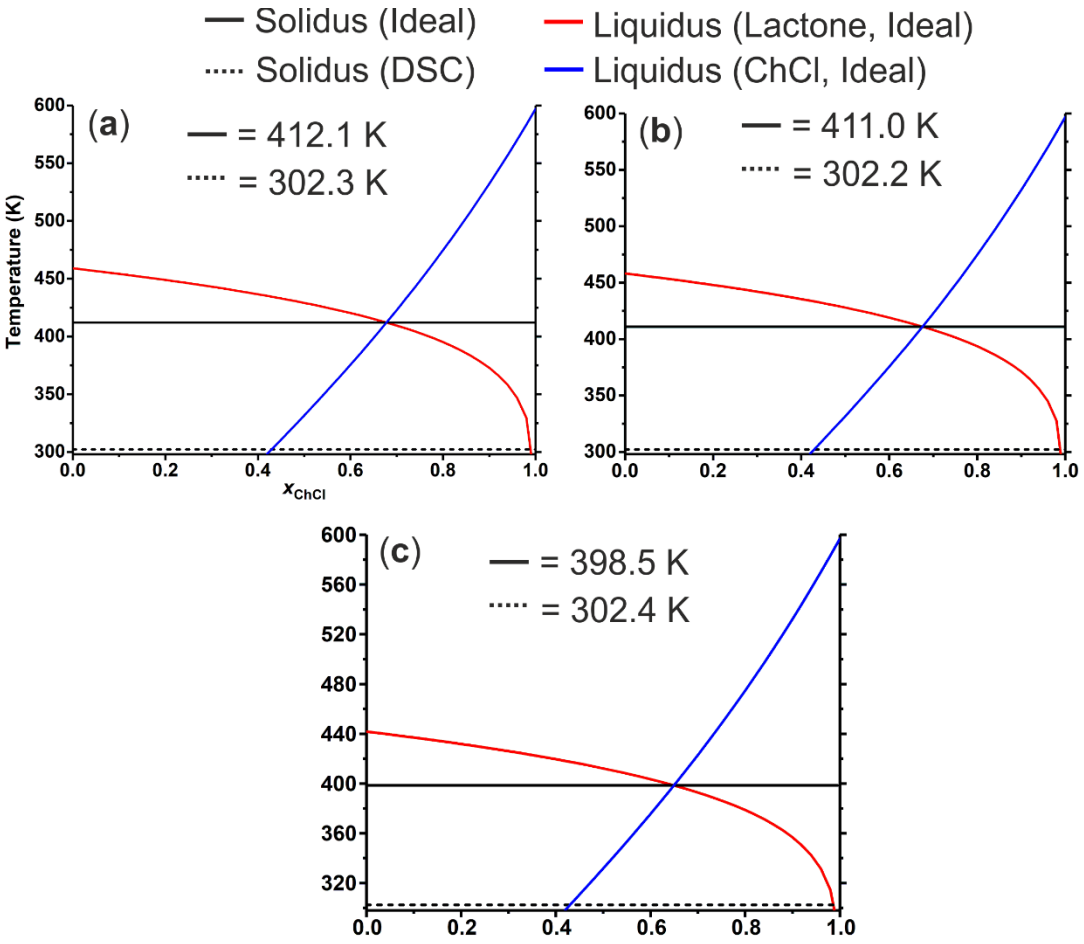

Appendix Figure D.8: Theoretical ideal SLE phase diagrams of (**a**) L-GLac:ChCl, (**b**) D-GLac:ChCl and (**c**) Glu-1,5-Lac:ChCl and comparison with the corresponding experimentally measured solidi. Originally in colour.

Appendix E

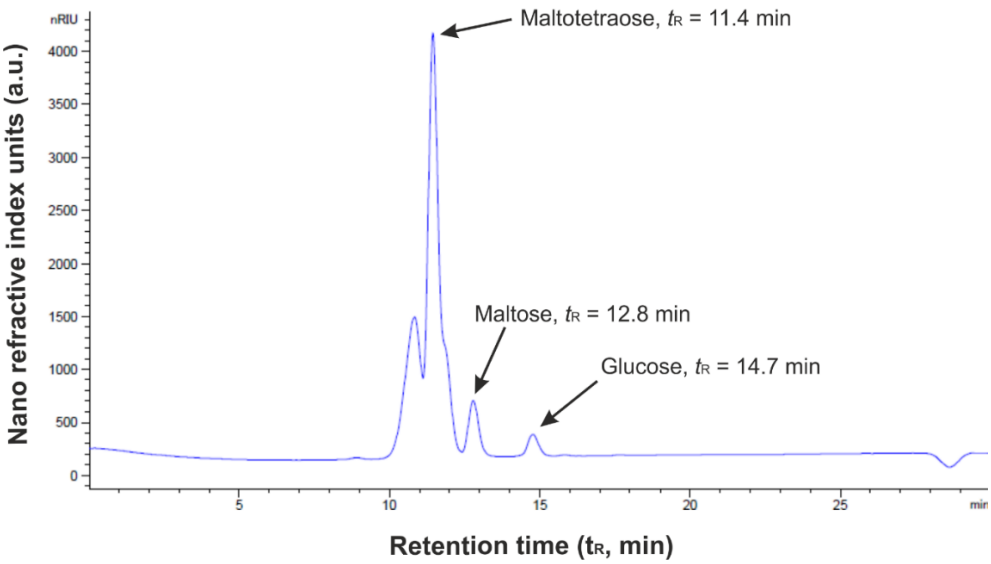

Appendix Figure E.1: HPLC chromatogram of as-received Mylose 351® glucose syrup with specific species identified therein. Originally in colour.

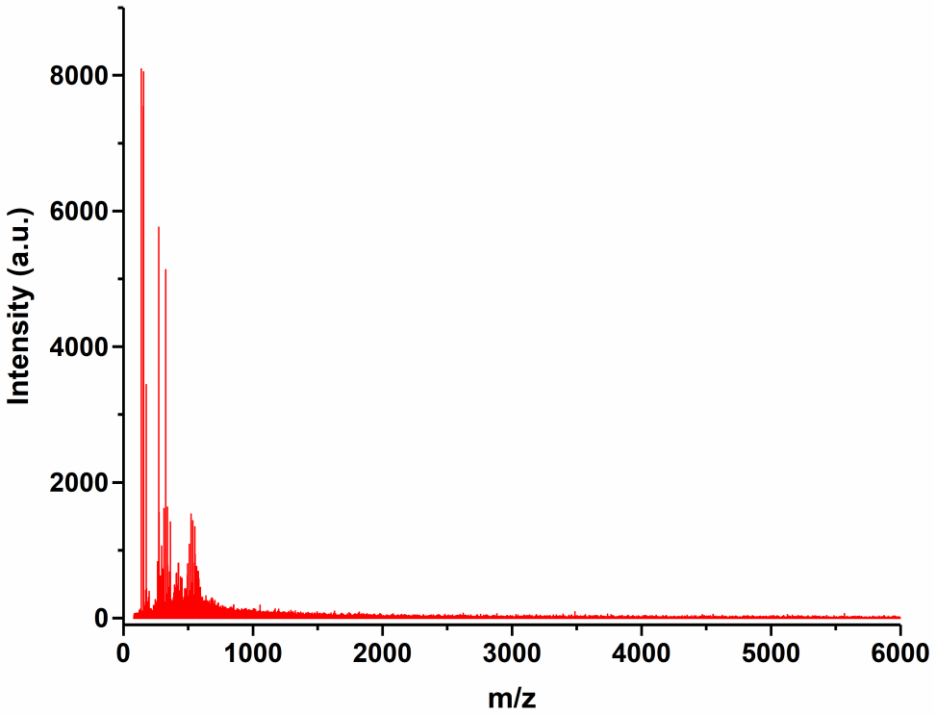

Appendix Figure E.2: MALDI-TOF-MS spectrum for 2,5-dihydoxybenzoic acid matrix used for the analysis of MYL. Originally in colour.

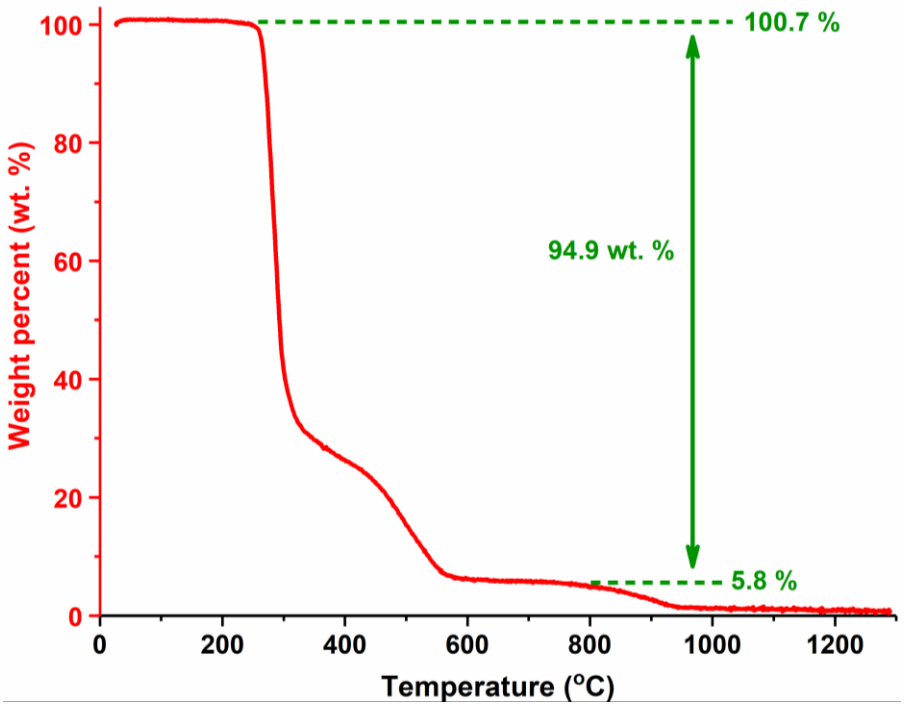

Appendix Figure E.3: TGA of collated floridoside extract (FLO) used in the preparation of model aqueous confections. Originally in colour.

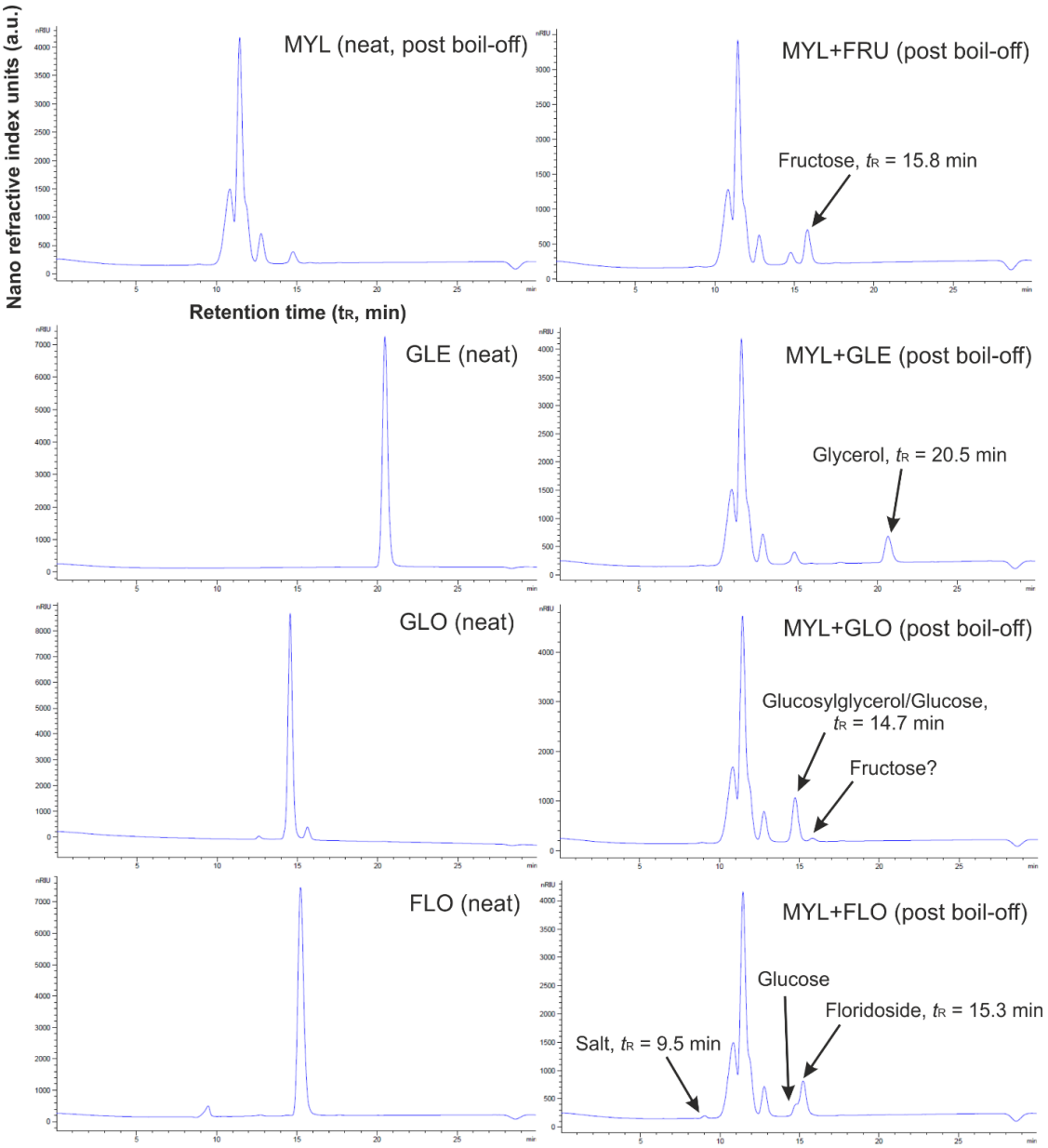

Appendix Figure E.4: HPLC chromatographs of neat model confection ingredients (left) and model confections following completion of boil-off experiments (right). Originally in colour.

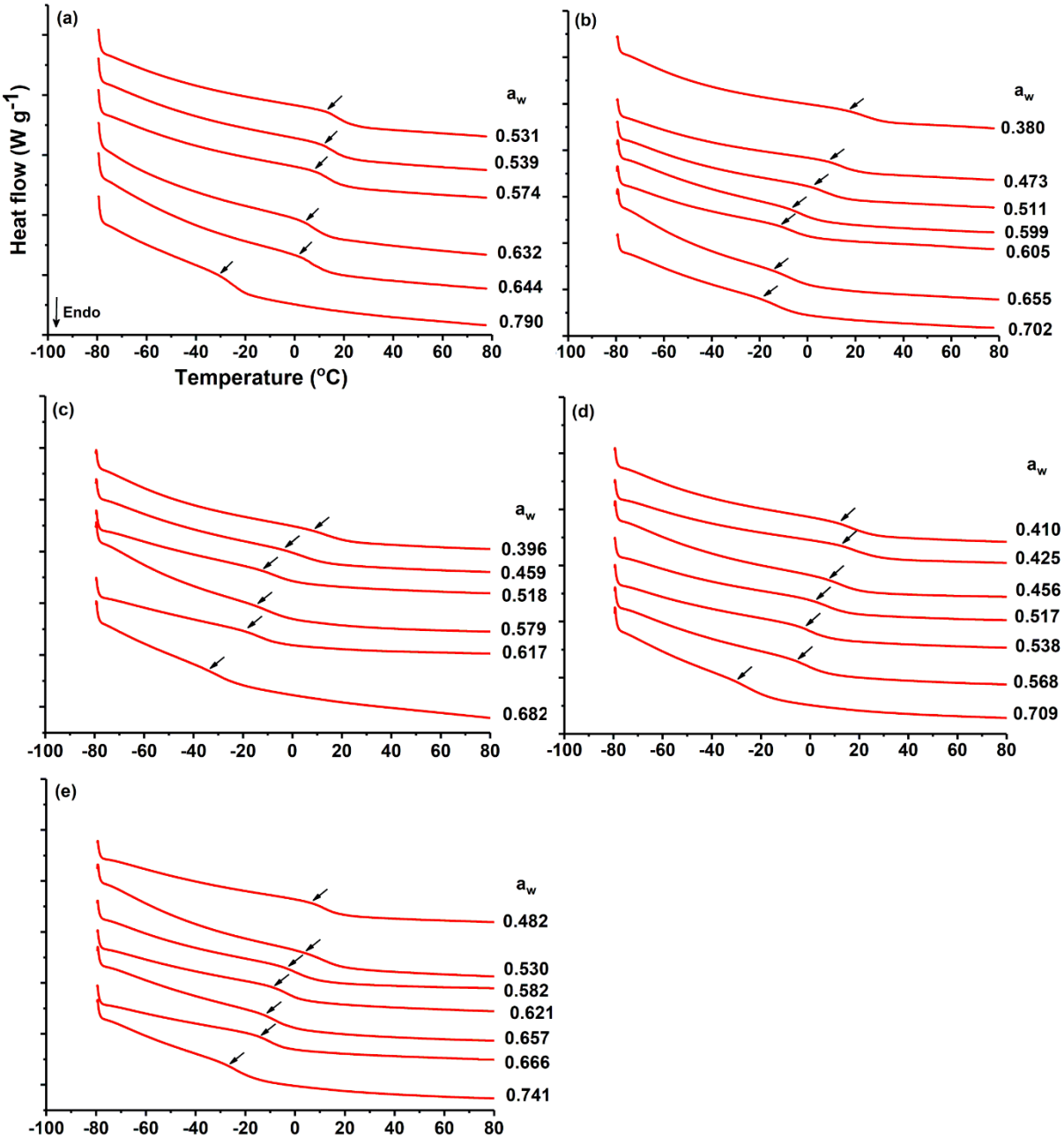

Appendix Figure E.5: Second heat cycles of model confections at varying a_w, large *y*-axes tick marks correspond to 0.2 W g^{-1}: (**a**) MYL, (**b**) MYL+FRU, (**c**) MYL+GLE, (**d**) MYL+DES, (**e**) MYL+GLO. Arrows indicate onset of T_g. Originally in colour.

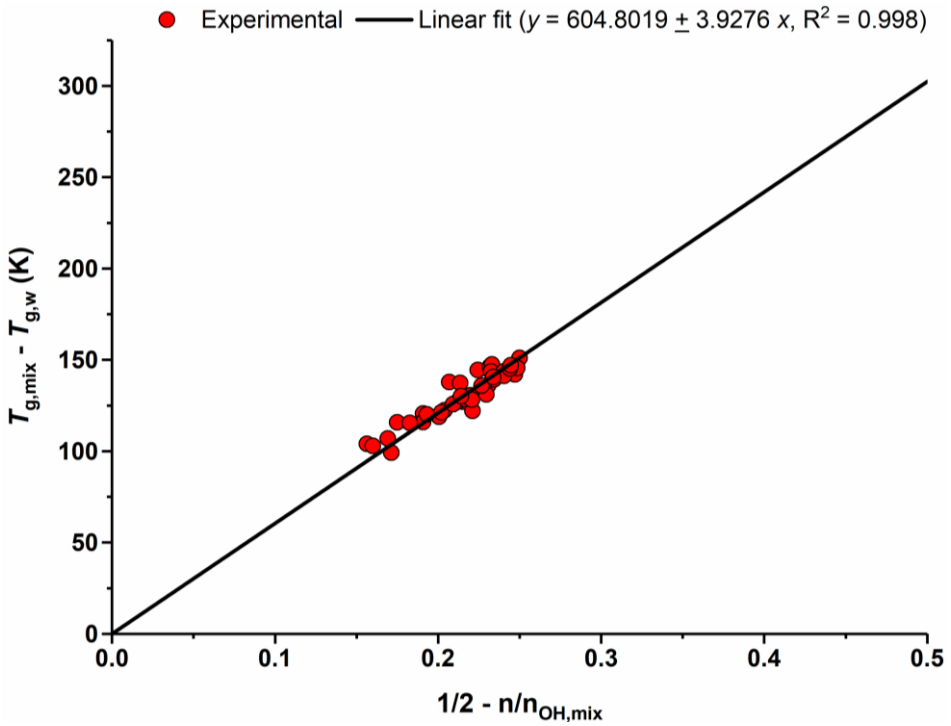

Appendix Figure E.6: Linear fit (and parameters thereof) of experimental T_g (onset) of model aqueous confections plotted against the inverse average number of OH groups per molecule within the mixture as calculated via **Equation 7.1**. Originally in colour.

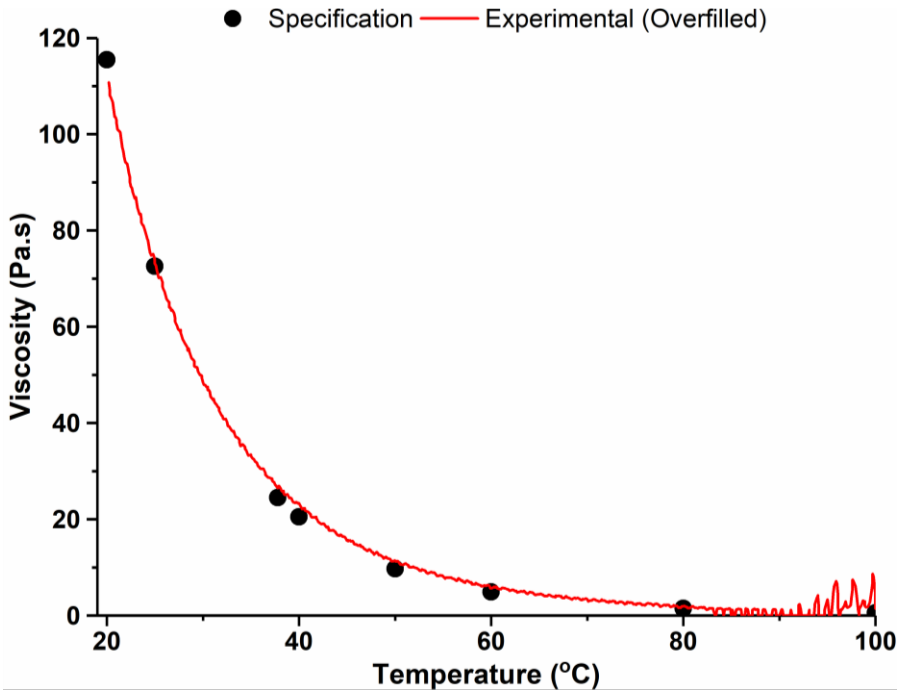

Appendix Figure E.7: Comparison of experimental viscosity recorded for a 115 Pa.s viscosity standard with the manufacturer's specifications (at 10 s^{-1}). Originally in colour.

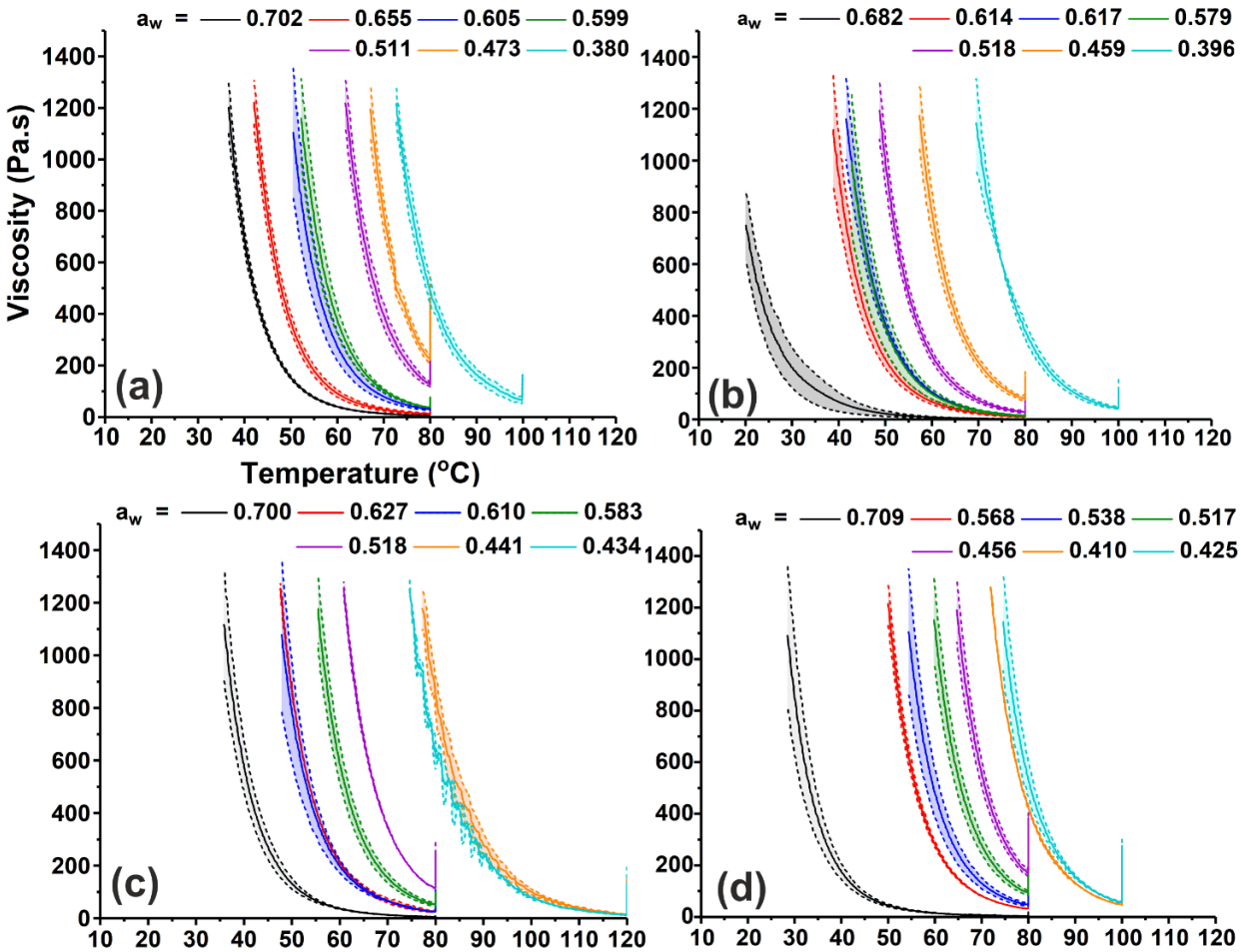

Appendix Figure E.8: Viscosity of model confectionery systems based on (**a**) MYL+FRU, (**b**) MYL+GLE, (**c**) MYL+FLO and (**d**) MYL+DES as a function of temperature at constant shear rate (10 s^{-1}). The shaded area and dashed lines of each curve represent $\pm$ 1 standard deviation and the limits thereof, respectively. Originally in colour.

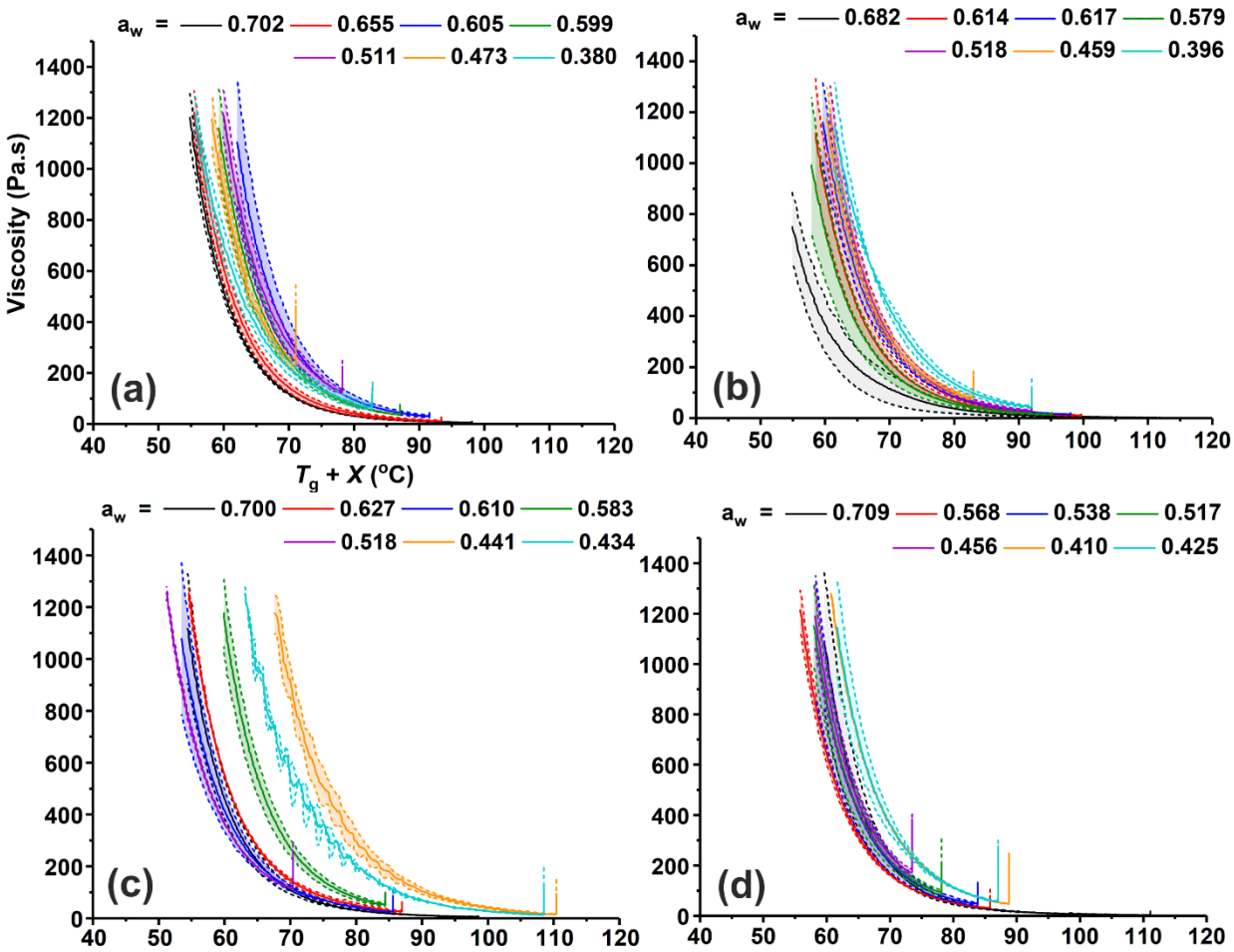

Appendix Figure E.9: Viscosity of model confectionery systems based on (**a**) MYL+FRU, (**b**) MYL+GLE, (**c**) MYL+FLO and (**d**) MYL+DES as a function $T_g + X$ °C at constant shear rate (10 s^{-1}). The shaded area and dashed lines of each curve represent $\pm$ 1 standard deviation and the limits thereof, respectively. Originally in colour

Appendix Table E.1: Tabulated composition of selected solutes present within Mylose 351® used during the present study as provided by the manufacturer (*DE* value determined as 33).

Solute	Concentration (wt. %)
Glucose	2.2
Maltose	6.8
Maltotriose	11.2
Maltotetraose	50.1
Total[a]	78.8

[a]Identity/quantity of other solutes not given.

Abbreviations and Symbols

AAD	Average Absolute Deviation
Asco	L-ascorbic acid
ATR-FTIR	Attenuated Total Reflectance - Fourier Transform Infrared
a_w	Water activity
a.u.	Arbitrary units
C_i	Constant *i* within the Williams-Landel-Ferry Model
CCDC	Cambridge Crystallographic Data Centre
ChCl	Choline chloride
CHN	Carbon, Hydrogen and Nitrogen microanalysis
cm	Centimetre
D-GLac	D-Gulono-1,4-lactone
DE	Dextrose Equivalent
DEPT-135	Distortionless Enhancement by Polarisation Transfer (using a 135 degree decoupler pulse) Nuclear Magnetic Resonance Spectroscopy
DES	Deep Eutectic Solvent
DES	Glucrono-6,3-lactone:ChCl, 1:1 Deep Eutectic Solvent
DMG	*N,N*-dimethylglycine
DMSO	Dimethyl sulfoxide
d.p.	Decimal places
DP	Degree of polymerisation
DRIFT-NIR	Diffuse Reflectance Fourier Transform - Near Infrared Spectroscopy
DSC	Differential Scanning Calorimetry
dTG	First derivative of Thermogravimetric Analysis curve
Ect	Ectoine
e^i	Exponential of *i*
E_a	Arrhenius activation energy
ECHA	European Chemicals Agency
EtOAc	Ethyl acetate
EtOH	Ethanol
ERH	Equilibrium Relative Humidity

F_I	Anhydrous floridoside crystal form I
F_{II}	Anhydrous floridoside crystal form I
FDA	Food and Drug Administration (USA)
F_h	Monohydrated floridoside crystal form
FLO	Floridoside-rich solid extracted from *Palmaria palmate*
FolAc	Folic Acid
FRU	Fructose
FTIR	Fourier-Transform Infrared Spectroscopy
g	Gramme
G_{ij}	Kirkwood Buff integral between components *i* and *j*
G_{ij}^{∞}	Kirkwood Buff integral between components *i* and *j* at infinite dilution of solute
GLE	Glycerol
GLO	Glycoin (*ca*. 90 wt. %)
GluLac	Glucurono-6,3-lactone
Glu-1,5-Lac	Glucono-1,5-lactone
Glycoin	bitop glycoin ® (2-α-*O*-D-glucopyranosyl glycerol)
Gly-T	Vacuum oven dried bitop glycoin ®
GRAS	Generally Recognised As Safe
h	Hour
HBD	Hydrogen Bond Donor
HIS	High intensity sweetener
HOD	Partially deuterated water
HPLC	High Performance Liquid Chromatography
HyEct	Hydroxyectoine
Hz	Hertz
ICP-OES	Inductively Coupled Plasma Optical Emission Spectroscopy
iPrOH	Isopropyl alcohol
J	Joule
K	Degree Kelvin
KBI	Kirkwood-Buff Integral

KF	Karl Fischer Titration
kg	Kilogramme
kJ	Kilojoule
k_{GT}	Gordon-Taylor constant
K_N	Norrish constant
kV	Kilovolt
L	Litre
LC-MS	Liquid Chromatography - Mass Spectrometry
L-GLac	L-Gulono-1,4-lactone
ln	Natural logarithm
$\log_{10}$	Log base 10
m/z	Mass-to-charge ratio
MALDI-TOF-MS	Matrix-assisted Laser Desorption Ionisation – Time of Flight Mass Spectrometry
mbar	Millibar
MCT	Mercury Cadmium Telluride
MeOH	Methanol
mg	Milligramme
MHz	Megahertz
min	Minutes
mix	Mixture
mL	Millilitre
mol	Mole
M_r	Molecular mass
mW	Milliwatt
MYL	Mylose 351® glucose syrup
N	Number
NADES	Natural Deep Eutectic Solvent
NCD	Non-Communicable Diseases
ND	Not detected or Not determined
NicAc	Nicotinic Acid

n_{OH}	Number of hydroxyl groups
n_{OH}^{eff}	Effective number of hydroxyl groups
nm	Nanometre
NMR	Nuclear Magnetic Resonance
$P2_12_12_1$	$P2_12_12_1$ orthorhombic crystal system
Pa	Pascal
PanAc	Pantothenic Acid
Pas	Pascal-second
PHE	Public Health England
ppm	Parts per million
pXRD	Powder X-Ray Diffraction
R	Universal gas constant
R^2	Coefficient of determination
RDF	Radial Distribution Function
RH	Relative Humidity
r.h.s.	Right hand side of equation
s	Second
S,Cl,Br,F	Sulfur, Chlorine, Bromine and Fluorine microanalysis
STA	Simultaneous Thermal Analysis
T	Absolute temperature in Kelvin (unless otherwise stated)
TBA	*tert*-butyl alcohol
T_{eu}	Eutectic or solidus temperature
T_g	Glass transition temperature
TGA	Thermogravimetric Analysis
TG-IR	Thermogravimetric Analysis – Infrared Spectroscopy
T_m	Fusion temperature
T_{max}	Maximum fusion temperature
t_R	Retention time
TW	This work
UCM	Untreated Crystalline Material (obtained from *Palmaria palmata* surface)

UCM-T	Untreated Crystalline Material (obtained from *Palmaria palmata* surface) dried *in vacuo*
UCM-90	Untreated Crystalline Material (obtained from *Palmaria palmata* surface) heated to 90 ^{o}C in sealed DSC pan
VTXRD	Variable Temperature Small Angle X-Ray Scattering
v/v	Liquid concentration in volume fraction
w_i	Weight fraction of component *i*
WLF	Williams-Landel-Ferry model
wt. %	Solute concentration in weight percent
x_s	Mole fraction of solute
x_w	Mole fraction of water
y_w	Water activity coefficient
α-GPC	L-α-glycerophosphorylcholine
Å	Angström
ΔH_i	Enthalpy of *i*
ΔT_{max}	Difference in maximum fusion temperature
κ_T^{∞}	Isothermal compressibility of pure liquid water at 298 K
^{o}	Degree
^{o}C	Degree Celsius
µA	Microampere
µm	Micrometre
μ_i	Chemical potential of *i*
^{1}H	Hydrogen-1 Nuclear Magnetic Resonance Spectroscopy
^{13}C	Carbon-13 Nuclear Magnetic Resonance Spectroscopy
$\tilde{\nu}$	Wavenumber
∂	Derivative
δ	Chemical shift in parts per million
η	Viscosity
η_0	Pre-exponential constant in Arrhenius equation
$\eta\ (T)$	Viscosity at temperature *T*
$\eta\ (T_g)$	Viscosity at temperature T_g
2Θ	Angle between incident and reflected X-rays

λ	Wavelength
ω	Torsion angle around O_6-C_6-C_5-O_5
Φ	Torsion angle around O_5-C_1-O_1-C_7
$\sum i$	Sum of i

References

1. L. V. Strashynska, *Business, Economics, Sustainability, Leadership and Innovation*, 2019, **2**, 61-69.
2. M. Ng *et al*., *Lancet*, 2014, **384**, 766-781.
3. M. Escobar, J. Veerman, S. Tollman, M. Bertram and K. Hofman, *BMC Public Health*, 2013, **13**, 1072.
4. A. Thow and C. Hawkes, *Public Health Nutrition*, 2014, **17**, 2151-2155.
5. D. Osborn, A. Cutter and F. Ullah, *Universal Sustainable Development Goals: Understanding the Transformational Challenge for Developed Countries, Report of a study by Stakeholder Forum*, Stakeholder Forum, 2015.
6. *Guideline: sugars intake for adults and children*, World Health Organization, 2015.
7. A. D. McNaught, *Pure and Applied Chemistry*, 1996, **68**, 1919-2008.
8. Scientific Advisory Committee on Nutrition, *Carbohydrates and Health*, The Stationery Office,2015.
9. Public Health England, *Sugar Reduction: Achieving the 20%, A technical report outlining progress to date, guidelines for industry, 2015 baseline levels in key foods and next steps*, Gov.uk, 2017.
10. UK pushes ahead with sugar tax, http://www.bbc.co.uk/news/health-38212608, (accessed 21st June, 2017).
11. Public Health England, *Fermented (yoghurt) drinks: A supplementary report to the sugar reduction guidelines, outlining the drinks included and separate guidelines set*, Gov.uk, 2019.
12. Public Health England, *Sugar reduction: progress between 2015 and 2018*, Gov.uk, 2019.
13. Sustainable Development Goals (SDGs) and Disability, https://www.un.org/development/desa/disabilities/about-us/sustainable-development-goals-sdgs-and-disability.html, (accessed 16th July, 2020).
14. *Nestlé in society, Creating Shared Value and meeting our commitments 2016*, Nestlé, 2016.
15. Y. Goryakin, A. Aldea, Y. Guillemette, A. Lerouge, A. Feigl, M. Devaux and M. Cecchini, in The Heavy Burden of Obesity: The Economics of Prevention, OECD Publishing, Paris, 2019, ch. 6.
16. Nestle axes low sugar chocolate due to weak sales, https://www.bbc.co.uk/news/business-51439407 (accessed 19th March, 2020).
17. Coca-Cola Life axed in the UK, https://www.beveragedaily.com/Article/2017/04/07/Coca-Cola-Life-axed-in-the-UK (accessed 14th April, 2017).
18. A. D. E. Van Laar, C. Grootaert and J. Van Camp, *Critical Reviews in Food Science and Nutrition*, 2020, DOI: 10.1080/10408398.2020.1743966.
19. R. W. Hartel, J. H. von Elbe and R. Hofberger, in *Confectionery Science and Technology*, Springer International Publishing, Cham, 2018, ch. 2, pp. 39-67.
20. R. C. L. Bosworth, *Nature*, 1946, **157**, 447.
21. P. S. Taoukis and M. Richardson, in *Water Activity in Foods: Fundamentals and Applications*, ed. G. V. Barbosa-Cánovas, A. J. Fontana Jr., S. J. Schmidt, T. P. Labuza, Blackwell Publishing Ltd, 2nd edn., 2020, ch. 16, pp. 385-424.
22. R. Touger-Decker and C. van Loveren, *The American Journal of Clinical Nutrition*, 2003, **78**, 881S-892S.
23. Sugars and dental caries, https://www.who.int/news-room/fact-sheets/detail/sugars-and-dental-caries (accessed 12th June, 2020).

24. R. Clemens, J. Jones, M. Kern, S. Lee, E. Mayhew, J. Slavin and S. Zivanovic, *Comprehensive Reviews in Food Science and Food Safety*, 2016, **15**, 433-470.
25. P. Prinz, *European Journal of Clinical Nutrition*, 2019, **73**, 1216-1223.
26. A. Lenhart and W. D. Chey, *Advances in Nutrition*, 2017, **8**, 587-596.
27. S. Struck, D. Jaros, C. S. Brennan and H. Rohm, *International Journal of Food Science and Technology*, 2014, **49**, 1963-1976.
28. G. Livesey, *Nutrition Research Reviews*, 2003, **16**, 163-191.
29. K. K. Mäkinen, Journal of Food: Microbiology, Safety & Hygiene, 2017, **2**, DOI: 10.4172/2476-2059.1000115.
30. R. G. M. van der Sman, *Journal of Physical Chemistry B*, 2013, **117**, 16303-16313.
31. R. G. M. van der Sman, *Food Hydrocolloids*, 2016, **56**, 144-149.
32. T. Chades, S. M. Scully, E. M. Ingvadottir and J. Orlygsson, *Frontiers in Microbiology*, 2018, **9**, DOI: 10.3389/fmicb.2018.01931.
33. S. Chattopadhyay, U. Raychaudhuri and R. Chakraborty, *Journal of Food Science and Technology-Mysore*, 2014, **51**, 611-621.
34. P. Putnik, I. Bezuk, F. J. Barba, J. M. Lorenzo, I. Polunić and D. Kovačević Bursać, in *Agri-Food Industry Strategies for Healthy Diets and Sustainability*, eds. F. J. Barba, P. Putnik and D. B. Kovačević, Academic Press, 2020, ch. 5, pp. 123-152.
35. N. d. S. Santana, M. G. Mothe and C. G. Mothe, *Journal of Thermal Analysis and Calorimetry*, 2019, **138**, 3577-3586.
36. G. Servant, C. Tachdjian, X.-Q. Tang, S. Werner, F. Zhang, X. Li, P. Kamdar, G. Petrovic, T. Ditschun, A. Java, P. Brust, N. Brune, G. E. DuBois, M. Zoller and D. S. Karanewsky, *Proceedings of the National Academy of Sciences of the United States of America*, 2010, **107**, 4746-4751.
37. K. Xu, H. Lu, B. Qu, H. Shan and J. Song, *Separation and Purification Technology*, 2010, **72**, 406-409.
38. F. A. Tomás-Barberán and M. N. Clifford, *Journal of the Science of Food and Agriculture*, 2000, **80**, 1073-1080.
39. T. Jalili, E. Mah, D. M. Medeiros and R. E. C. Wildman, in *Handbook of Nutraceuticals and Functional Foods*, eds. R. E. C. Wildman and R. S. Bruno, 2019, ch. 10. DOI: 10.1201/9780429195594-10.
40. R. W. Hartel, J. H. von Elbe and R. Hofberger, in *Confectionery Science and Technology*, Springer International Publishing, Cham, 2018, ch. 1, pp. 3-37.
41. J. E. Zimeri and J. L. Kokini, *Carbohydrate Polymers*, 2002, **48**, 299-304.
42. H. Treichel, S. M. Golunski, A. F. Camargo, T. Scapini, T. A. Modkovski, B. Venturin, E. R. Bordin, V. Rossetto and A. J. Mossi, in *Bioprocessing for Biomolecules Production*, eds. G. Molina, V. K. Gupta, B. N. Singh, N. Gathergood, John Wiley & Sons, Ltd, 3rd edn., 2019, ch. 11, pp. 239-254.
43. S. P. Singh, J. S. Jadaun, L. K. Narnoliya and A. Pandey, *Applied Biochemistry and Biotechnology*, 2017, **183**, 613-635.
44. D. L. Hofman, V. J. Van Buul and F. J. P. H. Brouns, *Critical Reviews in Food Science and Nutrition*, 2016, **56**, 2091-2100.
45. S. Miyazato, C. Nakagawa, Y. Kishimoto, H. Tagami and H. Hara, *European Journal of Nutrition*, 2010, **49**, 165-171.
46. J. Raudonus, J. Bernard, H. Janßen, J. Kowalczyk and R. Carle, *Food Research International*, 2000, **33**, 41-51.

47. Á.-M. González-Montemayor, A. C. Flores-Gallegos, L. E. Serrato-Villegas, M. G. López-Pérez, J. C. Montañez-Sáenz and R. Rodríguez-Herrera, in *Natural Beverages*, eds. A. M. Grumezescu and A. M. Holban, Academic Press, 2019, ch. 6, pp. 143-177.
48. D. W. Ball, *Journal of Chemical Education*, 2007, **84**, 1643-1646.
49. J. Mingaila, D. Ciuldiene, P. Viskelis, E. Bartkevicius, V. Vilimas and K. Armolaitis, *Forests*, 2020, **11**, DOI: 10.3390/f11040365.
50. S. B. Sulaiman, MSc. thesis, Universiti Sains Malaysia, 2016.
51. C. V. Ratnavathi and U. D. Chavan, in *Sorghum Biochemistry*, eds. C. V. Ratnavathi, J. V. Patil and U. D. Chavan, Academic Press, San Diego, 2016, ch. 5, pp. 253-310.
52. J. L. Willems and N. H. Low, *Journal of Agricultural and Food Chemistry*, 2012, **60**, 8745-8754.
53. I. Manrique, A. Parraga and M. Hermann, in *Yacon syrup: Principles and processing*, Swiss agency for development and cooperation, Lima, Peru, 2005, ch. 5, pp. 19-22.
54. R. C. Wang and R. W. Hartel, *Journal of Food Engineering*, 2020, **284**, DOI: 10.1016/j.jfoodeng.2020.110067.
55. T. Matsuo, R. Ishii, T. Iida, T. Yamada, S. Takamine and Y. Shirai, *Current Topics in Toxicology*, 2011, 41-49.
56. N. Hayashi, T. Yamada, S. Takamine, T. Iida, K. Okuma and M. Tokuda, *Journal of Functional Foods*, 2014, **11**, 152-159.
57. War on diabetes: New Nutrition Innovation technology slashes sugar while boosting protein and fibre, https://www.foodnavigator-asia.com/Article/2019/05/21/War-on-diabetes-New-Nutrition-Innovation-technology-slashes-sugar-while-boosting-protein-and-fibre (accessed 2nd July, 2019).
58. US pat., US8911806B2, 2014.
59. WO pat., WO2017093309A1, 2017.
60. H. Nakagawa and T. Oyama, *Frontiers in Chemistry*, 2019, **7**, DOI: 10.3389/fchem.2019.00731.
61. S. Ur-Rehman, Z. Mushtaq, T. Zahoor, A. Jamil and M. A. Murtaza, *Critical Reviews in Food Science and Nutrition*, 2015, **55**, 1514-1528.
62. Y. Roos and M. Karel, *Biotechnology Progress*, 1991, **7**, 49-53.
63. M. A. Mensink, H. W. Frijlink, K. van der Voort Maarschal and W. L. J. Hinrichs, *Carbohydrate Polymers*, 2015, **130**, 405-419.
64. C. Ribeiro, J. E. Zimeri, E. Yildiz and J. L. Kokini, *Carbohydrate Polymers*, 2003, **51**, 273-280.
65. A. Lazaridou, C. G. Biliaderis, N. Bacandritsos and A. G. Sabatini, *Journal of Food Engineering*, 2004, **64**, 9-21.
66. S. Bhatta, T. Stevanovic and C. Ratti, *Drying Technology*, 2020, **38**, 1138-1150.
67. W. Mu, W. Zhang, Y. Feng, B. Jiang and L. Zhou, *Applied Microbiology and Biotechnology*, 2012, **94**, 1461-1467.
68. S. Roy, J. Chikkerur, S. C. Roy, A. Dhali, A. P. Kolte, M. Sridhar and A. K. Samanta, *Journal of Food Science*, 2018, **83**, 2699-2709.
69. K. D. Roe and T. P. Labuza, *International Journal of Food Properties*, 2005, **8**, 559-574.
70. G. N. Lewis, *Proceedings of the American Academy of Arts and Sciences*, 1907, **43**, 259-293.
71. G. N. Lewis and M. Randall, *Thermodynamics and the free energy of chemical substances*, McGraw-Hill, 1923.
72. A. J. Fontana Jr. and B. P. Carter, in *Water Activity in Foods: Fundamentals and Applications*, ed. G. V. Barbosa-Cánovas, A. J. Fontana Jr., S. J. Schmidt, T. P. Labuza, Blackwell Publishing Ltd, 2nd edn., 2020, ch. 8, pp. 207-226.
73. F.-M. Raoult, *C.R. Acad. Sci. Paris*, 1887, **104**, 1430-1433.

74. E. W. Meijer, *Angewandte Chemie International Edition*, 2001, **40**, 3783-3789.
75. W. J. Scott, *Australian Journal of Biological Sciences*, 1953, **6**, 549-564.
76. D. A. A. Mossel and J. Westerdijk, *Antonie van Leeuwenhoek*, 1949, **15**, 190-202.
77. Y. H. Roos, in *Water Activity in Foods: Fundamentals and Applications*, ed. G. V. Barbosa-Cánovas, A. J. Fontana Jr., S. J. Schmidt, T. P. Labuza, Blackwell Publishing Ltd, 2nd edn., 2020, ch. 3, pp. 27-44.
78. R. Ergun, R. Lietha and R. Hartel, *Critical Reviews in Food Science and Nutrition*, 2010, **50**, 162-192.
79. T. P. Labuza and C. R. Hyman, *Trends in Food Science & Technology*, 1998, **9**, 47-55.
80. T. P. Labuza and B. Altunakar, in *Water Activity in Foods: Fundamentals and Applications*, ed. G. V. Barbosa-Cánovas, A. J. Fontana Jr., S. J. Schmidt, T. P. Labuza, Blackwell Publishing Ltd, 2nd edn., 2020, ch. 7, pp. 161-206.
81. P. Piccone, S. L. Rastelli and P. Pittia, *11th International Congress on Engineering and Food*, 2011, **1**, 1509-1515.
82. D. Grover, *Journal of the Society of Chemical Industry-London*, 1947, **66**, 201-205.
83. R. Money and R. Born, *Journal of the Science of Food and Agriculture*, 1951, **2**, 180-185.
84. M. Le Maguer, in *Physical Chemistry in Foods*, eds. H. G. Schwartzberg and R. W. Hartel, Marcel Dekker, New York, 1992, ch. 1, pp. 1-45.
85. P. P. Lewicki, in *Food Properties Handbook,* ed. M. S. Rahman, CRC Press, 2nd edn., 2009, ch. 3, pp. 33-66.
86. A. M. Sereno, M. D. Hubinger, J. F. Comesana and A. Correa, *Journal of Food Engineering*, 2001, **49**, 103-114.
87. R. S. Norrish, *International Journal of Food Science & Technology*, 1966, **1**, 25-39.
88. J. Chirife, G. Favetto and C. Fontan, *Journal of Applied Bacteriology*, 1984, **56**, 259-268.
89. R. Baeza, A. Pérez, V. Sánchez, M. C. Zamora and J. Chirife, *Food and Bioprocess Technology*, 2010, **3**, 87-92.
90. O. Fysun, M. Stoeckel, K. Thienel, F. Waschle, S. Palzer and J. Hinrichs, *Chemie Ingenieur Technik*, 2015, **87**, 1327-1333.
91. K. Ross, *Food Technology*, 1975, **29**, 26-&.
92. A. K. Salameh, L. J. Mauer and L. S. Taylor, *Journal of Food Science*, 2006, **71**, E10-E16.
93. M. Burg and J. Ferraris, *Journal of Biological Chemistry*, 2008, **283**, 7309-7313.
94. C. Argyropoulos, H. Rondon-Berrios, D. S. Raj, D. Malhotra, E. I. Agaba, M. Rohrscheib, Z. Khitan, G. H. Murata, J. I. Shapiro and A. H. Tzamaloukas, *Cureus*, 2016, **8**, DOI: 10.7759/cureus.596.
95. D. Martin, R. Ciulla and M. Roberts, *Applied and Environmental Microbiology*, 1999, **65**, 1815-1825.
96. S. Bougouffa, A. Radovanovic, M. Essack and V. Bajic, *Database-the Journal of Biological Databases and Curation*, 2014, DOI: 10.1093/database/bau100
97. P. Yancey, *Journal of Experimental Biology*, 2005, **208**, 2819-2830.
98. P. H. Yancey, *Science progress*, 2004, **87**, 1-24.
99. J. Chirife, C. Fontan and O. Scorza, *Journal of Food Technology*, 1980, **15**, 383-387.
100. L. Slade and H. Levine, *Critical Reviews in Food Science and Nutrition*, 1991, **30**, 115-360.
101. J. M. Aguilera and M. Karel, *Critical Reviews in Food Science and Nutrition*, 1997, **37**, 287-309.
102. K. Ivanov, A. Stoimenova, D. Obreshkova and L. Saso, *Biotechnology & Biotechnological Equipment*, 2013, **27**, 3620-3626.
103. C. Held and G. Sadowski, *Fluid Phase Equilibria*, 2016, **407**, 224-235.

104. R. Lang, T. Lang, M. Bader, A. Beusch, V. Schlagbauer and T. Hofmann, *Journal of Agricultural and Food Chemistry*, 2017, **65**, 1613-1619.
105. EFSA Panel on Dietetic Products, Nutrition and Allergies, *EFSA Journal*, 2011, **9**, 2071.
106. W. Lau and N. Vaziri, *Clinical Science*, 2017, **131**, 3-12.
107. M. Velasquez, A. Ramezani, A. Manal and D. Raj, *Toxins*, 2016, **8**, DOI: 10.3390/toxins8110326.
108. C. Kanitsoraphan, P. Rattanawong, S. Charoensri and V. Senthong, *Current nutrition reports*, 2018, **7**, 207-213.
109. L. Czech, L. Hermann, N. Stoeveken, A. A. Richter, A. Hoeppner, S. H. J. Smits, J. Heider and E. Bremer, *Genes*, 2018, **9**, DOI: 10.3390/genes9040177.
110. D. Mueller, T. Lindemann, K. Shah-Hosseini, O. Scherner, M. Knop, A. Bilstein and R. Moesges, *European Archives of Oto-Rhino-Laryngology*, 2016, **273**, 2591-2597.
111. J. Klein, T. Schwarz and G. Lentzen, *Journal of Dairy Research*, 2007, **74**, 446-451.
112. A. M. A. Omara, A. E.-M. M. Sharaf, A. A. El-Hela, A. A. M. Shahin, H. A. A. El-Bialy and M. Z. El-Fouly, *Biotechnology Letters*, 2020, **42**, 1003-1017.
113. C. Held, T. Neuhaus and G. Sadowski, *Biophysical Chemistry*, 2010, **152**, 28-39.
114. US Pat., US20040006222A1, 2004.
115. WO Pat., WO2008071797A1, 2008.
116. WO Pat., WO2003003856A1, 2003.
117. E. Tuboly, R. Gáspár, M. O. Ibor, K. Gömöri, B. Kiss, G. Strifler, P. Hartmann, P. Ferdinandy, M. Bartekova, M. Boros and A. Görbe, *Molecular and Cellular Biochemistry*, 2019, **460**, 195-203.
118. A. M. Brownawell, E. L. Carmines and F. Montesano, *Food and Chemical Toxicology*, 2011, **49**, 1303-1315.
119. J. Kim, Y. Song, S. J. Lee, J. E. Lee, M.-Y. Chung, I.-H. Kim and B. H. Kim, *Biotechnology Progress*, 2020, **36**, e2910.
120. A. Oyeneye, J. Shen, Y. Y. Shim, T. J. Tse and M. J. T. Reaney, *ACS omega*, 2020, **5**, 12486-12494.
121. A. Zumbe, A. Lee and D. Storey, *British Journal of Nutrition*, 2001, **85**, S31-S45.
122. S. Kadoya, K. Fujii, K. Izutsu, E. Yonemochi, K. Terada, C. Yomota and T. Kawanishi, *International Journal of Pharmaceutics*, 2010, **389**, 107-113.
123. R. W. Hartel, R. Ergun and S. Vogel, *Comprehensive Reviews in Food Science and Food Safety*, 2011, **10**, 17-32.
124. M. Hagemann, *Fems Microbiology Reviews*, 2011, **35**, 87-123.
125. U. Karsten, S. Gors, A. Eggert and J. West, *Phycologia*, 2007, **46**, 143-150.
126. JP Pat., JP2014062121A, 2014.
127. JP Pat., JPH10245333A, 1998.
128. J. Becker and C. Wittmann, *Current opinion in biotechnology*, 2020, **65**, 118-128.
129. H. S. Yoon, W. Nelson, S. C. Lindstrom, S. M. Boo, C. Pueschel, H. Qiu and D. Bhattacharya, in *Handbook of the Protists*, eds. J. M. Archibald, A. G. B. Simpson and C. H. Slamovits, Springer International Publishing, Cham, 2017.
130. K. Morgan, J. Wright and F. Simpson, *Economic Botany*, 1980, **34**, 27-50.
131. L. Kollau, M. Vis, A. van den Bruinhorst, A. C. C. Esteves and R. Tuinier, *Chemical Communications*, 2018, **54**, 13351-13354.
132. A. P. Abbott, G. Capper, D. L. Davies, R. K. Rasheed and V. Tambyrajah, *Chemical Communications*, 2003, 70-71.
133. A. P. Abbott, D. Boothby, G. Capper, D. L. Davies and R. K. Rasheed, *Journal of the American Chemical Society*, 2004, **126**, 9142-9147.

134. C. Clarke, W. Tu, O. Levers, A. Brohl and J. Hallett, *Chemical Reviews*, 2018, **118**, 747-800.
135. M. Faggian, S. Sut, B. Perissutti, V. Baldan, I. Grabnar and S. Dall'Acqua, *Molecules*, 2016, **21**, 10.3390/molecules21111531.
136. Y. Marcus, in *Deep Eutectic Solvents*, 2019, ch. 2, pp. 13-44.
137. Q. H. Zhang, K. D. Vigier, S. Royer and F. Jerome, *Chemical Society Reviews*, 2012, **41**, 7108-7146.
138. E. L. Smith, A. P. Abbott and K. S. Ryder, *Chemical Reviews*, 2014, **114**, 11060-11082.
139. S. Khandelwal, Y. Tailor and M. Kumar, *Journal of Molecular Liquids*, 2016, **215**, 345-386.
140. Y. Chen and T. Mu, *Green Energy & Environment*, 2019, **4**, 95-115.
141. A. Krishnan, K. P. Gopinath, D.-V. N. Vo, R. Malolan, V. M. Nagarajan and J. Arun, *Environmental Chemistry Letters*, 2020, DOI: 10.1007/s10311-020-01057-y.
142. P. Xu, G.-W. Zheng, M.-H. Zong, N. Li and W.-Y. Lou, *Bioresources and Bioprocessing*, 2017, **4**, 34.
143. D. O. Abranches, M. A. R. Martins, L. P. Silva, N. Schaeffer, S. P. Pinho and J. A. P. Coutinho, *Chemical Communications*, 2019, **55**, 10253-10256.
144. M. A. R. Martins, S. P. Pinho and J. A. P. Coutinho, *Journal of Solution Chemistry*, 2019, **48**, 962-982.
145. E. Durand, J. Lecomte and P. Villeneuve, *Biochimie*, 2016, **120**, 119-123.
146. Y. H. Choi, J. van Spronsen, Y. T. Dai, M. Verberne, F. Hollmann, I. Arends, G. J. Witkamp and R. Verpoorte, *Plant Physiology*, 2011, **156**, 1701-1705.
147. A. Gertrudes, R. Craveiro, Z. Eltayari, R. L. Reis, A. Paiva and A. R. C. Duarte, *ACS Sustainable Chemistry & Engineering*, 2017, **5**, 9542-9553.
148. WO Pat., WO2011155829A1, 2011.
149. S. Bajkacz and J. Adamek, *Food Analytical Methods*, 2017, **11**, 1330-1344.
150. B. Tang, W. Bi, H. Zhang and K. H. Row, *Chromatographia*, 2014, **77**, 373-377.
151. M. Ruesgas-Ramon, M. C. Figueroa-Espinoza and E. Durand, *Journal of Agricultural and Food Chemistry*, 2017, **65**, 3591-3601.
152. Y. T. Dai, J. van Spronsen, G. J. Witkamp, R. Verpoorte and Y. H. Choi, *Analytica Chimica Acta*, 2013, **766**, 61-68.
153. R. Ahmadi, B. Hemmateenejad, A. Safavi, Z. Shojaeifard, A. Shahsavar, A. Mohajeri, M. Heydari Dokoohaki and A. R. Zolghadr, *Physical Chemistry Chemical Physics*, 2018, **20**, 18463-18473.
154. P. Kumari, Shobhna, S. Kaur and H. K. Kashyap, *ACS Omega*, 2018, **3**, 15246-15255.
155. O. S. Hammond, D. T. Bowron and K. J. Edler, *Angewandte Chemie International Edition*, 2017, **56**, 9782-9785.
156. M. Zdanowicz and T. Spychaj, *Polimery*, 2011, **56**, 861-864.
157. A. P. Abbott, A. D. Ballantyne, J. P. Conde, K. S. Ryder and W. R. Wise, *Green Chemistry*, 2012, **14**, 1302-1307.
158. A. C. Galvis-Sanchez, A. M. M. Sousa, L. Hilliou, M. P. Goncalves and H. K. S. Souza, *Green Chemistry*, 2016, **18**, 1571-1580.
159. S. Ramesh, R. Shanti and E. Morris, *Carbohydrate Polymers*, 2013, **91**, 14-21.
160. A. A. Shamsuri and R. Daik, *Bioresources*, 2012, **7**, 4760-4775.
161. WO. Pat., WO2015165738A1, 2015.
162. WO. Pat., WO2015044139A1, 2015.
163. T. Jeliński, M. Przybyłek and P. Cysewski, *Pharmaceutical Research*, 2019, **36**, DOI: 10.1007/s11095-019-2643-2.

164. C. Georgantzi, A. E. Lioliou, N. Paterakis and D. P. Makris, *Agronomy*, 2017, **7**, DOI: 10.3390/agronomy7030054.
165. E. Yilmaz and M. Soylak, *Talanta*, 2015, **136**, 170-173.
166. C. G. González, N. R. Mustafa, E. G. Wilson, R. Verpoorte and Y. H. Choi, *Flavour and Fragrance Journal*, 2018, **33**, 91-96.
167. R. G. M. van der Sman, I. A. F. van den Hoek and S. Renzetti, *Food Hydrocolloids*, 2020, **109**.
168. Y. H. Roos, in *Handbook of Food Engineering*, ed. D. R. Heldman, D. B. Lund and C. Sabliov, CRC Press, 3rd edn., 2006, ch. 3, pp. 287-352.
169. Y. H. Roos, *Annual Review of Food Science and Technology*, 2010, **1**, 469-496.
170. M. G. Abiad, M. T. Carvajal and O. H. Campanella, *Food Engineering Reviews*, 2009, **1**, 105-132.
171. M. L. Williams, R. F. Landel and J. D. Ferry, *Journal of the American Chemical Society*, 1955, **77**, 3701-3707.
172. M. Quintas, T. R. S. Brandão, C. L. M. Silva and R. L. Cunha, *Journal of Food Engineering*, 2006, **77**, 844-852.
173. M. E. Yildiz and J. L. Kokini, *Journal of Rheology*, 2001, **45**, 903-912.
174. M. Bocqué, C. Voirin, V. Lapinte, S. Caillol and J.-J. Robin, *Journal of Polymer Science Part A: Polymer Chemistry*, 2016, **54**, 11-33.
175. T. Mekonnen, P. Mussone, H. Khalil and D. Bressler, *Journal of Materials Chemistry A*, 2013, **1**, 13379-13398.
176. B. Saberi, S. Chockchaisawasdee, J. B. Golding, C. J. Scarlett and C. E. Stathopoulos, *International Journal of Biological Macromolecules*, 2017, **104**, 345-359.
177. J. Ubbink, *Current Opinion in Food Science*, 2018, **21**, 72-78.
178. L. Greenspan, *Journal of Research of the National Bureau of Standards Section a-Physics and Chemistry*, 1977, **81**, 89-96.
179. C. Macrae, L. Sovago, S. Cottrell, P. Galek, P. McCabe, E. Pidcock, M. Platings, G. Shields, J. Stevens, M. Towler and P. Wood, *Journal of Applied Crystallography*, 2020, **53**, 226-235.
180. H. Günzler and H.-U. Gremlich, in *IR Spectroscopy: An Introduction*, Weinheim: Wiley-VCH, 2002, ch.2, pp. 9-36.
181. G.M. Barrow, in *The Structure Of Molecules*, ed. R. Johnsen, W. A. Benjamin, Inc., 1963, ch. 3, pp. 59-88.
182. B. C. Smith, in *Fundamentals of Fourier Transform Infrared Spectroscopy*, ed. B. C. Smith, CRC Press, 2nd edn., 2011, ch. 2, pp. 19-53.
183. B. C. Smith, in *Fundamentals of Fourier Transform Infrared Spectroscopy*, ed. B. C. Smith, CRC Press, 2nd edn., 2011, ch. 4, pp. 87-146.
184. Ametek Brookfield Inc., *More Solutions to Sticky Problems*, Brookfield Engineering Laboratories, 2017.
185. G. Burrell, N. Dunlop and F. Separovic, *Soft Matter*, 2010, **6**, 2080-2086.
186. P. Gabbott, in *Principles and Applications of Thermal Analysis*, ed. P. Gabbott, Blackwell Publishing Ltd., 2008, ch. 1, pp. 1-50.
187. R. Bottom, in *Principles and Applications of Thermal Analysis*, ed. P. Gabbott, Blackwell Publishing Ltd., 2008, ch. 3, pp. 87-118.
188. N. Saadatkhah, A. C. Garcia, S. Ackermann, P. Leclerc, M. Latifi, S. Samih, G. S. Patience and J. Chaouki, *Canadian Journal of Chemical Engineering*, 2020, **98**, 34-43.
189. J. Van Humbeeck, in Handbook of Thermal Analysis and Calorimetry *Volume 1 Principles and Practices*, ed. M. E. Brown, Elsevier Science B.V., 1998, ch. 11, pp. 497-508.

190. J. Mullens, in Handbook of Thermal Analysis and Calorimetry *Volume 1 Principles and Practices*, ed. M. E. Brown, Elsevier Science B.V., 1998, ch. 12, pp. 509-546.
191. L. J. Mauer and R. L. Bradley Jr, in *Food Analysis*, ed. S. Nielsen, Springer Cham., 2017, ch. 15, pp. 257-286.
192. V. K. Pecharsky and P. Y. Zavalij, In *Fundamentals of Powder Diffraction and Structural Characterization of Materials*, ed. V. K. Pecharsky and P. Y. Zavalij, Springer US, 2nd edn., 2009, ch. 7, pp. 133-149.
193. CrysAlisPro, Version 1.171.34.41., Oxford Diffraction Ltd.
194. Empirical absorption correction using spherical harmonics, implemented in SCALE3 ABSPACK scaling algorithm within CrysAlisPro software, Version 1.171.34.40, Oxford Diffraction Ltd.
195. O. Dolomanov, L. Bourhis, R. Gildea, J. Howard and H. Puschmann, *Journal of Applied Crystallography*, 2009, **42**, 339-341.
196. G. Sheldrick, *Acta Crystallographica a-Foundation and Advances*, 2015, **71**, 3-8.
197. G. M. Sheldrick, SHELXL-97 program for crystal structure refinement, 1997.
198. J. Nielsen, M. B. Andreasen, M. Pedersen and M. K. Rasmussen, *International Journal of Thermophysics*, 2015, **36**, 577-588.
199. N. D. D. Carareto, E. S. Monteiro Filho, P. A. Pessôa Filho and A. J. A. Meirelles, *Brazilian Journal of Chemical Engineering*, 2010, **27**, 173-181.
200. R. Guine, C. Almeida, P. Correia and M. Mendes, *Food and Bioprocess Technology*, 2015, **8**, 1113-1125.
201. M. Frosch, M. Bilde and O. F. Nielsen, *Journal of Physical Chemistry A*, 2010, **114**, 11933-11942.
202. O. F. Nielsen, M. Bilde and M. Frosch, *Spectroscopy (New York)*, 2012, **27**, 565-569.
203. S. J. Schmidt, in *Water Activity in Foods: Fundamentals and Applications*, ed. G. V. Barbosa-Cánovas, A. J. Fontana Jr., S. J. Schmidt, T. P. Labuza, Blackwell Publishing Ltd, 2nd edn., 2020, ch. 4, pp. 61-122.
204. M. Karel and D. Lund, *Physical Principles of Food Preservation*, CRC Press, Boca Raton, 2003.
205. G. Scatchard, *Journal of the American Chemical Society*, 1921, **43**, 2387-2406.
206. G. Scatchard, *Journal of the American Chemical Society*, 1921, **43**, 2406-2418.
207. R. H. Stokes and R. A. Robinson, *Journal of Physical Chemistry*, 1966, **70**, 2126-2131.
208. A. A. Zavitsas, *Chemistry-a European Journal*, 2010, **16**, 5942-5960.
209. A. Gharsallaoui, B. Rogé, J. Génotelle and M. Mathlouthi, *Food Chemistry*, 2008, **106**, 1443-1453.
210. B. Subbiah, U. K. M. Blank and K. R. Morison, *Food Chemistry*, 2020, **326**.
211. A. Apelblat, *Journal of Solution Chemistry*, 2010, **39**, 738-742.
212. Z.-H. Yang, *Journal of Physical Chemistry B*, 2019, **123**, 2459-2460.
213. A. A. Zavitsas, *Journal of Physical Chemistry B*, 2012, **116**, 10055-10069.
214. T. H. Lilley, *Journal of Food Engineering*, 1994, **22**, 13-25.
215. T. H. Lilley and R. L. Sutton, *Water Relationships in Foods: Advances in the 1980s and Trends for the 1990s*, 1991, 291-304.
216. M. Starzak, S. D. Peacock and M. Mathlouthi, *Critical Reviews in Food Science and Nutrition*, 2000, **40**, 327-367.
217. M. Starzak and M. Mathlouthi, *Food Chemistry*, 2006, **96**, 346-370.
218. A. VanHook, *Zuckerind*, 1987, **112**, 597-600.
219. H. S. Frank and M. W. Evans, *The Journal of Chemical Physics*, 1945, **13**, 507-532.
220. H. S. Frank and F. Franks, *Journal of Chemical Physics*, 1968, **48**, 4746-4757.
221. M. Caurie, *International Journal of Food Science and Technology*, 2005, **40**, 295-303.

222. M. C. Allan, E. N. Grush, B. P. Rajwa, C. E. Butzke and L. J. Mauer, *Food Analytical Methods*, 2019, **12**, 2753-2763.
223. O. Miyawaki, A. Saito, T. Matsuo and K. Nakamura, *Bioscience, Biotechnology and Biochemistry*, 1997, **61**, 466-469.
224. Y. Sato and O. Miyawaki, *Food Chemistry*, 2016, **190**, 594-598.
225. K. Shiraga, A. Adachi, M. Nakamura, T. Tajima, K. Ajito and Y. Ogawa, *Journal of Chemical Physics*, 2017, **146**.
226. R. Giangiacomo, *Food Chemistry*, 2006, **96**, 371-379.
227. M. A. Kabayama and D. Patterson, *Canadian Journal of Chemistry*, 1958, **36**, 563-573.
228. D. T. Warner, *Nature*, 1962, **196**, 1055-1058.
229. M. D. Tait, A. Suggett, F. Franks, S. Ablett and P. A. Quickenden, *Journal of Solution Chemistry*, 1972, **1**, 131-151.
230. F. Franks, D. S. Reid and A. Suggett, *Journal of Solution Chemistry*, 1973, **2**, 99-113.
231. F. Franks, J. R. Ravenhill and D. S. Reid, *Journal of Solution Chemistry*, 1972, **1**, 3-16.
232. F. Franks, in *Water: A Matrix of Life*, ed. F. Franks, The Royal Society of Chemistry, 2000, ch. 5, pp. 41-52.
233. H. Hirose, H. Sano, G. Mizutani, M. Eguchi, T. Ooya and N. Yui, *Polymer Journal*, 2006, **38**, 1093-1097.
234. A. M. Seuvre and M. Mathlouthi, *Food Chemistry*, 2010, **122**, 455-461.
235. J. Kirkwood and F. Buff, *Journal of Chemical Physics*, 1951, **19**, 774-777.
236. A. Ben-Naim, *The Journal of Chemical Physics*, 1977, **67**, 4884-4890.
237. R. Stenner, N. Matubayasi and S. Shimizu, *Food Hydrocolloids*, 2016, **54**, 284-292.
238. S. Shimizu, *Food and Function*, 2015, **6**, 3228-3235.
239. S. Shimizu, *Chemical Physics Letters*, 2013, **582**, 129-133.
240. K. Miyajima, M. Sawada and M. Nakagaki, *Bulletin of the Chemical Society of Japan*, 1983, **56**, 1954-1957.
241. H. D. Ellerton, P. J. Dunlop, D. E. Mulcahy and G. Reinfelds, *Journal of Physical Chemistry*, 1964, **68**, 398-402.
242. M. V. Galmarini, J. Chirife, M. C. Zamora and A. Pérez, *LWT - Food Science and Technology*, 2008, **41**, 628-631.
243. S. Shimizu and P. E. Smith, *Chemphyschem*, 2017, **18**, 2243-2249.
244. A. Ben-Naim, *Molecular theory of solutions*, Oxford University Press, 2006.
245. Y. Sato, S. Kawabuchi, Y. Irimoto and O. Miyawaki, *Food Hydrocolloids*, 2004, **18**, 527-534.
246. J. Rosgen, B. M. Pettitt and D. W. Bolen, *Protein Science*, 2007, **16**, 733-743.
247. R. Jackson-Atogi, P. K. Sinha and J. Roesgen, *Biophysical Journal*, 2013, **105**, 2166-2174.
248. P. K. Smith and E. R. B. Smith, *Journal of Biological Chemistry*, 1940, **132**, 57-64.
249. O. Miyawaki, M. Dozen and K. Nomura, *Biophysical Chemistry*, 2014, **185**, 19-24.
250. M. Di Gioacchino, M. A. Ricci, S. Imberti, N. Holzmann and F. Bruni, *Journal of Molecular Liquids*, 2020, **301**, DOI: 10.1016/j.molliq.2019.112407.
251. G. Zimbitas, A. Jawor-Baczynska, M. J. Vesga, N. Javid, B. D. Moore, J. Parkinson and J. Sefcik, *Colloids and Surfaces a-Physicochemical and Engineering Aspects*, 2019, **579**, DOI: 10.1016/j.colsurfa.2019.123633.
252. S. Paul and G. N. Patey, *Journal of Physical Chemistry B*, 2006, **110**, 10514-10518.
253. A. Oren, in *Algae and Cyanobacteria in Extreme Environments*, ed. J. Seckbach, Springer Netherlands, Dordrecht, 2007, pp. 639-655.
254. X. Tan, Q. Luo and X. Lu, *Applied Microbiology and Biotechnology*, 2016, **100**, 6131-6139.

255. F. Takenaka, H. Uchiyama and T. Imamura, *Bioscience Biotechnology and Biochemistry*, 2000, **64**, 378-385.
256. A. Ruiz-Matute, M. Sanz, M. Moreno-Arribas and I. Martinez-Castro, *Journal of Chromatography a*, 2009, **1216**, 7296-7300.
257. F. Takenaka and H. Uchiyama, *Bioscience, Biotechnology, and Biochemistry*, 2000, **64**, 1821-1826.
258. T. Sawangwan, *Functional Foods in Health and Disease*, 2015, **5**, 427-436.
259. WO pat., WO2010049136A2, 2010.
260. WO pat., WO2008034158A2, 2008.
261. US pat., US20160120795A1, 2016.
262. JP pat., JP2004331576A, 2004.
263. Glycoin natural, The Cell Energizer, https://www.bitop.de/en/products/cosmetic-active-ingredients/glycoin (accessed 4th February 2019)
264. ECHA, https://echa.europa.eu/registration-dossier/-/registered-dossier/24596 (accessed 24th June 2020)
265. B. Roenneke, N. Rosenfeldt, S. M. Derya, J. F. Novak, K. Marin, R. Kraemer and G. M. Seibold, *Microbial Cell Factories*, 2018, **17**, DOI: 10.1186/s12934-018-0939-2.
266. J. Bolivar, C. Luley-Goedl, E. Leitner, T. Sawangwan and B. Nidetzky, *Journal of Biotechnology*, 2017, **257**, 131-138.
267. J. Bolivar, D. Valikhani and B. Nidetzky, *Biotechnology Journal*, 2019, **14**, 10.1002/biot.201800244.
268. M. Karplus, *Journal of Chemical Physics*, 1959, **30**, 11-15.
269. J. E. Gurst, *Journal of Chemical Education*, 1991, **68**, 1003-1004.
270. F. M. Albini, C. Murelli, G. Patritti and M. Rovati, *Synthetic Communications*, 1994, **24**, 1651-1661.
271. J. Lu, P. Wang, Q. Wang, Y. Wang and M. Jiang, *Molecules*, 2018, **23**, DOI: 10.3390/molecules23051177.
272. H. Nakano, T. Kiso, K. Okamoto, T. Tomita, M. Bin Abdul Manan and S. Kitahata, *Journal of Bioscience and Bioengineering*, 2003, **95**, 583-588.
273. T. Nihira, Y. Saito, K. Ohtsubo, H. Nakai and M. Kitaoka, *Plos One*, 2014, **9**, 10.1371/journal.pone.0086548.
274. Y. Liu, B. Bhandari and W. Zhou, *Journal of Agricultural and Food Chemistry*, 2006, **54**, 5701-5717.
275. Y. Roos, *Carbohydrate Research*, 1993, **238**, 39-48.
276. F. Montanes, A. Olano, E. Ibanez and T. Fornari, *Aiche Journal*, 2007, **53**, 2411-2418.
277. US Pat., US20190127812A1, 2019.
278. J. G. Veneral, T. Benazzi, M. A. Mazutti, F. A. P. Voll, L. Cardozo-Filho, M. L. Corazza, R. Guirardello and J. Vladimir Oliveira, *Journal of Chemical Thermodynamics*, 2013, **58**, 398-404.
279. B. J. Murray, *Atmospheric Chemistry and Physics*, 2008, **8**, 5423-5433.
280. Y. Roos and M. Karel, *International Journal of Food Science & Technology*, 1991, **26**, 553-566.
281. M. Gordon and J. S. Taylor, *Journal of Applied Chemistry*, 1952, **2**, 493-500.
282. G. Scatchard, W. Hamer and S. Wood, *Journal of the American Chemical Society*, 1938, **60**, 3061-3070.
283. O. D. Bonner and Breazeal.Wh, *Journal of Chemical and Engineering Data*, 1965, **10**, 325-327.
284. A. M. Rudakov and V. V. Sergievskii, *Russian Journal of Physical Chemistry*, 2006, **80**, 1804-1808.

285. M. Mathlouthi and B. Rogé, *Food Chemistry*, 2003, **82**, 61-71.
286. M. C. Allan, E. Grush and L. J. Mauer, *Food Research International*, 2020, **127**, DOI: 10.1016/j.foodres.2019.108717.
287. S. Scholl, PhD Thesis, University of Illinois at Urbana-Champaign, 2014.
288. H.-J. Tong, J. P. Reid, D. L. Bones, B. P. Luo, U. K. Krieger, *Atmospheric Chemistry and Physics*, 2011, **11**, 4739-754.
289. J. Rosgen, B. Pettitt and D. Bolen, *Biophysical Journal*, 2005, **89**, 2988-2997.
290. D. J. Davis, C. Burlak and N. P. Money, *Mycological Research*, 2000, **104**, 800-804.
291. S. A. Cooke, S. O. Jonsdottir and P. Westh, *Journal of Chemical and Engineering Data*, 2002, **47**, 1185-1192.
292. C. Marcolli and T. Peter, *Atmospheric Chemistry and Physics*, 2005, **5**, 1545-1555.
293. H. Colin and E. Gueguen, *Comptes Rendus Hebdomadaires Des Seances De L Academie Des Sciences*, 1930, **190**, 653-655.
294. S.-Y. Li, Y. Shabtai and S. Arad, *Journal of Phycology*, 2002, **38**, 931-938.
295. Q. Luo, Z. Zhu, Z. Zhu, R. Yang, F. Qian, H. Chen and X. Yan, *Plos One*, 2014, **9**, 10.1371/journal.pone.0094354.
296. F. Qian, Q. Luo, R. Yang, Z. Zhu, H. Chen and X. Yan, *Journal of Applied Phycology*, 2015, **27**, 621-632.
297. M. Martinez-Garcia and M. van der Maarel, *AMB Express*, 2016, **6**.
298. M. Kim, Y. Li, P. Dewapriya, B. Ryu and S. Kim, *BMB Reports*, 2013, **46**, 398-403.
299. WO pat., WO2017132755A1, 2017.
300. CN Pat*.,* CN105395434A, 2016.
301. EP Pat*.,* EP 1652435B1, 2017.
302. WO Pat*.,* WO2001066100A3, 2002.
303. CN Pat., CN105494599A, 2016.
304. JP. Pat., JP2011057610A, 2011.
305. K. Ishihara, C. Oyamada, Y. Sato, T. Suzuki, M. Kaneniwa, H. Kunitake and T. Muraoka, *Fisheries Science*, 2010, **76**, 1015-1021.
306. Microorganisms & Microbial-Derived Ingredients Used in Food (Partial List), https://www.fda.gov/food/generally-recognized-safe-gras/microorganisms-microbial-derived-ingredients-used-food-partial-list (accessed 7th November 2018).
307. P. Cherry, C. O'Hara, P. J. Magee, E. M. McSorley and P. J. Allsopp, *Nutrition Reviews*, 2019, **77**, 307-329.
308. B. Grote, *Reviews in Aquaculture*, 2019, **11**, 25-41.
309. A. Courtois, C. Simon-Colin, C. Boisset, C. Berthou, E. Deslandes, J. Guezennec and A. Bordron, *Marine Drugs*, 2008, **6**, 407-417.
310. Y. Li, Y. Li, S. Lee, Z. Qian and S. Kim, *Journal of Agricultural and Food Chemistry*, 2010, **58**, 578-586.
311. R. Rødde, K. Varum, B. Larsen and S. Myklestad, *Botanica Marina*, 2004, **47**, 125-133.
312. C. Simon-Colin, F. Michaud, J. Leger and E. Deslandes, *Carbohydrate Research*, 2003, **338**, 2413-2416.
313. M. A. Le Pape, J. Grua-Priol, C. Prost and M. Demaimay, *Journal of Agricultural and Food Chemistry*, 2004, **52**, 550-556.
314. G. Kulshreshtha, A. Critchley, B. Rathgeber, G. Stratton, A. H. Banskota, J. Hafting and B. Prithiviraj, *Journal of Marine Science and Engineering*, 2020, **8**, DOI: 10.3390/jmse8070511.
315. S. P. Pinho and E. A. Macedo, *Journal of Chemical and Engineering Data*, 2005, **50**, 29-32.

316. S. Cox, L. Noronha, T. Herald, S. Bean, S.-H. Lee, R. Perumal, W. Wang and D. Smolensky, *Heliyon*, 2019, **5**, e01589.
317. F. P. Byrne, S. Jin, G. Paggiola, T. H. M. Petchey, J. H. Clark, T. J. Farmer, A. J. Hunt, C. Robert McElroy and J. Sherwood, *Sustainable Chemical Processes*, 2016, **4**, 7.
318. Q.-W. Zhang, L.-G. Lin and W.-C. Ye, *Chinese Medicine*, 2018, **13**, DOI: 10.1186/s13020-018-0177-x.
319. B. Thollas and C. Boisset, *Synlett*, 2007, 1736-1738.
320. C. Simon-Colin, N. Kervarec, R. Pichon and E. Deslandes, *Carbohydrate Research*, 2002, **337**, 279-280.
321. M. Li, D. Constantinescu, L. Wang, A. Mohs and J. Gmehling, *Industrial & Engineering Chemistry Research*, 2010, **49**, 4981-4988.
322. J. S. Craigie, J. McLachlan and R. D. Tocher, *Canadian Journal of Botany*, 1968, **46**, 605-611.
323. C. Vonthron-Senecheau, J. Santos, I. Mussio and A. Rusig, *Carbohydrate Research*, 2008, **343**, 2697-2698.
324. A. Nezzal, L. Aerts, M. Verspaille, G. Henderickx and A. Redl, *Journal of Crystal Growth*, 2009, **311**, 3863-3870.
325. J. Chirife and S. L. Resnik, *Journal of Food Science*, 1984, **49**, 1486-1488.
326. M. Allan, L. S. Taylor and L. J. Mauer, *Food Chemistry*, 2016, **195**, 2-10.
327. M. Mathlouthi, G. Benmessaoud and B. Roge, *Food Chemistry*, 2012, **132**, 1630-1637.
328. J. E. Williamson, R. De Nys, N. Kumar, D. G. Carson and P. D. Steinberg, *Biological Bulletin*, 2000, **198**, 332-345.
329. H. Colin, *Bulletin du Muséum national d'histoire naturelle.*, 1934, **6**, 153-155.
330. H. Nagase, N. Ogawa, T. Endo, M. Shiro, H. Ueda and M. Sakurai, *Journal of Physical Chemistry B*, 2008, **112**, 9105-9111.
331. J. Kirk, S. Dann and C. Blatchford, *International Journal of Pharmaceutics*, 2007, **334**, 103-114.
332. F. Sussich, R. Urbani, F. Princivalle and A. Cesaro, *Journal of the American Chemical Society*, 1998, **120**, 7893-7899.
333. M. Falk, *Spectrochimica Acta Part A: Molecular Spectroscopy*, 1984, **40**, 43-48.
334. S. E. Hogan and G. Buckton, *International Journal of Pharmaceutics*, 2000, **207**, 57-64.
335. H. Zhu, C. Yuen and D. Grant, *International Journal of Pharmaceutics*, 1996, **135**, 151-160.
336. M. Allan and L. J. Mauer, *Data in Brief*, 2017, **12**, 364-369.
337. T. Steiner and W. Saenger, *Acta Crystallographica Section B*, 1992, **48**, 819-827.
338. B. G. Osbourne, in *Encyclopedia of Analytical Chemistry*, ed. R.A. Meyers and R.J. McGorrin, John Wiley & Sons, Ltd., 2006, DOI: 10.1002/9780470027318.a1018
339. J. Lu and S. Rohani, *Current Medicinal Chemistry*, 2009, **16**, 884-905.
340. U. Karsten, K. D. Barrow and R. J. King, *Plant Physiology*, 1993, **103**, 485-491.
341. N. K. Jain and I. Roy, *Protein Science*, 2009, **18**, 24-36.
342. D. Kilburn, S. Townrow, V. Meunier, R. Richardson, A. Alam and J. Ubbink, *Nature Materials*, 2006, **5**, 632-635.
343. L. Meneses, F. Santos, A. R. Gameiro, A. Paiva and A. R. C. Duarte, *JoVE*, 2019, e60326.
344. S. H. Zeisel and K. A. da Costa, *Nutrition Reviews*, 2009, **67**, 615-623.
345. A. Hijo, G. J. Maximo, M. C. Costa, E. A. C. Batista and A. J. A. Meirelles, *ACS Sustainable Chemistry & Engineering*, 2016, **4**, 5347-5369.
346. F. Bergua, M. Nuez, J. Muñoz-Embid, C. Lafuente and M. Artal, *Journal of Molecular Liquids*, 2018, **258**, 106-113.
347. WO pat., WO2017165287A1, 2017.

348. T. Shrestha and N. G. Bisset, *Phytochemistry*, 1991, **30**, 3285-3287.
349. M. Orfanoudaki, A. Hartmann, H. Miladinovic, H. Nguyen Ngoc, U. Karsten and M. Ganzera, *Marine Drugs*, 2019, **17**, DOI: 10.3390/md17060356.
350. J. A. P. Coutinho, S. I. Andersen and E. H. Stenby, *Fluid Phase Equilibria*, 1995, **103**, 23-39.
351. S. Chelouche, D. Trache, C. M. S. S. Neves, S. P. Pinho, K. Khimeche and M. Benziane, *Thermochimica Acta*, 2018, **666**, 197-207.
352. E. A. Crespo, L. P. Silva, J. O. Lloret, P. J. Carvalho, L. F. Vega, F. Llovell and J. A. P. Coutinho, *Physical Chemistry Chemical Physics*, 2019, **21**, 15046-15061.
353. L. Fernandez, L. P. Silva, M. A. R. Martins, O. Ferreira, J. Ortega, S. P. Pinho and J. A. P. Coutinho, *Fluid Phase Equilibria*, 2017, **448**, 9-14.
354. K. Wysoczanska, G. Sadowski, E. A. Macedo and C. Held, *Industrial & Engineering Chemistry Research*, 2019, **58**, 7362-7369.
355. Y. Corvis, M. C. Menet, P. Negrier, M. Lazerges and P. Espeau, *New Journal of Chemistry*, 2013, **37**, 761-768.
356. G. Barone, G. D. Gatta, D. Ferro and V. Piacente, *Journal of the Chemical Society, Faraday Transactions*, 1990, **86**, 75-79.
357. J. Haneef and R. Chadha, *AAPS PharmSciTech*, 2018, **19**, 1191-1204.
358. M. W. Davey, M. Van Montagu, D. Inze, M. Sanmartin, A. Kanellis, N. Smirnoff, I. J. J. Benzie, J. J. Strain, D. Favell and J. Fletcher, *Journal of the Science of Food and Agriculture*, 2000, **80**, 825-860.
359. J. P. Higgins, T. D. Tuttle and C. L. Higgins, *Mayo Clinic Proceedings*, 2010, **85**, 1033-1041.
360. K. Nishinari, Y. Fang, S. Guo and G. O. Phillips, *Food Hydrocolloids*, 2014, **39**, 301-318.
361. G. Hua and K. Odelius, *ACS Sustainable Chemistry & Engineering*, 2016, **4**, 4831-4841.
362. W. Liu, K. Zhang, J. Chen and J. Yu, *Journal of Molecular Liquids*, 2018, **260**, 173-179.
363. J. M. Silva, R. L. Reis, A. Paiva and A. R. C. Duarte, *ACS Sustainable Chemistry & Engineering*, 2018.
364. CN pat., CN106397082A, 2017.
365. P. A. de Jongh, P. K. Paul, E. Khoshdel, P. Wilson, K. Kempe and D. M. Haddleton, *Polymer International*, 2017, **66**, 59-63.
366. Á. Mourelle-Insua, I. Lavandera and V. Gotor-Fernández, *Green Chemistry*, 2019, **21**, 2946-2951.
367. H. Flores and P. Amador, *Journal of Chemical Thermodynamics*, 2004, **36**, 1019-1024.
368. M. Stacey, *Journal of the Chemical Society (Resumed)*, 1939, 1529-1531.
369. V. Petrouleas, R. Lemmon and A. Christensen, *Journal of Chemical Physics*, 1978, **68**, 2243-2246.
370. X. Q. Meng, K. Ballerat-Busserolles, P. Husson and J. M. Andanson, *New Journal of Chemistry*, 2016, **40**, 4492-4499.
371. L. P. Silva, L. Fernandez, J. H. F. Conceicao, M. A. R. Martins, A. Sosa, J. Ortega, S. P. Pinho and J. A. P. Coutinho, *ACS Sustainable Chemistry & Engineering*, 2018, **6**, 10724-10734.
372. P. J. Smith, C. B. Arroyo, F. Lopez Hernandez and J. C. Goeltz, *The Journal of Physical Chemistry B*, 2019, **123**, 5302-5306.
373. C. Florindo, F. S. Oliveira, L. P. N. Rebelo, A. M. Fernandes and I. M. Marrucho, *ACS Sustainable Chemistry & Engineering*, 2014, **2**, 2416-2425.
374. N. R. Rodriguez, A. van den Bruinhorst, L. Kollau, M. C. Kroon and K. Binnemans, *ACS Sustainable Chemistry & Engineering*, 2019, **7**, 11521-11528.
375. M. Bierenstiel and M. Schlaf, *European Journal of Organic Chemistry*, 2004, **2004**, 1474-1481.

376. R. Craveiro, I. Aroso, V. Flammia, T. Carvalho, M. T. Viciosa, M. Dionisio, S. Barreiros, R. L. Reis, A. R. C. Duarte and A. Paiva, *Journal of Molecular Liquids*, 2016, **215**, 534-540.
377. T. H. Jang, S. C. Park, J. H. Yang, J. Y. Kim, J. H. Seok, U. S. Park, C. W. Choi, S. R. Lee and J. Han, *Integrative Medicine Research*, 2017, **6**, 12-18.
378. M. Gilmore, M. Swadzba-Kwasny and J. D. Holbrey, *Journal of Chemical and Engineering Data*, 2019, **64**, 5248-5255.
379. E. A. Crespo, L. P. Silva, M. A. R. Martins, M. Bulow, O. Ferreira, G. Sadowski, C. Held, S. P. Pinho and J. A. P. Coutinho, *Industrial & Engineering Chemistry Research*, 2018, **57**, 11195-11209.
380. A. R. Abbott, G. Capper and S. Gray, *Chemphyschem*, 2006, **7**, 803-806.
381. A. Abbott, R. Harris, K. Ryder, C. D'Agostino, L. Gladden and M. Mantle, *Green Chemistry*, 2011, **13**, 82-90.
382. L. Slade, M. Kweon and H. Levine, *Critical Reviews in Food Science and Nutrition*, 2020, DOI: 10.1080/10408398.2020.1729694.
383. T. Kimura and T. Nakakuki, *Starch-Starke*, 1990, **42**, 151-157.
384. M. Kweon, L. Slade and H. Levine, *Cereal Chemistry*, 2016, **93**, 568-575.
385. M. Kweon, L. Slade and H. Levine, *Cereal Chemistry*, 2016, **93**, 576-583.
386. E. J. Lee, Y. Moon and M. Kweon, *LWT*, 2020, **131**, 109565.
387. D. S. Reid, in *Water Activity in Foods: Fundamentals and Applications*, ed. G. V. Barbosa-Cánovas, A. J. Fontana Jr., S. J. Schmidt, T. P. Labuza, Blackwell Publishing Ltd, 2nd edn., 2020, ch. 2, pp. 13-26.
388. M. Dupas-Langlet, J. Dupas, S. Samain, M.-I. Giardiello, V. Meunier and L. Forny, *Journal of Food Engineering*, 2016, **184**, 53-62.
389. M. Dupas-Langlet, V. Meunier, M. Pouzot and J. Ubbink, *Carbohydrate Polymers*, 2019, **213**, 147-158.
390. M. Roussenova, J.-C. Andrieux, M. A. Alam and J. Ubbink, *Carbohydrate Polymers*, 2014, **102**, 566-575.
391. M. T. Kalichevsky, E. M. Jaroszkiewicz and J. M. V. Blanshard, *Polymer*, 1993, **34**, 346-358.
392. P. Y. Mikus, S. Alix, J. Soulestin, M. F. Lacrampe, P. Krawczak, X. Coqueret and P. Dole, *Carbohydrate Polymers*, 2014, **114**, 450-457.
393. K. Kawai and Y. Hagura, *Carbohydrate Polymers*, 2012, **89**, 836-841.
394. S. H. Kim, G. A. Jeffrey, R. D. Rosenstein and P. W. Corfield, *Acta Crystallographica*, 1967, **22**, 733-743.
395. M. Wang, MSc. Thesis, University of Illinois at Urbana-Champaign, 2017.
396. R. Chetana, S. Krishnamurthy and S. R. Y. Reddy, *European Food Research and Technology*, 2004, **218**, 345-348.
397. W. P. Schellart, *Journal of Structural Geology*, 2011, **33**, 1079-1088.
398. A. J. Davies, *Measurement Science and Technology*, 2015, **26**, DOI: 10.1088/0957-0233/26/12/127001.
399. I. Siemons, R. G. A. Politiek, R. M. Boom, R. G. M. van der Sman and M. A. I. Schutyser, *Food Research International*, 2020, **131**, DOI: 10.1016/j.foodres.2020.108988.
400. G. Barra, H. Chisholm and J. Mitchell, in *Gums and Stabilizers for the Food Industry 12*, ed. P. A. Williams and G. O. Phillips, Royal Society of Chemistry, London, 2004, pp. 450-460.
401. R. A. Lipasek, N. Li, S. J. Schmidt, L. S. Taylor and L. J. Mauer, *Journal of Agricultural and Food Chemistry*, 2013, **61**, 9241-9250.

402. A. Claude, S. Bondu, F. Michaud, N. Bourgougnon and E. Deslandes, *Carbohydrate Research*, 2009, **344**, 707-710.
403. N. Borges, C. D. Jorge, L. G. Goncalves, S. Goncalves, P. M. Matias and H. Santos, *Extremophiles*, 2014, **18**, 835-852.
404. L. Petigny, M. Z. Özel, S. Périno, J. Wajsman and F. Chemat, in *Green Extraction of Natural Products*, ed. F. Chemat and J. Strube, Wiley-VCH Verlag GmbH & Co. KGaA, 2015, ch. 7, pp. 237-264.
405. S. R. C. Warr, R. H. Reed, J. A. Chudek, R. Foster and W. D. P. Stewart, *Planta*, 1985, **163**, 424-429
406. P. A. Harnedy, M. B. O'Keeffe and R. J. FitzGerald, *Food Chemistry*, 2015, **172**, 400-406.
407. H. Noda, H. Amano, K. Abo and Y. Horiguchi, *Nippon Suisan Gakkaishi*, 1981, **47**, 57-62.
408. K. Jorgensen and P. T. Olesen, *Food Additives & Contaminants Part B-Surveillance*, 2018, **11**, 198-200.
409. D. Giustarini, I. Dalle-Donne, R. Colombo, A. Milzani and R. Rossi, *Nitric Oxide-Biology and Chemistry*, 2008, **19**, 252-258.
410. S. Cabani, P. Gianni, V. Mollica and L. Lepori, *Journal of Solution Chemistry*, 1981, **10**, 563-595.
411. S. Sirimulla, M. Lerma and W. C. Herndon, *Journal of Chemical Information and Modeling*, 2010, **50**, 194-204.
412. I. Gheorghe, C. Stoicescu and F. Sirbu, *Journal of Molecular Liquids*, 2016, **218**, 515-524.
413. H. Zhao, *Biophysical Chemistry*, 2006, **122**, 157-183.
414. I. Pitkänen, J. Suuronen and J. Nurmi, *Journal of Solution Chemistry*, 2010, **39**, 1609-1626.